Dynamic water flood optimization with smart wells using optimal control theory

Proefschrift

ter verkrijging van de graad van doctor
aan de Technische Universiteit Delft,
op gezag van de Rector Magnificus prof. dr. ir. J.T. Fokkema,
voorzitter van het College voor Promoties,
in het openbaar te verdedigen op dinsdag 12 oktober 2004 om 15:30 uur

door

Dirk Roelof BROUWER

doctorandus in de geochemie
geboren te Assen

Dit proefschrift is goedgekeurd door de promotor:
Prof. ir. C.P.J.W. van Kruijsdijk

Toegevoegd promotor:
Dr. ir. J.D. Jansen

Samenstelling promotiecommissie:

Rector Magnificus,	voorzitter
Prof. ir. C.P.J.W. van Kruijsdijk,	Technische Universiteit Delft, promotor
Dr. ir. J.D. Jansen,	Technische Universiteit Delft, toegevoegd promotor
Prof. dr. ir. A.W. Heemink,	Technische Universiteit Delft
Prof. dr. K. Aziz,	Stanford University
Prof. ir. O.H. Bosgra,	Technische Universiteit Delft
Dr. J.F.B.M. Kraaijevanger,	Shell International Exploration and Production
Dr. ir. C.B.M. te Stroet,	TNO-NITG

ISBN: 90-9018615-8

The research for this thesis was financially supported by Shell International Exploration and Production

to Barbara

Contents

Chapter 1
Introduction

1.1 Background

1.1.1 The demand for energy

The global demand for energy is large, and will only become larger in the future. Figure 1.1 shows that a large part of this energy is provided by fossil fuels, i.e. coal, oil and gas.

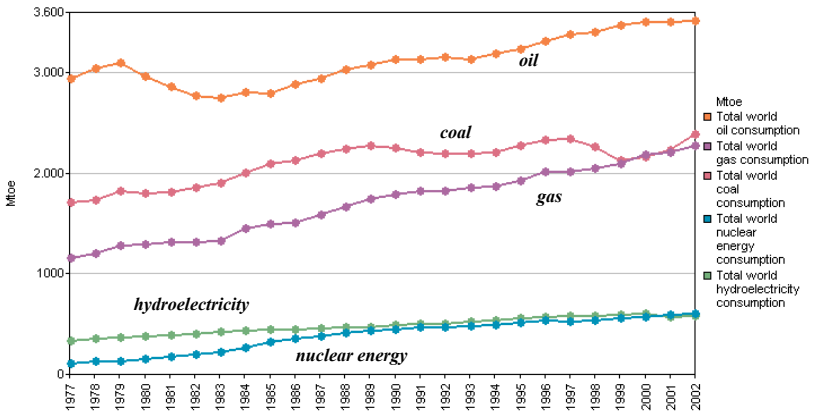

Figure 1.1: World consumption of primary energy. Million tonnes of oil equivalent (source: BP Statistical review of world energy)

For environmental reasons there are currently increasing efforts to switch from coal to oil to gas to renewables. The latter group comprises energy sources like wind, water, solar and biomass based energy sources. Nuclear energy is another important source of energy but is controversial, mainly because there are significant issues with the waste products. For most renewable energy sources technology is still at a too immature stage to make it a serious

alternative. For these reasons oil and gas will remain essential in meeting global energy requirements in the decades to come.

It becomes increasingly difficult for oil companies to meet the large demand for fossil fuels. An increasing number of large oil fields are already at a mature stage, and the number of new significant oil fields found per year decreases gradually. Smaller fields are still regularly found, but at the current oil price it is often not economical to exploit them. As a direct result it becomes more and more difficult to maintain economic reserves at a desirable level, as reflected in Figure 1.2. Therefore, oil companies are making great efforts to reduce the costs for developing and maintaining oil fields.

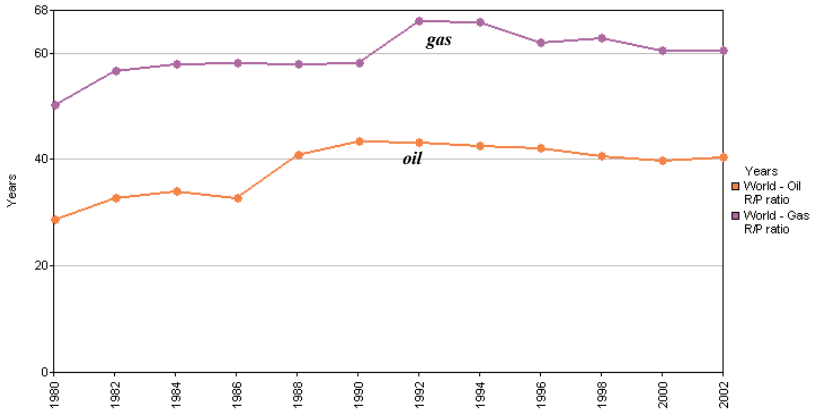

Figure 1.2: Worlds oil and gas reserves-production ratio. (source: BP Statistical review of world energy)

1.1.2 Oil reservoirs

Oil and gas resources are generally contained in sandstones or limestones beneath the earth surface, typically at a depth between 1-5 km. The rock containing the oil is generally referred to as the reservoir rock. It has a relatively high porosity (fraction of the rock that can be occupied by fluids) and permeability. The latter means that the individual fluid-containing pores are well connected and that fluids can consequently easily flow through the porous network. The areal coverage of oil fields may range from only a few to a few hundred square kilometers, whereas the thickness of the reservoir rock may range from only a few to hundreds of meters. Figure 1.3 shows a schematic vertical cross-section of an oil reservoir. In the figure, overlying the oil-bearing reservoir rock there is a rock formation that is imper-

meable to fluids, i.e. it acts as a seal for the oil below. This impermeable rock formation is generally referred to as a cap rock. At the bottom the oil reservoir may be bounded by rocks having a low porosity and permeability (referred to as non-reservoir rock) and/or by a water-bearing zone. The interface between the oil- and water-bearing zones is generally referred to as the oil-water contact. The oil is produced to the surface through production wells that are drilled and completed in the oil-bearing reservoir rock. A variety of well types can be distinguished.

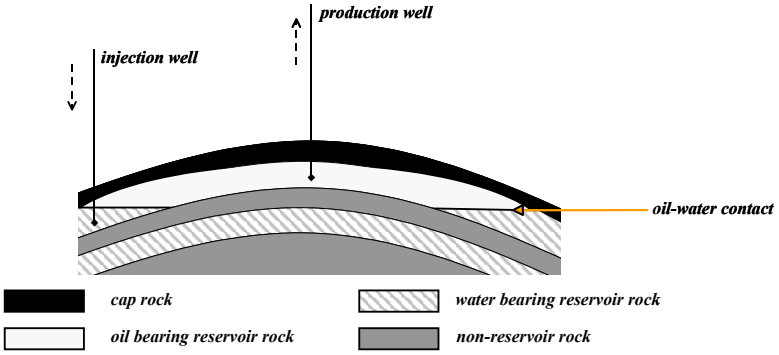

Figure 1.3: Schematic vertical cross-section of an oil reservoir bounded by a cap rock at the top and an aquifer and non-reservoir rock at the bottom.

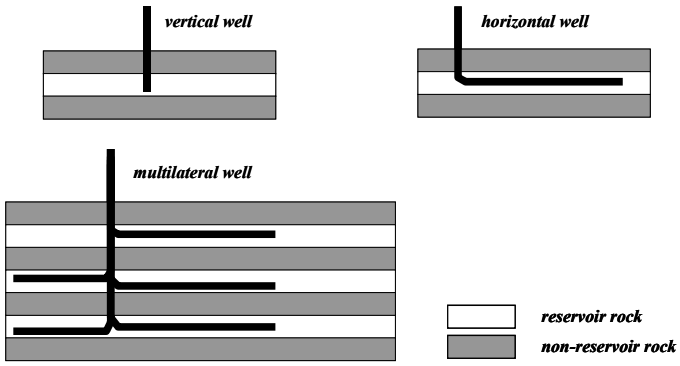

Figure 1.4: Well types

1.1.3 Well types

Conventional wells

Up to the early eighties mainly vertical wells (Figure 1.4) were used in the industry. Deviated wells have been drilled frequently as of the early seventies to allow multi-well developments from a single offshore platform. However, these wells still ended vertically, i.e. they penetrated the reservoir vertically. A drawback of vertical wells is often that their contact area with the reservoir is small, because in most reservoirs the areal extension is significantly larger that the vertical extension. At the end of the eighties it became technically possible to drill horizontal wells (Figure 1.4). They have a much larger contact area with the reservoir, as a result of which higher production rates can generally be achieved. The development of multilateral wells (Figure 1.4) enabled a further increase in the contact area between well and reservoir, generally at lower costs than if separate horizontal wells would be drilled.

Smart wells

In the last few years, the need to produce cheaper and to produce more oil from a reservoir has resulted in the development of a variety of technologies to better measure and control the production process through the wells. Typically, these technologies are installed within the well and can be operated remotely. A well equipped with this type of technology is generally referred to as a smart, intelligent, or instrumented well. A schematic description of it is given in Figure 1.5.

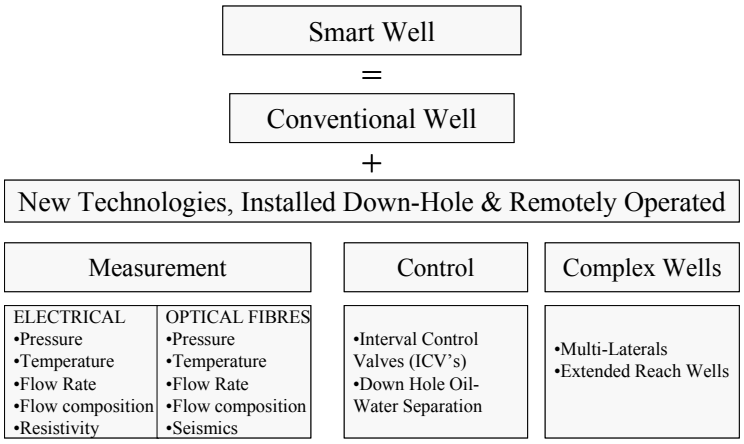

Figure 1.5: Schematic description of a smart well.

Sensors have been developed for permanent down-hole measurement of for instance temperature, pressure, resistivity, fluid composition, and acoustic velocities. With these sensors much more and much more detailed information on several processes occurring in the well and in the near-well reservoir region can be obtained than with conventional wells.

Apart from measurement equipment major progress has been made in the development of technology to control the production process. This technology comprises down-hole hydrocyclones and down-hole valves. The development of down-hole hydrocyclones enables oil-water separation down in the well. The separated water can then directly be reinjected into the reservoir for pressure support. This may reduce costs of surface facilities significantly and reduce problems associated with high (water) production rates. The development of down-hole valves enables the splitting up of wells into a number of segments, as shown schematically in Figure 1.6, that can be controlled individually and remotely. They were initially developed to be able to shut in that part of the production well that produces large volumes of water, without having to enter the well from the surface. This is particularly important at sea, where the costs of a well intervention are high. Implementing down-hole control valves in multilateral wells (Figure 1.4) enables commingled (simultaneous) production from different reservoirs, as flow from each branch of the multilateral can be regulated.

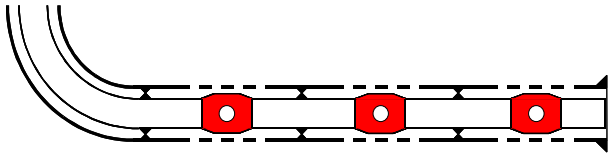

Figure 1.6: Smart horizontal well, consisting of three segments, each having a down-hole control valve.

The potential benefits of smart wells over conventional wells become apparent when considering the oil production process.

1.1.4 The production process

The production process for gas reservoirs generally consists of only one phase. Due to the low density and viscosity the gas flows relatively easily to the surface, and the pressure decline in the reservoir, resulting from the extraction of gas, is slow due to the high compressibility of the gas.

Contrary to gas reservoirs, the production process of oil reservoirs generally consists of a number of phases. During the primary recovery phase the pressure in the reservoir is high enough to produce the oil through the production well to the surface at sufficiently high rates. The decrease in reservoir pressure, resulting from the extraction of oil causes this flow towards the surface to occur at a decreasing rate. The decline in reservoir pressure and the

decrease in flow rates are more severe as for gas reservoirs, due to the lower compressibility and higher density of oil compared to gas. At a certain point in time economic production rates can only be maintained by installing a pump in the well or by repressurizing the reservoir through the injection of gas and/or water. The phase during which fluids are injected for pressure maintenance is generally referred to as the secondary recovery phase. Injection of these fluids is generally done through wells at some distance from the production wells, as schematically depicted in Figure 1.3.

Ideally, as the production process continues the injected fluids will slowly move through the reservoir in the direction of the producer(s), in the meantime displacing all the oil in between. In reality, however, that does not happen. Due to spatially varying rock properties (heterogeneities) there may exist preferential flow paths in the reservoir through which the injected fluids channel towards the producer. Oil located outside these channels may as a result be bypassed, and instead production of injected gas and/or water may start at an early stage. Identification of these preferential flow paths is difficult, because only a small part of the reservoir can be accessed through the wells. Furthermore, the geological model of the reservoir, describing the rock properties is constructed based on a restricted number of indirect measurements, like well logs, core samples, and seismics. The spatial resolution and measurement errors generally differ with the type of measurement. Apart from uncertainties in the rock properties there are also uncertainties in the fluid properties, in the amount of oil present in the reservoir, in the location of the oil-water contact, and in the size of the communicating water zone (aquifer) below this oil-water contact. Because of all the uncertainties it is difficult to define the best location of the wells within the reservoir. A drawback of conventional wells is that there is little that can be done to control the production process if it evolves differently than expected.

As a result of the uncertainties and the lack of control on the production process with conventional wells, typically only 20-40% of the oil in place can be recovered economically. Hence there is potentially large scope for increasing the worlds recoverable oil reserves by increasing the percentage of oil that can be recovered from the reservoir. The capacity of smart wells to near-continuously monitor and control the production process may enable this.

1.2 Closed loop control

Maximum benefit from the measurement and control equipment of a smart well is expected when used in an integrated monitoring and control approach, as schematically depicted in Figure 1.7. In this approach measurements obtained from smart well sensors (and other data sources) are used to construct or update a model describing the dynamic behavior of the system. In principle various types of models could be used, the type and complexity depending on the purpose they serve. In this thesis the model is the numerical representation of the reservoir and the wells, i.e. a reservoir simulator. Based on these models the production process can subsequently be optimized, for instance by optimizing the injection and produc-

tion strategy. As the process continues new measurements are used to update the model, based on which an update of the optimal injection and production strategy can be calculated. This thesis primarily focuses on the optimization part of this closed loop, shown in Figure 1.8. Based on a model of the real reservoir the aim is to find the optimum well operating strategy that maximizes the value from the reservoir.

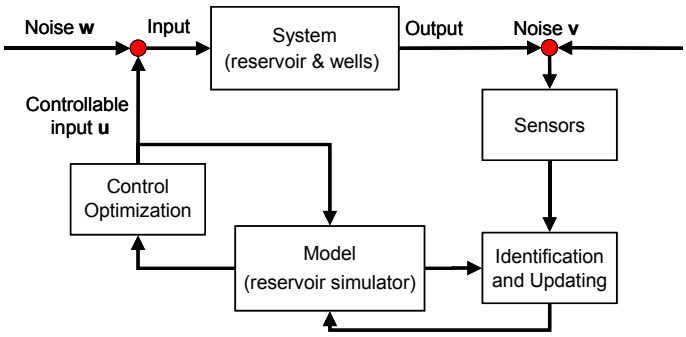

Figure 1.7: Schematic representation of model-based closed-loop control.

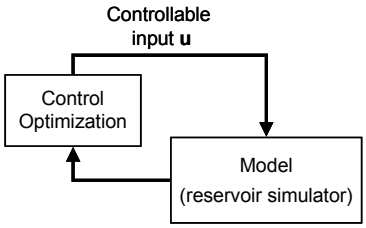

Figure 1.8: Model-based open loop control.

In particular optimization of the water flooding process with smart wells like in Figure 1.6 is investigated. Figure 1.9 shows a schematic of a reservoir with a horizontal, smart segmented injector along the left edge, and a horizontal, smart segmented producer along the right edge. Upon injection the water moves towards the production well where fluids are withdrawn from the reservoir, on its way displacing the oil that it encounters. The speed at which the oil-water front propagates in the direction of the producer generally differs from one place to the other, as shown schematically by the irregular shape of the oil-water

interface in Figure 1.9. This is, because the reservoir generally has spatially varying rock properties. The oil-water front shown in the figure corresponds to a particular injection and production strategy, i.e. a particular combination of valve-settings. By manipulating the down-hole valves it is to some extent possible to control the flow direction, and thereby the movement of this oil-water front in the reservoir. By doing so the flow of fluids through high permeability zones (channels) may be reduced and flow outside these zones may be increased, ideally displacing the oil everywhere in the reservoir. The question then is which combination of valve-settings would give the best displacement. Secondly, the question is what degree of improvement is possible by optimizing the valve-settings. Both expectedly depend on the type of heterogeneity in the reservoir. Physical and economical constraints on the wells and the valves will also affect how much can be improved by valve-setting optimization.

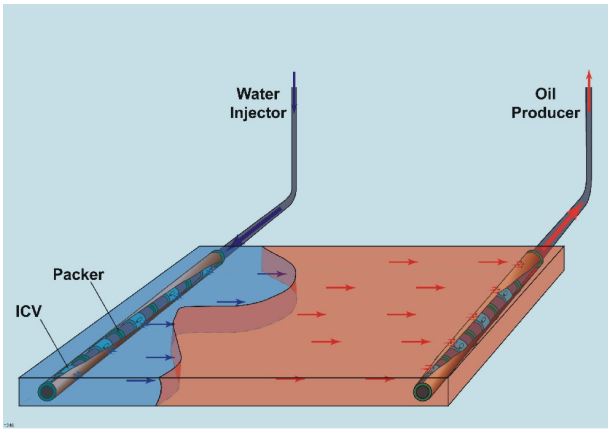

Figure 1.9: Schematic of horizontal reservoir with two horizontal, segmented smart wells.

1.3 Research objectives and approach

At present it is neither known what the optimum injection and production strategy is for a particular type of reservoir and operating constraints, nor what improvement could be achieved under these conditions. Since smart well technology increases the capital expenditure of the project it is important to know what its added value will be under certain conditions in order to justify its implementation. One objective of this thesis is to find for various types of reservoirs and operating conditions the combination of down-hole valve settings that optimizes

the water flood. A second objective is to investigate the potential for improvement as function of reservoir properties and operating constraints. For obvious reasons this study cannot be done on a real reservoir. Instead, a reservoir simulator is therefore used.

The problem of finding the optimal water flood constitutes an optimization problem where the objective is to maximize the water flood performance and the parameters to be optimized are the valve-settings in the smart wells. A major issue in this optimization problem is that the number of control parameters, i.e. the valve settings, to be optimized may be large. This is because a valve can, apart from its extreme settings (fully open and fully closed), generally have a number of intermediate settings. On top of this, the number of down-hole valves itself can be large, especially if multiple smart wells like the one shown in Figure 1.6 must be optimized simultaneously. Since these valves can be operated remotely they can in principle be changed frequently over time, thereby further increasing the number of control parameters that must be optimized. In addition the function evaluation may be long, as each requires a forward reservoir simulation. The combination of the large number of control parameters and the long function evaluation times require efficient algorithms to find the optimal operating strategy within reasonable computational time.

Roughly two types of optimization methods can be distinguished. Global optimization methods guarantee a global optimum solution, provided that enough function evaluations are done. In local optimization methods the optimum nearest to an initial guess will be found. If the response surface is rough, many local optima exist and in that case the optimum found generally depends on the initial guess. So, global optimization methods would in principle be preferable to use. However, global optimization methods are computationally more intensive than local optimization methods and in that respect less suitable for optimization problems where the number of control parameters and the computation time for one function evaluation are large.

The optimization method used in this study is therefore a local optimization method, that is gradient based. The gradients indicate the sensitivity of the objective function with respect to the controllable parameters. They can be obtained analytically or numerically, either forward or backward in time. From an implementation point of view the easiest approach generally is to calculate the gradients numerically. However, for large systems with a lot of control parameters to be optimized this becomes computationally expensive. With optimal control theory these gradients can be obtained more efficiently. The gradients are calculated backward in time with the aid of an adjoint equation. For the optimization problem investigated in this thesis optimal control theory is the only method available sofar that can provide gradients for the controls with sufficient computational efficiency.

In reality, the rock properties in the majority of the reservoir are unknown. The optimum water flooding strategy for a real reservoir must then be based on the limited information that is available. Developing robust algorithms for optimizing the production process at an early stage with scarce information can expectedly be helped through knowledge of the characteristics of an optimal water flood. Another aim of this study is therefore to try to extract (physical) principles behind an optimal water flood.

1.4 Outline of thesis

In chapter 2 work published in the open literature on optimization of the production process is discussed. The theory behind numerical reservoir simulation is treated in chapter 3. Optimal control theory and some properties and characteristics of the adjoint dynamic system will be treated in chapter 4. When numerically implementing a multi-phase flow optimal control problem it appeared important to address a number of issues in order to assure stability of the numerical scheme. Besides that, constraints on the controls must be taken into account. These issues are treated in chapter 5. In chapter 6 the optimization algorithm is applied to the optimization of several synthetic reservoir models. In chapter 7 results obtained in chapter 6 are discussed. Chapter 8 contains the main conclusions of this work and recommendations for future work.

Chapter 2
Optimization of the production process with smart wells

2.1 Benefits of smart wells from a conceptual viewpoint

One of the main benefits of a smart well is its ability to adapt to unexpected circumstances in the reservoir. This section describes from a conceptual viewpoint why flexibility is a beneficial feature in the production process.

Generally there may exist a difference in optimal well location and configuration during different stages of the recovery process, with respect to for example fractures. During the primary recovery phase, where production is due to fluid and rock expansion, the well should generally intersect as many fractures as possible to maximize its productivity, which means that the well should be at an angle to the main fracture system direction. During the secondary recovery phase, where a fluid is injected for pressure support, the well orientation should preferably be more parallel to the main fracture system direction, to avoid rapid advance of injected fluids towards the production wells. The optimum orientation for the primary recovery phase may thus correspond to the worst possible configuration for the secondary recovery phase. The actual well trajectory to be chosen therefore depends on which of the recovery phases is expected to be most important. This on its turn depends on factors like the size and strength of the aquifer and the gas cap, and the direction from which aquifer influx occurs. These factors are generally poorly known. Because of these uncertainties the ultimately resulting combination of well type, geometry, size, location, and orientation, will generally not be optimal. For conventional wells there is nothing that can be done to change this without significant extra costs. These may comprise costs related to identifying the down-hole conditions and workover costs. Furthermore, what is considered to be the optimal well location and configuration generally changes with time, as newly incoming information (seismics, production data, logs from other wells) generally leads to a change in reservoir description and optimal operating strategy. On top of this the completion of new wells may affect the performance of existing wells.

Even if the reservoir properties would be known a priori a smart well may still be beneficial. Contrary to a conventional well, the flexibility of a smart well enables it to adapt to changes in the oil-water and gas-oil contacts, in the reservoir properties (resulting from scaling, sand production, injection-induced fracturing, compaction, etc.), the completion of new wells, failure and maintenance in neighboring wells, maintenance and problems in the facilities, or maybe even changes in production in other fields (if quotas have to be met).

2.2 Work done on optimization of the production process with smart wells

A lot of work has been done on improving the production process in the last decades, both on the macro-scale (reservoir-scale) and the micro-scale (pore-scale). Improving the macro-scale displacement efficiency is mainly associated with getting a more uniform displacement of oil by the injected fluid throughout the reservoir, whereas improvements on the micro-scale are related to improving the flow of oil relative to that of the injected fluid. Giving a brief overview of all this work is beyond the scope of this thesis. Therefore the overview is restricted to optimization studies with smart wells.

Until recently most focus in the industry has been on the hardware aspects of a smart well. Development of operation strategies has stayed behind [Gai (2001)]. Down-hole valves were initially developed to be able to cut back unwanted water production, quickly and without intervention costs. Apart from this remedial, reactive application there may also be considerable scope to use smart well technology in a more proactive way. An overview of work done on both reactive and proactive optimization of reservoir flow with smart wells is given in the next sections.

2.2.1 Reactive control

The potential benefits of a smart well result from its flexibility to adapt to unexpected geological features or production conditions. Reactive control is one of the first types of smart well control investigated in the literature. It generally comprises an action on the down-hole valves upon water or gas breakthrough.

Yu *et al.* (2000) studied various types of smart completions in a simple reservoir with an oil rim bounded by a gas cap and an aquifer. Through reactive control smart wells were able to partly compensate for underestimated aquifer behavior and unexpected geological features. For a conventional completion the ultimate recovery was more sensitive to aquifer behavior and geological features than for a smart completion. For the cases investigated the improvements obtained with smart completions were attributed to a more efficient use of gas cap and aquifer energy. An on/off mode of operating the valve settings generally gave highest improvements.

Several authors studied the scope for using smart completions to counteract localized gas/water coning towards the heel of the well, caused by frictional pressure losses along the wellbore [Yeten and Jalali (2001), Sinha *et al.* (2001), Jansen *et al.* (2002)]. They primarily investigated homogeneous, thin oil rim reservoirs. The approaches in these studies generally comprised a proactive control (discussed further on page 14) during the period before water or gas breakthrough, that resulted in a more uniform inflow into the well. In the period after breakthrough a reactive control approach was used to control water or gas production, in which the down-hole valves were often operated in a cyclic way. Upon gas or water breakthrough they were closed and only reopened after some time in order to let the

cone somewhat recede. Hysteresis effects, however, were generally not considered, something that is expected to negatively affect the improvement [Jansen *et al.* (2002)]. In practice, these cyclic operating scenarios would require a coupled monitoring and control approach. For many synthetic examples the approach resulted in a significant delay of gas and water breakthrough, with the performance sometimes being close to that of the ideal, frictionless well (infinite conductivity well) [Sinha *et al.* (2001), Jansen *et al.* (2002)]. The prerequisite, however, is that the increased lift requirements for the instrumented wells do not result in lift problems. The robustness to improve the process for different geological features and fluid properties varied with the type of well instrumentation and the operational strategy.

Jansen *et al.* (2002) found that for the Smart Stinger Completion (SSC) in thin oil rims, the optimum valve-settings changed over time, due to a drop in reservoir pressure caused by production. The SSC was both effective in delaying water and gas breakthrough and in coning control for the post water breakthrough stage. For optimal design of the SSC a reasonable knowledge on the permeability distribution along the well is required.

In the Oseberg field most horizontal wells, producing from the remaining 20-40 [m] thick thin oil rim, experienced gas breakthrough near the heel of the well. Smart wells were deployed in order to be able to choke zones experiencing rapid gas breakthrough. Because the field production rate was limited by gas handling capacity, a reduction in gas production from the wells would immediately lead to increased oil production rates. Analysis of the first 9 months of production of one well showed the benefits of down-hole control valves. Apart from choking valves upon gas and water breakthrough they were also used for in-situ gas lift. The controlled commingled production resulted in an estimated acceleration of production by a factor of about three with respect to a sequential scenario. Comparison of uncontrolled and controlled commingled production also clearly showed the added value of reactive control [Erlandsen (2000), van Delden *et al.* (2001)].

2.2.2 Proactive Control

Proactive control scenarios are well operating strategies that do not start at the moment of gas or water breakthrough but in an earlier stage in order to prevent or delay it as much as possible. Typically, these scenarios typically require a greater knowledge of the reservoir than reactive control scenarios. Within proactive control strategies two main types can be distinguished, each requiring different knowledge on the reservoir properties. In the first kind of strategy, optimization of the valve-settings is done based only on well performance at the current time or forecasted well performance for a short period [Saputelli *et al.* (2003b)]. This approach requires relatively little information, mainly because the length of the optimization window is short. This kind of optimization algorithms will be referred to as *short-term* or *production* optimization algorithms. In the second type of optimization algorithm, the entire remaining production life span (remaining production window) is considered in the optimization. In this approach a reservoir model is needed to calculate the production forecast. In the remainder of this section this type of algorithms are referred to as *long-term* or *recovery* optimization algorithms.

Production optimization algorithms

Production optimization algorithms primarily use well information for instantaneous optimization of production. In a large number of reservoir settings a more uniform flow into the well results in delayed water or gas breakthrough and an improved macro-scale oil sweep. Valvatne *et al.* (2001) developed a semi-analytical solution to calculate the down-hole valve-settings needed to get a more uniform inflow into wells situated in highly heterogeneous reservoirs. For a smart well completed in multiple reservoirs with different pressure regimes they showed that apart from realizing a more uniform inflow, cross-flow between reservoirs could be avoided by proper choking. Yeten and Jalali (2001), Sinha *et al.* (2001) and Jansen *et al.* (2002) also used algorithms that gave a more uniform inflow into smart wells in the period before water or gas breakthrough. They investigated situations where a conventional well would suffer from preferential coning towards the heel due to frictional pressure losses along the wellbore.

Although the algorithms worked well for the relatively simple examples investigated, they may give suboptimal results for other, more realistic (thin oil rim) reservoirs. Finding production optimization algorithms that can effectively optimize for any kind of reservoir and any kind of operating conditions still requires significant effort. Furthermore, because the optimization window is short it is unknown how optimization of production will affect the long-term overall system performance, since short-term production and long-term recovery optimization may not be compatible [Yeten *et al.* (2002), Saputelli *et al.* (2003a)].

Recovery optimization algorithms

Brouwer *et al.* (2001) studied water flood optimization under rate-control for simple horizontal, two-dimensional systems with fully penetrating smart wells, each having 19 segments. Based on the productivity index for each segment the flow rates were redistributed in order to improve the cumulative oil recovery at the final simulation time. Various redistribution algorithms were explored. The algorithms resulted in flow profiles that do not change over time. Improvements in recovery over the base case were between 0-20% with a 7-168% delay in water breakthrough. Results from this study suggested that larger improvements would be possible by using more advanced, dynamic flow control algorithms.

There is little published literature on dynamic waterflood optimization. Roughly two methods can be distinguished in this respect, the *defensive control method*, developed by Yeten *et al.* (2002), and the *optimal control method* used by other authors [Asheim (1988), Virnovsky (1991), Virnovsky (1992), Zakirov *et al.* (1996), Sudaryanto and Yortsos (2001), Dolle *et al.* (2002)]. Recently, Yang *et al.* (2003) studied global optimization of displacement efficiency in hydrocarbon reservoirs at field scale. For the optimization they used a parallel genetic algorithm, in combination with a gradient-based algorithm to speed up the computational process. In the field case described, an increase in total oil rate of a few percent was established.

Optimal Control

A general literature review on applications of optimal control theory in the petroleum industry is postponed to section 4.2. A literature review of the application of optimal control theory to water flood optimization starts on page 33 of that section.

Defensive Control

This method was developed by Yeten *et al.* [Yeten *et al.* (2002), Yeten (2003)]. Although named differently it is a proactive control approach. The method uses a conjugate gradient based optimization technique in combination with a commercial reservoir simulator (ECLIPSE). The first step of the optimization consists of splitting the total simulation time up into a number of intervals (typically 3-10). Subsequently, the continuously variable valves are optimized for the first time interval. To this end each valve α is perturbed by $\Delta\alpha$ for the entire remaining simulation period in a separate simulation, and the change in the objective function ΔJ with respect to the nonperturbed case is evaluated. The valves are perturbed for the entire remaining simulation period to ensure that the settings determined for the early steps do not have detrimental effects at later times. Based on the gradients $\frac{\Delta J}{\Delta \alpha}$ the valve settings are optimized for the entire remaining simulation period with the conjugate gradient algorithm. After optimizing the first interval the simulation is restarted at the next optimization interval and the procedure is repeated until all intervals are optimized. The overall optimization may thus be considered as *n* independent optimization problems, were *n* equals the number of time intervals.

The advantage of the method is that it is straightforward to implement in an existing simulator, and that it can be used for complex reservoirs and complex well types. A drawback is that the method is computationally expensive if the number of controls to be optimized (equal to the product of the number of valves and the number of optimization intervals) is large. (For cases that were investigated with about 5 valves and 5 optimization periods $O\left(100\right)$ simulations were required, although the exact number was quite case-specific.)

The defensive control algorithm of Yeten *et al.* and the optimal control algorithm used by Brouwer and Jansen (2002) were compared on a two-phase, two-dimensional example [Yeten (2003)]. Despite the fact that the number of segments, the number of optimization steps, and the optimal control policies differed significantly the end results obtained in terms of cumulative oil and water production were similar.

Chapter 3
The reservoir model

3.1 Introduction

In the reservoir hydrocarbons and water often flow simultaneously. The hydrocarbons comprise many different components, that could in theory be considered separately. From a computational point of view this is however not desirable. On top of this, in practice bulk oil and gas production is considered rather than the production of each individual component. A simplified approach to model multi-phase reservoir flow is to consider at most three distinct pseudo-components. The bulk hydrocarbons are split up in a heavy, nonvolatile hydrocarbon pseudo-component, and a light volatile hydrocarbon pseudo-component. The light hydrocarbon component is assumed (partly) soluble in the heavy hydrocarbon phase, the solubility being a function of pressure and bulk hydrocarbon composition. The heavy hydrocarbon component is assumed to be insoluble in the light hydrocarbon component. The third distinct component that is considered is water. Mutual solubility of heavy hydrocarbon-water and light hydrocarbon-water is assumed zero. This simplified approach is called a black oil model.

The multi-phase flow formulation in this study is based on this black oil approach. It is discussed in section 3.2. Theory and equations behind reservoir simulation are well documented in a number of standard works on reservoir simulation [Peaceman (1977), Aziz and Settari (1986), Ertekin *et al.* (2001)]. Normally it would therefore be sufficient to refer to these books. The reason for discussing the equations in this thesis is the fact that the optimal control formulation is directly and entirely based on these equations.[1] Section 3.3 discusses some properties of the dynamic system. In section 3.4 the well model and the control valves are described.

3.2 The black oil formulation

In this study optimization of the water flooding process was investigated both for two-phase (oil and water) flow in the horizontal plane, and three-phase, three-dimensional flow. Two separate reservoir models were used. Since the three-phase, three-dimensional formulation is the most general, it is the one that will be discussed. The black oil formulation described

[1] Another reason for discussing the black oil formulation in some detail is the fact that this study is part of a larger project involving people from many different disciplines.

in the following sections is based on the formulation from Aziz and Settari (1986). The three phases that are distinguished are gas, oil, and water. The three components that are distinguished are the light and the heavy hydrocarbon pseudo-components and the water component.

3.2.1 Mass balance equations

In multi-phase flow the mass balance for each individual component (here considered equal to pseudo-component) per unit rock volume is

$$-\nabla \cdot \dot{\mathbf{m}} + \grave{q} = \frac{\partial m}{\partial t}, \tag{3.1}$$

which states that the difference in mass flowing into and out of a unit volume per unit time, plus the mass added or extracted through an external source per unit time and volume $\grave{q}$ $\left[\frac{kg}{s}\frac{1}{m^3}\right]$ must equal the change in mass per unit time and volume $\frac{\partial(m)}{\partial t}$ $\left[\frac{kg}{s}\frac{1}{m^3}\right]$. $\dot{\mathbf{m}}$ is a vector comprising the mass flow in *x*,*y*,*z*-direction and has unit $\left[\frac{kgm}{s}\frac{1}{m^3}\right]$. For a component c it is equal to the product of its density and the volumetric velocity of the phase l in which it is present, i.e. $\dot{\mathbf{m}}_c{=}\rho_c\mathbf{u}_l$. The total mass m of component c per unit rock volume can be expressed as the product of the component density ρ_c, the rock porosity ϕ, and the phase saturation S_l (The volume fraction of the pore space that is occupied by the phase l in which component c is present.), i.e. $m_c = \rho_c\phi S_l$. Substitution into eq. 3.1 then gives

$$-\nabla \cdot \rho_c\mathbf{u}_l = \frac{\partial}{\partial t}\left(\rho_c\phi S_l\right) - \rho_c\tilde{q}_l, \tag{3.2}$$

where the source term $\tilde{q}_l$ has unit $\left[\frac{1}{s}\right]$, and $\mathbf{u}_l$ $\left[\frac{m}{s}\right]$ is a vector with the phase velocities in *x*,*y*,*z*-direction. The porosity and density are a function of pressure. The component density is generally assumed to be a function of the phase pressure p_l, hence $\rho_c = \rho_c\left(p_l\right)$.

For the heavy hydrocarbon component the mass balance becomes

$$-\nabla \cdot \bar{\rho}_o\mathbf{u}_o = \frac{\partial}{\partial t}\left(\bar{\rho}_o\phi S_o\right) - \bar{\rho}_o\tilde{q}_o, \tag{3.3}$$

where $\bar{\rho}_o$ is the density of the heavy hydrocarbon component in the oil phase. For the water component the material balance is

$$-\nabla \cdot \rho_w\mathbf{u}_w = \frac{\partial}{\partial t}\left(\rho_w\phi S_w\right) - \rho_w\tilde{q}_w. \tag{3.4}$$

For the light hydrocarbon component the situation is slightly different since it is present both in the gas phase and in solution in the oil phase. The total mass equals the sum of the masses in the individual phases, i.e.

$$\dot{\mathbf{m}}_g = \bar{\rho}_{dg}\mathbf{u}_o + \rho_g\mathbf{u}_g, \tag{3.5}$$

$$m_g = \bar{\rho}_{dg}\phi S_o + \rho_g\phi S_g, \tag{3.6}$$

where $\bar{\rho}_{dg}$ is the density of the light hydrocarbon component dissolved in the oil phase. The mass balance then is

$$-\nabla \cdot \left(\bar{\rho}_{dg}\mathbf{u}_o + \rho_g \mathbf{u}_g\right) = \frac{\partial}{\partial t}\left(\bar{\rho}_{dg}\phi S_o + \rho_g \phi S_g\right) - \bar{\rho}_{dg}\tilde{q}_o - \rho_g \tilde{q}_{fg}. \tag{3.7}$$

The source terms $\bar{\rho}_{dg}\tilde{q}_o$ and $\rho_g \tilde{q}_{fg}$ represent respectively dissolved and free gas injection or production.

3.2.2 Constitutive equations - Darcy's Law

The fluid phase velocity $\mathbf{u}$ in permeable media is generally described through Darcy's law. For phase l it reads

$$\mathbf{u}_l = -\frac{k k_{rl}}{\mu_l}\nabla \Phi_l, \tag{3.8}$$

where $\nabla \Phi_l \left[\frac{Pa}{m}\right]$is the potential gradient, $k \left[m^2\right]$ the absolute permeability, $\mu \left[Pa\ s\right]$ the phase viscosity. The relative permeability k_{rl} represents a reduction in the permeability for phase l due to interference with others phases. The potential gradient can be expressed as

$$\nabla \Phi_l = \nabla p_l - \rho_l g \nabla h, \tag{3.9}$$

where p_l is the phase pressure, g is the gravitational acceleration $\left(g = 9.81\ \frac{m}{s^2}\right)$, and h is the depth. The density and viscosity are a function of both pressure and temperature. Constant temperature is assumed in the black model and the density and viscosity are assumed to be only a function of pressure, i.e. $\rho_l = \rho_l\left(p_l\right)$, and $\mu_l = \mu_l\left(p_l\right)$. The relative permeability is assumed to be only a function of saturation. In three-phase flow with a water-wet rock the relative permeability for the oil phase is typically taken to be a function of both the water (S_w) and the gas saturation (S_g), i.e. $k_{ro} = k_{ro}\left(S_w, S_g\right)$. The relative permeability for the water and gas phases is generally assumed to be a function of only their own phase saturation, i.e. $k_{rw} = k_{rw}\left(S_w\right)$ and $k_{rg} = k_{rg}\left(S_g\right)$ (A more detailed explanation is given in appendix A).

3.2.3 Formulation in terms of p_o, S_w, and S_g

Substituting Darcy's law into eqs. 3.3, 3.4, 3.7, and dividing by the component density at standard conditions, gives after some intermediate steps (described in appendix A) respectively

$$\nabla \cdot \left(\lambda_o\left(\nabla p_o - \rho_o g \nabla h\right)\right) = \frac{\partial}{\partial t}\left(\frac{1}{B_o}\phi S_o\right) - \frac{1}{B_o}\tilde{q}_o, \tag{3.10}$$

$$\nabla \cdot \left(\lambda_w\left(\nabla p_w - \rho_w g \nabla h\right)\right) = \frac{\partial}{\partial t}\left(\frac{1}{B_w}\phi S_w\right) - \frac{1}{B_w}\tilde{q}_w, \tag{3.11}$$

and

$$\begin{aligned} & \nabla \cdot \left(R_s \lambda_o \left(\nabla p_o - \rho_o g \nabla h \right) + \lambda_g \left(\nabla p_g - \rho_g g \nabla h \right) \right) \\ = \quad & \frac{\partial}{\partial t} \left(\frac{R_s}{B_o} \phi S_o + \frac{1}{B_g} \phi S_g \right) - \frac{1}{B_o} R_s \tilde{q}_o - \frac{1}{B_g} \tilde{q}_{fg}. \end{aligned} \tag{3.12}$$

In these equations λ_l is the mobility of phase l, defined as $\lambda_l = \frac{k_{rl}}{B_l \mu_l} k$. B_l $[-]$ is the formation volume factor for component l, describing the relation between the component volume at reservoir conditions and at surface conditions. The term R_s $[-]$ in eq. 3.12 is the solution gas oil ratio, describing the amount of light hydrocarbons dissolved in the heavy hydrocarbons. In this study B_l and R_s are assumed to be only a function of pressure. For saturated oil, R_s increases with pressure. The bubble point pressure (p_{bp}) is the pressure at which all light hydrocarbons are just dissolved in the oil phase. It depends on the bulk hydrocarbon composition in the reservoir. Above this pressure the oil is undersaturated, and R_s is therefore constant.

With 6 unknowns (p_o, p_w, p_g, S_o, S_w, and S_g), 6 equations are required to complete the system description. Apart from eqs. 3.10, 3.11 & 3.12 these comprise 3 additional equations. The first is a closure equation requiring that the sum of all fractional saturations must always be equal to one, i.e.

$$S_o + S_w + S_g = 1. \tag{3.13}$$

Furthermore, the relation between the individual phase pressures is given by the capillary pressure equations

$$p_{cow} = p_o - p_w = f_{cow} \left(S_w, S_g \right), \tag{3.14}$$

$$p_{cgo} = p_g - p_o = f_{cgo} \left(S_w, S_g \right), \tag{3.15}$$

where water is assumed to be the wetting phase, oil the intermediate wetting phase, and gas the nonwetting phase. Functions f_{cow} and f_{cgo} are generally empirical relations, derived from core experiments.

In eqs. 3.10, 3.11, 3.12 the primary variables are respectively p_o, p_w, and p_g. Generally a formulation with primary variables being the oil pressure p_o, the fractional water saturation S_w and the fractional gas saturation S_g is used in reservoir simulation. This formulation can be obtained by using eqs. 3.13, 3.14 & 3.15. Substitution of these equations into eqs. 3.10, 3.11, 3.12 then gives, after some intermediate steps (described in appendix A.1.5)

$$\nabla \cdot \left(\lambda_o \nabla p_o - \lambda_o \rho_o g \nabla h \right) = \frac{\partial}{\partial t} \left(\frac{1}{B_o} \phi \left(1 - S_w - S_g \right) \right) - \frac{1}{B_o} \tilde{q}_o, \tag{3.16}$$

$$\nabla \cdot \left(\lambda_w \nabla p_o - \lambda_w \frac{\partial p_{cow}}{\partial S_w} \nabla S_w - \lambda_w \frac{\partial p_{cow}}{\partial S_g} \nabla S_g - \lambda_w \rho_w g \nabla h \right) = \frac{\partial}{\partial t} \left(\frac{1}{B_w} \phi S_w \right) - \frac{1}{B_w} \tilde{q}_w, \tag{3.17}$$

$$\begin{aligned} & \nabla \cdot \left(\left(R_s \lambda_o + \lambda_g \right) \nabla p_o + \lambda_g \frac{\partial p_{cgo}}{\partial S_w} \nabla S_w + \lambda_g \frac{\partial p_{cgo}}{\partial S_g} \nabla S_g - R_s \lambda_o \rho_o g \nabla h - \lambda_g \rho_g g \nabla h \right) \\ = \quad & \frac{\partial}{\partial t} \left(\frac{R_s}{B_o} \phi \left(1 - S_w - S_g \right) + \frac{1}{B_g} \phi S_g \right) - \frac{1}{B_o} R_s \tilde{q}_o - \frac{1}{B_g} \tilde{q}_{fg}. \end{aligned} \tag{3.18}$$

3.2.4 Discrete formulation

Since the equations can generally not be solved analytically, they must be evaluated numerically. To this purpose the equations are discretized in space and in time. This is described in detail in section A.2. After discretization in space the result in matrix form is

$$\mathbf{B}\dot{\hat{\mathbf{p}}} = \hat{\mathbf{T}}\hat{\mathbf{p}} - \mathbf{T_4 h} + \hat{\mathbf{q}}, \tag{3.19}$$

where $\hat{\mathbf{p}}$ is the state vector containing the oil pressures (p_o) and the water and gas saturations (S_w and S_g) in all grid blocks, matrix $\hat{\mathbf{T}}$ contains the transmissibility terms, and matrix $\mathbf{B}$ contains storage terms. The product $\mathbf{T_4 h}$ is a vector containing the gravity terms, and $\hat{\mathbf{q}}$ a vector comprising the injection and production terms. In this formulation q has positive sign if fluid is injected, and negative sign if fluids are produced. A more detailed description of the individual terms in these vectors and matrices is given in sections A.2.1 - A.2.3.

For discretization in time the choice was made to calculate all states $\hat{\mathbf{p}}$ implicitly (at time step $n+1$), and the state dependent coefficients explicitly (at time step n). The main reason for this choice is that it is easier to implement than a fully implicit scheme. Eq. 3.19 then becomes

$$\mathbf{B}^n \left(\frac{\hat{\mathbf{p}}^{n+1}}{\Delta t^n} - \frac{\hat{\mathbf{p}}^n}{\Delta t^n} \right) = \hat{\mathbf{T}}^n \hat{\mathbf{p}}^{n+1} - \mathbf{T}_4^n \mathbf{h} + \hat{\mathbf{q}}^n. \tag{3.20}$$

If injection and production rates are assigned directly without using a well model, the fluid mobilities are calculated explicitly. This is also the case if a well model is used, but in this case the grid block pressure used in the well model is calculated implicitly, i.e.

$$\hat{\mathbf{q}}^n = -\hat{\mathbf{W}}^n \hat{\mathbf{p}}^{n+1} + \hat{\mathbf{W}}^n \hat{\mathbf{p}}_{wf}^n + \hat{\mathbf{w}}_{pc}^n, \tag{3.21}$$

where $\hat{\mathbf{p}}^{n+1}$ contains the grid block pressures and $\hat{\mathbf{p}}_{wf}^n$ the well flowing pressures at locations where a well is present, and zeros otherwise. The terms $\hat{\mathbf{W}}^n$ and $\hat{\mathbf{w}}_{pc}^n$ in eq. 3.21 contain well geometric factors and fluid mobilities. They are discussed in more detail appendix B. Substitution of eq. 3.21 into eq. 3.20 gives, after some rearranging

$$\hat{\mathbf{p}}^{n+1} = \left[\mathbf{I}\frac{1}{\Delta t^n} - (\mathbf{B}^n)^{-1} \hat{\mathbf{T}}^n + (\mathbf{B}^n)^{-1} \hat{\mathbf{W}}^n \right]^{-1} \left[\begin{array}{c} (\mathbf{B}^n)^{-1} \left(-\mathbf{T}_4^n \mathbf{h} + \hat{\mathbf{W}}^n \hat{\mathbf{p}}_{wf}^n + \hat{\mathbf{w}}_{pc}^n \right) \\ + \mathbf{I}\frac{\hat{\mathbf{p}}^n}{\Delta t^n} \end{array} \right], \tag{3.22}$$

which can also be written as

$$\begin{aligned} \mathbf{g}^n &= \mathbf{0} \qquad (3.23) \\ &= \left[-\mathbf{I}\frac{1}{\Delta t^n} + (\mathbf{B}^n)^{-1} \hat{\mathbf{T}}^n - (\mathbf{B}^n)^{-1} \hat{\mathbf{W}}^n \right] \hat{\mathbf{p}}^{n+1} \\ &\quad + (\mathbf{B}^n)^{-1} \left(-\mathbf{T}_4^n \mathbf{h} + \hat{\mathbf{W}}^n \hat{\mathbf{p}}_{wf}^n + \hat{\mathbf{w}}_{pc}^n \right) + \mathbf{I}\frac{\hat{\mathbf{p}}^n}{\Delta t^n}. \end{aligned}$$

Eq. 3.23 is used in the remainder of this thesis. In this formulation the system is unconditionally stable in the implicitly calculated states, but only conditionally stable in the explicitly calculated transmissibility terms. Because of this conditional stability in the transmissibility terms there is an upper limit to the time step size, determined by the Courant-Friedrich-Levy (CFL) condition [Aziz and Settari (1986), Hoffman (1992)].

3.2.5 Spatial weighting of parameters

In the discretized numerical scheme described above, average values for various coefficients are calculated at the grid block interfaces. Since a block centered discretization is used these coefficients are defined in the grid block center, and therefore they have to be converted to effective values at the grid block interface. For the permeability k this is done by taking the weighted harmonic average. With constant grid block size this is equal to

$$k_{1\frac{1}{2}} = \frac{1}{\frac{1}{2k_1} + \frac{1}{2k_2}}. \tag{3.24}$$

Generally the values for the weakly nonlinear pressure dependent coefficients at the grid block boundaries are approximated by taking the weighted arithmetic mean [Ertekin *et al.* (2001)]. With constant grid block size this yields for example for the oil viscosity μ_o

$$\mu_{o,1\frac{1}{2}} = \frac{\mu_{o,1} + \mu_{o,2}}{2}. \tag{3.25}$$

The weighted arithmetic mean was used to calculated average values at the grid block interface for the fluid viscosities μ_l, the formation volume factors B_l, and the solution gas oil ratio R_s. The strongly nonlinear coefficients are the saturation dependent relative permeabilities k_{r_l}, and capillary pressures p_{cow} & p_{cgo}. They were calculated according to the upstream weighting principle, i.e. the interface value is equal to the value in the grid block from where the flow is coming. For example, for the relative permeabilities k_{r_l} this becomes

$$\begin{aligned} k_{rl,1\frac{1}{2}} &= k_{rl,1}, \text{ if } \Phi_1 \geqq \Phi_2, \\ k_{rl,1\frac{1}{2}} &= k_{rl,2}, \text{ if } \Phi_1 < \Phi_2. \end{aligned} \tag{3.26}$$

3.3 Some properties of the dynamic system

In multi-phase flow in the reservoir different dynamic processes are occurring. One is related to the reservoir pressure dynamics. The potential gradient in the reservoir forms the driving force for the transport of fluids, which constitutes a second type of process.

The two types of processes show distinct dynamic behavior. A disturbance in the reservoir pressure at some location induces a pressure transient in the reservoir through which the system goes towards a new dynamic equilibrium pressure distribution. The (steep) pressure gradients induced by the disturbance quickly decay towards this new dynamic equilibrium pressure distribution. Contrary to disturbances in the reservoir pressure, disturbances in the saturation may not decay quickly, since the fluids are immiscible.

The differences in pressure and saturation dynamics are reflected in the eigenvalues of the reservoir simulator system matrix $\mathbf{A}$. In the discrete dynamic system formulation (eq. 3.22) the system matrix $\mathbf{A}$ equals

$$\mathbf{A} = \left[\mathbf{I} - (\mathbf{B}^n)^{-1}\,\hat{\mathbf{T}}^n \Delta t^n + (\mathbf{B}^n)^{-1}\,\hat{\mathbf{W}}^n \Delta t^n\right]^{-1}. \tag{3.27}$$

In the reservoir model formulation in this study, matrix $\mathbf{A}$ is taken constant during a time step, assuming that the states $\hat{\mathbf{p}}$ do not drastically change per time step. Eigenvalues of $\mathbf{A}$ were calculated for a simple two-dimensional, horizontal reservoir, containing 25 grid blocks. A random permeability field was used, shown in Figure 3.1. Furthermore, zero capillary pressures were used.

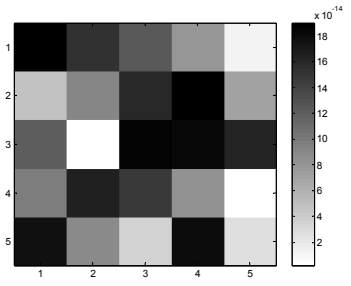

Figure 3.1: Top view of permeability distribution. Values along the axes correspond to the grid block number.

Since there are three unknowns per grid block (p_o, S_w, S_g) $\mathbf{A}$ has dimensions 75×75. Figure 3.2 shows the eigenvalues of $\mathbf{A}$. It shows a distinct distribution in the magnitude of the eigenvalues. Eigenvalues 1-50 all have value of 1 and will be referred to as group I.

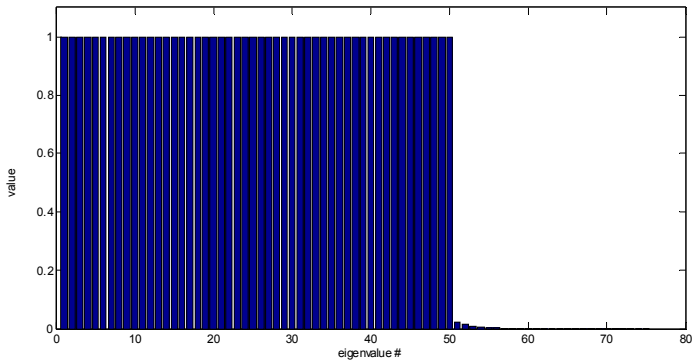

Figure 3.2: Eigenvalues for dynamic system of 25 grid blocks at time step $n = 20$. Eigenvalues are sorted on magnitude

Eigenvalues 51-75, shown in more detail in Figure 3.3, are of much smaller magnitude, and will be referred to as group II.

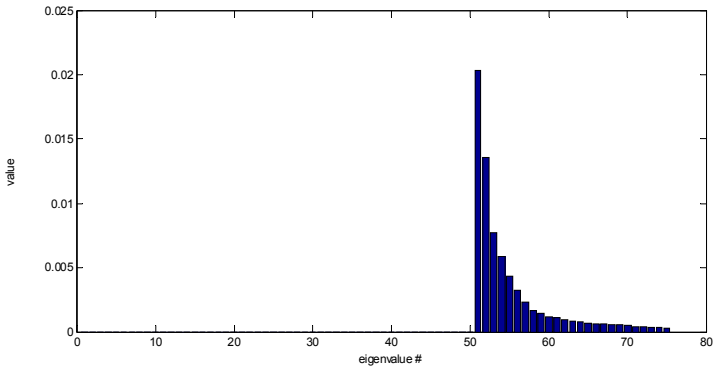

Figure 3.3: Eigenvalues 51-75 at time step $n = 20$. Eigenvalues are sorted on magnitude

The distinct magnitudes for eigenvalues of group I and II suggest they correspond to different types of processes. Group I, containing 50 eigenvalues, correspond to the water and gas saturation states, $\mathbf{S}_w$ and $\mathbf{S}_g$ respectively. The 25 eigenvalues of group II correspond to the oil pressure states $\mathbf{p}_o$. Since $\mathbf{A}$ contains coefficients that are nonlinear functions of the states, it would be more appropriate to do the eigenvalue analysis on the linearized equations. This is, however, outside the scope of this research.

3.4 The well model

3.4.1 General

A general formulation for the well model is

$$q_t = w\left(p_{wf} - p_{gb}\right), \tag{3.28}$$

where parameter w contains well geometric factors and rock and fluid properties of the reservoir directly around the well, p_{wf} is the well flowing pressure, and p_{gb} is the grid block pressure. A more detailed description of the well model is given in appendix B.

Through injection wells generally either only water or gas is injected. The amount of water or gas that is injected can thus be controlled directly and only depends on the total fluid mobility in the reservoir directly around the well and on p_{wf}. In this case the injection rate of the component equals the total injection rate, i.e. $q_{l_{inj}} = q_{t_{inj}}$. In a producer, however, the amounts of oil, water and gas that will be produced are determined by their mobilities directly around the well and by p_{wf}. So, although it is possible to control the total flow rate from the reservoir into the well by changing p_{wf}, the produced fluid composition cannot be controlled directly.

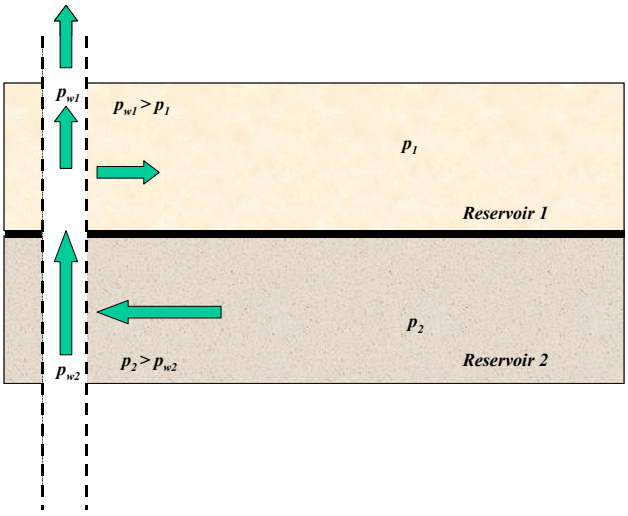

Figure 3.4: Cross-flow in a producer. Fluids produced from reservoir 2 are partly cross-flowing into reservoir 1.

3.4.2 Back- / cross-flow

The driving force for fluid flow into or out of the well is the difference in pressure between the wellbore and the reservoir. In case of a producer the pressure is highest in the reservoir and therefore fluids flow into the well. It may however sometimes occur that locally the pressure in the well is highest, inducing fluid flow from the wellbore into the reservoir. This could for example occur if the well is completed in multiple reservoirs, each having a different pressure regime. The result of this can be that fluids that are produced at some point along the well flow back into the reservoir at some other point, as schematically depicted in Figure 3.4. With smart wells, equipped with down-hole control valves this back-flow can in principle be

remedied by closing the valve. A prerequisite then of course is that the occurrence of it can be detected by the down-hole sensors. The valve could be reopened if the potential difference is again favorable. Because including back- and cross-flow in the optimization may lead to numerous (numerical) difficulties, the well model parameters are for each simulation chosen such that back-flow does not occur.

3.4.3 Control valves

An additional parameter needed in the well model is a down-hole valve to manipulate the flowrate per segment. This effect can be added to eq. 3.28, yielding

$$q_t = a_{icv} w \left(p_{wf} - p_{gb} \right). \tag{3.29}$$

In eq. 3.29 a_{icv} is simply a multiplication factor that has a value between 0 and 1. In this model the well rate can be changed by tuning of the interval control valve a_{icv}, if the well flowing pressure p_{wf} is kept constant. This valve multiplication factor represents a non-physical choke model. This approach is called the modeling of a choke as a pseudodevice [Holmes (2001)]. An additional valve that could in principle be controlled is the choke at the well head α_{wh}. Including its effect in eq. 3.29 yields

$$q_t = a_{wh} a_{icv} w \left(p_{wf} - p_{gb} \right), \tag{3.30}$$

where α_{wh} is again a multiplication factor. The well head choke could be formally included as a separate control in the optimization problem. If a wellbore flow model is used (possibly in the form of lift tables) there may be a difference between choking down-hole or at the surface. Furthermore, if the rates in all segments need to be cut back proportionally it may be preferable to do this by adjusting the well head choke a_{wh}, because an increased pressure drop over the valves may lead to increased wear and a quicker need for replacement, which can be done cheaper and more easily for the well head choke. In this study, however, instead of treating the two types of valves separately only the effective valve multiplication factor $\alpha_{eff} = a_{wh} a_{icv}$ is used as a control parameter. The final form of the well model is therefore

$$q_t = a_{eff} w \left(p_{wf} - p_{gb} \right). \tag{3.31}$$

Chapter 4
Optimal control theory

4.1 Introduction

The methods used for finding optimal control strategies for dynamic systems are similar to those used for static optimization problems, but the implementation is generally more complex. One reason is that instead of a fixed control value a dynamic control trajectory must be calculated. With optimal control theory it is possible to calculate the control strategy which forces the state from its initial value to its final value along a physically feasible trajectory, which at the same time minimizes or maximizes the value of the objective function. The resulting state trajectory is an optimal trajectory [Stengel (1994)]. Translated to the problem investigated in this thesis, the optimal control problem can be read as the problem of finding the injection and production strategy that directs the fluids through the reservoir in a way that gives best displacement efficiency or best economic performance. This optimal trajectory is affected both by the objective function and by the physical constraints of the dynamic system.

An overview of published work on optimal control theory in the petroleum industry is given in section 4.2. In sections 4.3, 4.4 & 4.5 the theory itself is discussed. Sofar, optimal control applications in the oil industry have primarily focused on the gradients obtained with the adjoint equation. Possibly, additional information can be extracted from the magnitudes of the adjoint states, i.e. the Lagrange multipliers, by considering their (physical) meaning. This is briefly treated in section 4.6. Section 4.7 treats the eigenvalues of the adjoint dynamic system matrix. Section 4.8 discusses how results obtained with the adjoint equation can be verified. Apart from constraints related to the dynamic system there are also constraints on the controls that must be taken into account in the optimization. These are discussed in section 4.9. A gradient based optimization algorithm is required to calculate the optimal control function, based on the gradients calculated in the adjoint equation. Section 4.10 gives a brief overview of experiences with various algorithms in optimal control applications in the oil industry. It also discusses the steepest descent algorithm used in this thesis.

4.2 Literature review of optimal control theory in the oil industry

Optimal control theory has been used for decades in various disciplines. Applications to large scale systems occur for instance in the area of meteorology, oceanography, hydrology, and petroleum engineering. In the petroleum industry, optimal control theory has a history going back to the 1970's. Sofar, there have mainly been applications in history matching, in optimization of enhanced oil recovery (EOR) methods, and in water flood optimization. These will be treated in some detail in the literature overview below. The application of optimal control theory to history matching and dynamic process optimization seem to have evolved largely independently. Few papers published on one of these areas have references to work done in the other area. Other applications are in the control of water injection into a layered formation, where optimal control theory was used to calculate the injection pressure that keeps injection at the prescribed rate in the presence of hydrofracture growth [Silin and Patzek (2000), Silin and Patzek (2001)]. Furthermore, it was used in aquifer [Zakirov and Zakirov (1999)], and reservoir geometry estimation [Palatnik and Aanonsen (1994)].

4.2.1 History matching

Single-phase flow

Chavent *et al.* (1973) studied history matching in single phase oil reservoirs. The objective was to minimize the difference between observed and actual pressures at the wells with the permeability-thickness product kh $[mD\ ft]$ and porosity-thickness product ϕh $[ft]$ as adjustable parameters. Although the intergridblock transmissivities found by the history matching procedure matched reasonably, within the grid blocks they locally deviated significantly from the actual values, and were not unique. They also found a local imprint of the initial guess on the final results. A steepest-descent algorithm was used to find the optimum.

Dougherty and Khairkhah (1975) used optimal control theory for history matching a gas reservoir. As in Chavent *et al.* (1973) the objective was also to minimize the difference between actual and observed pressure at the wells, by adjusting kh and ϕh. The optimum values kh and ϕh found were not unique, and different initial guesses for these parameters resulted in different final values found. Furthermore, the starting profile for the parameter combination ϕh appeared to be preserved in the optimum profile. The calculated pore volumes were in good agreement with the actual pore volume. Just like Chavent *et al.* (1973), it was found that although the average kh value was often in good agreement with the average value for the actual case, they locally often differed significantly from the actual value. Hard bounds on the allowed range for this parameter combination were required to keep the spread from being even larger. A rapid decrease in objective function value was found for early iterations, followed by a small or marginal decrease for subsequent iterations. In some case,

however, instead of becoming smaller, the objective function value actually became larger, when the control parameters were changed too much in one iteration.

Fasanino *et al.* (1986) studied single-phase history matching of 2D gas reservoirs using the adjoint method in combination with geostatistical information and the pilot point technique. The extra information was included in order to prevent non-plausible solutions in the permeability and porosity distributions from being found. Reportedly, they obtained reliable estimates for the transmissibility and porosity thickness product distributions.

Bi *et al.* (2000) studied the conditioning of three-dimensional stochastic channels to pressure data in single-phase reservoirs. At early iterations the change in model parameters often needed to be dampened to avoid slow convergence or convergence to unacceptable local optima, especially if the mismatch between observed and estimated model parameters was large. A Levenberg-Marquardt algorithm was used to provide this damping. The algorithm typically required in the order of 5 iterations to obtain convergence.

Zakirov *et al.* (1998) used optimal control theory for history matching a dual porosity gas reservoir. The paper does not address any details of the method.

Multi-phase flow

Wasserman *et al.* (1974) were among the first to use optimal control theory in history-matching multi-phase simulator models. However, instead of using a multi-phase optimal control formulation, they used an adjoint equation only for the pressure equation. The motivation for this simplified approach was that they were only history matching the pressures at the wells. They were also among the first to derive the optimal control algorithm using a spatially discretized formulation. Similarly to previous studies they found non-smooth solutions for the porosity-thickness distribution that locally deviated significantly from the actual values. They concluded that smoothing of the reservoir properties of the history-matched model in accordance with known geology was needed in order to avoid physically unrealistic solutions from being found. They empirically smoothed the distributions, which still gave a good history match despite increased standard deviations in many grid blocks. The irregularities found in the porosity-thickness distributions were attributed to the existence of many local minima.

Watson *et al.* (1979) studied history matching in two-phase petroleum reservoirs. Displacement in the reservoir model was unfavorable with a viscosity ratio $\frac{\mu_o}{\mu_w} = 5$. The porosity and absolute permeability distributions found locally deviated from the actual values, although the average values found matched reasonably well with the actual averages. They also history-matched the relative permeability coefficients for a one-dimensional case. (This may be because they used one relative permeability model for all the grid blocks, and thus only one *average* value had to be found.) Increased convergence rates were observed when the end-points of the relative permeability curves were specified. They also simultaneously history-matched porosity, absolute and relative permeability for a one-dimensional and a two-dimensional reservoir where absolute and relative permeability, and porosity where represented by a single zone. In the two-dimensional reservoir they also corrupted the observed

data with Gaussian distributed noise, but found no effect on the performance of the algorithm.

Chavent and Cohen (1980) used optimal control theory to estimate relative permeability curves and the capillary pressure function from drainage and imbibition experiments. Fluids were considered incompressible. The optimal control technique was applied to the discretized equations in order to get an exact calculation of the gradients. A discontinuous finite element approach was used to reduce the effects of numerical diffusion. To overcome problems associated with ill conditioning, the physical unknowns (relative permeabilities and capillary pressures) were replaced by functions that appeared as coefficients in the model equations. For each function one value was estimated.

Yang and Watson (1987) used optimal control theory in history matching simple two-phase reservoirs. In a one-dimensional example with homogeneous rock properties they simultaneously estimated absolute and relative permeabilities, and porosities. Constraints on the relative permeability functions were required to avoid physically unrealistic, non-monotonic curves from being found. Adding constraints also improved the efficiency of the method since it prevented the algorithm from searching ranges of parameter values that are not physically realistic. They also compared various gradient optimization methods. These will be briefly discussed in section 4.10.

Wu *et al.* (1999) studied the conditioning of geostatistical models to two-phase production data. The system investigated was a two-phase, two-dimensional, isotropic reservoir. Gravity and capillary effects, as well as rock compressibility were neglected. They derived a discrete adjoint method to calculate the sensitivities of wellbore pressure and water-oil ratio to reservoir simulator grid blocks permeabilities and porosities. This was applied to the problem of estimating the most probable reservoir model consistent with measurements of the water-oil ratio and the pressure data and to the problem of generating realizations that are conditioned to the production data. A different formulation was used for the forward simulator (standard finite-difference IMPES) as for the adjoint simulator (fully implicit). They found a good agreement between sensitivities obtained with numerical perturbation and with the adjoint method.

Wu (2000) used optimal control theory for integrating production data into reservoir models with a Newton-Raphson iterative scheme. The objective was to minimize the production mismatch while honoring the geostatistical data. (Reportedly the adjoint formulation differed from that used in previous studies [Wu *et al.* (1999)].) He expressed concerns about uniqueness and existence of the solution in the scheme. If the initial values were not sufficiently close to the true model, the solution could sometimes not be obtained (without regularization terms).

Li *et al.* (2001) studied history matching of three-dimensional, three-phase flow production data. The objective was to minimize the mismatch in flowing wellbore pressure, producing gas oil ratio (GOR) and water oil ratio (WOR). They found that conditioning to all production data (pressure, WOR, and GOR) gave a greater reduction in the uncertainty of the reservoir properties than obtained by only conditioning to pressure, only pressure and GOR or only pressure and WOR. Similar to Wu *et al.* (1999) they used the adjoint method to generate the

sensitivity coefficients. They found a good agreement between sensitivities obtained with numerical perturbation and with the adjoint method.

Wu and Datta-Gupta (2001) used optimal control theory to obtain sensitivity coefficients of the travel time with respect the permeability and porosity field for history matching purposes. They included a priori information in the history matching problem to avoid problems associated with solving an underdetermined problem. They applied it to history matching a reservoir model with 27 producers and 15 injectors thereby indicating the viability of the method for large-scale field applications. They found a good match in the water-cut production response, and a reasonably good match for the permeability field.

4.2.2 Production process optimization

First published work on the application of optimal control theory to production process optimization dates from the early eighties. Some of these studies addressed optimization of the production process at the micro-scale, others primarily focused on macro-scale optimization.

On the micro-scale the production process efficiency can be manipulated by for example manipulating the interfacial tension between fluids and/or the viscosity and/or relative permeability of fluids. The purpose is to improve the flow of oil with respect to the flow of gas and/or water, and to reduce the residual oil saturation. In general these kind of processes are addressed in tertiary, enhanced oil recovery projects. Optimization at the macro-scale involves maximizing the areal and vertical sweep of oil and/or gas in the reservoir.

Micro-scale optimization

The earliest applications of optimal control theory to production optimization were studied by Ramirez and his co-workers. They primarily investigated optimization of enhanced oil recovery (EOR) processes on the micro-scale. Various EOR processes were studied, like surfactant , polymer, and caustic flooding. The controls they optimized were the concentrations of the injected fluids, the total injection rates and the producer bottom hole pressure. In early work they used a partial differential formulation of the optimal control problem [Ramirez *et al.* (1984)], in later work they used a discrete formulation [Mehos (1986), Fathi and Ramirez (1987), Liu *et al.* (1990)].

Fathi and Ramirez (1984) applied optimal control theory to find the optimum injection policy of a surfactant slug for a one-dimensional chemical flood. The objective function was to maximize the oil recovery while minimizing the costs for the chemicals. Fluids were considered incompressible. In addition to the convective and dispersive mechanisms of mass transfer their model allowed for the irreversible adsorption of surfactant onto the solid matrix and surfactant partitioning between the fluid phases. They considered two different interfacial tension functions. The oil-phase viscosity was assumed constant and the water-phase viscosity was postulated to be an exponential function of the surfactant concentration. The irreducible water and residual oil saturations were taken to be a function of the capillary number. The uniqueness of the solution depended on the type of interfacial tension func-

tion used. Whereas the shape of the optimal injection function was not unique for every interfacial tension function, the amount of surfactant needed appeared to be unique. They also reported the difficulty of solving the adjoint partial differential equations backwards in time. The difficulty arose from the existence of discontinuities in the coefficients, resulting from two saturation shocks that form during a low tension flood (the first being the Buckley-Leverett shock at the oil-water front, the second being at the surfactant front where the surfactant slug contacts the connate water). Because of the difficulties associated with solving this adjoint system with discontinuities, they developed a similar but simpler quasi-linear adjoint formulation. In later work they studied surfactant flooding optimization using a streamtube reservoir simulator [Porzucek (1988)].

Fathi and Ramirez (1987) applied optimal control theory to optimize micellar/polymer flooding. They used a compositional model with 7 components, and investigated both the continuous and the discrete formulation. As an optimizer they used both a steepest descent and a conjugate gradient algorithm that was modified and extended to include bounds on the controls. The advantage of the conjugate gradient method was rapid convergence near the optimum, the drawback was that a good initial starting condition was needed for solution stability. Although generally less efficient the steepest descent algorithm always worked satisfactorily. In general, the convergence performance depended on the initial control strategies. Regularization was applied to increase the convergence rate. Although the optimal injection policies varied with the initial guess for the control parameters, the optimum performance was in some cases very similar. They also reported that the mathematical complexity of the equations describing immiscible flow had proven to be a serious obstacle for the application of optimal control theory. They also addressed the issue of numerical dispersion. If the numerical dispersion represented the physical dispersion, it could be used to replace the physical dispersion and simplify the calculations. This should also help in cancelling some computational difficulties they had in previous studies [Fathi and Ramirez (1984), Fathi (1986)].

Mehos (1986) and Mehos and Ramirez (1989) studied the optimization of the carbon dioxide miscible flooding process using optimal control theory. They considered slug, simultaneous injection, and WAG policies. For pragmatic reasons, they used a three-component, two-phase, two-dimensional, modified black oil model to describe the miscible displacement of oil by carbon dioxide. No free gas was assumed to exist, and gravity and capillary effects were ignored. The reservoir was taken to be homogeneous. Injection rates of CO_2 and water and the producer bottom hole pressures were taken as control parameters. In the optimal policies they often found a clear imprint of the starting policy. Although the optimum injection policy was found to be not unique the total volume injected was. Furthermore, all three optimum control policies gave approximately the same cumulative oil recovery, and the same value for the objective function. In the optimal control policy the production well was initially shut in. This was in agreement with results from other authors who suggested to shut in the production wells at the beginning in order to reduce the CO_2 mobility and increase the efficiency of the displacement.

Liu *et al.* (1990) studied the problem of steam flood optimization with optimal control theory using a discrete optimal control formulation. The objective was to maximize oil recovery

while minimizing the steam injection costs. The control parameters for optimization were the injection rate of steam and water, the steam quality, and the bottom-hole pressure in the production well. Upper and lower bounds on the controls were considered in some examples. The examples considered were simple two-dimensional models consisting of 28 grid blocks. Improvements obtained with respect to the base case were significant. Reportedly, they were due to higher injection and production rates, and a better sweep due to reduced oil viscosity. Trends found in the optimal control policies were considered to be important principles behind an optimal steam flood. They also studied the sensitivity of the individual controls, and found injection rate and bottom hole pressure to be the most sensitive. The scope for optimization was found to decrease for more restrictive constraints on the controls. They also found that the optimal profitability increased with decreased $\frac{k_v}{k_h}$ ratio, which was attributed to reduced steam override. Different optimal control functions were found for different initial control policies. Regularization of the calculated optimal control policies did not significantly affect the end-results. They too reported that finding a stable adjoint solution in itself could be a major mathematical problem. Especially for complicated EOR problems this was reported to be an important consideration. In later work Liu and Ramirez (1994b) investigated three-dimensional steamflood optimization for reservoir models that were matched to data from some real steamflooding projects. Improvements between 12-20% were realized. The time step size Δt in the forward simulation was automatically regulated by limits on the maximum changes in the states allowed. The time step size of the adjoint equation was regularized to a small constant value because the variation in the distributed states might not correspond to the variation of the distributed adjoint states. A quadratic interpolation was used in calculating the adjoint coefficients for unmatched time points. The non-smooth shapes of the optimal control policies were attributed to the time step size used. A further reduction in the time step size should smooth the resulting policies.

Macro-scale sweep optimization

Asheim (1986) and Asheim (1988) studied optimization of water flooding with two vertical injection wells, and a single vertical production well (artificial water drive). He also studied a scenario with two vertical production wells and a natural aquifer (natural water drive). The objective was to maximize the net present value (NPV) of the water flood. As a reference case he used rate-allocation in wells based on the permeability-thickness product. Improvements in NPV ranging from 2-11% were found, realized by improved sweep efficiency and delayed water breakthrough. He also found that the performance of an optimized water flood depended less on reservoir heterogeneity than a conventional water flood (the reference case), indicating that negative effects of reservoir heterogeneity could to some extent be compensated for by dynamic flow control. The optimization algorithm used was a commercially available nonlinear search program, based on the Generalized Reduced Gradient Method. Convergence of this optimizer was efficient with the optimal solution being found in only a few iterations.

Birnovskii (1988)[2] and Virnovsky (1991) investigated the optimization of both two-phase and three-phase flow in two-dimensional reservoirs. Gravity effects were not considered. Furthermore, fluids were taken to be incompressible, and mutually insoluble. They optimized both for well location, well type, and water flood efficiency and allowed wells to change from injector to producer and vice versa. To this end they started out with a large number of injection and production wells. In subsequent iterations a number of these wells were removed. (These were probably the wells with the lowest flow rates, although this is not clearly mentioned in the paper.) Distinct stages in the optimized production process were found, corresponding to drainage of the low permeable part of the reservoir, followed by a stage during which the main goal was to get a uniform displacement front. For two-dimensional water flood optimization the optimum distribution of flow rates among the wells was to assign low flow rates to wells in the high permeability areas. Significant improvements of up to 50% in cumulative oil recovery were achieved.

Zakirov *et al.* (1996) studied optimization of allocation of available gas and water handling capacity between individual wells against a common production platform, while including (in)equality constraints on the production in the optimization. They used a fully-implicit, three-dimensional, black oil simulator. The control parameters were the bottom hole pressures in the wells. In the optimum scenario production was such that the gas-oil-ratio (GOR) in both wells was equal at all times. This was interpreted to correspond to an equal gas-front movement through the reservoir. The evolution of the water-oil ratio was not similar in both wells. Improvements of 5-10% were obtained for the two-producer scenarios. An important observation was that maximizing plateau production may not necessarily be optimal with respect to obtaining the best economy over the fields life time. Similar observations were done in other studies [Virnovsky (1991), Yeten *et al.* (2002), Yeten (2003)].

Sudaryanto (1998), Sudaryanto and Yortsos (2000), and Sudaryanto and Yortsos (2001) studied optimization of water flooding at the time of water breakthrough. They considered two-dimensional reservoirs with two vertical injection wells and a single vertical production well. Fluids were taken to be incompressible. A "bang bang" optimal control formulation was used in which wells operate only at the extremes (fully open or closed). The displacement process was optimized by optimizing the switch times for opening or closing the injection wells. As a reference case they used a control scenario in which the injection rates remain constant throughout the displacement process and are chosen such as to get simultaneous breakthrough at the producer. Results obtained from simulations, were compared with experiments conducted with a Hele-Shaw cell[3], giving good agreement.

In most of the examples considered the permeability field was assumed to be known. In some cases however they assumed the permeability distribution to be unknown and simply treated those cases as homogeneous. For virtually all these cases they found improvements with respect to their base case. Only for 2 out of 400 cases they found a slight decrease in

---

[2] The name of the author is not spelled correctly in the article. His real name is G.A. Virnovsky.

[3] A Hele-Shaw cell is sometimes used in experiments to study laminar flow, the flow occurring in between two closely-spaced parallel plates.

performance (order 1%). These slight decreases both occurred for reservoir models where the true permeability field had a random distribution, i.e. the grid block values were uncorrelated.

In most cases they studied the production rate was constant. However, they also studied optimization with constraints on well injection rates. For these cases they found both improvement in displacement efficiency and acceleration of production compared to the constant base case, partly due to the fact the total injection rates in the optimized case were sometimes higher than in the base case. For some initial control policies no switch time could be calculated; in those cases the optimization had to be restarted with a different initial policy.

Dolle *et al.* (2002) studied dynamic water flood optimization with optimal control theory on simple two-dimensional reservoirs. In their approach the Jacobian was calculated numerically. Results were compared to those obtained with a static optimization algorithm [Brouwer *et al.* (2001)], in which optimization was done with time-independent injection and production rates. For most cases results obtained with optimal control theory were found to be an improvement over the static optimization algorithms. In some cases, however, the static optimization algorithm performed better. This was attributed to local optima and to problems with the stability of the adjoint equation.

4.3 Moment of discretization in optimal control problem

In principle the optimization could be approached in two ways. One is to use a continuous optimal control formulation in which the discretization for the dynamic system, the adjoint equations, and the objective function is only done as the last step. This is generally referred to as the *differentiate-then-discretize* approach. The other possibility is to start directly with a discrete optimal control formulation. This is generally referred to as the *discretize-then-differentiate* approach.

Differentiate-then-discretize approach

In this approach discretization is done separately for the objective function, the dynamic system, and the adjoint equation. Upon discretization truncation errors will be introduced since the discrete formulation is generally a low order approximation. These truncation errors may be different for the different components in the optimization problem, and the resulting derivatives may therefore not be exact [Ulbrich (2001)].

Discretize-then-differentiate approach

This approach starts with a discrete formulation of the optimal control problem, and thus with a discrete description of the dynamic system and the objective function. Since the adjoint

is derived from this discrete description it yields the exact gradient of the discrete objective function.

According to several studies [Chavent (1979), Chavent *et al.* (1980), Mehos (1986), Ulbrich (2001)] it is better to apply optimal control theory according to the *discretize-then-differentiate* approach if a discrete, numerical approximation of the dynamic system is to be optimized. In this study we therefore followed this approach. It must be noted, however, that this issue still subject of recent research [Li and Petzold (2003)].

4.4 General theory

Optimal control theory exists both for continuous as well as discrete problems [Luenberger (1979)]. Which formulation should be used is dependent on the problem investigated. In addition, the optimal control formulation itself can also vary with the problem that is studied. In this thesis a fixed terminal time, free terminal state formulation was used. It means that the time interval for which optimization is conducted is fixed. Furthermore, it means that there is no constraint on the final states, i.e. the oil pressures, the water saturations, and the gas saturations. The formulation will be discussed in detail in section 4.4.1.

Alternatively, the optimal control problem could be formulated as a free terminal time problem, as was done by Sudaryanto and Yortsos (2001). In such a formulation the end time is part of the optimization problem. The optimal control problem could also be formulated as a fixed terminal state problem. The problem with this formulation, however, is that the constraints on the final states may not be feasible, i.e. it may not be possible to achieve them by any combination of controls. Especially for a complex system as a reservoir it may be difficult to assess in advance the feasibility of final constraints on the states.

4.4.1 The optimal control problem - Fixed terminal time, free terminal states

Optimal control is a gradient-based optimization technique that allows one to find those values of the input (control) variables $\mathbf{u}$ that minimize or maximize a certain scalar objective function $\mathcal{J}$, subject to the constraints on the states $\mathbf{x}$ imposed by the dynamic system. In this study, an objective function is used that accumulates over time, i.e.

$$\mathcal{J} = \sum_{n=0}^{N-1} \mathcal{J}^n \left(\mathbf{x}^n, \mathbf{u}^n\right), \tag{4.1}$$

where n is the time step, and N is the final time step. Because $\mathcal{J}$ is a function of the states $\mathbf{x}$ which in turn is a function of $\mathbf{u}$, the influence of changes in $\mathbf{u}$ on the magnitude of $\mathcal{J}$ cannot be derived directly. Furthermore, the optimal value of $\mathcal{J}$ depends on which $\mathbf{x}$ are feasible.

This problem can be approached as a constrained optimization problem, where the constraint is formed by the dynamic system, that has the general form

$$\mathbf{g}^n\left(\mathbf{x}^{n+1}, \mathbf{x}^n, \mathbf{u}^n\right) = \mathbf{0}, \tag{4.2}$$

and initial state vector $\mathbf{x}_o$. The dynamic system (eq. 4.2) is formally included as a constraint by adding it to the objective function $\mathcal{J}$ with a set of Lagrange multipliers $\boldsymbol{\lambda}$ (different from λ used for mobility in chapter 3). The resulting equation is called the modified objective function $\bar{\mathcal{J}}$

$$\bar{\mathcal{J}} = \sum_{n=0}^{N-1} \left[\mathcal{J}^n\left(\mathbf{x}^n, \mathbf{u}^n\right) + \left(\boldsymbol{\lambda}^{n+1}\right)^T \mathbf{g}^n\left(\mathbf{x}^{n+1}, \mathbf{x}^n, \mathbf{u}^n\right)\right]. \tag{4.3}$$

Next an auxiliary function, $\mathcal{L}^n$, is defined as

$$\mathcal{L}^n\left(\mathbf{x}^{n+1}, \mathbf{x}^n, \mathbf{u}^n, \boldsymbol{\lambda}^{n+1}\right) = \mathcal{J}^n\left(\mathbf{x}^n, \mathbf{u}^n\right) + \left(\boldsymbol{\lambda}^{n+1}\right)^T \mathbf{g}^n\left(\mathbf{x}^{n+1}, \mathbf{x}^n, \mathbf{u}^n\right). \tag{4.4}$$

Substitution into eq. 4.3 gives

$$\bar{\mathcal{J}} = \sum_{n=0}^{N-1} \mathcal{L}^n\left(\mathbf{x}^{n+1}, \mathbf{x}^n, \mathbf{u}^n, \boldsymbol{\lambda}^{n+1}\right). \tag{4.5}$$

A first order approximation of the sensitivity of $\bar{\mathcal{J}}$ with respect to $\mathbf{x}^{n+1}$, $\mathbf{x}^n$, $\mathbf{u}^n$, and $\boldsymbol{\lambda}^{n+1}$ is obtained by taking the first variation of $\bar{\mathcal{J}}$ (noting that $\delta\mathbf{x}^0 = \mathbf{0}$),

$$\begin{aligned}\delta\bar{\mathcal{J}} &= \sum_{n=1}^{N-1}\left(\frac{\partial\mathcal{L}^n}{\partial\mathbf{x}^n}\right)\delta\mathbf{x}^n + \sum_{n=0}^{N-1}\left(\frac{\partial\mathcal{L}^n}{\partial\mathbf{x}^{n+1}}\right)\delta\mathbf{x}^{n+1} + \sum_{n=0}^{N-1}\left(\frac{\partial\mathcal{L}^n}{\partial\mathbf{u}^n}\right)\delta\mathbf{u}^n \\ &\quad + \sum_{n=0}^{N-1}\left(\frac{\partial\mathcal{L}^n}{\partial\boldsymbol{\lambda}^{n+1}}\right)\delta\boldsymbol{\lambda}^{n+1},\end{aligned} \tag{4.6}$$

where $\frac{\partial\mathcal{L}^n}{\partial\mathbf{x}^n}$, $\frac{\partial\mathcal{L}^n}{\partial\mathbf{x}^{n+1}}$, $\frac{\partial\mathcal{L}^n}{\partial\mathbf{u}^n}$, and $\frac{\partial\mathcal{L}^n}{\partial\boldsymbol{\lambda}^{n+1}}$ are row vectors. By changing the index of summation, the second term in the right hand side of eq. 4.6 can be written as

$$\begin{aligned}\sum_{n=0}^{N-1}\left(\frac{\partial\mathcal{L}^n}{\partial\mathbf{x}^{n+1}}\right)\delta\mathbf{x}^{n+1} &= \sum_{n=1}^{N}\left(\frac{\partial\mathcal{L}^{n-1}}{\partial\mathbf{x}^n}\right)\delta\mathbf{x}^n \\ &= \left(\frac{\partial\mathcal{L}^{N-1}}{\partial\mathbf{x}^N}\right)\delta\mathbf{x}^N + \sum_{n=1}^{N-1}\left(\frac{\partial\mathcal{L}^{n-1}}{\partial\mathbf{x}^n}\right)\delta\mathbf{x}^n.\end{aligned} \tag{4.7}$$

Substituting eq. 4.7 into eq. 4.6 gives

$$\begin{aligned}\delta\bar{\mathcal{J}} &= \sum_{n=1}^{N-1}\left(\frac{\partial\mathcal{L}^{n-1}}{\partial\mathbf{x}^n} + \frac{\partial\mathcal{L}^n}{\partial\mathbf{x}^n}\right)\delta\mathbf{x}^n + \sum_{n=0}^{N-1}\left(\frac{\partial\mathcal{L}^n}{\partial\mathbf{u}^n}\right)\delta\mathbf{u}^n \\ &\quad + \sum_{n=0}^{N-1}\left(\frac{\partial\mathcal{L}^n}{\partial\boldsymbol{\lambda}^{n+1}}\right)\delta\boldsymbol{\lambda}^{n+1} + \left(\frac{\partial\mathcal{L}^{N-1}}{\partial\mathbf{x}^N}\right)\delta\mathbf{x}^N.\end{aligned} \tag{4.8}$$

From eq. 4.8 it is not directly obvious what the effect of a change in the control $\mathbf{u}$ is, since a change in it will also lead to a change in the states $\mathbf{x}$. Eq. 4.8 can, however, be simplified in a number of steps. The third term in the right hand side of eq. 4.8 is zero because $\frac{\partial \mathcal{L}^n}{\partial \boldsymbol{\lambda}^{n+1}} = (\mathbf{g}^n)^T = \mathbf{0}^T$. Further simplification of eq. 4.8 can be obtained by a proper choice of the Langrange multipliers. The last term in eq. 4.8 is always zero if the following is imposed:

$$\frac{\partial \mathcal{L}^{N-1}}{\partial \mathbf{x}^N} = \mathbf{0}^T. \tag{4.9}$$

This condition is called the *Final Condition*, which after substitution of eq. 4.4 can be written as

$$\left(\boldsymbol{\lambda}^N\right)^T \frac{\partial \mathbf{g}^{N-1}}{\partial \mathbf{x}^N} = \mathbf{0}^T. \tag{4.10}$$

On top of this, the first term in the right hand side of eq. 4.8 can be set to zero by imposing

$$\frac{\partial \mathcal{L}^{n-1}}{\partial \mathbf{x}^n} + \frac{\partial \mathcal{L}^n}{\partial \mathbf{x}^n} = \mathbf{0}^T \tag{4.11}$$

for $n = 1, 2, .., N-1$. Substitution of eq. 4.4 into eq. 4.11 gives, after some rearranging

$$(\boldsymbol{\lambda}^n)^T \left(\frac{\partial \mathbf{g}^{n-1}}{\partial \mathbf{x}^n}\right) = -\left(\boldsymbol{\lambda}^{n+1}\right)^T \frac{\partial \mathbf{g}^n}{\partial \mathbf{x}^n} - \frac{\partial \mathcal{J}^n}{\partial \mathbf{x}^n}. \tag{4.12}$$

Eq. 4.12 is known as the *adjoint* or *co-state* equation. Using the *Final Condition* (eq. 4.10) to give initial condition $\boldsymbol{\lambda}^N$, eq. 4.12 can be integrated backwards in time. After all Lagrange multipliers have been calculated eq. 4.8 simplifies to

$$\delta \bar{\mathcal{J}} = \sum_{n=0}^{N-1} \left(\frac{\partial \mathcal{L}^n}{\partial \mathbf{u}^n}\right) \delta \mathbf{u}^n = \sum_{n=0}^{N-1} \left[\frac{\partial \mathcal{J}^n}{\partial \mathbf{u}^n} + \left(\boldsymbol{\lambda}^{n+1}\right)^T \frac{\partial \mathbf{g}^n}{\partial \mathbf{u}^n}\right] \delta \mathbf{u}^n. \tag{4.13}$$

Eq. 4.13 shows the first order change in the objective function resulting from a change in the control vector $\mathbf{u}$. In the optimum this first order variation is zero. If the controls $\mathbf{u}$ are unconstrained this yields

$$\frac{\partial \mathcal{L}^n}{\partial \mathbf{u}^n} = \mathbf{0}^T. \tag{4.14}$$

If the control is constrained the optimal control policy optimizes (maximizes or minimizes) $\mathcal{L}^n$. Thus for a maximization problem

$$\mathcal{L}^n\left(\mathbf{x}^{n+1}, \mathbf{x}^n, \mathbf{u}^n_{opt}, \boldsymbol{\lambda}^{n+1}\right) \geq \mathcal{L}^n\left(\mathbf{x}^{n+1}, \mathbf{x}^n, \mathbf{u}^n, \boldsymbol{\lambda}^{n+1}\right). \tag{4.15}$$

This is called the *Pontryagin Maximum Principle* [Luenberger (1979)].

4.4.2 Optimization procedure

The optimization problem is a *two-point boundary value problem*, since initial conditions for the dynamic system and the adjoint are specified at opposite sides of the time interval

[Stengel (1994)]. Solution of the optimization problem consists of repeating the following steps until the optimal control vector $\mathbf{u}$ has been found for each time step:

1. Numerical simulation of the dynamic system behavior by numerical solution of eq. 4.2 from time interval 0 to N, with an initial choice for $\mathbf{u}$, using $\mathbf{x}^0$ as initial conditions
2. Evaluation of the objective function
3. Calculation of the Lagrange multipliers by backward numerical solution of the adjoint equation (eq. 4.12), using the *Final Condition* (eq. 4.10) as initial condition
4. Computation of the gradients $\frac{\partial \mathcal{L}^n}{\partial \mathbf{u}^n}$:
5. Computation of an improved control vector $\mathbf{u}$, using the gradients $\frac{\partial \mathcal{L}^n}{\partial \mathbf{u}^n}$
6. Repetition of steps 2-5 until no further improvement can be found

Because the process is gradient-based, a local optimum may be computed and therefore the results may depend on the initial choice of $\mathbf{u}$. The partial derivatives $\frac{\partial \mathcal{J}^n}{\partial \mathbf{x}^n}$, $\frac{\partial \mathbf{g}^n}{\partial \mathbf{x}^n}$, $\frac{\partial \mathbf{g}^{n-1}}{\partial \mathbf{x}^n}$, $\frac{\partial \mathbf{g}^n}{\partial \mathbf{u}^n}$, and $\frac{\partial \mathcal{J}^n}{\partial \mathbf{u}^n}$ depend on the discretization of the dynamic system and the objective function.

4.5 Application to water flood optimization

In the previous section the general formulation of the optimal control problem was discussed. In this section a brief summary of its application to the water flood optimization problem is given. In this study the objective is to maximize the Net Present Value (NPV) of the water flooding process. It generally comprises costs of water injection and water production, and revenues of oil and gas production. In this study separate water injection costs were not considered. Instead, the oil production price and the water production costs were assumed to be a net price and cost respectively, including costs of associated water injection. The objective function $\mathcal{J}$ is thus evaluated only at the production wells and is defined as

$$\begin{aligned} \mathcal{J} &= \sum_{n=0}^{N-1} \sum_{k=1}^{N_{prod}} \frac{-r_o \left(q_o^*\right)_k^n - r_w \left(q_w^*\right)_k^n - r_g \left(q_g^*\right)_k^n}{\left(1+\frac{b}{100}\right)^{\tau^n}} \Delta t^n \\ &= \sum_{n=0}^{N-1} \mathcal{J}^n, \end{aligned} \tag{4.16}$$

where r_o is the oil price $\left[\frac{\$}{m^3}\right]$ and has positive sign, r_w is the water cost $\left[\frac{\$}{m^3}\right]$ and has a negative sign, and r_g is the gas price $\left[\frac{\$}{m^3}\right]$. q_o^*, q_w^*, and q_g^* are rates at surface conditions $\left[\frac{m^3}{s}\right]$, which are negative for production. Δt is the time step size $[s]$, b is the discount rate

per year $[\%]$, τ is the number of years $[-]$, n is the time step, N is the final time step, and N_{prod} equals the number of production wells. The dynamic system is the reservoir simulator, discussed in detail in chapter 3 and appendix A. Its most general form is

$$\mathbf{g}^n = \mathbf{0}. \tag{4.17}$$

It is a function of the states $\hat{\mathbf{p}}$ and the control parameters. If the control parameters are the total liquid injection and production rates $\mathbf{q}$ in the wells (The scenario described in section 4.9.1.), eq. 4.17 equals

$$\mathbf{g}^n\left(\hat{\mathbf{p}}^{n+1}, \hat{\mathbf{p}}^n, \mathbf{q}^n\right) = \mathbf{0}. \tag{4.18}$$

If a well model is used (sections 3.4 & 4.9.2), the control parameters may be the effective valve settings α_{eff} in the wells, which will be referred to as $\boldsymbol{\alpha}$. Eq. 4.17 is in that case

$$\mathbf{g}^n\left(\hat{\mathbf{p}}^{n+1}, \hat{\mathbf{p}}^n, \boldsymbol{\alpha}^n\right) = \mathbf{0}. \tag{4.19}$$

For the remainder of this section the control is taken to be $\boldsymbol{\alpha}$. With $\mathcal{L}^n$ defined as

$$\mathcal{L}^n\left(\hat{\mathbf{p}}^{n+1}, \hat{\mathbf{p}}^n, \boldsymbol{\alpha}^n, \boldsymbol{\lambda}^{n+1}\right) = \mathcal{J}^n\left(\hat{\mathbf{p}}^n, \boldsymbol{\alpha}^n\right) + \left(\boldsymbol{\lambda}^{n+1}\right)^T \mathbf{g}\left(\hat{\mathbf{p}}^{n+1}, \hat{\mathbf{p}}^n, \boldsymbol{\alpha}^n\right), \tag{4.20}$$

the *Final Condition* (eq. 4.10) in the water flood optimization problem equals

$$\frac{\partial \mathcal{L}^{N-1}}{\partial \hat{\mathbf{p}}^N} = \mathbf{0}^T, \tag{4.21}$$

and the *adjoint equation* equals

$$\left(\boldsymbol{\lambda}^n\right)^T = \left[-\left(\boldsymbol{\lambda}^{n+1}\right)^T \frac{\partial \mathbf{g}^n}{\partial \hat{\mathbf{p}}^n} - \frac{\partial \mathcal{J}^n}{\partial \hat{\mathbf{p}}^n}\right] \left(\frac{\partial \mathbf{g}^{n-1}}{\partial \hat{\mathbf{p}}^n}\right)^{-1}. \tag{4.22}$$

After the Lagrange multipliers have been calculated the gradients $\frac{\partial \mathcal{L}^n}{\partial \boldsymbol{\alpha}^n}$ can be calculated. These gradients form the input for the steepest descent optimizer, that will be discussed in section 4.10. A summary of the derivatives in eq. 4.22 is given in appendix C.

4.6 Interpretation of the adjoint equation

In the oil industry, the optimal control method is primarily used to calculate gradients with respect to the controllable parameters. The meaning of the Lagrange multipliers has, to our knowledge, not yet been addressed in the petroleum industry.

4.6.1 Lagrange multipliers

Lagrange multipliers are used to find a function's extremum under constrained conditions. They integrate the constraints into the objective function that is to be optimized. If the value of the Lagrange multiplier equals zero under optimized conditions, the constraint does not affect the value of the objective function (the constraint is not active). If it has a nonzero

value the constraint does affect the optimal objective function value (the constraint is active). The larger the magnitude of the multiplier the larger the effect of the constraint is on the value of the optimized function [Strang (1986)]. In the optimum, the Lagrange multiplier value is thus an indication of the cost of the associated constraint, reflecting the sensitivity of the objective function with respect to a change in the constraint [Fletcher (1987)]. In the optimum this sensitivity of the objective function $\mathcal{J}$ with respect to a constraint g^{j-1} can be expressed as [Kraaijevanger (2004)]

$$d\mathcal{J}_j = -\left(\lambda^j\right)^T dg^{j-1}, \tag{4.23}$$

in which $\mathcal{J}_j$ represents the cost-to-go objective function which is evaluated from the time step of perturbation to the end time step (see also eq. E.2). The cost-to-go objective function and the derivation of eq. 4.23 are described in more detail in sections E.1 & E.2 of appendix E.

4.6.2 Adjoint equation

In optimal control theory the dynamic system is added to the objective function as an equality constraint with (a set of) Lagrange multipliers. This constraint must be satisfied for each point in space and time that is to be optimized. Therefore, there is a separate Lagrange multiplier for each constraining equation at each time step. Largely analogous to section 4.6.1 the Lagrange multipliers in an optimal control problem represent the objective function's *sensitivity to dynamic effects* on the optimal trajectory [Stengel (1994)]. After evaluating the adjoint equation, the first variation in the cost-to-go objective function at some arbitrary time step j is given by

$$d\mathcal{J}_j = -\left(\lambda^j\right)^T \frac{\partial g^{j-1}}{\partial x^j} dx^j. \tag{4.24}$$

The derivation of eq. 4.24 is given in section E.1 of appendix E. In systems where $\frac{\partial g^{j-1}}{\partial x^j} = 1$ (see appendix E for more detail), eq. 4.24 reduces to

$$d\mathcal{J}_j = -\left(\lambda^j\right)^T dx^j \tag{4.25}$$

In eq. 4.25 the Lagrange multiplier directly gives the sensitivity of the objective function with respect to small changes in the state.

4.6.3 Other potential applications of Lagrange multiplier values

Eqs. 4.24 & 4.25 indicated that, along the optimal trajectory, the values of the Lagrange multipliers $\boldsymbol{\lambda}$ reflect the sensitivity $\left(\text{ a scaled sensitivity if } \frac{\partial g^{j-1}}{\partial x^j} \neq 1\right)$ of the objective function with respect to slight changes in the corresponding states. The value of the Lagrange multipliers may thus give an estimate of how much the optimum objective function value would change if constraints on the states could be changed. Constraints on the pressure at a location

close to existing wells may be manipulated by stimulation or water shutoff methods. In more distant areas in the reservoir this may be achieved by completing new wells. A more detailed discussion on the physical meaning of the Lagrange multipliers is postponed to section 5.7.

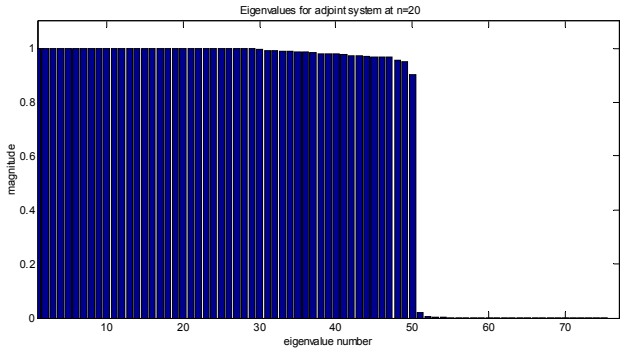

Figure 4.1: Eigenvalues of adjoint system matrix at time step $n = 20$.

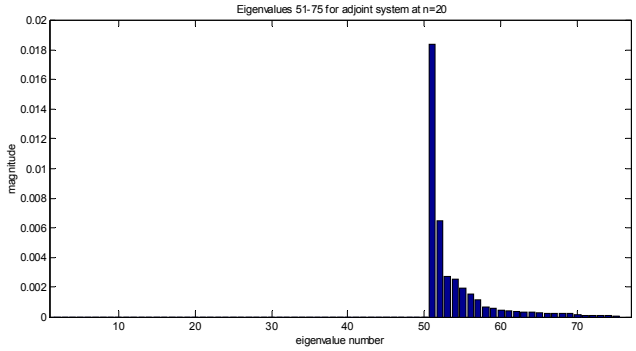

Figure 4.2: eigenvalues 51-75 for adjoint at time step 20. Eigenvalues are sorted on magnitude.

4.7 Eigenvalues of the adjoint equation

In section 3.3 the eigenvalues of the dynamic system were briefly discussed. In this section the eigenvalues of the adjoint equation are discussed. Figure 4.1 shows the absolute magnitude of the eigenvalues at time step $n = 20$ for the adjoint, corresponding to the dynamic system described in section 3.3. The complex modulus was plotted since a few eigenvalues were complex, although the imaginary part was very small ($O\left(10^{-9}\right)$). Just as was the case for the dynamic system, the eigenvalues of the adjoint can be split up in distinct groups. Eigenvalues 1-25 are approximately 1. Some of them are slightly larger than one, and some of the eigenvalues in this group have a very small imaginary part. The fact that some of the eigenvalues are larger than 1 suggest that the adjoint is strictly spoken not stable. The fact that the difference is very small suggests that it is related to numerical round-off errors. Eigenvalues 26-50 are within the range 0.90-1. Eigenvalues 51-75 are close to zero, as shown in Figure 4.2. Overall, the eigenvalue distribution of the adjoint resembles that of the dynamic system, the main differences are found for eigenvalues 26-50.

4.8 Verification of gradients obtained with optimal control theory

The validation of a numerical scheme is generally done by comparison with a reference solution. For simple systems the results obtained with a numerical reservoir simulator can be compared with results from analytical solutions, laboratory experiments or other numerical reservoir simulators. This cannot be done so easily for the adjoint scheme. First of all there are not yet any reference solutions for the adjoint. Secondly, its behavior is not only determined by the dynamic system to which it is adjoint, but also by the objective function which derivatives with respect to the states $\frac{\partial \mathcal{J}}{\partial \mathbf{x}}$ form the source for the adjoint equation (see eq. 4.12 in this respect).

Validation of the gradients obtained with optimal control theory can be done by comparison with gradients obtained with numerical perturbation. Eq. 4.13 describes the relation between a change in the control $\delta \mathbf{u}$ and a change in the objective function $\delta \bar{\mathcal{J}}$ if the appropriate Lagrange multipliers have been calculated. It is repeated below

$$\delta \bar{\mathcal{J}} = \sum_{n=0}^{N-1} \left(\frac{\partial \mathcal{L}^n}{\partial \mathbf{u}^n} \right) \delta \mathbf{u}^n. \tag{4.26}$$

For a single control at time n this relation is

$$\frac{\delta \bar{\mathcal{J}}}{\delta {u_i}^n} = \frac{\partial \mathcal{L}^n}{\partial {u_i}^n}. \tag{4.27}$$

Eq. 4.27 states that a change in the objective function due to a change in the control at point i and time n is equal to the gradient $\frac{\partial \mathcal{L}^n}{\partial {u_i}^n}$ at that point i and time n. The gradient on the left

hand side can be obtained by numerically perturbing the forward simulation. This is done with the aid of two reservoir simulations. In the first, a reservoir simulation is run with a particular control function and the objective function is calculated. In the second simulation the control i is perturbed at time step n, and the objective function for this run is evaluated. The ratio of the difference in objective function over the difference in the control must then be (approximately) the same as the gradient $\frac{\partial \mathcal{L}^n}{\partial {u_i}^n}$, i.e.

$$\frac{\Delta \bar{\mathcal{J}}}{\Delta u_i^n} = \frac{\bar{\mathcal{J}}_2 - \bar{\mathcal{J}}_1}{u_{i,2}^n - u_{i,1}^n} \approx \frac{\partial \mathcal{L}^n}{\partial u_i^n}. \tag{4.28}$$

It must be kept in mind that the value of the numerically obtained gradient $\frac{\Delta \bar{\mathcal{J}}}{\Delta u_i^n}$ may depend on the size of the perturbation. The perturbation should therefore be sufficiently small. A perturbation that is too small, however, may lead to inaccurate gradients due to numerical round off errors. Comparison of the gradients is discussed in some more detail in section 5.4.

4.9 Constraints on the controls

Sections 4.4 & 4.5 discussed how the dynamic system is included as a constraint in the optimization procedure. In addition, constraints on the control function must be taken into account. In the water flood optimization problem these constraints are the well operating constraints. In this study, two types of well operating scenarios are investigated. In the first scenario no well model is used, instead total liquid injection and production rates $\mathbf{q}$ are controlled directly. In this scenario the field injection and production rate is kept constant and balanced, therefore it is referred to as the rate-controlled scenario[4]. The constraints on the controls for this scenario are described in section 4.9.1. In the second scenario a well model is used. It has been described in section 3.4. In this scenario the well flowing pressures in the injector and producers are fixed, and the injection and production rates are controlled by the valve-settings α_{eff} in the wells. The constraints on the controls for this scenario are described in section 4.9.2.

There are a number of ways to include these constraints into the optimization procedure. Equality constraints on the controls could be included in the optimization in the same way as the dynamic system. For inequality constraints, however, this becomes more complex. Instead, we will follow a more ad hoc approach in including the constraints on the controls. Its discussion is postponed until section 5.8.

[4] This operating scenario was only used in two-phase flow (oil and water) cases with very low (numerical) compressibility. In these cases constant liquid density was assumed, although compressibility was not zero. The resulting error in the mass balance was found to be very small ($<10^{-4}$ %).

4.9.1 Constant field injection and production rate

In this scenario the field injection and production rates are constant and balanced, i.e.

$$\left|q_{t_{inj}}\right| = \left|q_{t_{pr}}\right| = q_{field} = \text{constant.} \tag{4.29}$$

The controllable parameters are the liquid injection and production rates $\mathbf{q}$ in the individual wells. Since the total injection and production rates are constant this scenario can be considered a purely rate-controlled scenario. It is implicitly assumed that well injection and production pressures will never become a limiting factor. In this formulation, injection rates have positive sign, and production rates negative sign. For injectors the constraints are

$$0 \leq q_{inj_i} \leq q_{field}, \tag{4.30}$$

$$\sum_{i=1}^{N_{inj}} q_{inj_i} = q_{field}, \tag{4.31}$$

where q_{inj_i} is the injection rate in well i, q_{field} is the total injection rate, and N_{inj} equals the number of injectors.

For the producers the constraints are

$$-q_{field} \leq q_{prod_j} \leq 0, \tag{4.32}$$

$$\sum_{j=1}^{N_{prod}} q_{prod_j} = -q_{field}, \tag{4.33}$$

where q_{prod_j} is the production rate in well j, and N_{prod} equals the number of producers. In chapters 6 & 7 this scenarios is referred to as the *rate-controlled scenario*.

4.9.2 Constant well flowing pressure

In this scenario a simple well model is used (described in section 3.4 and appendix B). The well flowing pressure p_{wf} is equal and constant for all injection wells, and for all production wells. Of course, it is different for injection and production wells. They are taken constant because control on the flow rates is done through manipulation of the valve-settings α_{eff} in the wells, i.e. the valve-settings α_{eff} are the controllable parameters. In this scenario we only considered purely pressure constrained operating conditions, i.e. the well flowing pressures in the injector and the producer are always the factor limiting the injection and production rates. Any change in valve-setting will lead to a change in the field injection and production rates. For both injectors and producers the effective valve-settings a_{eff} must satisfy

$$0 \leq a_{eff} \leq 1. \tag{4.34}$$

For the injectors the rates should be nonnegative and the well flowing pressure is equal and constant for all injection wells

$$0 \leq q_{inj_i}, \tag{4.35}$$
$$p_{wf} = p_{wf_{inj}}. \tag{4.36}$$

For the producers the rates should be nonpositive and the well flowing pressure is equal and constant for all production wells

$$q_{prod_j} \leq 0, \tag{4.37}$$
$$p_{wf} = p_{wf_{prod}}. \tag{4.38}$$

To satisfy constraints in eqs. 4.35 & 4.37 requires backflow to be avoided. Section 3.4.2 described how this was achieved. In chapters 6 & 7 this scenario is referred to as the *pressure-constrained scenario*.

4.9.3 Mixed-operating constraints

The purely rate controlled and purely pressure constrained scenarios represent the extremes in well operating conditions that are possible. In general, however, there may be distinct stages in the production process during which different constraints are active. If the total injection or production rates exceed the maximum field rates the wells need to be cut back. During this stage the production is rate constrained. In practice this is generally done by choking at the well head. In a simulator this may be done by choking at the well head if a wellbore flow model is used, or by adjusting the well flowing pressures to reduce the drawdown. In this study, however, the well flowing pressure is not taken to be a control variable. Therefore the cutting back of production should be realized by partially closing the valves α_{eff}. If the desired field injection and production rates are higher than can be realized with the injector and producer well flowing pressures, the production becomes pressure-constrained.

For optimization under mixed operating conditions the valve settings should again satisfy

$$0 \leq a_{eff} \leq 1. \tag{4.39}$$

The constraints on the injectors are

$$0 \leq q_{inj_i} \leq q_{field}, \tag{4.40}$$
$$\sum_{i=1}^{N_{inj}} q_{inj_i} \leq q_{field}. \tag{4.41}$$

Since control of the injection rate is done by the valve-settings the well flowing pressure is fixed, i.e.

$$p_{w_{inj}} = p_{wf_{inj}}. \tag{4.42}$$

Similarly for the producers

$$-q_{field} \leq q_{prod_j} \leq 0, \tag{4.43}$$

$$-q_{field} \leq \sum_{j=1}^{N_{prod}} q_{prod_j}, \tag{4.44}$$

$$p_{w_{prod}} = p_{wf_{prod}}. \tag{4.45}$$

4.10 Gradient based optimization algorithms

Figure 4.3 shows a flow chart of the optimization procedure. The adjoint only serves to calculate the gradients of $\mathcal{L}$ with respect to the control. A gradient-based optimization algorithm must subsequently be used to calculate the optimal control function. There are various gradient-based methods that can be used to this end. In section 4.10.1 a brief literature overview of experiences with various gradient-based optimization methods in previous optimal control studies is given. In section 4.10.2 the steepest descent algorithm used in this study is described.

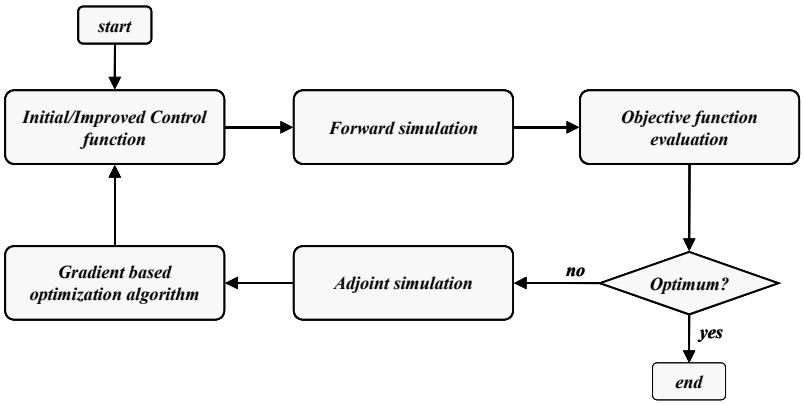

Figure 4.3: Flow chart for dynamic water flood optimization

Convergence to the optimum was assumed if the objective function value hardly increased for a number of subsequent iterations. If the optimal controls are unconstrained, the existence of the optimum may be assessed based on the gradients $\frac{\partial \mathcal{L}^n}{\partial \mathbf{u}^n}$, since eq. 4.14 showed that these should then be zero in the optimum. In that case the flowchart in Figure 4.3 would change slightly, with the adjoint simulation being done prior to assessing convergence to the

optimum. The difficulty with the latter approach, however, is it only holds if the controls are unconstrained.

4.10.1 Literature overview

Various methods were used and compared in previous optimal control studies on history matching and dynamic process optimization. A comparison between the steepest descent method, a conjugate gradient method, a quasi-Newton Method and a Fixed Direction Set method was done by Jacobs (1993). He compared the four methods and concluded that the quasi-Newton method performed best for his test case. For the case he considered, the number of iterations required to achieve an optimum was about a factor 2-3 lower for the quasi-Newton method than for the steepest descent method. Yang and Watson (1987) used optimal control theory in history matching simple two-phase reservoirs. They compared performance of the steepest descent, a conjugate gradient, and two types of quasi-Newton methods. The quasi-Newton methods were generally most efficient and accurate, and could best be used in combination with parameter inequality constraints. Their performance was often an order of magnitude better than the steepest descent methods. Only for (near) quadratic objective functions they found the conjugate gradients method to be more efficient. From the quasi-Newton methods they investigated the Broyden-Fletcher-Goldfarb-Shanno (BFGS) and the Self-Scaling Variable Metric (SSVM) formulations, the latter being more efficient when the number of unknown parameters was large.

Wu *et al.* (1999) and Wu (2000) studied the conditioning of geostatistical models to two-phase production data, using Gauss-Newton and Newton-Raphson methods. Although generally efficient for quickly locating local minima of the objective function, convergence and local minima problems were sometimes encountered when the data mismatch was large, resulting in a poor match of the observed production data. Bi *et al.* (2000) reported that at early iterations in the history match optimization, the change in model parameters often needed to be dampened to avoid slow convergence or convergence to unacceptable local optima, especially when the mismatch between observed and estimated model parameters was large. They used a Levenberg-Marquardt algorithm to provide this damping. Their algorithm generally required on the order of 5 iterations to obtain convergence.

Fathi and Ramirez (1987) applied optimal control theory to optimize a micellar/polymer flooding enhanced oil recovery system. As an optimizer they used both a steepest descent and a conjugate gradient algorithm that was modified and extended to include bounds on the controls. The conjugate gradient method appeared not always superior in performance, it often showed tendencies toward instability, especially in situations where the initial control strategy was far from optimal. Although generally less efficient, the steepest descent algorithm always worked satisfactorily.

Asheim (1986) and Asheim (1988) studied the optimization of natural water drive and water drive by injection for a two-dimensional oil-water system for constant total injection and production rates. The optimization algorithm he used was a commercially available

nonlinear search program, based on the Generalized Reduced Gradient Method. The optimal solution was typically found in only a few iterations.

4.10.2 Method used in this study

In this study only a steepest descent based method was used. Since its performance was satisfactory with an optimum typically being found within 5-15 iterations, a more advanced algorithm was not investigated. In the steepest descent method the controls $\mathbf{u}$ are updated according to

$$\left(\mathbf{u}^n_{new}\right)^T = \left(\mathbf{u}^n_{old}\right)^T + \varepsilon \frac{\partial \mathcal{L}^n}{\partial \mathbf{u}^n}, \tag{4.46}$$

where ε is a weighting factor, and $\left(\mathbf{u}^n_{new}\right)^T$, $\left(\mathbf{u}^n_{old}\right)^T$, and $\frac{\partial \mathcal{L}^n}{\partial \mathbf{u}^n}$ are row vectors. If the weighting factor ε is chosen small, it takes a large number of evaluations before the optimum is reached. A too large value, on the other hand, can cause spurious results if the new control function is beyond the optimum. A choice for the weighting factor was determined empirically. At first, the weighting factor ε^* was calculated that maximizes $\Delta\bar{\mathcal{J}}$, based on the gradients $\frac{\partial \mathcal{L}^n}{\partial \mathbf{u}^n}$. This was done based on the method described by Ray (1981). Its determination requires a number of trial runs in which

$$\Delta\bar{\mathcal{J}} = \sum_{n=0}^{N-1} \left(\frac{\partial \mathcal{L}^n}{\partial \mathbf{u}^n} \right) \Delta \mathbf{u}^n \tag{4.47}$$

is optimized. The weighting factor ε^* optimizes eq. 4.47. The actual weighting factor ε_r chosen for iteration r was at most half of the weighting factor ε^*_r, i.e.

$$\varepsilon_r = \frac{1}{2}\varepsilon^*_r. \tag{4.48}$$

However, this approach sometimes gave too large changes in the controls, especially at early iterations. An additional restriction on the change in controls per iteration was therefore imposed by not allowing $\mathcal{L}$ to change by more than a certain percentage ζ per iteration. This maximum allowable change $\Delta\mathcal{L}_r$ was increased for each subsequent iteration r according to the relation

$$\Delta\mathcal{L}_r = r\zeta, \tag{4.49}$$

up to some preset maximum $\Delta\mathcal{L}^{\max}$, with an associated weighting factor $\varepsilon^{\max}_r$. The smallest of the two weighting factors $\varepsilon^{\max}_r$ and ε_r was used in 4.46 to calculate the new control function. The result of all this is that the controls are not changed drastically at early iterations where the solution is generally still far from the optimum, the gradients $\frac{\partial \mathcal{L}^n}{\partial \mathbf{u}^n}$ are generally large, and the shape of the control function may still change significantly, but allowed to change more when the solution comes closer to the optimum, in order to speed up convergence. Instead of using the gradients $\frac{\partial \mathcal{L}^n}{\partial \mathbf{u}^n}$ directly, they were rescaled first. This will be discussed in section 5.8.

Chapter 5
Issues related to numerical implementation

5.1 Introduction

The previous chapter discussed the theoretical background of optimal control theory and its application to water flood optimization. Upon numerical implementation of the optimal control problem some problems were encountered, mainly with the adjoint equation. These aspects are discussed in sections 5.2, 5.3, and 5.4. To investigate some of the issues mentioned in section 5.4, some tests were done on a simple one-dimensional fractional flow problem. They are described in sections 5.5 & 5.6. Section 5.7 discusses the physical meaning of the Lagrange multipliers for this simple system. Section 5.8 describes how constraints on the controls were implemented. Some preliminary observations on how the computation time for calculating the adjoint may be reduced are briefly mentioned in section 5.9.

5.2 Difficulties in adjoint applications - Literature overview

This section gives a literature overview of problems reported in adjoint applications in meteorology, oceanography and the petroleum industry.

Meteorology and oceanography

Issues with adjoint applications have been reported in the area of meteorology and oceanography [Li and Droegemeier (1993), Xu (1996)]. Li and Droegemeier (1993) investigated the influence of diffusion, and errors associated with its representation, on the adjoint data assimilation technique. They investigated how diffusion influences the retrieval of the initial state given a set of observations at later times. If the model diffusion is represented incorrectly or if numerical diffusion is exceedingly large, the retrieved fields could be substantially distorted, especially for small scale features. They argued that because the two models associated with the adjoint methodology (forward-in-time prediction model and its associated backward-in-time adjoint) contain irreversible diffusive effects, which can be both physical and numerical in nature, information contained in the initial state may be damped, and in some cases even lost completely, as the physical system evolves. In such cases it may be difficult or even impossible to infer the initial field from observations at later times. They conducted some numerical tests on a constant diffusion model. It was observed that in cases

where the diffusivity of the observations was identical to that used in the assimilation runs, the cost function showed similar convergence behavior for various diffusivities. However, the number of iterations required to achieve a certain accuracy increased with increasing diffusivity. This was attributed to the increasing difficulty of retrieving small scale features when larger diffusivities are used. In cases where the diffusivity in the adjoint model was larger than that in the observations (obtained with forward model with low diffusivity), amplification of the estimated initial state occurs. For early iterations the error between real and retrieved initial state decreased but started to increase again for subsequent iterations. The increase in error was attributed to spurious amplification of small-scale features (noise). This effect increased with diffusivity mismatch and length of the assimilation window. In cases where the diffusivity for the observations was larger than that for the forward and adjoint model smoothing of the retrieved initial states occurred. Initially, the error between real and retrieved initial state decreased rapidly, but at large iteration numbers it increased again, due to the spurious damping induced by the diffusion process. Finally the error converged to some higher-than minimum level. From this they concluded that for the cases considered there existed an optimal number of iterations for the minimization process.

Derber (1989) developed a variational continuous assimilation approach for dealing with various sorts of errors that may be related to both the data and the model itself. He added a correction term to the governing equations to serve as a control variable, obtained forecasts superior to those obtained with a more traditional adjoint approach.

In meteorology and oceanography instead of the formal adjoint approximate adjoints are generally used. It is not clear if all problems reported in adjoint applications are referring to approximate or exact adjoints.

Petroleum engineering

Fathi and Ramirez (1987) reported the mathematical complexity of the equations describing immiscible flow to be a serious obstacle for the application of optimal control theory in this area. They reported that non-smooth coefficients in the adjoint, arising from the physical nature of the system may lead to difficulties in getting a stable numerical adjoint scheme. They investigated many numerical schemes for the solution of the continuous adjoint equation in their surfactant flooding optimization study, but none of them resulted in a stable solution [Ramirez (1987)]. The difficulty was in the existence of discontinuities in the coefficients, that occur because two saturation shocks form during a surfactant flood, the first being the Buckley-Leverett shock, the second shock being at the surfactant front where the surfactant slug contacts the connate water. Smooth approximations of these coefficients were required to get a stable scheme. This work was all based on a continuous optimal control formulation, in later work they went to a discrete formulation. They also addressed the issue of numerical dispersion. If the numerical dispersion represents the physical dispersion, it can be used to replace the physical dispersion and simplify the calculations. This should also help in cancelling some computational difficulties they encountered in previous studies [Fathi and Ramirez (1984), Fathi (1986)].

Liu *et al.* (1990) investigated optimization of the steam flooding process with optimal control theory. They reported that finding a stable adjoint scheme in itself could be a major mathematical problem. Especially for complicated EOR problems this was an important aspect to consider. For the examples considered they found nonsmooth shapes of the optimal control functions. Reportedly smaller time steps should result in smoother control functions.

Sudaryanto (1998) encountered computational problems in calculating the optimum switch time for the case of miscible, variable mobility displacements, in which a finite difference method was used to simulate the forward and adjoint equations. They found that the objective function reached a maximum at a switch time that was different than the switch time at which the derivative $\frac{\partial \mathcal{L}}{\partial u}$ was zero. As a result, the optimization stopped at a suboptimal value in a number of cases. This problem did not occur in their streamtube formulation. They attributed the computational problems in the finite difference formulation to numerical (round off) errors in solving the large system of linear state and adjoint equations. They also had to use small time steps in order to avoid stability problems with the adjoint equation (Sudaryanto, personal communication).

5.3 Stability aspects of the adjoint equation

Some problems concerning the stability of the adjoint were encountered in this study. Analysis of the stability of the adjoint equation was done with the matrix method. The stability was assessed based on the eigenvalues of the adjoint amplification matrix $\mathbf{G}_{\mathrm{adj}}$, which is defined as:

$$\begin{aligned} \boldsymbol{\lambda}^n &= -\left[\left(\frac{\partial \mathbf{g}^n}{\partial \mathbf{x}^n}\right)\left(\frac{\partial \mathbf{g}^{n-1}}{\partial \mathbf{x}^n}\right)^{-1}\right]^T \boldsymbol{\lambda}^{n+1} - \left[\left(\frac{\partial \mathcal{J}^n}{\partial \mathbf{x}^n}\right)\left(\frac{\partial \mathbf{g}^{n-1}}{\partial \mathbf{x}^n}\right)^{-1}\right]^T \\ &= \mathbf{G}_{\mathrm{adj}}\boldsymbol{\lambda}^{n+1} - \mathbf{q}_{\mathrm{adj}}. \end{aligned} \tag{5.1}$$

In this equation matrix $\mathbf{G}_{\mathrm{adj}}$ is the amplification matrix and vector $\mathbf{q}_{\mathrm{adj}}$ is the source/sink to the adjoint dynamic system.

5.3.1 Spatial weighting

In section 3.2.5 spatial weighting of various parameters in the discrete dynamic system was discussed. The relative permeabilities k_{rl} and capillary pressures p_{cow} and p_{cgo} are calculated according to the upstream weighting principle. The adjoint equation inherits this upstream weighting. Using this formal adjoint gave good results for simple, small dynamic systems (small number of grid blocks) with a small number of time steps, but for larger systems it resulted in stability problems in the adjoint equation. Applying the upstream weighting principle to the adjoint itself, noting that in the adjoint flow is in the direction of increasing potential, resulted in a more stable scheme. The parameters that were upstream-weighted in

the adjoint were the same parameters for which upstream weighting is used in the original dynamic system, including their derivatives. It must be stressed that whether or not this upstream weighting should be done separately is subject of debate, the opinions differing from one expert to the other. It should therefore be considered in conjunction with the stability of the adjoint scheme, and with validation of the gradients obtained against those obtained with numerical perturbation methods (section 4.8). Further research in this area is, however, definitely necessary.

5.3.2 Time weighting

In this section the effect of time weighting on the stability of the adjoint equation is discussed. Two different time discretizations for the adjoint were investigated. One adjoint formulation was based on the semi-implicit dynamic system equations, as described in chapter 3. Secondly, an adjoint formulation based on a fully-implicit discretization of the forward dynamic system was investigated. The calculation of the forward problem was for both done with a semi-implicit reservoir simulator as discussed in chapter 3, assuming that for small time steps the results obtained with a semi-implicit and fully implicit reservoir simulator are sufficiently similar. In general, however, numerical dispersion is larger in a fully-implicit formulation.

Adjoint resulting from a semi-implicit dynamic system formulation

This adjoint formulation results from a time discretization of the dynamic system according to eq. 3.23. For the dynamic system this means that the scheme is unconditionally stable in its states, but only conditionally stable with respect to the transmissibility terms. For the latter the Courant-Friedrichs-Lewy (CFL) condition holds, which states that a fluid particle should not move more than one spatial step-size Δx in one time step Δt [Peaceman (1977), Fletcher (1987)].

Adjoint resulting from a fully-implicit dynamic system formulation

This adjoint formulation results from a fully-implicit dynamic system formulation. For the dynamic system itself this means that the scheme is unconditionally stable in the states and in the implicitly calculated transmissibility terms.

Comparison of results obtained with different adjoint formulations

The gradients $\frac{\partial \mathcal{L}}{\partial \tilde{\mathbf{q}}}$ obtained from the semi-implicit and fully-implicit adjoints were compared for two different time step sizes at which dynamic system and adjoints were integrated forward and backward in time respectively. The total simulation time was fixed and equal for both cases. The reservoir model on which the comparison was done, was a horizontal reser-

voir with dimensions of 450 by 450 [m], consisting of 45 by 45 grid blocks, with 45 injectors and 45 producers. The permeability field is shown in Figure 5.1.

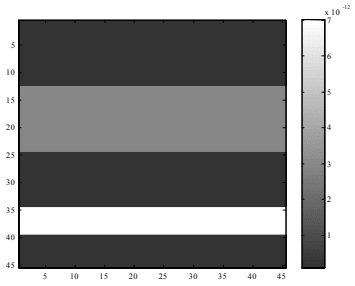

Figure 5.1: Top view of permeability $[m^2]$ distribution in reservoir. 45 injectors are aligned along the left edge, 45 producers along the right edge.

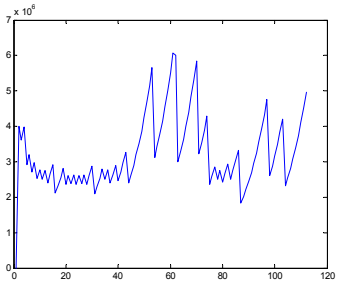

Figure 5.2: Time step size versus time step number for Case II.

In the forward simulation the injectors and producers were operated at equal rate. Since, the controls were the injection and production rates, the gradients with respect to the controls were $\frac{\partial \mathcal{L}}{\partial \tilde{\mathbf{q}}}$. In Case I the time step size was small and constant to ensure stability in the reservoir simulation. The total number of time steps for the simulation in this case was 1800. In Case II, the time step size was much larger, varying in time, and chosen such as to cause

local instabilities in the reservoir simulation[5]. The total number of time steps in this case was 111. Figure 5.2 shows the time step size versus time step n for Case II.

Case I: small, constant time step size

Figure. 5.3 & 5.4 show the improved injection and production rates as function of time step n for all injectors and producers in Case I, calculated after the first iteration. Each row in the left graph of Figure 5.3 shows the injection rate as function of time step for one injection well. Thus row 15 shows the injection rate as function of time step for injector number 15. The grey-scale shows the value of the flow rate, where black is a low, and white a high rate. The injection and production rates in Figure 5.3 & 5.4 were calculated from the gradients $\frac{\partial \mathcal{L}^n}{\partial \tilde{\mathbf{q}}^n}$. Since these gradients are directly calculated from the Lagrange multipliers they are a good way of comparing both formulations. Differences in the Lagrange multipliers will result in different gradients $\frac{\partial \mathcal{L}^n}{\partial \tilde{\mathbf{q}}^n}$ and thus into a different control function for the injectors and producers. Figure 5.3 & 5.4 show that in Case I the resulting control functions are similar for the semi-implicit and fully-implicit adjoints, suggesting that the adjoints are also similar. For small time steps this suggests that, although only the semi-implicit adjoint formulation is formally adjoint to the dynamic system, for practical purposes the fully-implicit adjoint can also be considered compatible/adjoint to the semi-implicit dynamic system description. This is attributed to the fact that for small time steps a semi-implicit and fully-implicit formulation of the forward problem give similar results. Therefore, we expect their adjoints also to give similar results.

This is in agreement with results obtained independently by Wu (1999) and Wu *et al.* (1999). For the forward problem they used a standard IMPES scheme whereas the adjoint was based on a fully-implicit form of the difference equations. This was done under the assumption that the pressures and saturations obtained with the IMPES procedure are for small time steps sufficiently similar to those obtained with a fully-implicit scheme. Results they obtained suggested this to be a fair assumption.

The fact that one adjoint formulation seems compatible to different forward schemes is an important result when considering implementation in commercial simulators. The latter may use different degrees of implicitness for different grid blocks, depending on time step and stability requirements. If the formal adjoint would be required for each grid block and time step, implementation would be significantly more complicated. Another important fact in this respect is that, contrary to the forward simulation, a fully-implicit formulation of the adjoint does not necessarily require more calculation time than a semi-implicit formulation. No iterating is required because the coefficients in the adjoint are known at all time steps, and because the adjoint equations are linear in the Lagrange multipliers.

[5] The maximum stable time step size exists because in the formulation in this study the transmissbilities were calculated explicitly. In a fully implicit scheme these instabilities would not occur.

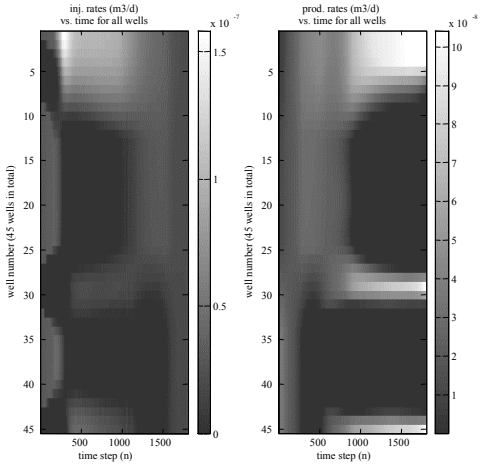

Figure 5.3: Improved injection & production rates for the injectors (left) and the producers (right) obtained with the semi-implicit formulation of the adjoint. Results for Case I.

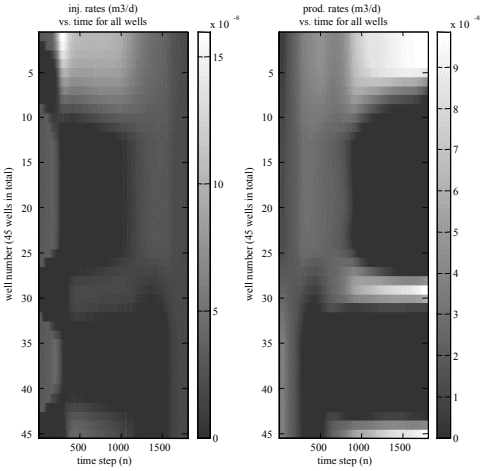

Figure 5.4: Improved injection & production rates for the injectors (left) and the producers (right) obtained with the fully-implicit formulation of the adjoint. Results for Case I.

Case II: large, variable time step size

Figure 5.5 & 5.6 show the improved injection and production rates as function of time step n for the injectors and producers in Case II, calculated after the first optimization loop. Figure 5.5 shows that with the semi-implicit adjoint formulation oscillating injection and production rates are calculated for a large number of time steps. The rates are in no way comparable to those in Figure 5.3. The oscillating rates result from an unstable adjoint equation. The instability could be due to the large time step size that was used, or it could be due to the instabilities in the reservoir simulation, or due to a combination of the two. Figure 5.6 shows the improved rates obtained with the fully-implicit adjoint formulation. The rates are similar to those in Figure 5.4 (and Figure 5.3). The absolute values are slightly different, which is attributed to the fact that on average much larger time steps were used, affecting the accuracy of the calculation. The reason why Figure 5.6 looks a little 'blocky' is related to the fact it was generated from only 111 time steps, compared to 1800 for Figure 5.3 & 5.4.

So the fully-implicit adjoint remained stable and only seemed to suffer from reduced accuracy due to the larger time step size. It even remained stable for a partly and temporarily unstable forward simulation. The semi-implicit adjoint was only stable for small time steps. For the objective function used, the stability properties of the adjoint formulations thus seem to reflect those of the corresponding dynamic system formulations.

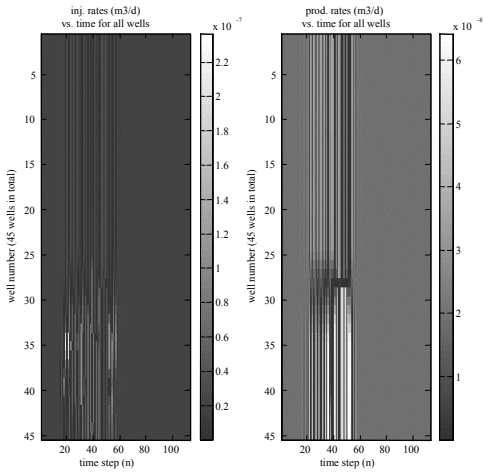

Figure 5.5: Improved injection & production rates for the injectors (left) and the producers (right) obtained with the semi-implicit formulation of the adjoint. Results for Case II.

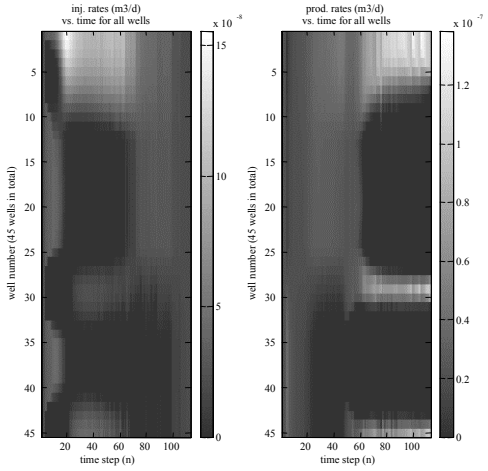

Figure 5.6: Improved injection & production rates for the injectors (left) and the producers (right) obtained with the fully-implicit formulation of the adjoint. Results for Case II.

5.4 Gradients obtained with optimal control theory

A few papers on the application of optimal control theory to history matching discuss the comparison between gradients obtained by numerical perturbation and the gradients $\frac{\partial \mathcal{L}}{\partial \mathbf{u}}$ obtained with optimal control theory, as described in section 4.8.

Wu (1999) and Wu *et al.* (1999) found differences between numerically obtained gradients and adjoint-based gradients smaller than 1%. Wu and Datta-Gupta (2001) also compared sensitivities obtained with the perturbation and the optimal control method, finding similar gradients. The small differences were attributed to the fact that sensitivities obtained with the perturbation method depend on the magnitude of the perturbation.

In this study, however, the agreement between numerically obtained gradients and gradients $\frac{\partial \mathcal{L}}{\partial \mathbf{u}}$ varied from case to case. A number of tests were conducted on a simple three dimensional reservoir with two-phase flow (oil and water). The dimensions of the reservoir were $100 \times 100 \times 30$ $\left[m^3\right]$ modelled by $10 \times 10 \times 3$ grid blocks. In the upper layer a simple high permeability streak is located, as shown in Figure 5.7. The other two layers were homogeneous with a permeability of 10^{-13} $\left[m^2\right]$. The injectors and producers are located along the left and right edge in the upper layer respectively, each grid block containing a separate injector/producer. In this comparison the valve-settings $\boldsymbol{\alpha}$ were taken to be the control vari-

able. The simulation was run for a short period in which water breakthrough in the producer did not occur, with 72 time steps in total. Numerical gradients $\frac{\Delta \mathcal{J}}{\Delta \alpha_{eff}}$ (with $\mathcal{J}$ being the objective function) were calculated for time steps 5-65 in increments of 5. Figure 5.8 shows the gradients $\frac{\Delta \mathcal{J}}{\Delta \alpha_{eff}}$ and $\frac{\partial \mathcal{L}}{\partial \alpha_{eff}}$ for injector 4.

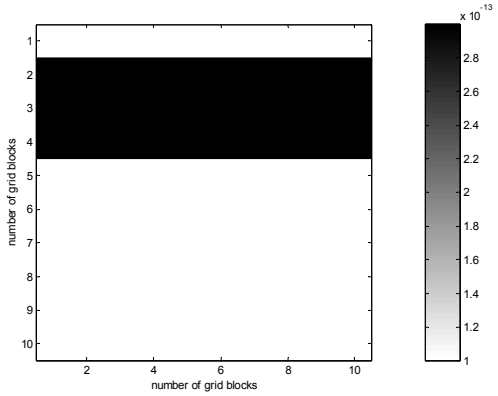

Figure 5.7: Permeability in upper layer (top view). Labels along y-axis correspond both to grid block and well number.

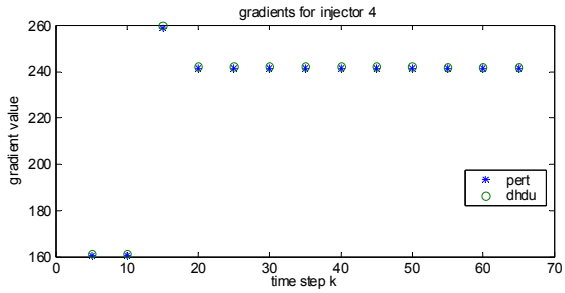

Figure 5.8: Comparison of gradients obtained with numerical perturbation $\frac{\Delta \mathcal{J}}{\Delta \alpha_{eff}}$ (pert) and with the adjoint method $\frac{\partial \mathcal{L}}{\partial \alpha_{eff}}$ (dhdu) for injector number 4. Magnitude of perturbation was 10^{-7}.

The maximum difference in gradients in this case was $0.54\ \%$ at time step $k = 5$. The change in magnitude of the gradients for time steps 5, 10, and 15 is due to a change in time step size of integration. Similar results were obtained for the producer with the error being slightly smaller. Often, however, larger differences between gradients obtained with numerical perturbation $\left(\frac{\Delta \mathcal{J}}{\Delta \alpha_{eff}}\right)$ and the adjoint method $\left(\frac{\partial \mathcal{L}}{\partial \alpha_{eff}}\right)$ were observed. Generally close to the end time the agreement in gradients is good, but closer to the starting time a growing discrepancy in gradients was often observed. The fact that a combination of a semi-implicit dynamic system description and a fully-implicit adjoint formulation were used may introduce errors in the gradients obtained with optimal control theory. However, results from section 5.3 suggests these differences to be rather small. Furthermore, experiences from other studies do not suggest significant problems in this respect [Wu (1999), Wu *et al.* (1999)]. A number of other possible reasons for this discrepancy are discussed below.

Numerical errors

Sudaryanto (1998) found errors in the gradients $\frac{\partial \mathcal{L}}{\partial \mathbf{u}}$ when optimizing a miscible, variable mobility displacement, with a finite difference method. These were attributed to numerical (round off) errors in solving the large system of state and adjoint equations. Since both forward and adjoint equations are typically integrated over hundreds of time steps the build-up of numerical errors may become significant, especially since a large number of eigenvalues of both the forward system and the adjoint are close to or equal to unity. Numerical errors introduced at any stage may as a result hardly or not decay.

Fathi and Ramirez (1987) discussed the effect of numerical diffusion/dispersion in optimal control applications. They mentioned that, if the numerical dispersion represents the physical dispersion, it can be used to replace the physical dispersion and simplify the calculations. This treatment should aid in obviating the computational difficulties encountered in earlier studies [Fathi and Ramirez (1984), Fathi (1986)]. Li and Droegemeier (1993) reported that a misrepresentation of diffusion in the forward and adjoint models could lead to a spurious amplification or smoothing of the retrieved initial state, an effect that increased drastically with the number of time steps, and with mismatch between real and modeled diffusion. Their paper was discussed in some detail in section 5.2. The effect of numerical dispersion is investigated for a simple one dimensional fractional flow problem in section 5.5.

Time step size.

For accuracy reasons there are in the forward simulation generally upper limits to the allowed change in the states per time step. The time step size is controlled to prevent changes in for instance pressure and saturations to exceed these maximum allowed changes. Liu and Ramirez (1994a) suggested in their steam flood optimization study that, because changes in the states may not necessarily coordinate with changes in the adjoint states, a different time step size control may be required for the adjoint as for the forward simulation. To this end, they reduced the time step size in the adjoint equation to a small, constant value. In comput-

ing the adjoint coefficients they used quadratic interpolation of the states for unmatched time points. They found nonsmooth shapes of the optimal control functions. Reportedly, smaller time steps should result in smoother control functions. The effect of time step size on the smoothness of the gradients will be briefly discussed in section 5.6.

Formulation of the dynamic system

The forward problem was formulated with p_o, S_w, S_g as primary variables. Resultingly, the adjoint contains derivatives like

$$\frac{\partial k_{rl}}{\partial S_l}, \frac{\partial P_{clk}}{\partial S_l}, \tag{5.2}$$

which are generally still nonlinear $\left(\frac{\partial k_{rl}}{\partial S_l} = \frac{\partial k_{rl}}{\partial S_l}(S_l)$ and $\frac{\partial P_{clk}}{\partial S_l} = \frac{\partial P_{clk}}{\partial S_l}(S_l)\right)$. Furthermore, abrupt changes in these derivatives may occur, in particular at the saturation extremes (S_{wc}, S_{or}, S_{gc}, $S_{g\max}$). It may be interesting to investigate other formulations of the dynamic system in which the primary variables are for example p_o, p_w, and p_g. The derivatives for the capillary pressure and the relative permeabilities are simpler in the latter formulation, i.e.

$$\frac{\partial p_{cow}}{\partial p_o} = \frac{\partial (p_o - p_w)}{\partial p_o} = 1, \tag{5.3}$$

$$\frac{\partial p_{cow}}{\partial p_w} = \frac{\partial (p_o - p_w)}{\partial p_w} = -1, \tag{5.4}$$

$$\frac{\partial p_{cow}}{\partial p_g} = \frac{\partial (p_o - p_w)}{\partial p_g} = 0, \tag{5.5}$$

$$\frac{\partial k_{rl}}{\partial p_l} = 0, \tag{5.6}$$

which are all constants. In addition, there are slightly different requirements for different dynamic system formulations. If p_o, S_w, S_g are the primary variables, a simulation can be run with zero capillary pressure, whereas for a formulation with p_o, p_w, p_g formulation at least a small (dummy) capillary pressure must always be used [Aziz and Settari (1986)]. Similarly, there may be different requirements for the corresponding adjoints.

Sensitivities for the controls as function of time

A complicating factor in the optimization may arise from the fact that the magnitude of the gradients can for a single control vary by orders of magnitude over time, as shown in Figure 5.9.

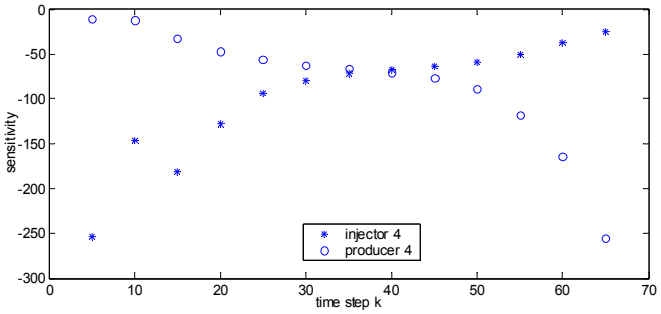

Figure 5.9: Numerical gradients for injector and producer, obtained with perturbation method. Magnitude of perturbation was 10^{-7}. Permeability in the matrix is 10^{-13} $[m^2]$, in the high permeability zone $1.3{\times}10^{-12}$. Contrast factor between high and low (matrix) permeability zone: 13. Total number of time steps: 72.

It shows the gradients, obtained with numerical perturbation, for injector number 4 and producer number 4 as a function of time. In the waterflood considered, with a permeability field similar to the one in Figure 5.7, significant water breakthrough occurred around time step 30. Apart from the large change in gradient magnitude, the figure shows that the trends in gradients are opposite for injector and producer. Going forward in time an increase in producer sensitivity, and a decrease in injector sensitivity are observed, which is attributed to the movement of the water front from injector towards the producer. Going backwards in time, the increase in sensitivity for the injector may require non-diffusive behavior of the adjoint equation, which may from a computational point of view be difficult.

5.5 The effect of numerical dispersion

Some studies reported issues with the adjoint method that are related to numerical dispersion [Fathi and Ramirez (1987), Li and Droegemeier (1993)]. The effect of numerical dispersion on the optimal control method was investigated for a simple, one-dimensional fractional flow example with incompressible fluids and zero capillary pressure. A comparison between the gradients obtained with optimal control theory (in this section defined as $\frac{\Delta \mathcal{H}}{\Delta q_t^n}$) and the gradients obtained with numerical perturbation (in this section defined as $\frac{\Delta J}{\Delta q_t^n}$) was done to explore this effect, assuming that, if present, it will show up as errors in the gradients $\frac{\Delta \mathcal{H}}{\Delta q_t^n}$.

The one dimensional fractional flow equation for incompressible fluids without capillary pressure is, after Aziz and Settari (1986),

$$\frac{\partial S_w}{\partial t} = -\frac{u_t}{\phi}\frac{\partial f_w\left(S_w\right)}{\partial x} - \frac{q_w}{\phi} + \frac{f_w\left(S_w\right)q_t}{\phi}, \tag{5.7}$$

where S_w is the water saturation $[-]$, u_t the total fluid velocity $\left[\frac{m}{s}\right]$, ϕ the porosity $[-]$, $f_w\left(S_w\right)$ the fractional flow of water $[-]$, x the distance in the *x*-direction $[m]$, and q_w and q_t are respectively the water and total injection rates $\left[\frac{1}{s}\right]$.

The term $\frac{\partial f_w}{\partial x}$ is discretized with an upstream weighting scheme, assuming the flow is from i to $i+1$ (from left to right), i.e.

$$\left[\frac{\partial f_w}{\partial x}\right]_i \approx \frac{f_{w_i} - f_{w_{i-1}}}{\Delta x}. \tag{5.8}$$

Substituting eq. 5.8 into eq. 5.7 and discretizing explicitly in time (and replacing $\approx$ with $=$) gives, after some rearranging

$$\begin{aligned} S_{w_i}^{n+1} &= \frac{\Delta t}{\phi}\left[-u_{t_i}^n\left(\frac{f_{w_i} - f_{w_{i-1}}}{\Delta x}\right) - q_{w_i}^n + f_{w_i}^n q_{t_i}^n\right] + S_{w_i}^n \\ &= f_i^n. \end{aligned} \tag{5.9}$$

The time step size Δt is taken to be constant and the porosity ϕ is the same in every grid block. The left boundary ($i = 0$) is a no-flow boundary, hence $u_{t_0}^n = 0$. All flow at this location is due to the injection of water. The initial saturation at this boundary equals the connate water saturation, just as in all other grid blocks. The connate water saturation S_{wc} and the residual oil saturation S_{or} were taken zero. The objective function to be optimized is again the net present value (NPV) objective function, which for this problem is defined as

$$\begin{aligned} J &= \sum_{n=0}^{N-1}\left(-V_{gb}\frac{\left[\left(1 - f_w^n\right)r_o + f_w^n r_w\right]q_t^n \Delta t^n}{\left(1+b\right)^{\tau^n}}\right) \\ &= \sum_{n=0}^{N-1} J^n, \end{aligned} \tag{5.10}$$

where V_{gb} is the grid block volume $\left[m^3\right]$, r_o is the unit oil revenue $\left[\frac{\$}{m^3}\right]$ which is of positive sign, r_w is the unit water cost $\left[\frac{\$}{m^3}\right]$ which is of negative sign, b is the discount factor per year $[\%]$, τ is the cumulative time in number of years $[-]$. The total production rate equals the total injection rate q_w^n, since flow is incompressible. Parameter n represents the discrete time step, and N the final time step. The objective function is evaluated from the rates at the right boundary ($i = r$). Parameter J^n represents the cash flow for time step n [\$].

The optimal control formulation, and the derivatives are given in appendix D. The control parameter in this case is the total rate q_t which has negative sign.

5.5.1 First order relative permeability model, zero numerical dispersion

If a first order relative permeability model (straight lines), constant total mobility, unit viscosity ratio for the fluids, and first order upstream weighting are used, the displacement is non-dispersive if there is no numerical dispersion. This can be realized by choosing the time step size such that the CFL-condition

$$C_{CFL} = \frac{u_t \Delta t}{\phi \Delta x} \tag{5.11}$$

is equal to 1 [Aziz and Settari (1986), Hoffman (1992)]. It means that with every time step, the front moves by one grid block. To achieve this the parameter values $u_t = -0.02 \times 10^{-2}$ $\left[\frac{m}{s}\right]$, $\Delta x = 10\ [m]$, $\phi = 0.2\ [-]$, and $\Delta t = 10^4\ [s]$ were used. Furthermore, the number of grid blocks equals 20, r_o is 80 $\left[\frac{\$}{m^3}\right]$, and r_w is -20 $\left[\frac{\$}{m^3}\right]$. Figure 5.10 shows the fractional flow of water f_w as function of water saturation.

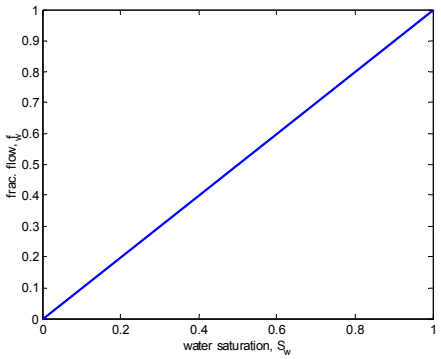

Figure 5.10: Fractional flow as function of saturation for first order powerlaw model with unit viscosity ratio, constant total mobility. $S_{wc} = S_{or} = 0$.

The total simulation time is $2.5 \times 10^5\ [s]$, which is longer than the breakthrough time of $2 \times 10^5\ [s]$. As a result the entire *x*-interval is completely water saturated at the end time (not shown). The gradients $\frac{\Delta J}{\Delta q_t^n}$ and $\frac{\partial \mathcal{H}^n}{\partial q_t^n}$ are shown in Figure 5.11. The upper picture shows that gradients are exactly equal. The gradients are of positive sign, indicating that an increase in the magnitude of the flowrate will lead to a decrease in the value for the objective function. The values of the gradients do not change with time step, indicating that a unit increase in the flow rate at any time step will have the same effect.

The lower picture in Figure 5.11 shows the cash flow J^n versus time step n. It shows that water breakthrough occurs between $n = 20$ and $n = 21$. In one time step production goes from pure oil to pure water production.

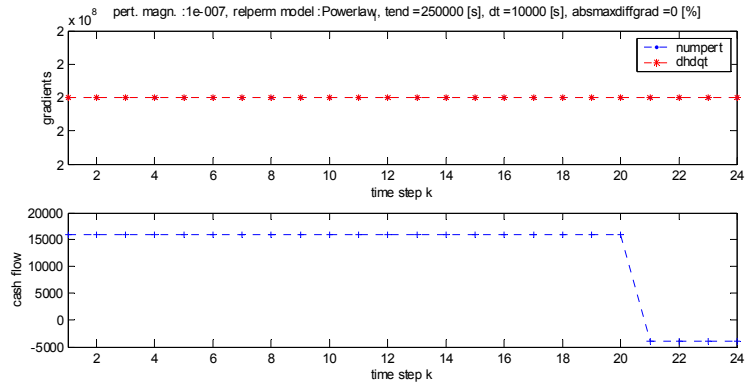

Figure 5.11: Gradients $\frac{\Delta J}{\Delta q_t^n}$ (numpert) and $\frac{\partial \mathcal{H}^n}{\partial q_t^n}$ (dhdqt) and cash flow [$ per time step].

Figure 5.12 shows the Lagrange multipliers for all grid blocks and time steps. Each row in the figure contains the Lagrange multipliers for all grid blocks at one time step. In this example there are only two values for the Lagrange multipliers. All Lagrange multipliers that are depicted white have a value of zero, all multipliers indicated in gray have a value of -20000. A discussion of the values of the Lagrange multipliers is postponed to section 5.7.

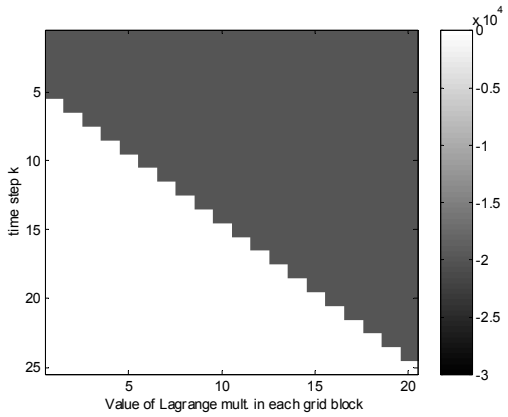

Figure 5.12: Lagrange multipliers for all grid blocks and time steps. (First order powerlaw model, zero numerical dispersion)

5.5.2 First order relative permeability model, nonzero numerical dispersion

Results from section 5.5.1 suggest that in the absence of numerical dispersion the computed gradients are correct. In the present section numerical dispersion is introduced by reducing the time step size to 5×10^3 $[s]$ ($\Delta t = 0.5 \times \Delta t_{C_{CFL}=1}$).

Gradient comparison was done for three examples. In the first example, with a total simulation time of 1×10^5 $[s]$, no water breakthrough occurred. Gradients $\frac{\Delta J}{\Delta q_t^n}$ and $\frac{\partial \mathcal{H}^n}{\partial q_t^n}$ had identical values. In the second example, with a total simulation equal to 2.5×10^5 $[s]$, a mixture of oil and water was produced at the end time. The gradients $\frac{\Delta J}{\Delta q_t^n}$ and $\frac{\partial \mathcal{H}^n}{\partial q_t^n}$ were the same within numerical precision, with a maximum difference in gradients of $O\left(10^{-9}\right)$ $[\%]$. In the third example, with a total simulation time equal to 4×10^5 $[s]$, only water was produced at the end time, as shown by the cash flow curve in Figure 5.13. Again, the gradients $\frac{\Delta J}{\Delta q_t^n}$ and $\frac{\partial \mathcal{H}^n}{\partial q_t^n}$ were the same within numerical precision.

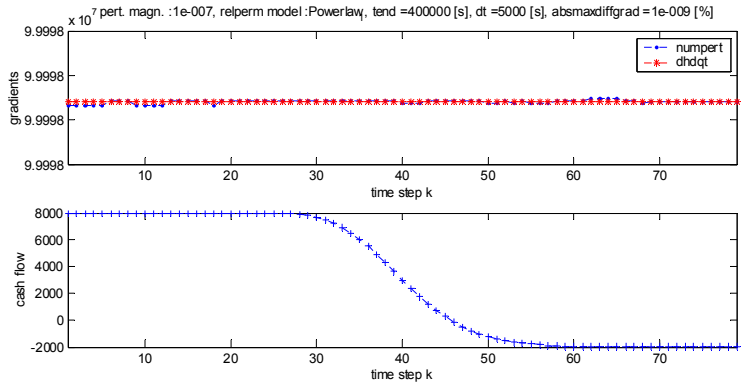

Figure 5.13: Gradients $\frac{\Delta J}{\Delta q_t^n}$ (numpert) and $\frac{\partial \mathcal{H}^n}{\partial q_t^n}$ (dhdqt) and cash flow [$ per time step].

The results for the three examples considered suggest that numerical dispersion is not a problem if a first order relative permeability model is used.

5.6 The effect of the time step size

The previous section showed that for a straight-line relative permeability model the gradients obtained with numerical perturbation and optimal control theory were the same within numerical precision. In this section gradient comparison is done for a system with a second order relative permeability model. As in the previous section the fluid viscosities are taken to be the same. Figure 5.14 shows the fractional flow curve as function of saturation. Contrary to section 5.5.1 the derivative $\frac{\partial f_w}{\partial S_w}$ is now a function of saturation. Gradient comparison was done for three cases, one with a total simulation time shorter than the time of water breakthrough and two with a total simulation time longer than the water breakthrough time. The latter two only differed from eachother in the time step size of integration.

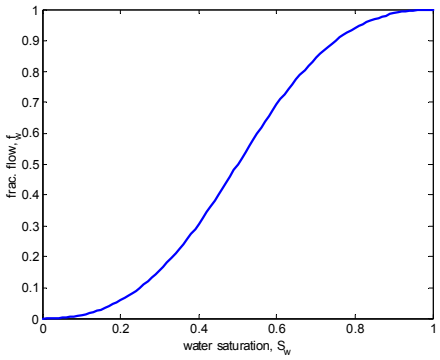

Figure 5.14: Fractional flow as function of saturation for second order powerlaw model with $k_{rw}|_{S_w=1-S_{or}} = k_{ro}|_{S_w=S_{wc}} = 1$*, unit viscosity ratio, and* $S_{wc} = S_{or} = 0$*.*

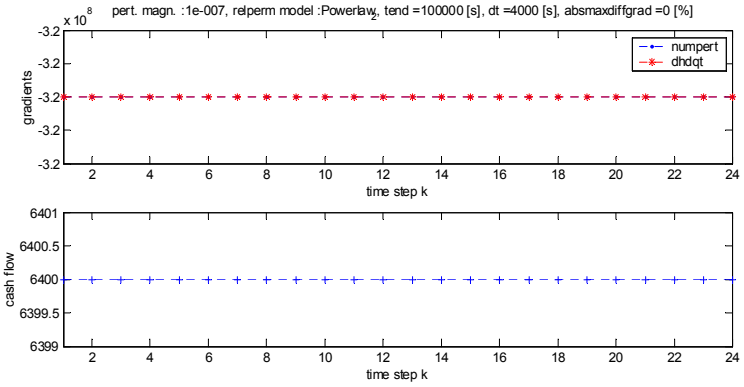

Figure 5.15: Gradients $\frac{\Delta J}{\Delta q_t^n}$ *(numpert) and* $\frac{\partial \mathcal{H}^n}{\partial q_t^n}$ *(dhdqt) and cash flow [$ per time step].*

No water breakthrough

The end simulation time in this case was 1×10^5 $[s]$, which is less than the breakthrough time, as the cash flow curve in Figure 5.15 shows. The time step size Δt was 4×10^3 $[s]$. The figure also shows that the gradients are identical. In this example the Lagrange multipliers

were zero for all grid blocks and time steps, indicating that the system dynamics do not influence the value of the objective function.

Water breakthrough

The end simulation time in this case was 2.2×10^5 $[s]$, which is more than the breakthrough time. Figure 5.16 shows the results for Δt equal to 4×10^3 $[s]$. The gradients $\frac{\Delta J}{\Delta q_t^n}$ and $\frac{\partial \mathcal{H}^n}{\partial q_t^n}$ are not identical for all time steps, although differences are small (1.94 %). Contrary to those in section 5.5.1, the gradients are not of constant magnitude, and furthermore the change in gradient magnitude is nonsmooth for a number of time steps.

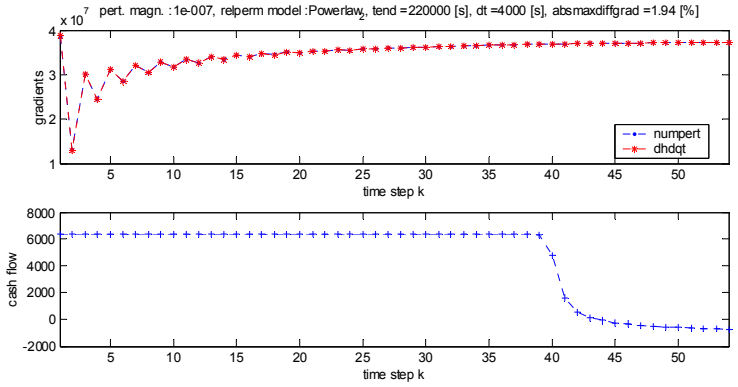

Figure 5.16: Gradients $\frac{\Delta J}{\Delta q_t^n}$ (numpert) and $\frac{\partial \mathcal{H}^n}{\partial q_t^n}$ (dhdqt) and cash flow [$ per time step].

Figure 5.17 shows the results for Δt equal to 2×10^3 $[s]$. Differences between gradients $\frac{\Delta J}{\Delta q_t^n}$ and $\frac{\partial \mathcal{H}^n}{\partial q_t^n}$ are smaller with a maximum absolute difference of 0.11 %. Again the magnitude of the gradients is not constant, the change in magnitude, however, is smoother than in Figure 5.16. The values of the Lagrange multipliers are shown in Figure 5.18.

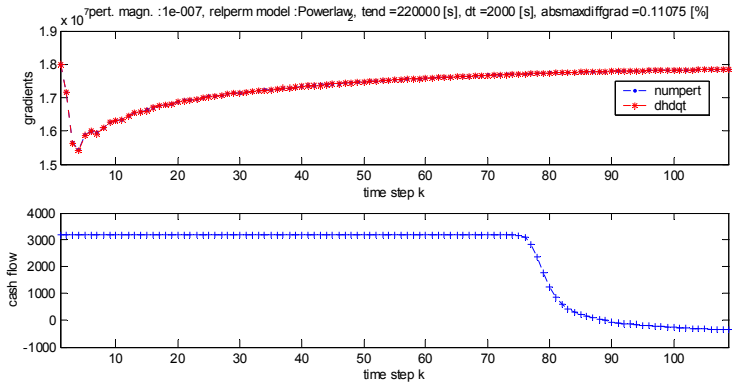

Figure 5.17: Gradients $\frac{\Delta J}{\Delta q_t^n}$ (numpert) and $\frac{\partial \mathcal{H}^n}{\partial q_t^n}$ (dhdqt) and cash flow [$ per time step].

The fact that the error is smaller for smaller time steps size may be due to differences in numerical dispersion. However, a decreased time step size in this case also means the derivative $\frac{\partial f_w}{\partial S_w}$ is calculated more frequently, yielding a more accurate sensitivity.

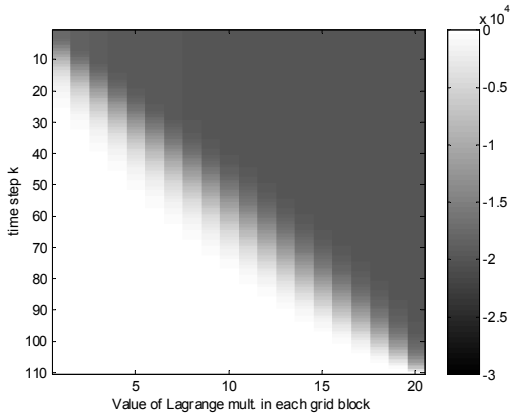

Figure 5.18: Lagrange multipliers for all grid blocks and time steps. $\Delta t = 2 \times 10^3$ $[s]$

The time step size may thus affect the smoothness of the gradients, and thereby the smoothness of the optimal control functions. This is in agreement with observations from Liu

and Ramirez (1994a), who found nonsmooth shapes of the optimal control functions in their steamflood optimization study. They reported that smaller time steps should result in smoother optimal control functions. Figure 5.16 & 5.17 also show that regularization of the gradients may sometimes be desirable.

5.7 Meaning of the Lagrange multiplier values

Figure 5.12 showed that the Lagrange multipliers for case with a first order relative permeability model and zero numerical dispersion either had a value of zero or a value of -20000. These values are discussed in some more detail in this section.

For the fractional flow problem the Lagrange multipliers have the same units as the NPV objective function [$], as can be derived from eqs. 5.7 & D.11. Section 4.6 discussed that the Lagrange multipliers in the adjoint equation reflect the objective function's sensitivity to perturbations in the constraint on the optimal trajectory. Because for the fractional flow example $\frac{\partial g^{j-1}}{\partial x^j} = 1$, they directly give the sensitivity with respect to perturbations in the states. For the one dimensional fractional flow problem eq. 4.25 can be written as (leaving out the time indices)

$$dJ = -\lambda dS_w. \tag{5.12}$$

Eq. 5.12 shows that if a Lagrange multiplier has a value of zero, a change in the water saturation does not influence the objective function value. In Figure 5.12 the value of the nonzero Lagrange multiplier found was -20000 [$], hence

$$dJ = +20000 dS_w \quad [\$]\,. \tag{5.13}$$

Eq. 5.13 states that the maximum value of the objective function J would increase by 20000 $ if a unit increase in the constraint on the maximum water saturation ($S_w^* = 1 - S_{or}$) in the corresponding grid block would be possible. For the one dimensional example considered, a unit increase in the maximum possible water saturation would lead to a shock front at saturation $S_w = 2 - S_{or}$ in the associated grid block. As a result, the production of water would be delayed by one time step, instead oil production would occur. With $S_{wc} = S_{or} = 0$, the total fluid volume V_f in one grid cell is

$$V_f = \Delta x \Delta y \Delta z \phi = 10 \times 10 \times 10 \times 0.2 = 200 \ \left[m^3\right]. \tag{5.14}$$

The value of the liquid in a grid block filled with water (J_w^*) is equal to the product $r_w V_f$, hence with $r_w = -20 \left[\frac{\$}{m^3}\right]$

$$J_w^* = -20 \times 200 = -4000 \ [\$]\,. \tag{5.15}$$

With an oil price r_o of $80 \left[\frac{\$}{m^3}\right]$ the value of the liquid in a grid block filled with oil (J_o^*) is

$$J_o^* = 80 \times 200 = 16000 \ [\$]\,. \tag{5.16}$$

Since production of a volume V_f of water is replaced by production of a volume V_f of oil, the change in the value for the objective function ΔJ upon a unit change in the maximum water saturation is

$$\begin{aligned} \Delta J &= J_o^* - J_w^* \\ &= 16000 - -4000 = +20000 \ [\$] \,. \end{aligned} \tag{5.17}$$

Comparison shows that, for $\Delta S_w = 1$, eqs. 5.13 and 5.17 are the same. For this example the Lagrange multiplier value thus reflects the cost of the physical constraint on S_w. In this case nothing can be done to change this constraint. However, in other cases it may be possible to influence constraints on the states. Constraints on the reservoir pressure may at some locations for instance be manipulated by completing new wells at that location, or by stimulation or water shutoff methods. The values of the Lagrange multipliers may then provide information on suitable locations for new wells, as well as information on the optimal well trajectory for either these new wells or side tracks from existing wells. Constraints on for instance the residual oil saturation may be changed by injecting gas instead of water.

The (physical) meaning of the Lagrange multipliers changes with the objective function that is used. By proper choice of the objective function it may be possible to let the Lagrange multipliers provide information regarding constraints/costs that one wants to investigate.

5.8 Constraints on the controls

Upon calculating the optimal control function the constraints on the controls must be taken into account. Equality constraints could be included in the same way as the dynamic system. Including inequality constraints is, however, more complex. Instead of formally including the constraints, a more ad hoc approach was followed in the present study. It involved rescaling of the gradients before using them in the steepest descent optimizer (discussed in section 4.10.2). The scaling was done in two steps. In the first step, the gradients were rescaled into modified gradients, referred to as $\frac{\partial \mathcal{L}^*}{\partial u}$, that include information on the constraints on the controls. This rescaling was different for the rate-controlled case where no well model is used (section 4.9.1) , and the pressure constrained case where a well model is used (section 4.9.2). Secondly, the gradients were scaled between $+1$ and -1 by dividing them by the largest absolute gradient value.

5.8.1 Constant total injection and production rate

In the rate-controlled scenario no well model was used. The controls are the injection and production rates q_t per well segment. Eqs. 4.29-4.33 showed the constraints for this scenario. Since the total injection and production rates must remain constant the optimization comes down to optimal allocation of injection and production over the individual injector and producer segments. More flow should go to the favorable injectors/producers and less

to the unfavorable injectors/producers. At time step n injectors/producers are considered favorable if their associated gradients $\frac{\partial \mathcal{L}}{\partial \mathbf{u}}$ are higher than the average of all injectors/producers at that time step, and unfavorable is their gradient is lower than this average. All favorable gradients will have positive sign and all unfavorable gradients will have negative sign, if at each time step n the mean injector gradient value is subtracted from the individual injector gradients and the mean producer gradient value from the individual producer gradients. The advantage of this approach is that the amplitude of the (differences in) gradients is preserved. The resulting gradients will be referred to as modified gradients. The modified gradients $\frac{\partial \mathcal{L}^*}{\partial \mathbf{u}}$ for the rate-controlled case are then:

$$\left(\frac{\partial \mathcal{L}^*}{\partial u_{inj}}\right)_i^n = \left(\frac{\partial \mathcal{L}}{\partial q_{t_{inj}}}\right)_i^n - \frac{1}{N_{inj}} \sum_{i=1}^{N_{inj}} \left(\frac{\partial \mathcal{L}}{\partial q_{t_{inj}}}\right)_i^n \tag{5.18}$$

for the injectors, and

$$\left(\frac{\partial \mathcal{L}^*}{\partial u_{prod}}\right)_j^n = \left(\frac{\partial \mathcal{L}}{\partial q_{t_{prod}}}\right)_j^n - \frac{1}{N_{prod}} \sum_{j=1}^{N_{prod}} \left(\frac{\partial \mathcal{L}}{\partial q_{t_{prod}}}\right)_j^n \tag{5.19}$$

for the producers. In eqs. 5.18 & 5.19 n is the time step, N_{inj} the number of injectors, and N_{prod} the number of producers. As a second step, the modified gradients were scaled between -1 and $+1$.

5.8.2 Constant well flowing pressure

In this scenario a well model is used and the controls are the effective valve settings α_{eff} in the injectors and producers. The operating constraints are given in eqs. 4.34 - 4.45. Positive gradients indicate that the valve should be opened further. However, if the valve is already on its maximum setting it cannot be opened further. In a modified gradient $\frac{\partial \mathcal{L}^*}{\partial u}$ it is desirable to include the capacity to further open or close the valve, in order to make the gradients more directly interpretable.

For controls with positive gradients this can be achieved by multiplying the original gradient by the potential to further open the valve. This was done in the following way

$$\left(\frac{\partial \mathcal{L}^*}{\partial u_{pos}}\right)_l^n = \left(a_{eff_l}^{\max} - a_{eff_l}\right)^n \left(\frac{\partial \mathcal{L}}{\partial \alpha_{pos}}\right)_l^n, \tag{5.20}$$

where $a_{eff_l}^{\max}$ is the maximum valve aperture (with $a_{eff_l}^{\max} = 1$ in this study), and a_{eff_l} is the current valve position (value between 0 and 1). If the original gradient is positive, but the valve aperture is already at its maximum, the modified gradient $\frac{\partial \mathcal{L}^*}{\partial u_{pos}}$ is zero. Similarly, for a negative gradient

$$\left(\frac{\partial \mathcal{L}^*}{\partial u_{neg}}\right)_r^n = \left(a_{eff_r} - a_{eff_r}^{\min}\right)^n \left(\frac{\partial \mathcal{L}}{\partial \alpha_{neg}}\right)_r^n, \tag{5.21}$$

where $a_{eff_r}^{\min}$ is the minimum valve aperture (with $a_{eff_r}^{\min} = 0$ in this study), and a_{eff_r} is the current valve position (value between 0 and 1). This means that if the original gradient is

negative, but the valve aperture is already at its minimum, the modified gradient $\frac{\partial \mathcal{L}^*}{\partial u_{neg}}$ will be zero.

The result of the rescaling is that controls that can be significantly changed are weighed heavier in the steepest descent method than controls that are already close to their limits. As a second step the modified gradients $\frac{\partial \mathcal{L}^*}{\partial \mathbf{u}}$ were scaled between -1 and $+1$.

5.9 Computational efficiency of the adjoint

One drawback of the adjoint method is that all states from the forward simulation must be stored. Furthermore, although the adjoint method is efficient in calculating the gradients, the adjoint simulation generally still is computationally demanding. For the cases considered in this study, the computation time for calculating the adjoint is about twice that of the forward system.

The similarity in control strategy for case 1 and 2 in section 5.3, shown in Figure 5.4 & 5.6, suggests that for that example a reduction in the number of time steps of integration of the adjoint equation may be possible without affecting the calculated control strategy. A few other studies also observed that the adjoint may be simulated with larger time step size than the forward scheme [Wu (1999), Dolle *et al.* (2002)]. It is then easiest to calculate the adjoint for a subset of the forward time steps as it avoids the need of having to interpolate the states for unmatched time points. Preliminary tests from this study suggest that in some cases calculating the adjoint for a subset of the forward time steps gave similar improvements per iteration as an adjoint calculated for the full set of time steps, at least for early iterations. In other cases however, the adjoint based on a full set of time steps gave a steeper improvement. Further investigation in this respect is required.

Chapter 6
Optimization results

6.1 Introduction

The optimal control based optimization, described in chapters 3, 4 & 5, was applied to a number of synthetic reservoir models. In section 6.2 a number of two-dimensional, two-phase models containing one smart injector and one smart producer are considered. The scope for improvement is investigated for various permeability distributions, well operating conditions, fluid viscosities, lengths of the optimization window, and discount rates. In reality the reservoir model is of course largely unknown. Optimization should in that case be done based on the most likely reservoir description, which is expected to change as more information, from for example production data, becomes available. In section 6.3 the optimal control based optimization algorithm is combined with a data assimilation method that regularly updates the description of the system based on production data. In sections 6.2 & 6.3 optimization was done from the start of the production process, i.e. for virgin reservoirs. Since a large number of oil fields already have a production history it is also important to consider the scope for water flood optimization in mature reservoirs. This is done in section 6.4. In section 6.5 optimization of a two-dimensional reservoir model with multiple smart injectors and producers is considered. Water flood optimization is not necessarily restricted to smart wells. In section 6.6 the optimization of a two-dimensional field scale pattern flood with vertical wells is considered. Since the wells are not segmented they could be controlled from the surface. In section 6.7, a two-phase, three-dimensional example is discussed. Finally, in section 6.8 optimization of a simple three-phase, three-dimensional reservoir is considered. For the examples in sections 6.2 - 6.6, a two-phase, two-dimensional dynamic system and adjoint formulation was used. For the examples discussed in sections 6.7 & 6.8 a three-dimensional, three-phase formulation for the dynamic system and adjoint was used.

Since the optimization is gradient based it may find a local optimum. Furthermore, the optimization procedure used may not always have converged completely to the absolute local optimum, due to the restricted number of optimization cycles allowed, or due to difficulties with the adjoint equation described in chapter 5. The optimum results obtained in this study therefore represent the lower limit of possible improvement.

6.2 Two-phase flow: 1 smart injector and 1 smart producer

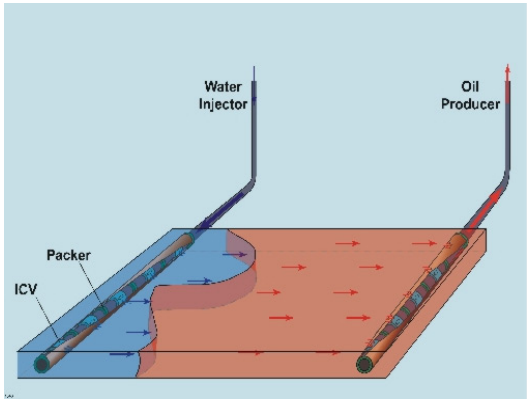

Figure 6.1: Schematic of water flooding with smart, horizontal wells.

Figure 6.1 shows a schematic of a horizontal, two-dimensional reservoir. A smart injector, consisting of a number of segments, is located along the left edge. Similarly, a smart producer is located along the right edge. In this section the scope for water flood optimization for a setting similar to the one shown in the figure is investigated.

Reservoir model

The reservoir model considered in this section is horizontal, square, and two-dimensional. The dimensions are 450×450×10 $\left[m^3\right]$, modeled with 45×45×1 grid blocks. The reservoir boundaries are no-flow boundaries, and the liquids in the reservoir are oil and water, having a viscosity of 1 $[mPa\ s]$. The relative permeabilities are straight such that the total liquid mobility is independent of saturation. Since only water and oil are present, low liquid compressibilities of 1×10^{-10} $\left[Pa^{-1}\right]$ were used. The capillary pressure was taken to be zero. As in Figure 6.1, the injector is located along the left and the producer along the right edge. Each well was divided in 45 segments such that each grid block penetrated by a well represents one segment. Each segment was modeled as a separate well. Optimization was done for three permeability fields, top views of which are shown in figure 6.2. The porosity distribution is homogeneous with $\phi = 0.2$. Figure 6.2 also shows the well locations. In all cases, the principal axes of the high permeability zones are aligned with the main flow direction. These types of heterogeneities have a large impact negative on the macro-scale sweep efficiency, and on early water breakthrough and are in consequence important to investigate [Brouwer *et al.* (2001), Brouwer and Jansen (2002)]. The main difference between the het-

erogeneity types is in the relative amount of oil present in the high permeability zones, in the position of these zones with respect to the wells and the no-flow boundaries, and in the contrast between high and low permeability zones. In heterogeneity type 1 the streak contains about 5-15 % of the oil in place. The contrast in permeability between high permeability streak and the rest of the reservoir is about a factor 20-40. In heterogeneity type 2 the streaks contain about 15-25 % of the oil in place. The contrast in permeability between high permeability zones and the rest of the reservoir is about a factor 25-40. The high permeability zones in heterogeneity type 3 contain about 30-40 % of the oil in place. The contrast in permeability between high and low permeability zones is about a factor 10-30. The initial water saturation in all reservoirs was 0.101.

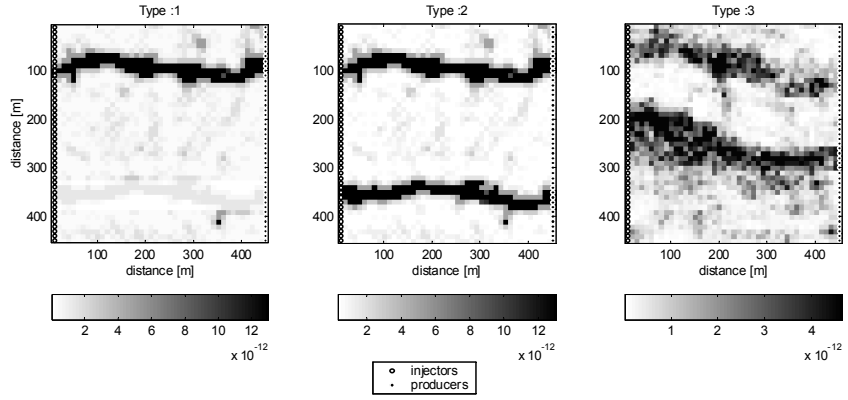

Figure 6.2: Permeability distribution and well locations for heterogeneity type 1 (left), type 2 (centre), and type 3 (right). Top view.

Economic parameters

The relative prices for oil and water production determine the maximum water cut for which the cash flow is positive, i.e. the maximum profitable water cut. In this study, a maximum profitable water cut of 80% was used. To this end the revenue of oil produced was set to \$80 per m^3, the total cost of water produced was set to \$20 per m^3. These are net prices that include costs of associated water injection, which was not considered separately. Both discounted and non-discounted cases were considered. For the discounted cases, the discount factor b was chosen per case such as to obtain a 50% reduction in the oil value and the water costs at the end of the production period.

Approach

For each reservoir the optimized results are compared with results from the corresponding reference case. These reference cases reflect a conventional water flooding scenario. They also served as initial guess for the optimal control function in the optimization procedure. The optimization was done for both rate-controlled operating conditions, in which no well model was used, and pressure-constrained conditions in which a well model was used. In the rate-controlled cases the total injection and production rate was constant and balanced for the entire simulation period. In the pressure-constrained case, total injection rates are approximately equal to total production rates, because of the low liquid compressibilities. The total production time was fixed per case.

6.2.1 Pressure-constrained optimization, one pore volume

In this case the total production time was set such that in the reference case cumulative injection was the equivalent of about one pore volume (PV) of liquids in place. With $S_{wc} = 0.1$ and $S_{or} = 0.1$ this corresponds to the equivalent of about 1.25 mobile oil volume in place. For an ideal displacement this would thus be sufficient to sweep all the oil. The final oil-water saturation distributions for the reference cases are shown in Figure 6.9. It shows significant areas that are still oil saturated.

Scope for improvement

Tables 6.1 shows the results for reference case and the pressure-constrained optimized case, with zero discounting. Table 6.2 shows the results for the discounted cases. The shaded areas indicate where an improvement with respect to the reference case was obtained. For all cases considered an improvement in NPV with respect to the reference case was found, ranging from 10 – 53% .

For heterogeneity types 1 and 3 the increase in NPV resulted from a slight to moderate decrease in oil production combined with a large decrease in water production. This can also be derived from Figure 6.3, which shows the (cumulative) reference and optimized production rates for heterogeneity type I. The decrease in cumulative oil production is due to the maximum profitable water cut of 80%. Allowing a higher maximum profitable water cut (i.e. lower relative water costs) will cause a smaller decrease in cumulative oil production, but also a smaller decrease in cumulative water production.

Type 1
Pressure constrained optimization

	cum oil*	cum water*	cum liq*	mob PV	NPV**
base case	0.19	0.21	0.41	1.26	11.36
opt case	0.18	0.04	0.22	0.68	13.97
diff(%)	-5.5	-82.5	-45.7	-45.7	23.1

Type 2
Pressure constrained optimization

	cum oil*	cum water*	cum liq*	mob PV	NPV**
base case	0.19	0.22	0.41	1.27	10.98
opt case	0.22	0.05	0.27	0.85	16.81
diff(%)	16.2	-76.4	-33.2	-33.2	53.0

Type 3
Pressure constrained optimization

	cum oil*	cum water*	cum liq*	mob PV	NPV**
base case	0.243	0.178	0.421	1.30	15.93
opt case	0.236	0.041	0.276	0.85	18.12
diff(%)	-2.9	-77.1	-34.3	-34.3	13.7

* units: million m3 ** units: million $

Table 6.1: Results reference and pressure-constrained optimized cases. No discounting.

Type 1
Pressure constrained optimization

	cum oil*	cum water*	cum liq*	mob PV	NPV**
base case	0.19	0.21	0.41	1.26	9.14
opt case	0.18	0.03	0.21	0.63	10.58
diff(%)	-8.5	-87.1	-49.5	-49.5	15.7

Type 2
Pressure constrained optimization

	cum oil*	cum water*	cum liq*	mob PV	NPV**
base case	0.19	0.22	0.41	1.27	9.20
opt case	0.22	0.07	0.29	0.91	12.65
diff(%)	16.5	-68.0	-28.6	-28.6	37.4

Type 3
Pressure constrained optimization

	cum oil*	cum water*	cum liq*	mob PV	NPV**
base case	0.243	0.178	0.421	1.30	13.01
opt case	0.239	0.065	0.304	0.94	14.33
diff(%)	-1.4	-63.4	-27.7	-27.7	10.1

* units: million m3 ** units: million $

Table 6.2: Results reference and pressure-constrained optimized cases. Discounting.

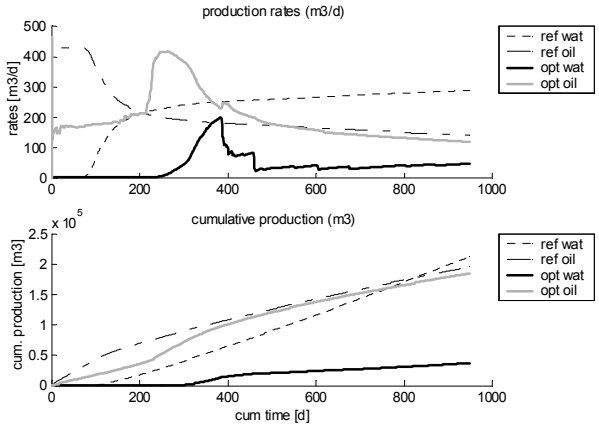

Figure 6.3: Heterogeneity type 1. (Cumulative) production rates for reference and pressure-constrained optimized cases. No discounting.

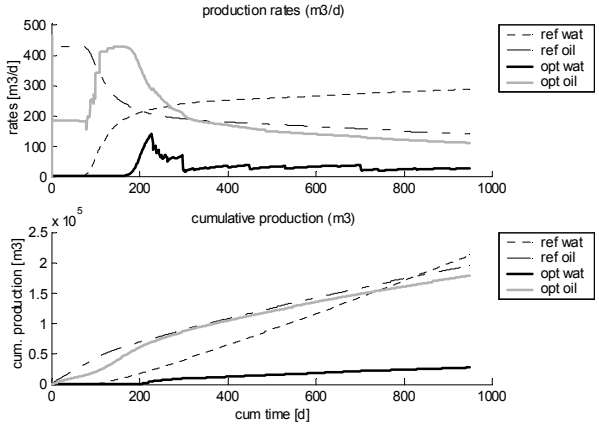

Figure 6.4: Heterogeneity type 1. (Cumulative) production rates for reference and pressure-constrained optimized cases. Discounting.

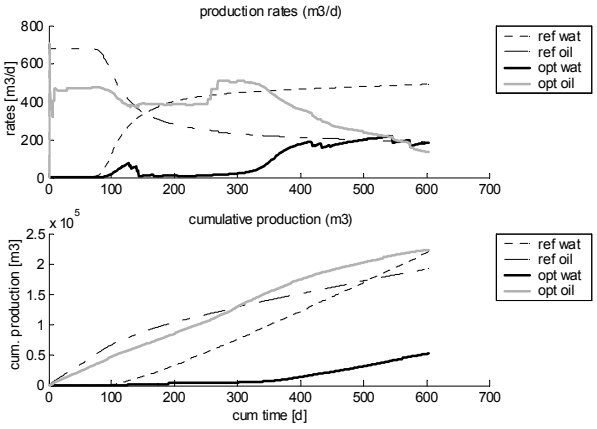

Figure 6.5: Heterogeneity type 2. (Cumulative) production rates for reference and pressure-constrained optimized cases. No discounting.

Figure 6.3 shows that for heterogeneity type 1 the length of the oil plateau production period is similar to the one in the reference case, but plateau production rates occur later in time. Water production is also delayed but in addition drastically reduced. Resultingly, total liquid production rates as well as water injection rates are reduced significantly. The delay in early oil production is largely compensated for in a later stage. Similar observations were made by Yeten *et al.* (2002) and van Delden *et al.* (2001) on a synthetic and a real field example respectively.

Contrary to heterogeneity type 1 and 3, the improvement in NPV for heterogeneity type 2 resulted from both an increase in cumulative oil production and a decrease in water production, as also shown in Figure 6.5. The reason for this difference in scope for improvement will be discussed in section 7.3.3. The results for heterogeneity type 2 will be discussed in more detail on pages 143 - 144.

Tables 6.1 & 6.2 show that for all cases the improvement in NPV with respect to the reference case is lower for the discounted cases than for the undiscounted cases. This is due to the increased importance of accelerated oil production, as for heterogeneity type 2 can be seen by comparison of figs 6.5 & 6.6, and for heterogeneity type 1 by comparison of Figure 6.3 & 6.4. The increased need for high early production rates negatively affects the capacity to reduce water production.

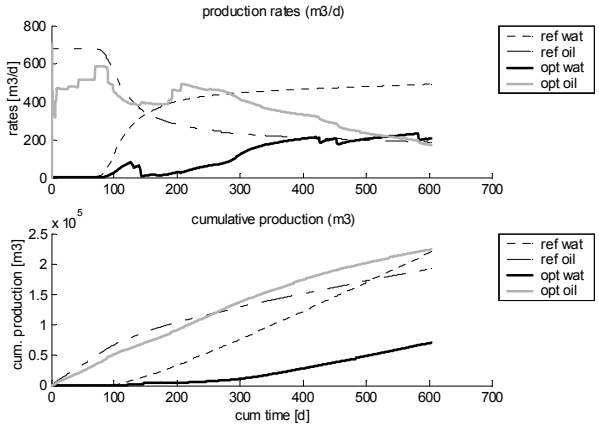

Figure 6.6: Heterogeneity type 2. (Cumulative) production rates for reference and pressure-constrained optimized cases. Discounting.

Optimum valve-settings

In the reference case all valves are fully open. Figure 6.7 shows the optimum valve-settings for the undiscounted optimized cases. For most of the time there is at least one injector or producer segment closed. Figure 6.8 shows the optimum valve-settings for the discounted case. The increased need for high early oil production rates is reflected in the fact that fewer injector valves are closed compared to the non-discounted case. In most pressure-constrained cases the optimum valve-settings take one of the two extremes possible: open or closed. This type of control in which the controls only operate on the extremes, is sometimes also referred to as a 'bang-bang' control [Sudaryanto (1998), Sudaryanto and Yortsos (2000), Sudaryanto and Yortsos (2001)]. For these examples simple on/off valves may be sufficient to optimize water flooding. A more detailed discussion on the type of control is postponed to section 7.4.1. The optimal control functions, shown in fig 6.7, resulted in significantly different oil-water distribution in the reservoir, than for a conventional water flood, as comparison of Figure 6.9 & 6.10 shows.

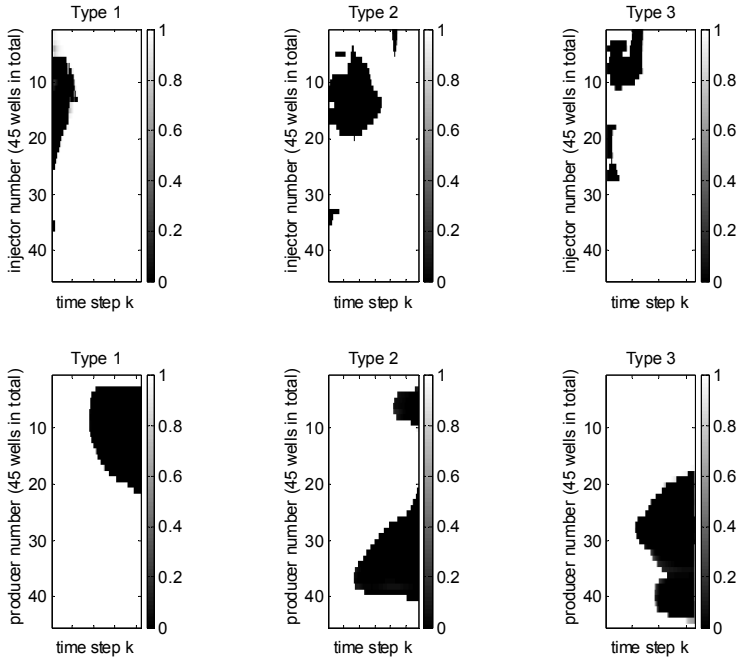

Figure 6.7: Optimum valve-settings for heterogeneity type 1 (left), type 2 (middle) and type 3 (right). The top row shows the optimum settings for the injectors, the bottom row for the producers. The segment number, shown along the vertical axis corresponds to the row number of the grid block in which the segment is completed. No discounting.

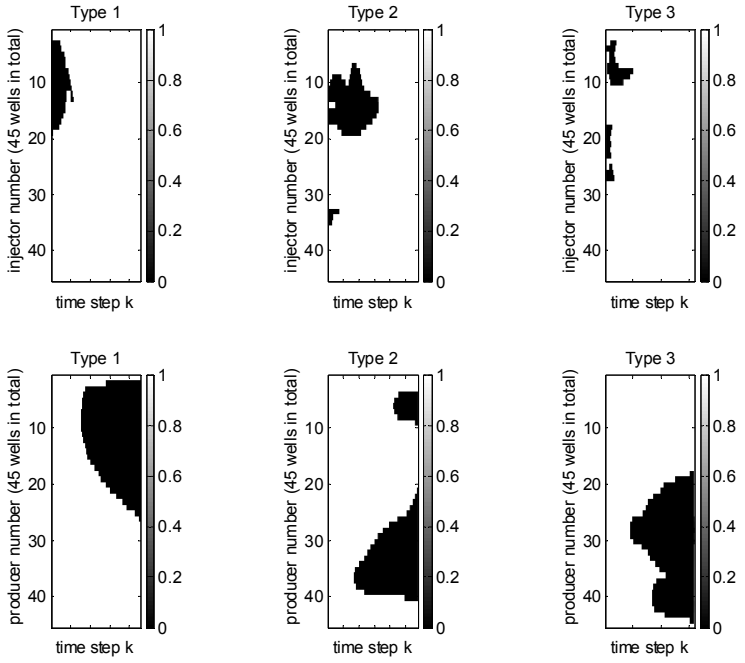

Figure 6.8: Optimum valve-settings for injector and producer segments. Discounting.

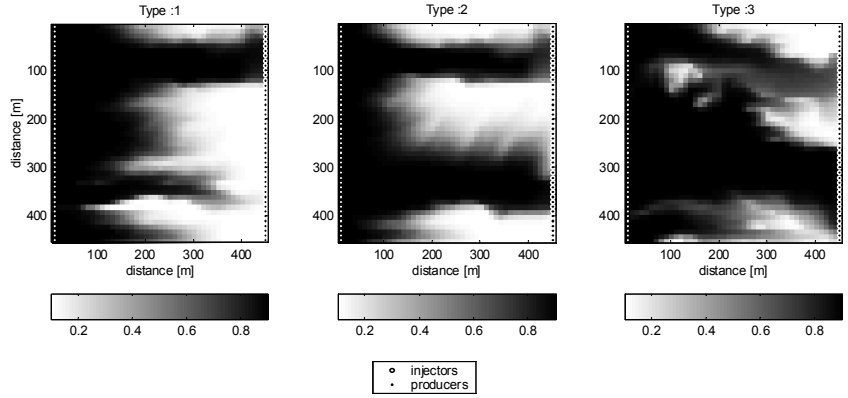

Figure 6.9: Oil-water saturation distribution in reservoir for reference (not optimized) cases after production of about one PV of liquid. Oil-saturated areas are depicted in white, water saturated areas in black.

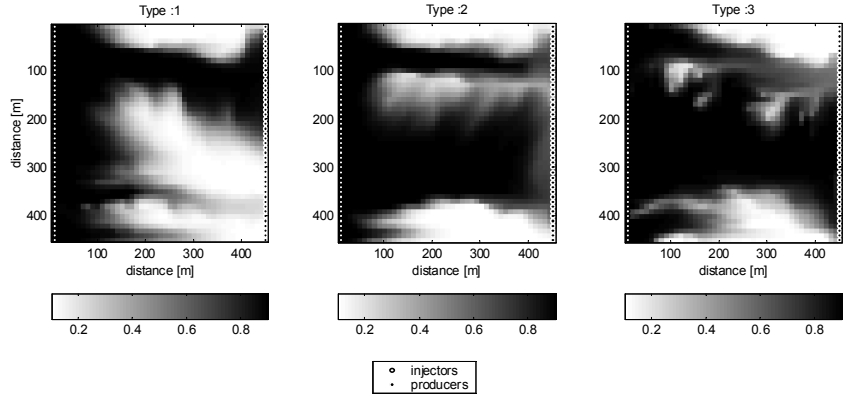

Figure 6.10: Final oil-water saturation distribution in reservoir for optimized, pressure-constrained cases without discounting. Oil-saturated areas are depicted in white, water saturated areas in black.

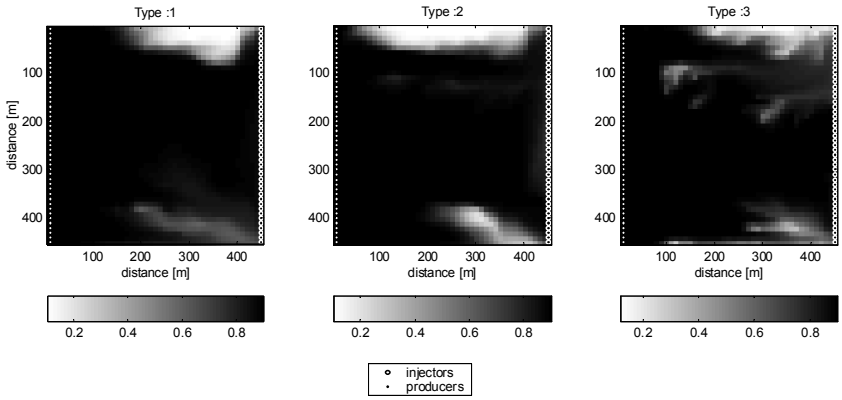

Figure 6.11: Final oil-water saturation distribution in reservoir for non-discounted optimal rate-controlled cases after one PV of liquid production. Oil-saturated areas are depicted in white, water saturated areas in black.

6.2.2 Pressure-constrained optimization, two pore volumes

In the cases considered so far the optimization was done for one PV of liquid production (see tables 6.1 & 6.2). The improvement obtained varied considerably from case to case. This is mainly due to the fact that the main benefit is in cutting back unprofitable water production, i.e. water production that does not carry significant amounts of oil. The chance of this happening is generally larger when the total number of PV's injected/produced is larger. As a result, the scope for optimization should improve for longer production periods. To verify this, the optimization was done for two PV's of production for heterogeneity types 1 & 2. Results for undiscounted reference and optimized cases are shown in table 6.3. Improvements in NPV with respect to the reference case are 46 % and 63 % for heterogeneity type 1 and 2 respectively, indeed higher than the improvements obtained for one PV of production (respectively 21 % and 53 % , table 6.1). Table 6.3 also shows that now in both cases the improvement is realized by a moderate decrease in cumulative oil production, and a large decrease in water production.

6.2.3 Pressure-constrained optimization, variable end time

Results from the previous sections showed that under pressure constrained operating conditions with fixed end time, NPV optimization often resulted from a large decrease in water

Type 1
Pressure constrained optimization

	cum oil*	cum water*	cum liq*	mob PV	NPV**
base case	0.30	0.52	0.81	2.51	13.29
opt case	0.26	0.07	0.33	1.03	19.34
diff(%)	-11.8	-85.6	-58.8	-58.8	45.5

Type 2
Pressure constrained optimization

	cum oil*	cum water*	cum liq*	mob PV	NPV**
base case	0.28	0.54	0.82	2.53	11.68
opt case	0.25	0.05	0.30	0.94	19.01
diff(%)	-10.6	-90.1	-62.9	-62.9	62.8

* units: million m3 ** units: million $

Table 6.3: Results for reference and pressure-constrained optimized cases for 2 PV production in the reference case. No discounting.

production and a slight decrease in oil production. Figure 6.3, 6.4, 6.5 and 6.6 also show that contrary to the reference cases, the optimized cases still produce at a low water cut at the end time. If the end time would be determined by the moment at which the cash flow becomes negative, this would expectedly be reached earlier in the reference case. In the optimized case, increased cumulative oil recovery may then result from extension of the production period with positive cash flow. The scope for optimization may thus be different if the end time is flexible. Table 6.4 and Figure 6.12 illustrate this for heterogeneity type 1. In the reference case the cash flow becomes zero at about 1672 days. In the optimized case the production period with positive cash flow is significantly longer, yielding a 5.8 % higher ultimate oil recovery at 2895 days. At this point the cash flow was still positive, although very small (86 $\frac{\$}{day}$). For a more accurate estimate of the scope for improved with free terminal time, a free terminal time optimal control formulation should be used. This is beyond the scope of this research.

Type 1
Pressure constrained optimization

	cum oil*	cum water*	cum liq*	mob PV	NPV**	t_end***
base case	0.279	0.437	0.715	2.2	13.65	1672
opt case	0.295	0.139	0.434	1.3	20.91	2895
diff(%)	5.8	-68.2	-39.3	-39.3	53.2	

* units: mill ** units: million $ *** units: days

Table 6.4: Results for reference and pressure-constrained optimized cases with variable time.

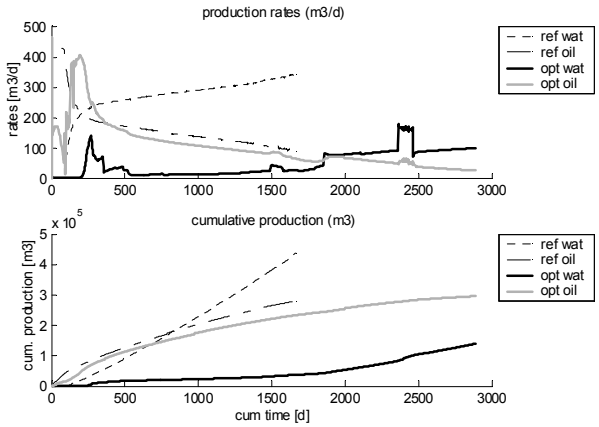

Figure 6.12: Heterogeneity type 1. (Cumulative) production rates for reference and pressure-constrained optimized case. No discounting

6.2.4 Rate-controlled optimization, one pore volume

Section 6.2.1 discussed water flood optimization for one PV production under pressure-constrained well operating conditions. In this section optimization under rate-controlled operating conditions is investigated.

Scope for improvement

Tables 6.5 and 6.6 show results for reference and optimized cases under rate-control. The shaded areas again indicate where improvement with respect to the reference case was ob-

Type 1
Rate controlled optimization

	cum oil*	cum water*	cum liq*	mob PV	NPV**
base case	0.193	0.213	0.406	1.25	11.25
opt case	0.295	0.111	0.406	1.25	21.46
diff(%)	52.8	-48.0	0.0	0.0	90.8

Type 2
Rate controlled optimization

	cum oil*	cum water*	cum liq*	mob PV	NPV**
base case	0.201	0.209	0.410	1.27	11.94
opt case	0.287	0.123	0.410	1.26	20.58
diff(%)	42.9	-41.4	-0.1	-0.1	72.3

Typ 3
Rate controlled optimization

	cum oil*	cum water*	cum liq*	mob PV	NPV**
base case	0.242	0.177	0.420	1.30	15.91
opt case	0.293	0.126	0.420	1.29	21.00
diff(%)	21.0	-28.8	0.0	0.0	32.0

* units: million m3 ** units: million $

Table 6.5: Results for reference and rate-controlled optimized cases. No discounting.

tained. For all cases an improvement in NPV was found, ranging from 32-91% . In all cases the improvement in NPV was achieved by a combination of an increase in cumulative oil production and a decrease in cumulative water production. Figure 6.11 shows the final saturation distributions in the reservoir for the optimized cases. It is clear that the sweep is much better than in the reference cases (Figure 6.9).

Type 1
Rate controlled optimization

	cum oil*	cum water*	cum liq*	mob PV	NPV**
base case	0.193	0.213	0.406	1.25	9.06
opt case	0.297	0.109	0.406	1.25	17.06
diff(%)	53.8	-48.9	0.0	0.0	88.3

Type 2
Rate controlled optimization

	cum oil*	cum water*	cum liq*	mob PV	NPV**
base case	0.201	0.209	0.410	1.27	9.84
opt case	0.291	0.119	0.410	1.26	16.55
diff(%)	44.9	-43.2	-0.1	-0.1	68.2

Typ 3
Rate controlled optimization

	cum oil*	cum water*	cum liq*	mob PV	NPV**
base case	0.243	0.177	0.420	1.30	12.99
opt case	0.305	0.115	0.419	1.29	17.51
diff(%)	25.5	-35.2	-0.1	-0.1	34.8

* units: million m3 ** units: million $

Table 6.6: Results for reference and rate-controlled optimized cases. Discounting.

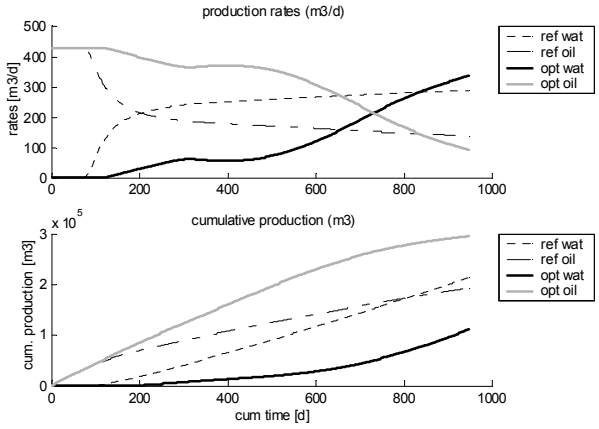

Figure 6.13: Reference and rate-controlled optimized (cumulative) production rates. Heterogeneity type 1. No discounting.

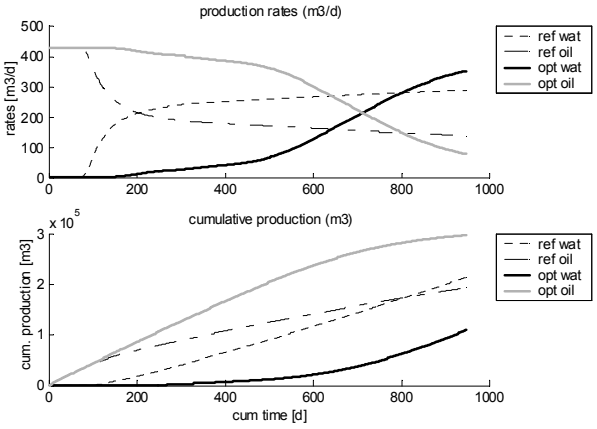

Figure 6.14: Reference and rate-controlled optimized (cumulative) production rates. Heterogeneity type 1. Discounting.

Figure 6.13 shows the reference and optimized production rates for heterogeneity type 1. The plateau production is extended with respect to the reference case, and the oil production rate remains higher for most of the subsequent period. At the end of the production period cumulative oil production is approximately 53% higher than in the reference case, and reduction in cumulative water production is about 48%. Figure 6.14 shows production results for the discounted case. The main difference with the undiscounted case is that the plateau production period is extended somewhat more. The extension of the plateau production period relative to that in the undiscounted cases was observed for all discounted cases. The reason for this is that due to the discounting there is more emphasis on high, early oil production rates and low early water production rates. Tables 6.5 & 6.6 show a weak trend in NPV between the undiscounted and discounted cases. The tables show that cumulative oil production is higher for the discounted cases, although the differences are small. Applying the optimal control functions obtained for the discounted cases to the non-discounted cases would give slightly better results for the latter. The differences could result from the existence of local optima. Alternatively, the differences in the results may be within the accuracy of the optimizer.

Tables 6.5 & 6.6 also show that the performance of the conventional water flood varies more with the permeability field than the performance of the optimized water flood. For the non-discounted reference cases the NPV range is 11.25 - 15.91$\left[10^6\ \$\right]$, for the optimized cases it equals 20.58 - 21.45 $\left[10^6\ \$\right]$. This indicates that by optimized flow control the negative impact of geological features can to some extent be eliminated.

Optimum injection and production rates

The reference injection and production rates per segment for heterogeneity type 1, 2 and 3 are shown in Figure 6.15. The high flow rates in a number of the segments in the reference case coincide with zones of high permeability (Figure 6.2). The optimum injection and production rates per segment are shown in Figure 6.16 for the undiscounted case. They differ significantly from the reference case. The general difference for the producers is that whereas production is mainly from the high permeability zones in the reference cases, it is much more from the low permeability zones in the optimized cases. The optimum injection rates for heterogeneity type 1 and 2 show that injection switches frequently from one (group of) injector(s) to another, especially at the early stage. The optimum injection rates for type 3 do not show this frequent switching. The switching frequency may thus vary with the type of heterogeneity. It may, however, also be a numerical artefact of the optimization procedure, as will be discussed in section 7.4.1. The principles behind optimum injection and production policies are in agreement with those observed in earlier studies [Asheim (1988), Virnovsky (1992), Zakirov *et al.* (1996), Brouwer *et al.* (2001)]. They will be discussed in more detail in chapter 7.

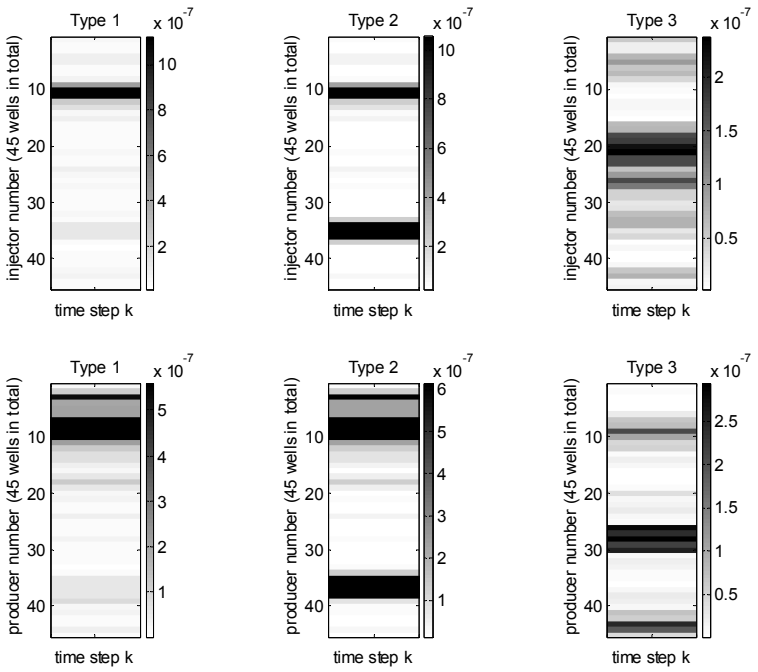

Figure 6.15: Injection rates (top row)and production rates (bottom row) for each well segment for reference (not-optimized) cases. The segment number, shown along the vertical axis corresponds to the row number of the grid block in which the segment is completed. Dark colors indicate high rates, light colors low rates. Rate units $\left[\frac{1}{s}\right]$.

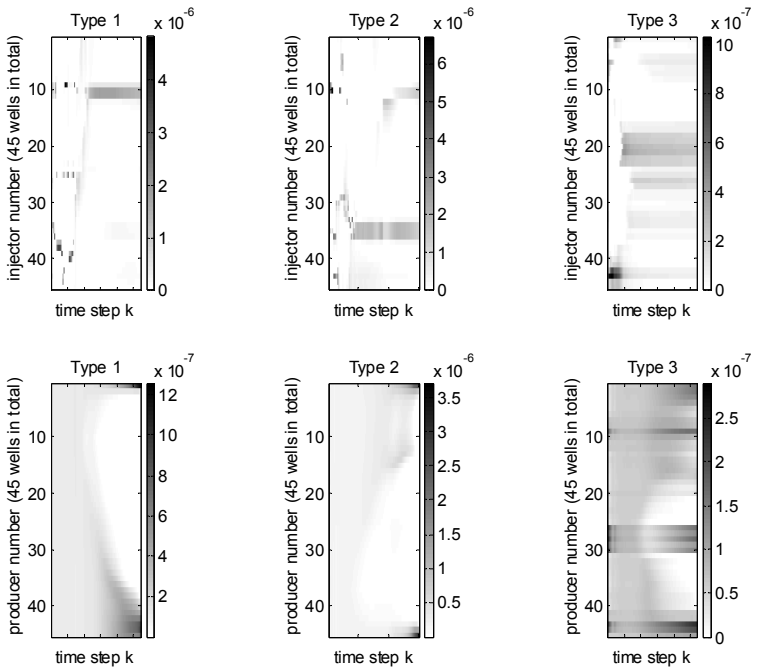

Figure 6.16: Optimal injection rates (top row) and production rates (bottom row) as function of time for non-discounted, rate-controlled cases. Rate units $\left[\frac{1}{s}\right]$.

6.2.5 Pressure- versus rate-constrained optimization

The results from the previous sections show that the scope for optimization depends strongly on the well operating constraints. The two types of constraints investigated represent the extremes of what is possible in practice. It is unlikely that wells can entirely be completely operated on rate constraints, because a too high injection pressure may induce fractures in the reservoir, or a too high drawdown in the producer may for instance cause excessive sand production. It is also unlikely that wells are operated purely on pressure constraints during the entire production process. In the well there may be lift problems causing a decrease in gross production rates as soon as water breaks through or well die-out (zero flow) at a particular water cut. In these situations a reduction in water cut increases the total well rate.

Another possibility may be that field injection or production rates are restricted by surface facilities, rather than flowing well bore pressures. In that case reducing the cycling of water from injectors to producers may directly increase the oil production rate.

6.2.6 Non-unit mobility ratio: Unfavorable displacement

In a non-unit mobility ratio reservoir the total mobility varies with saturation. The rock-fluid and fluid parameters determining the fluid mobility of a phase are the relative permeabilities and the fluid viscosities. Under purely rate-controlled well operation the field injection and production rates are independent of the total mobility in the reservoir. The optimal fluid trajectory and hence the optimal control policy will however change. If production is pressure-constrained the situation is different since a change in the total mobility in the reservoir causes a change in the total injection and production rates. A decreasing fluid mobility may cause the production to go from rate-constrained to pressure-constrained. An increasing fluid mobility in the reservoir will result in increasing well rates and production may as a result go from pressure- to rate-constrained. A third possibility is that the total mobility is minimal at some intermediate water saturation. In this case the production may go from rate- to pressure- to rate-constrained.

In this section the scope for water flood optimization under unfavorable displacement conditions (with a viscosity ratio $\frac{\mu_o}{\mu_w} = 10$) and rate-controlled well operating conditions is investigated for heterogeneity types 1 and 3. As for the unit mobility case, the optimization was done for production, equivalent to 1.25 mobile oil volume in place (MOIP) for heterogeneity type 1, and 1.30 for heterogeneity type 3. For both reference and optimized cases, however, the cash flow became negative before the end time. For the optimized cases this happened close before the end time, for the reference cases this happened earlier. Resultingly, large improvements in NPV were found (170% and 54 % for type 1 and 3 respectively), because the NPV at the end time was lower than the maximum, occurring at an earlier stage). Since production would in reality be stopped at a negative cash flow the results are shown for the production period in which the cash flow is positive.

Table 6.7 shows the results for the reference and optimized cases. Compared to unit mobility displacement conditions (table 6.5) the water flood efficiency is in an absolute sense much worse if displacement conditions are unfavorable, because of the much higher cumulative water production and the much lower cumulative oil production. Comparison of the tables, however, shows that the relative improvement in NPV obtained by water flood optimization is larger under unfavorable displacement conditions. These findings are in agreement with results from Sudaryanto (1998) who found that the absolute displacement efficiency at water breakthrough decreases with increasing mobility ratio $\frac{\mu_o}{\mu_w}$, but the efficiency ratio (improvement of optimized water flood with respect to the reference case) increases with increasing mobility ratio.

For these examples no reduction in water production was achieved because the production periods were not the same. For heterogeneity type 1 the cash flow in the reference case became negative at about 538 days of production. In the optimized case this only happened

Type 1
Unfavorable displacement (muo/muw=10)

	cum oil*	cum water*	cum liq*	mob PV	NPV**
base case	0.078	0.152	0.230	0.71	3.25
opt case	0.151	0.246	0.397	1.22	7.21
diff(%)	93.2	62.1	72.7	72.7	121.7

Type 3
Unfavorable displacement (muo/muw=10)

	cum oil*	cum water*	cum liq*	mob PV	NPV**
base case	0.114	0.175	0.289	0.89	5.64
opt case	0.162	0.246	0.408	1.26	8.06
diff(%)	42.2	40.6	41.2	41.2	43.0

* units: million m3 ** units: million $

Table 6.7: Water flooding results under unfavorable displacement conditions.

at 927 days. For heterogeneity type 3 the cash flow in the reference case became negative at 1196 days, and only at approximately 1687 days in the optimized case.

Figure 6.17 & 6.18 show reference and optimized production rates for heterogeneity type 1 and 3 respectively. Little delay of water breakthrough is realized with respect to the reference case, which is due to the unfavorable viscosity ratio. The figures show that the scope for improvement is both in acceleration of production and extension of the production period.

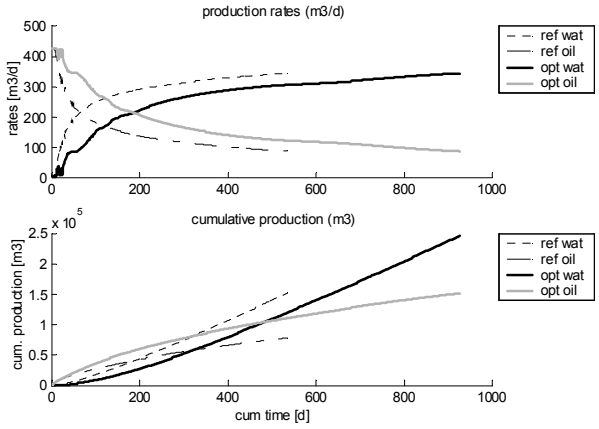

Figure 6.17: Reference and optimized (cumulative) production rates for heterogeneity type 1, under unfavorable displacement conditions.

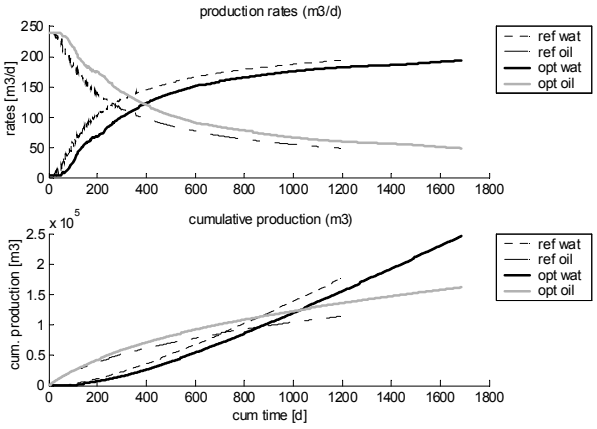

Figure 6.18: Reference and optimized (cumulative) production rates for heterogeneity type 3, under unfavorable displacement conditions.

For these cases, rather than delaying water breakthrough the optimization seemed to be in minimizing the fractional flow of water. Here too the performance of the conventional water flood depends more on the permeability field than the performance of the optimized water flood. The NPV's for the reference cases are 3.25 and 5.64 [million $] for heterogeneity type 1 and 3 respectively, and 7.21 & 8.06 [million $] for the optimized cases.

The saturation distributions at the time at which production was stopped due to a negative cash flow are shown for reference and optimized cases in respectively Figure 6.19 & 6.20. They show that the reservoir is swept better in the optimized cases.

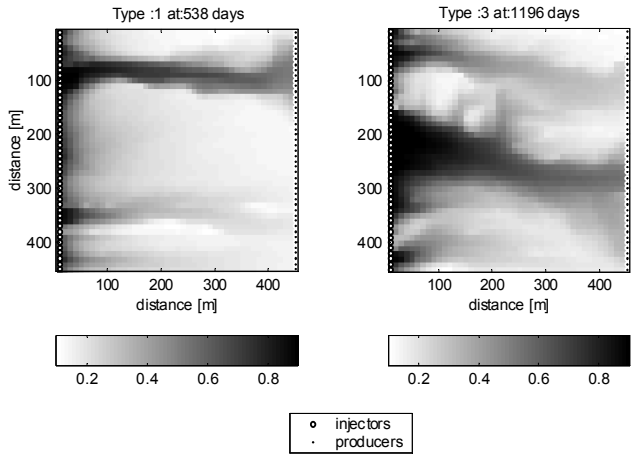

Figure 6.19: Final saturation distribution for reference cases, heterogeneity types 1 and 3 at the day the cashflow becomes negative.

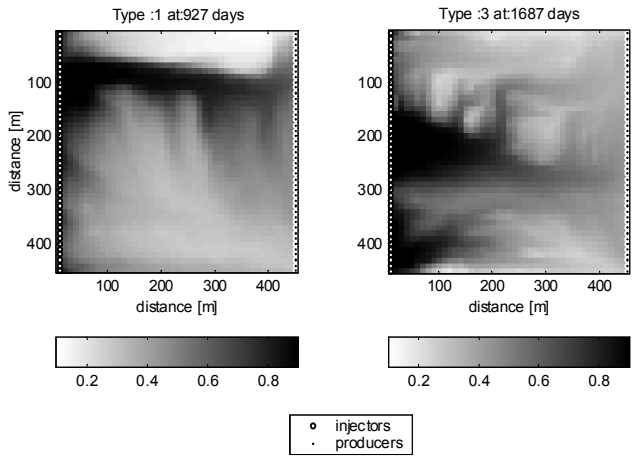

Figure 6.20: Final saturation distribution for optimized cases, heterogeneity types 1 and 3 at the day the cash flow becomes negative.

The optimal control functions for heterogeneity types 1 and 3 are shown in Figure 6.21. They look similar to those for the unit mobility case (Figure 6.16), although a more frequent switching between injectors is observed for heterogeneity type 3. The high frequent switching and very detailed control functions may be due to the fact that near the end time there are few areas left where the fractional flow of water is below 0.8, as a result a detailed control strategy is required to keep the produced water cut below the maximum profitable of 80%. However, the frequent switching may also be a numerical artefact of the optimization procedure, as will be discussed in section 7.4.1.

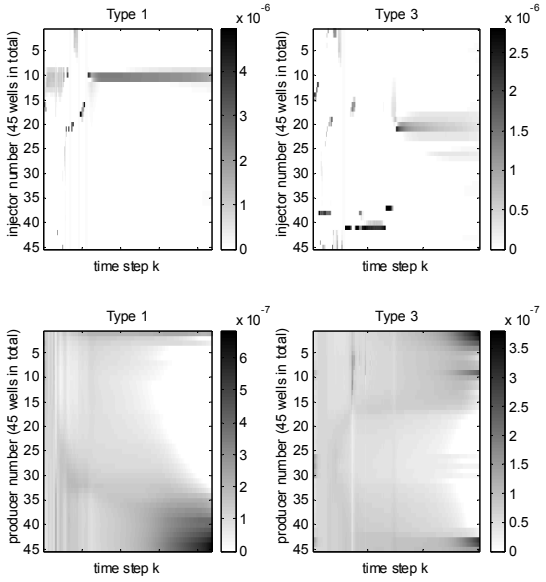

Figure 6.21: Optimal well rates under unfavorable displacement conditions.

6.3 Optimization under uncertainty in reservoir properties

In the previous section optimization was done for a known reservoir model. In reality, however, the reservoir properties are largely unknown, particularly at the early production stage.

In those cases the reservoir properties must be estimated from the data that is available with the aid of a parameter identification method (Figure 1.7).

In this section the optimization of the water flooding process is considered for a synthetic reservoir model that has an initially unknown permeability distribution. To this end, the water flooding optimization algorithm is combined with a parameter identification method, in a closed loop approach (Figure 1.7). As the water flooding process progresses an update of the permeability distribution is calculated at various points in time, based on production data. After the update the optimal injection and production strategy is (re)calculated for the remainder of the production process. A flow chart of the closed-loop optimization procedure is shown in Figure 6.22.

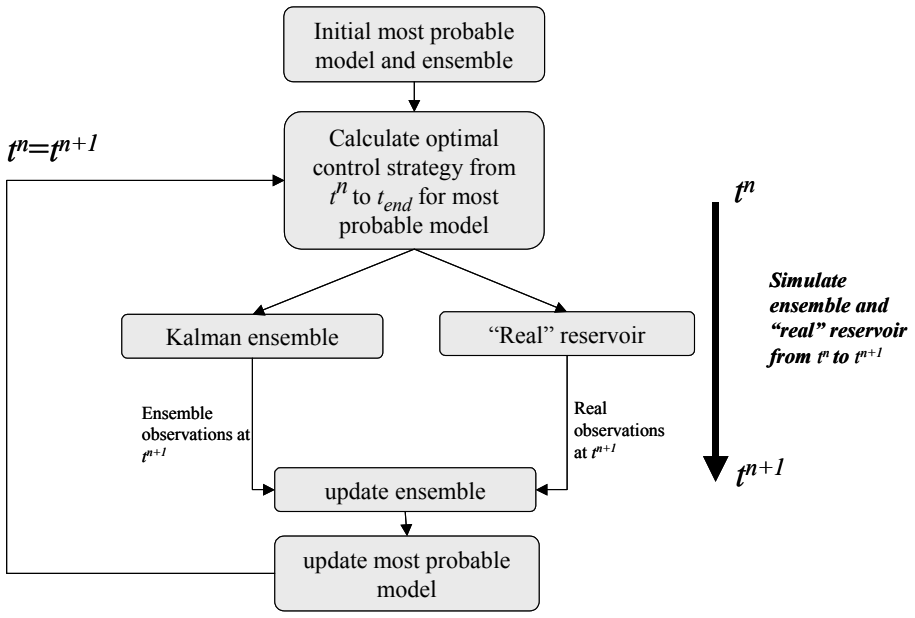

Figure 6.22: Flow chart of closed loop optimization procedure.

As the permeability in the reservoir is initially assumed unknown, the initial optimal control function must be calculated for the initially estimated permeability field. In this example, at the start of the production process the permeability field was assumed to be homogeneous, as shown in the upper left picture of Figure 6.23. The reason for this choice is the following: Sudaryanto (1998), Sudaryanto and Yortsos (2000) and Sudaryanto and Yortsos (2001) found for the examples they considered that if the permeability field is unknown, some improvement can often still be achieved by assuming the permeability distribution to be homogeneous and to calculate the optimal control function for this homogeneous reservoir model.

Similar findings were done in this study for rate-controlled well operating conditions. In the absence of any information on the permeability field a good initial guess for it may therefore be a homogeneous permeability distribution, and a good initial guess for the optimal control function may then be the control function that gives optimal displacement for this homogeneous field.

After start of the production process an improved estimate of the permeability distribution was obtained from production data, with the aid of the ensemble Kalman filter data assimilation method from Naevdal *et al.* (2003)[6]. Naevdal *et al.* (2002a), Naevdal *et al.* (2002b) and Naevdal *et al.* (2003) used the ensemble Kalman filtering technique to update the reservoir model description by assimilating the production data. Both dynamic variables, such as pressures and saturations, and static parameters, such as the permeabilities, were updated in the reservoir model, giving improved forecasts. For the examples considered, the main trends in the permeability field could often be estimated quickly with the filter method, in some cases already after a few days.

The Kalman filter computations are based on an ensemble of realizations of the reservoir model. The filter consists of sequentially running a forecast step, followed by an analysis step. The forecast step consists of running a reservoir simulation for each of the model realizations up to the time at which new measurements are to be assimilated, yielding the forecasted states $\mathbf{s}_f^n$ for the analysis step. At the analysis step, the analyzed state $\mathbf{s}_a^n$ of each ensemble member is computed according to

$$\mathbf{s}_a^n = \mathbf{s}_f^n + \mathbf{K}^n \left(\mathbf{d}^n - \mathbf{H}\mathbf{s}_f^n \right), \tag{6.1}$$

where matrix $\mathbf{H}$ gives the correspondence between the state vector $\mathbf{s}_f^n$ and the measurements in vector $\mathbf{d}^n$. Matrix $\mathbf{K}^n$ is the Kalman gain matrix, which at time n is

$$\mathbf{K}^n = \mathbf{P}^n \mathbf{H}^T \left(\mathbf{H}\mathbf{P}^n \mathbf{H}^T + \mathbf{R}^n \right)^{-1}. \tag{6.2}$$

Matrix $\mathbf{P}^n$ in eq. 6.2 is the error covariance matrix for the states of the system at time step n, and matrix $\mathbf{R}^n$ is the covariance matrix for the measurement errors at time step n. The method is described in detail in Naevdal *et al.* (2003).

The size of the ensemble was taken to be 100. An initial constant pressure and connate water saturation distribution were assumed for each ensemble member. The 100 realizations for the permeability field were generated based on the initial homogeneous estimate, using a mean correlation length of 20 grid blocks with a standard deviation of 1 grid block.

The initial optimum injection and production strategy was applied to the real reservoir (in this study replaced by a numerical reservoir model representing the true reservoir), and to the 100 realizations in the ensemble. At t_1 the first analysis step was conducted. The forecasted and the measured pressures were compared, and an update of the analyzed state of each ensemble member was computed. From the updated ensemble an update of the mean pressure, saturation, and permeability distribution was calculated, based on which the

[6] This work was done in close cooperation with Geir Naevdal from Rogaland Research (Norway) during his three-month stay as a visiting scientist at Delft University of Technology.

Initial permeability estimate	202	(mD)
Mean correlation length	20	(grid blocks)
St. dev correlation length	1	(grid block)
Size of ensemble	100	
Variance in ln perm field*	1.5	

* In the Kalman filter all permeability related parameters were expressed in millidarcies

Table 6.8: Values used in the Kalman filter.

optimum injection and production strategy was recalculated for the remaining producing period. This cycle was repeated at various points in time.

The production data were the pressures in the grid blocks in which a well was completed. The error in the pressure measurements was taken to be low, with a standard deviation of 0.2 Bar. In addition, liquid injection and production rates were assumed known without error in all wells. The total simulation time was fixed at 949 days. The true permeability field for this example was heterogeneity type 1, shown in Figure 6.2. It also shows the locations of the injection and production wells. Apart from the permeability all rock, fluid and rock-fluid properties were assumed known. They are described in section 6.2. Table 6.8 shows values for some of the parameters used in the Kalman filter.

The mean forecasts for the permeability field at the measurement times are shown in Figure 6.23. Already after a few days a reasonable estimate of the trend in the permeability field was obtained. Although the exact permeability field was not retrieved, the main large scale variations in the permeability field were and this may be most important for water flood optimization purposes.

After each update (Figure 6.23) the optimal control function was recalculated for the remaining producing period. Upon recalculating the optimal control function, only three iterations were done instead of iterating until convergence was obtained, mainly to reduce computational time. In addition, however, a too detailed optimal control function may not be desirable at an early stage, because the estimated states might change considerably at the next assimilation time. Since there were 10 assimilation times at which the control function was recalculated, the total number of iterations equalled 30. This was expected sufficient, since for the examples discussed in section 6.2 typically 5-20 iterations were required for convergence.

Figure 6.24 shows the resulting production rates. The production rates for the reference case and the optimized production rates, based on an a priori known permeability distribution (section 6.2), are included for comparison. The production rates resulting from the combined optimization-assimilation (closed-loop) approach are significantly better than those for the reference case. Furthermore, the figure shows that they are quite close to the optimal production rates that would result if the permeability field would have been known in advance. Figure 6.25 shows the final saturation distributions in the reservoir for the reference case, for the rate-controlled optimized case with an a priori known permeability field, and for the

closed-loop optimized case. The final saturation for the closed-loop optimized case is close to that of the optimized case with an a priori known permeability field.

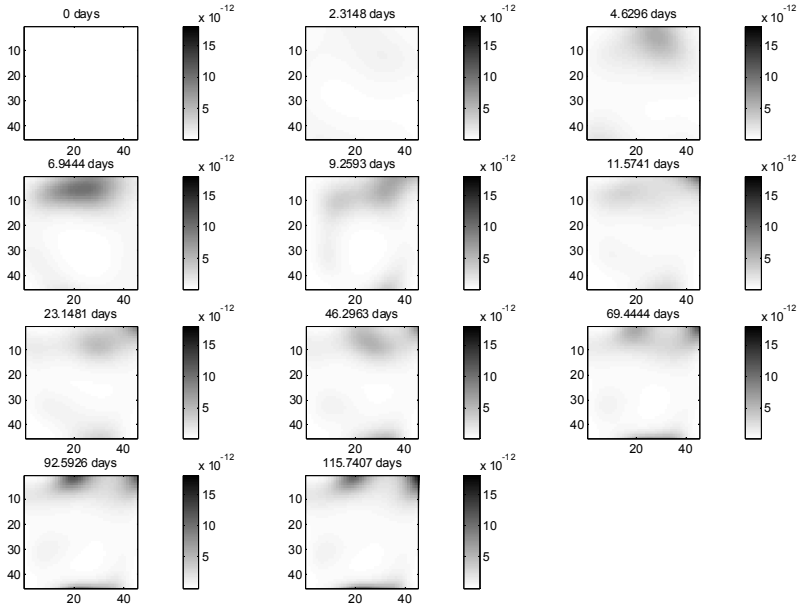

Figure 6.23: Mean forecast for permeability field. Units $\left[m^2\right]$.

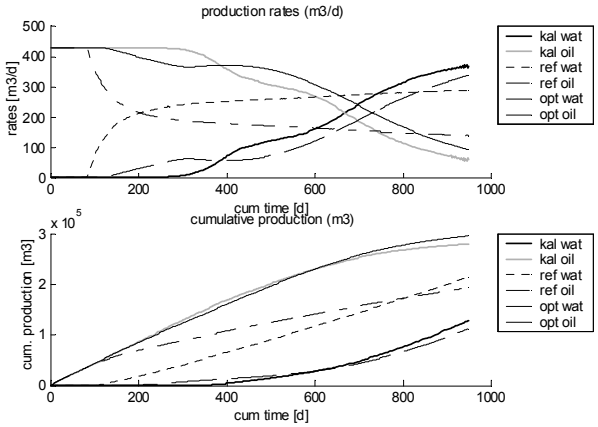

Figure 6.24: Production rates for the reference case, the optimized case for a known permeability field, and the closed-loop optimized case.

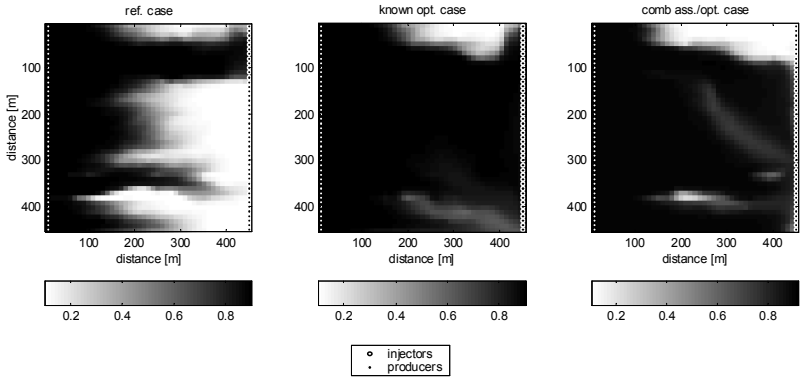

Figure 6.25: Final saturation for the reference case, the rate-controlled optimized case for a known permeability field, and the closed-loop optimzed case.

The early results in this section show that significant improvement in the water flooding process may in principle be feasible with a closed-loop approach, even if the permeability distribution in the reservoir is initially unknown. However, significant effort is still required

to test its feasibility for various geological features, for three-dimensional reservoirs, and larger measurement errors.

6.4 Optimization in mature reservoirs

In section 6.2 optimization was done for reservoirs that do not yet have any production history. Since a large number of oil fields already have been producing for many years it is also important to consider the scope for water flood optimization in these mature reservoirs. If the scope is significant it may be worthwhile to equip existing conventional wells with smart well instrumentation in order to improve the remainder of the production process.

In this section the scope for water flood optimization in mature reservoirs is discussed. The reservoir model considered was heterogeneity type 1, discussed in section 6.2. In that section the results are shown for optimized flow control, starting at $t = 0$ days, i.e. 0 PV production. In this section optimization starting at a later time is investigated, i.e. at 189 days (0.2PV), 378 days (0.4 PV), 568 (0.6 PV), and 757 days (0.8 PV). The end time was kept fixed at 949 days, corresponding to about 1 PV of production.

6.4.1 Scope for improvement

The results for pressure- and rate-constrained optimization are shown in table 6.9 & 6.10, and in Figure 6.26. They show that significant improvement can still be realized if optimized flow control starts at a later stage of the waterflooding process. The scope for improvement reduces with later deployment of optimized flow control, but only significantly if its time as fraction of the total production time is very short, i.e. if it starts close to the end time. The reduction in scope with decreased dynamic flow control time, with the scope ultimately reducing to zero, partly results from the fact that the end time was fixed in this example. The results in table 6.9 and in Figure 6.26 thus actually represent the scope for improvement as function of the fractional optimized flow control period (the optimized flow control period t_{df} as fraction of the total production period t_{tot}), with control starting at $t_{tot} - t_{df}$. If the end time would be flexible, the scope for improvement would be higher, as will be explained later in this section.

Rate Control

	time (days)	time step k	PV	rec. moboil @ start*	impr. NPV (%)
1 0.0PV	0.0	1	0	0	90.8
2 0.2PV	189.1	176	0.2	0.21	88.6
3 0.4PV	378.1	339	0.4	0.32	83.5
4 0.6PV	567.2	503	0.6	0.42	69.2
5 0.8PV	756.2	666	0.8	0.51	38.6
6 1.0PV	945.3	829	1	0.60	0

Pressure Control

	time (days)	time step k	PV	rec. moboil @ start*	impr. NPV (%)
1 0.0PV	0.0	1	0	0	23.1
2 0.2PV	189.3	176	0.2	0.21	18.3
3 0.4PV	378.5	339	0.4	0.32	18.3
4 0.6PV	567.8	503	0.6	0.42	16.3
5 0.8PV	757.0	667	0.8	0.52	11.1
6 1.0PV	946.3	830	1	0.60	0.0

*cumulative oil production as fraction of total mobile oil in place at start of dynamic control

Table 6.9: Improvement with respect to reference case for rate and pressure controlled well operating conditions, with flow control starting after 0.2, 0.4, 0.6, and 0.8 PV of production.

Type 1, Pressure constrained optimization

	cum oil*	cum water*	cum liq*	mob PV	NPV**
base case	0.195	0.212	0.407	1.26	11.36
0 PV					
	cum oil*	cum water*	cum liq*	mob PV	NPV**
opt case	0.184	0.037	0.221	0.68	13.97
diff(%)	-5.5	-82.5	-45.7	-45.7	23.1
0.2 PV					
	cum oil*	cum water*	cum liq*	mob PV	NPV**
opt case	0.185	0.069	0.254	0.78	13.44
diff(%)	-5.0	-67.6	-37.6	-37.6	18.3
0.4 PV					
	cum oil*	cum water*	cum liq*	mob PV	NPV**
opt case	0.185	0.069	0.254	0.78	13.44
diff(%)	-5.0	-67.6	-37.6	-37.6	18.3
0.6 PV					
	cum oil*	cum water*	cum liq*	mob PV	NPV**
opt case	0.194	0.115	0.309	0.95	13.20
diff(%)	-0.6	-45.7	-24.1	-24.1	16.3
0.8 PV					
	cum oil*	cum water*	cum liq*	mob PV	NPV**
opt case	0.198	0.163	0.361	1.11	12.61
diff(%)	1.8	-23.1	-11.2	-11.2	11.1

* units: million m3 ** units: million $

Table 6.10: Results for pressure-constrained optimization.

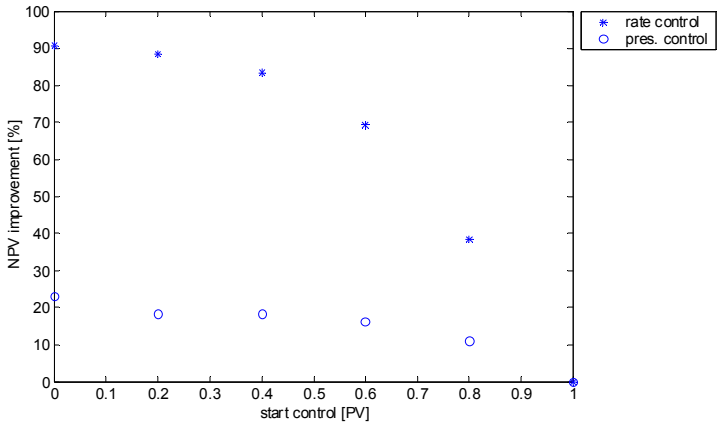

Figure 6.26: Improvement in NPV with respect to the reference case versus the time of start of optimized flow control (expressed in PV already produced).

For pressure-constrained optimization starting at the beginning of the production process, the improvement is realized by a moderate decrease in cumulative oil recovery and a large decrease in water production. With control starting at a later stage the scope changes more towards a combined increase in cumulative oil recovery and decrease in water production, as shown in table 6.10.

Figure 6.27 shows that at the start of control the water production rates go down, and the oil production rates go up. This is due to a change in the flow paths along which fluids move through the reservoir, induced by closing a number of the producer segments. For optimized control starting at 0.2 PV no improvement was found compared to the case where control starts at 0.4 PV. Various strategies were found that gave approximately (within 0.1%) the same results as for the 0.4 PV control function, however with a different strategy. The reason for this is likely to be due to local optima, or inaccuracies in the optimization method. Figure 6.30 shows that the control strategy changes significantly between 0 and 0.4 PV, which may cause difficulties as the local optima may also change quickly in this interval. Finally, it was decided to use the same control function for the 0.2 PV and the 0.4 PV case.

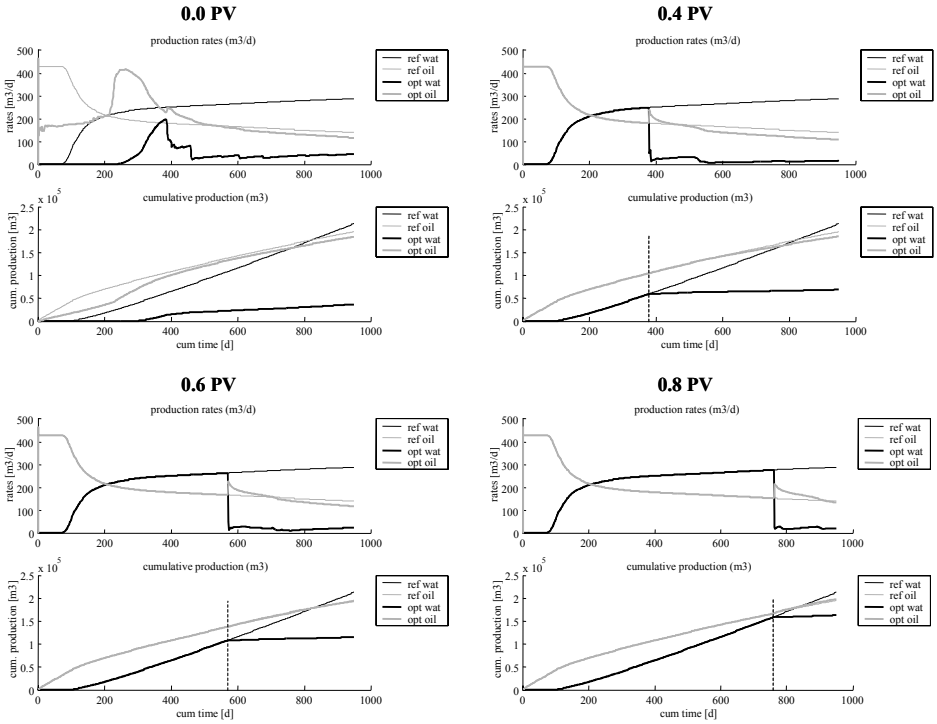

Figure 6.27: Results for reference and pressure-constrained optimized case with optimized control starting at 0, 0.4, 0.6, and 0.8 PV production. Vertical bars indicate start of optimization.

Figure 6.28 & 6.29 show the reference and optimized production rates under rate-controlled well operating conditions. For all, the oil production rates go back to (almost) the plateau rate, and water production back to almost zero upon start of optimized flow control. The figures show that in all cases there is accelerated production, increased cumulative oil recovery and reduced water production. The scope for improvement decreases with decreasing dynamic flow control time, but only significantly if the optimization starts at a late stage. Besides, Figure 6.29 shows that for the cases where the optimization starts late, the oil production rates are still high at the end time. Extra improvement could be realized for these cases by extending the production period.

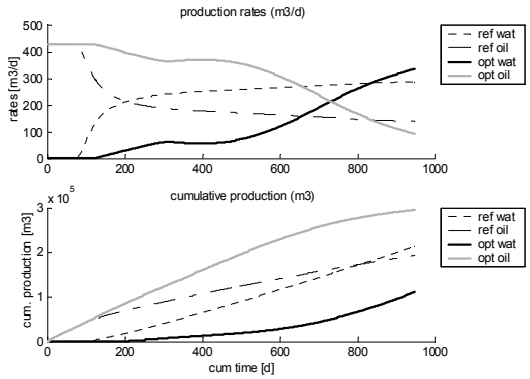

Figure 6.28: Results for reference and rate-controlled optimized case, with optimized control starting at 0 PV production.

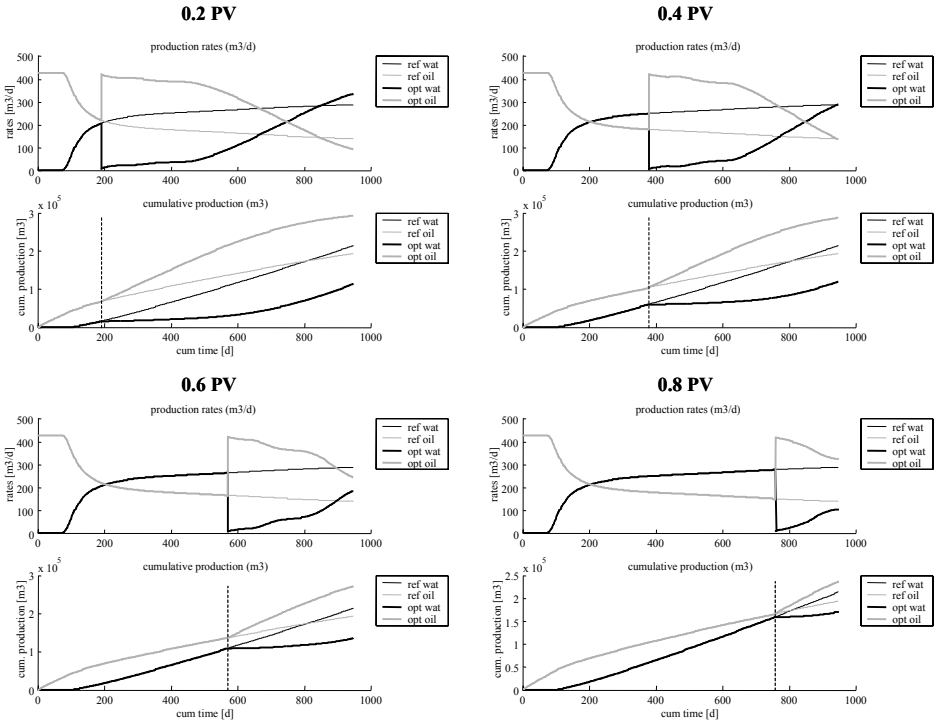

Figure 6.29: Results for reference and rate-controlled optimized case with optimized flow control starting at 0.2, 0.4, 0.6, and 0.8 PV production. Vertical bars indicate start of optimization.

6.4.2 Optimal control functions

Figure 6.30 shows the optimum valve-settings in the wells for the pressure-constrained optimized cases. Only for optimization starting at $t = 0$, choking occurs at the injection side. In all other cases choking only occurs at the producer wells. This may be attributed to the fact that for all other cases the optimization started at a time at which water breakthrough had already occurred. Furthermore, as optimized flow control starts later the optimization becomes more local, because relative to the remaining control time there is more oil in the reservoir. The optimum rates per segment for the rate-controlled scenarios are shown in Figure 6.31 & 6.32. The figures show that control is occurring both in injectors and producers. For optimization starting at 0.2 PV, the improvement in NPV is close to that of optimization starting at the beginning, i.e. at 0 PV. Comparison of the control functions for these two cases, how-

ever, shows that especially the injection strategy is different. This suggests that there may be multiple, significantly different control functions giving similar end results. One reason for the difference in control strategies may be that if optimization starts at 0 PV, the reservoir is almost completely depleted of oil close to the end time. The frequent switching at the injectors may in that case be required to produce the last (relatively small) amount of oil left in the reservoir. The high frequent switching may, however, also be a numerical artefact of the optimization procedure, as will be discussed in section 7.4.1.

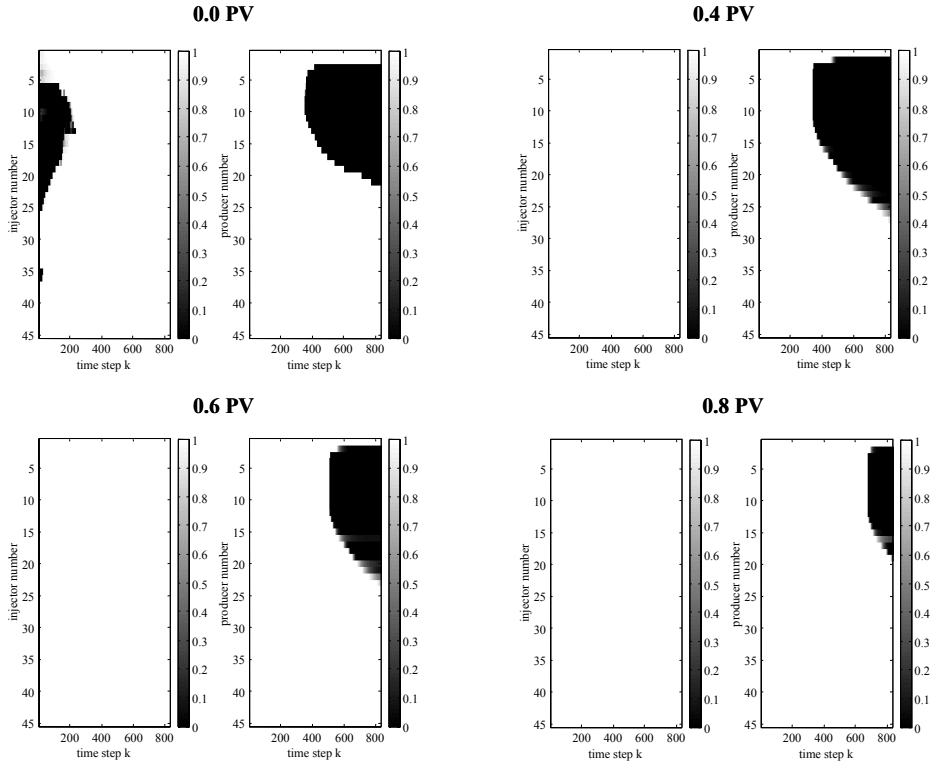

Figure 6.30: Valve-settings for optimization starting at 0.0, 0.4, 0.6, and 0.8 PV of production.

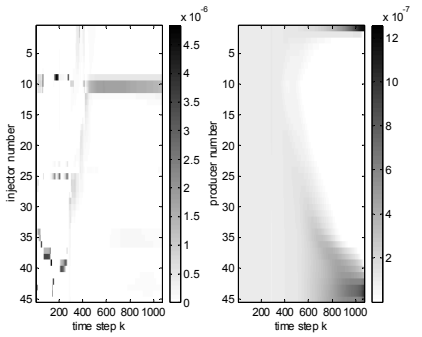

Figure 6.31: Optimal injection and production rates for rate-controlled optimization starting at 0 PV.

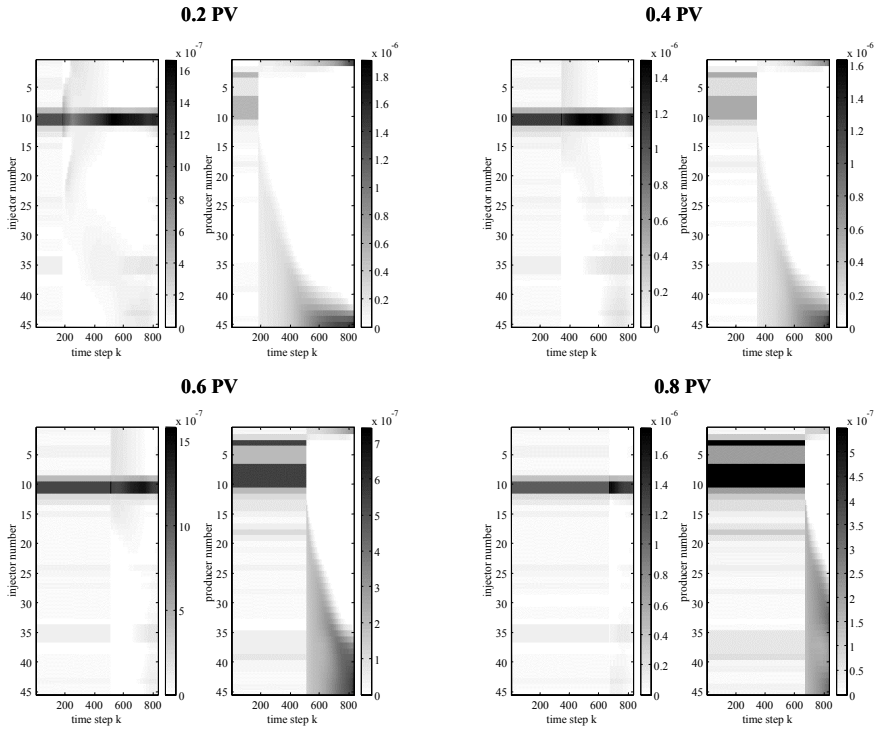

Figure 6.32: Optimum well rates with flow control starting at 0.2, 0.4, 0.6 and 0.8 PV production.

6.5 Multiple smart injectors and producers

In this section the optimization of a system with multiple injection and production wells, each consisting of 30 segments, is considered. Again, each segment is modeled as a separate well. A top view of the permeability field and the well locations are shown in Figure 6.33. The reservoir dimensions are $300\times1200\times10$ m^3, modelled with $30\times120\times1$ grid blocks.

Pressure constrained optimization	cum oil*	cum water*	cum liq*	mob PV	NPV**
base case	0.390	0.474	0.864	1.50	21.93
opt case	0.365	0.170	0.535	0.93	25.86
diff(%)	-6.5	-64.1	-38.1	-38.1	17.9
Rate controlled optimization					
base case	0.382	0.481	0.863	1.50	21.34
opt case	0.529	0.334	0.864	1.50	36.57
diff(%)	38.4	-30.5	0.0	0.0	71.4

* units: million m^3 ** units: million $

Table 6.11: Results for reference and optimized cases.

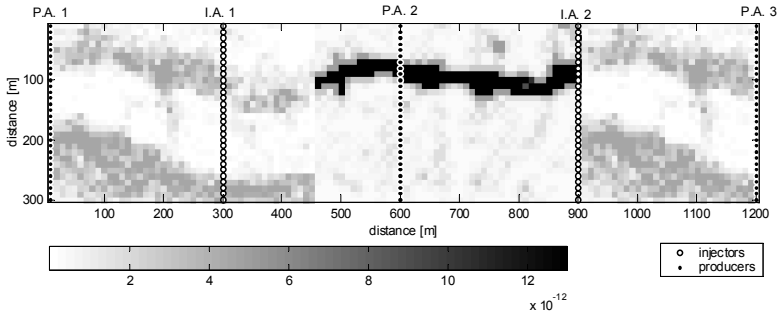

Figure 6.33: Top view of permeability field with 3 smart producers and two smart injectors, called respectively P.A.1, P.A.2, P.A.3, I.A.1, and I.A.2.

Other rock fluid properties are the same as in section 6.2. The optimization was done for cumulative production equivalent to 1.5 pore volumes of mobile oil in place, with zero discounting. As injection and production occur at different locations, multiple oil-water fronts are formed that move in different directions. The final saturation distribution for the reference case is shown in Figure 6.35.

6.5.1 Scope for improvement

The results for the reference case and for the pressure- and rate-controlled optimization are shown in table 6.11. Under pressure-constrained well operating conditions the improvement is realized by a moderate decrease in oil production and a significant reduction in water

production. The final saturation distribution is shown in Figure 6.36. For the rate-controlled case, there is an improvement in both cumulative oil and water production, as well as in acceleration of production. Figure 6.34 shows that in the optimized case water breakthrough occurs slightly earlier than in the reference case. Between day 60 and 850, however, the oil production rates are significantly higher in the optimized case. After 850 days the oil production rate is again lower, which is attributed to the fact that the reservoir is almost depleted of oil, as shown in Figure 6.37.

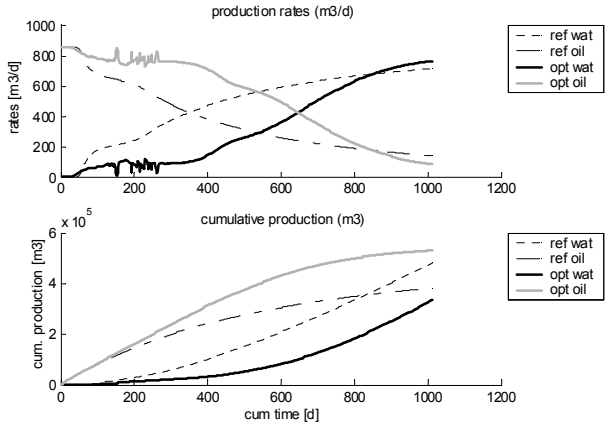

Figure 6.34: Production rates for reference and rate-controlled optimized case.

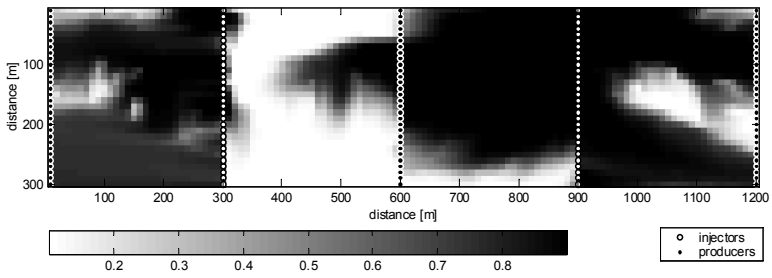

Figure 6.35: Final saturation for reference case.

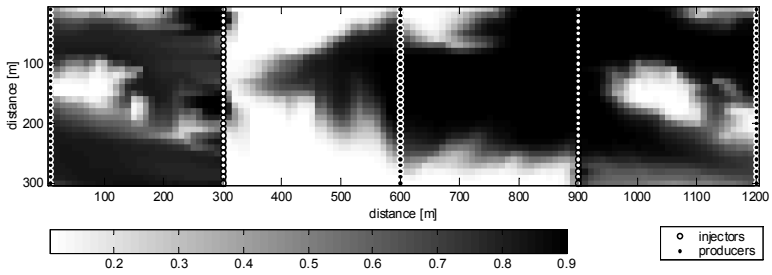

Figure 6.36: Final saturation for pressure-constrained optimized case.

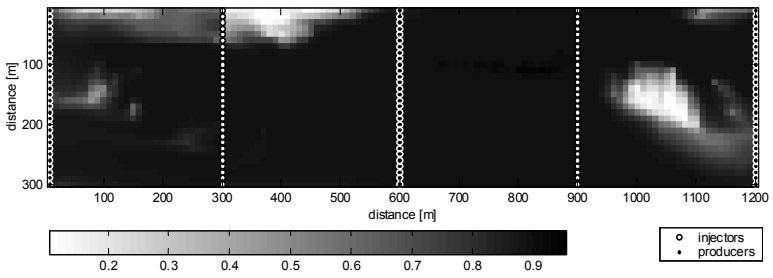

Figure 6.37: Final saturation for rate-controlled optimized case.

6.5.2 Optimal control functions

Figure 6.38 shows the optimum valve-settings for the pressure-constrained optimized case. Reduction of water production is entirely realized by choking at the production wells. All injectors remain open. Figure 6.39 shows the optimal well rates for the rate-controlled case. Flow control occurs both at the injectors and the producers. At the early stage injection and production switch frequently between wells, followed by a period during which changes in well rates are more gradual.

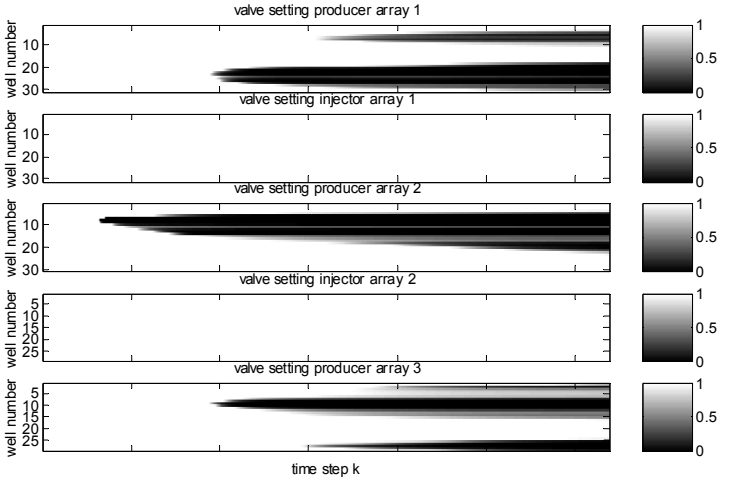

Figure 6.38: Optimum valve-settings for pressure-constrained optimization.

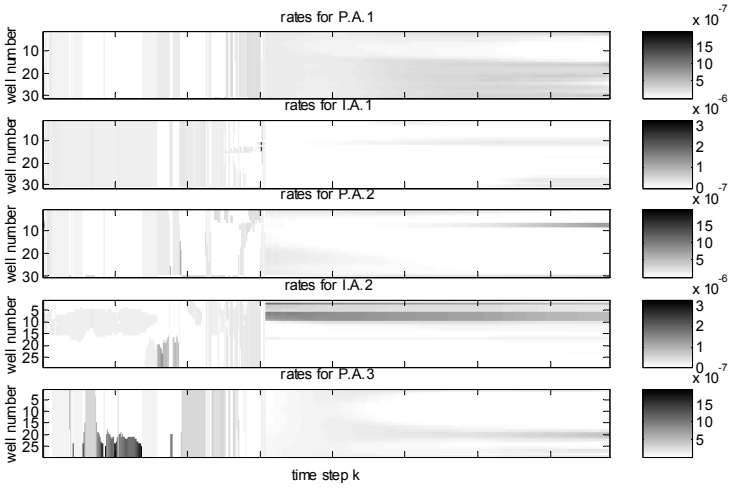

Figure 6.39: Optimal injection and production rates for rate-controlled optimization. Units [$\frac{1}{s}$].

6.6 Field-scale pattern flood optimization

Dynamic water flood optimization can also be done with (conventional) vertical wells, as long as they can be controlled individually. In this situation control may be the surface. In this two-dimensional, horizontal example a field-scale optimization with 36 vertical injection wells and 25 vertical production wells is considered. The field dimensions are $2020 \times 2020 \times 10$ m^3, modelled by $101 \times 101 \times 1$ grid blocks. The permeability field and well locations are shown in Figure 6.40. All other rock and fluid properties are as described in section 6.2. Optimization was done for cumulative production equivalent to 1.1 PV of mobile oil in place, with zero discounting. In this example the adjoint was for computational reasons calculated for a subset (one third) of the forward time steps. This was done under the assumption that the subset of pressures and saturations obtained are sufficiently similar to the set that would result from a fully implicit forward scheme with a three-times larger simulation time step size. It is noted that this may have negatively affected the results.

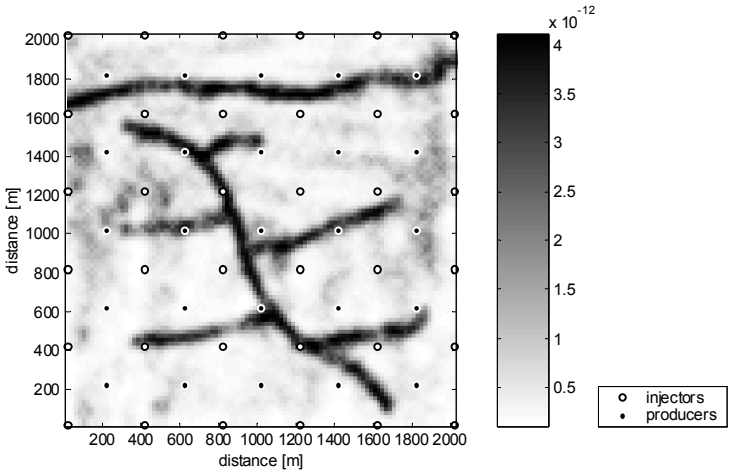

Figure 6.40: Top view of permeability field and well locations for field-scale optimization example.

6.6.1 Scope for improvement

Results are shown in table 6.12 and in Figures 6.41 & 6.42. Under pressure-constrained well operating conditions the main benefit is again in reduced water production, although a slight increase in cumulative oil recovery was also realized. The small-scale oscillations

Pressure constrained optimization					
	cum oil*	cum water*	cum liq*	mob PV	NPV**
base case	4.34	2.85	7.20	1.10	291.1
opt case	4.39	1.80	6.19	0.95	315.8
diff(%)	1.1	-36.9	-14.0	-14.0	8.5
Rate controlled optimization					
base case	4.38	2.81	7.19	1.10	295.21
opt case	5.01	2.17	7.19	1.10	358.69
diff(%)	14.4	-22.6	0.0	0.0	21.5

* units: million m^3 ** units: million $

Table 6.12: Results for pressure- and rate-controlled optimization.

in the production rates are attributed to the complexity of the flow pattern in combination with the explicit calculation of transmissibilities and production rates. For rate-controlled well operating conditions accelerated oil production, increased cumulative oil production, and decreased water production were realized.

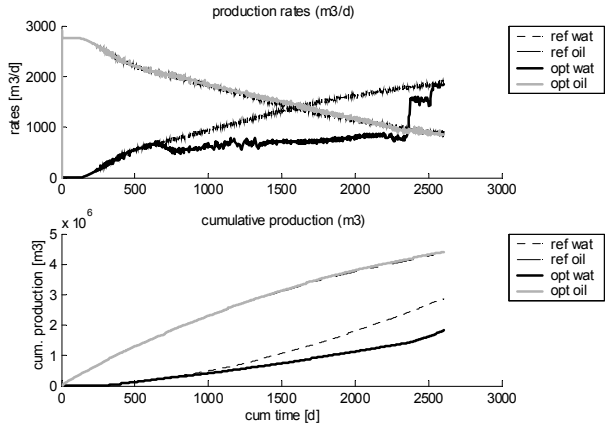

Figure 6.41: Production rates for reference case and pressure-constrained optimized case.

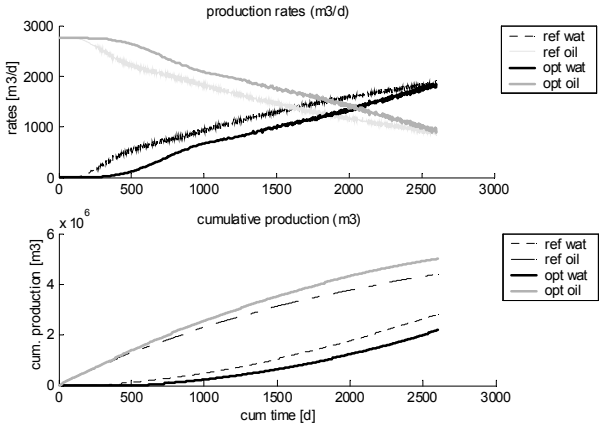

Figure 6.42: Production rates for reference and rate-controlled optimized case.

Figure 6.44 & 6.45 show the final saturations distribution for the reference and rate-controlled optimized case respectively. It shows increased sweep in quadrants $Q1$, $Q3$, and $Q4$ (see Figure 6.43 for definition of these areas). In quadrant $Q2$ this is not so obvious. In some areas within $Q2$ the sweep is improved, in others the sweep is less.

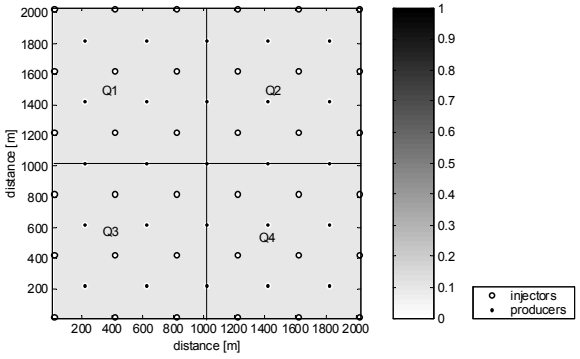

Figure 6.43: Definition of quadrants Q_1, Q_2, Q_3 and Q_4.

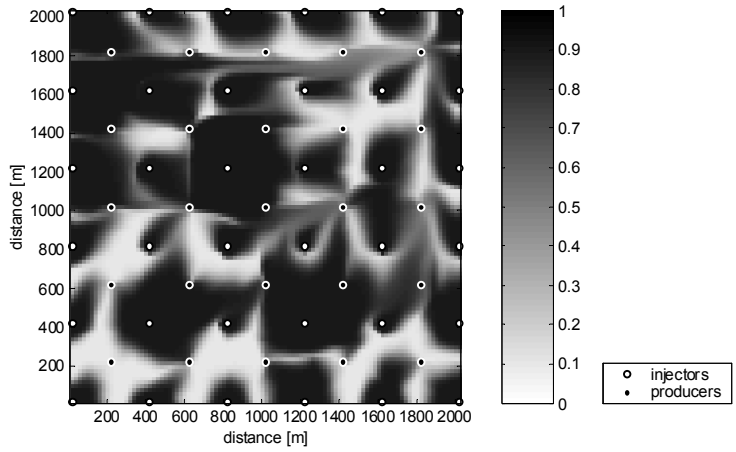

Figure 6.44: Final saturation distribution for reference case.

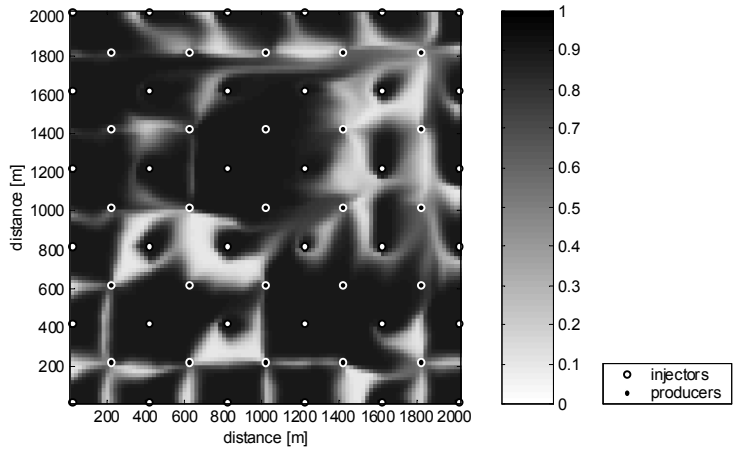

Figure 6.45: Final saturation distibution for rate-controlled optimized case.

6.6.2 Optimal control function

Figure 6.46 shows the optimum valve-settings for the pressure-constrained optimized case. All optimization is done at the production wells. Differently from the previous examples, producer valves are mainly closed at the intermediate stage.

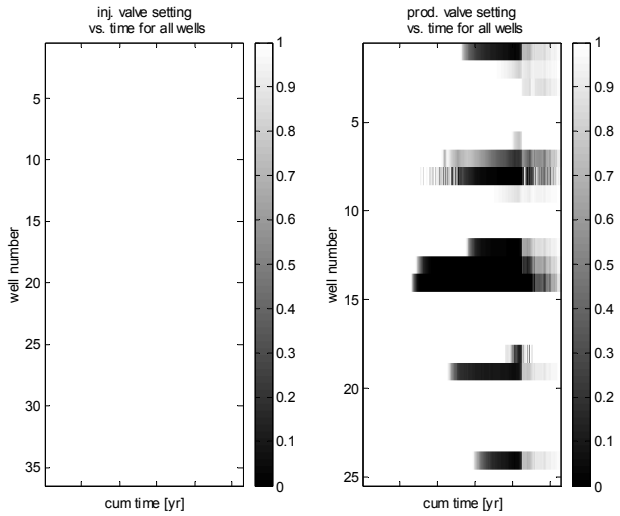

Figure 6.46: Optimum valve-settings for pressure-constrained optimization.

6.7 Two-phase, three-dimensional example

In the previous sections, water flood optimization in two dimensional, horizontal reservoir models was investigated. In this section, optimization for a two-phase, three-dimensional example was considered. Apart from the third dimension it differs from the reservoir models in the previous sections by the presence of gravity effects.

6.7.1 Reservoir model

The permeability field and well locations are shown in Figure 6.47. The reservoir dimensions in x-, y-, and z-direction are $300\times300\times30$ m^3 modelled with $30\times30\times3$ grid blocks. The

smart producer, consisting of 30 segments, is located at the right edge in the top layer, the smart injector, also consisting of 30 segments, is located at the left edge in the middle layer. The vertical permeability was taken to be a factor 10 lower than the horizontal permeability. The oil and water densities at standard conditions were respectively 850 and 1000 $\left[\frac{kg}{m^3}\right]$, and constant compressibility of 1×10^{-9} $\left[\frac{1}{Pa}\right]$ was taken for both liquids. Other properties are described in section 6.2. Optimization was done for cumulative production equivalent to 1.5 PV of mobile oil in place, with zero discounting.

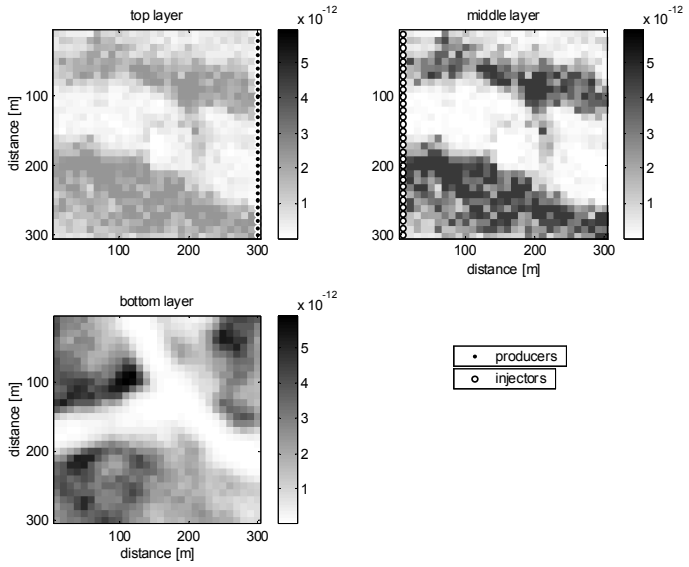

Figure 6.47: Permeability field and well locations.

6.7.2 Scope for improvement

For this case only optimization under pressure-constrained well operating conditions was investigated. The results for the reference and the optimized case are shown in table 6.13. As in most two-dimensional, pressure-constrained optimized cases the improvement is mainly in a reduction in water production; a slight improvement in cumulative oil recovery was however also realized. Figure 6.48 shows the production figures for the reference and the optimized

no discounting
Pressure constrained optimization

	cum oil*	cum water*	cum liq*	mob PV	NPV**
base case	0.389	0.263	0.652	1.51	25.81
opt case	0.392	0.140	0.532	1.23	28.58
diff(%)	0.9	-46.9	-18.4	-18.4	10.7

* units: million m3 ** units: million $

Table 6.13: Results for reference and optimized case.

case. In the optimized case the oil production rate is initially slightly below the plateau production, which is compensated for in a later stage. Water production is significantly reduced.

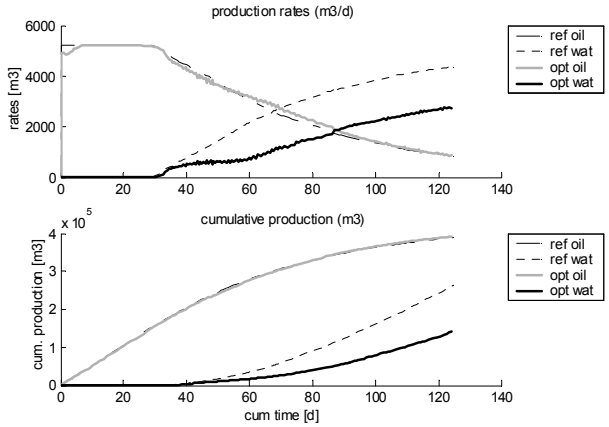

Figure 6.48: Production rates for reference and optimized case.

Figure 6.49 shows the final water saturation distribution for the reference case. The figure shows that most of the reservoir is saturated with water, leaving little scope for improving cumulative oil recovery.

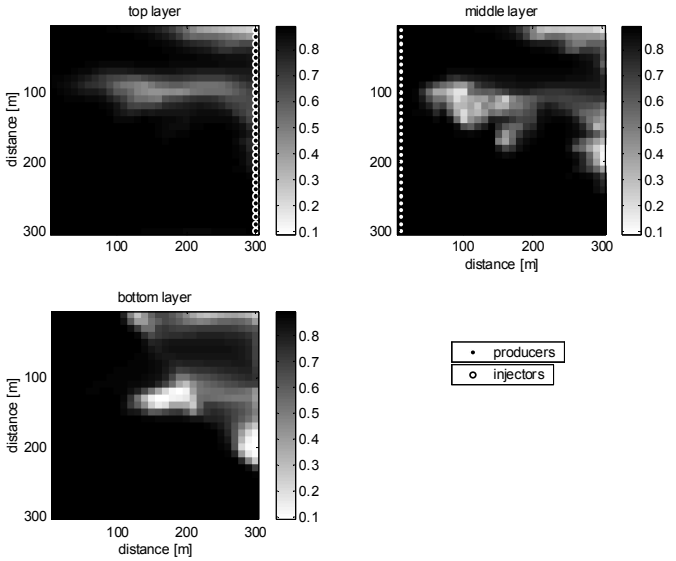

Figure 6.49: Final saturation distribution in reference case.

Figure 6.50 shows the optimum valve-settings for the injector and producer segments. Although most choking at the injectors occurs at the early stage, some also occur near the end of the producing period. Similarly, although most choking at the producers occurs near the end of the producing period, some also occurs at the early stage.

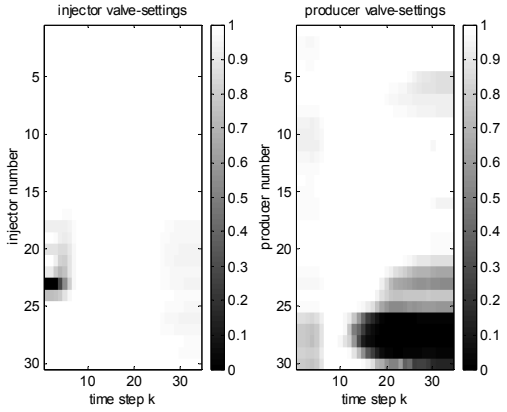

Figure 6.50: Optimum valve-settings.

6.8 Three-phase flow, three-dimensional case

In this section pressure-constrained optimization for a simple three dimensional reservoir is considered in the presence of a small gas cap.

6.8.1 Reservoir model

The reservoir dimensions in *x*-, *y*-, and *z*-direction are $300\times300\times30$ m^3, modelled with $30\times30\times6$ grid blocks. The reservoir is tilted by 10° in the y-direction. The permeability field is simple, with a high permeability streak in parts of layers 3, 4 and 5, as shown in Figure 6.51. The permeability in *x*-, and *y*-direction in the high permeability zone is 2×10^{-12} m^2. Outside of it the permeability equals 1×10^{-13} m^2. The permeability in the *z*-direction is 1% of that in the *x*- and *y*-direction.

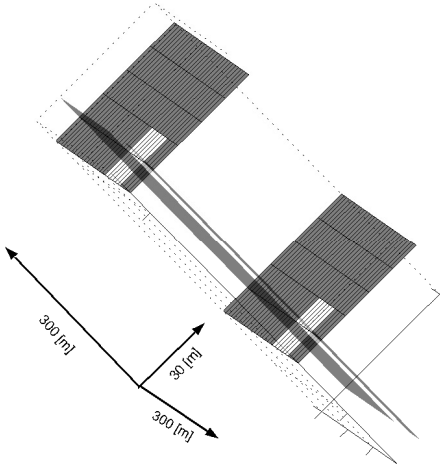

Figure 6.51: Slice of permeability field. Exagerated scale for z-direction.

The top of the reservoir is at 2200 m and the initial gas-oil contact at 2230 m. The locations of the wells and the gas-oil contact (GOC) are shown in Figure 6.52.

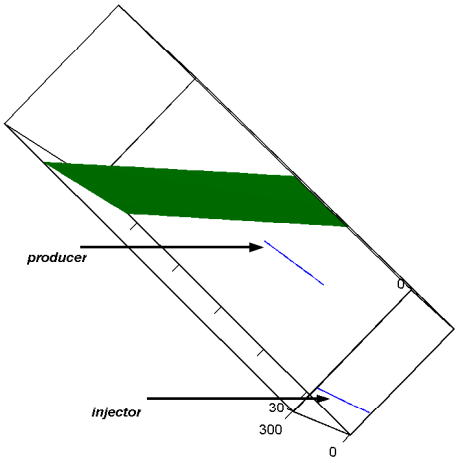

Figure 6.52: Location of gas-oil contact (flat surface), injection well (lower bar), and production well (upper bar). Exagerated scale for z-direction.

P [10^5Pa]	Bo [-]	w_dens [kg/m3]	g_dens [kg/m3]	Rs[m3/m3]
143	1.15	1090	100	40
183	1.2	1098	120	45
223	1.21	1105	140	46
263	1.2	1111	156	46
303	1.19	1116	172	46

*Table 6.14: PVT data, bubble point at 223*105 Pa.*

Pressure constrained optimization

	cum oil*	cum wat*	cum gas**	NPV***	cum w inj*
base case	46.32	99.28	4.26	1.72	163.17
opt case	45.24	13.71	4.16	3.36	80.38
diff(%)	-2.34	-86.19	-2.34	95.02	-50.74

*thousand m3, **million m3, *** million $

Table 6.15: Results for reference and optimized case.

Initially, in the entire reservoir the water saturation is at connate water saturation with $S_{wc} = 0.1$. Above the GOC the oil saturation is equal to the residual oil saturation S_{or} ($S_{or} = 0.1$). The well flowing pressure in the producer is kept slightly above the bubble point pressure to avoid gas coming out of solution directly around the well. The PVT data are shown in Table 6.14. Constant viscosities were used with $\mu_o = \mu_w = 1 \times 10^{-3}$ $[Pa\ s]$, and $\mu_g = 1 \times 10^{-5}$ $[Pa\ s]$. A Stone I relative permeability model was used.

For this example the adjoint was calculated for one-fifth of the time steps of the forward simulation. The total simulation time was 523 days. At the start of production the reservoir was at hydrostatic equilibrium.

6.8.2 Scope for improvement

Only pressure-constrained optimization was considered. In the reference case the cash flow became negative at 426 days, in the optimized case the cash flow remained positive for the entire simulation period. The results are shown in table 6.15 and in Figure 6.53 & 6.54. They show that the main improvement is in cutting back water production.

The optimum oil production rates are for most of the time lower than in the reference case, due to choking of the producer segments (Figure 6.55) that are located within the high permeability zone.

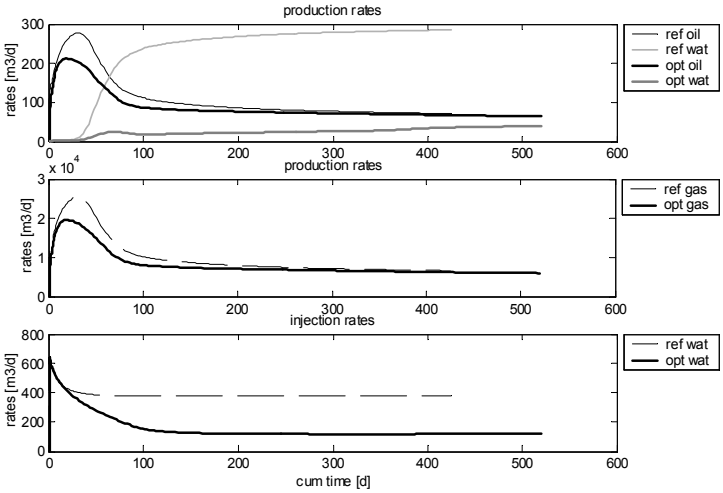

Figure 6.53: Injection and production rates

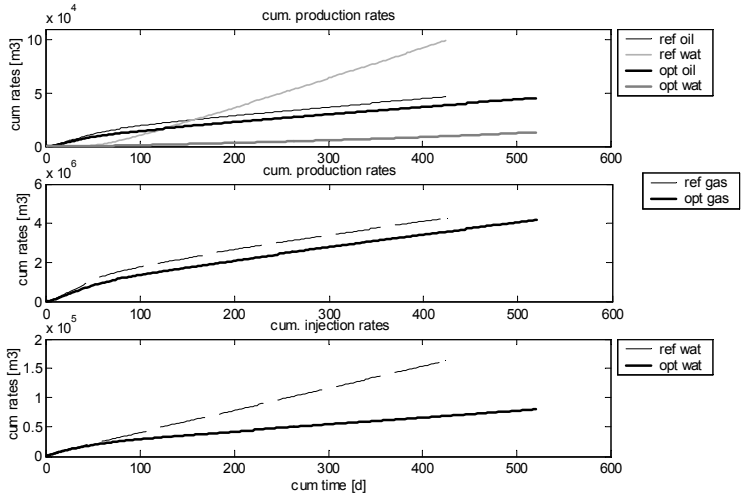

Figure 6.54: Cumulative injection and production rates.

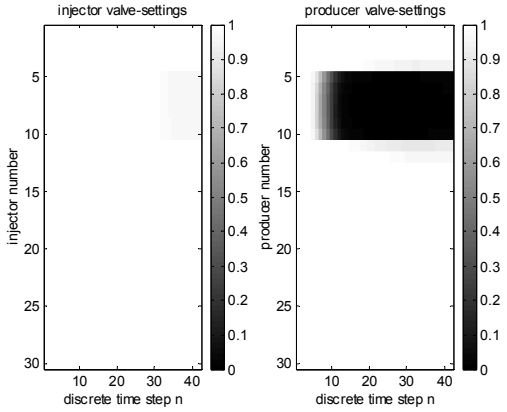

Figure 6.55: Optimum valve-settings

Chapter 7
Discussion

7.1 Introduction

The scope for water flood improvement by dynamic flow control as well as the shape of the optimal control function are affected by many factors. The optimum results obtained vary with the objective function and the length of the optimization period, as will be discussed in section 7.2. In section 7.3 the scope for improvement as function of reservoir properties, well operating constraints and relative well positions are treated. In section 7.4 some trends in the control functions are discussed. Section 7.5 addresses some possible principles behind an optimal water flood.

Results from chapter 6 showed that the scope for improvement and the associated optimal control functions vary with reservoir type, location of the wells and well operating conditions. Furthermore, factors related to the optimization method, such as convergence, local optima, numerical dispersion and adjoint issues may affect the results obtained. Some care must therefore be taken in interpreting trends for the optimized water floods. The trends discussed should therefore be considered as trends associated with an improved, rather than the optimal water flooding scenario.

7.2 Assessment of water flood efficiency

One objective of this study is to find the control function that gives the optimal trajectory of the injected water (front) through the reservoir. Results from chapter 6 showed that this control function as well as the scope for improvement may strongly depend on the discount rate, on the length of the optimization window, and on the fact of the length of the optimization window is fixed or variable.

Technical versus economical optimum

From a technical viewpoint the optimal control function may yield maximum oil recovery with minimum water injection and production. However, from a economic viewpoint this may not be optimal, especially if it is associated with low production rates. When optimizing the Net Present Value (NPV) objective function, with increasing discount rate the focus becomes more on the short term (production) optimization. This can be deduced from com-

parison of Figure 6.3 & 6.4, Figure 6.5 & 6.6, and Figure 6.13 & 6.14. Tables 6.1 & 6.2 in section 6.2.1 show that for pressure-constrained optimization the economical and technical optima are often more conflicting if discounting is applied, since the increased need for high early oil production rates resulted in a less efficient reduction of water production.

Length of the optimization window

The NPV objective function used in this study only comprises information on oil and water production rates. If the length of the optimization period is shorter than the time of water breakthrough, the only thing to be optimized is the oil production rate. If production is rate-controlled it does not matter from which part of the well the oil is produced. Similarly, if the length of the optimization period is such that water breakthrough occurs just close to the end, this water breakthrough can often be completely prevented with a slight, and often nonunique adjustment of the injection/production strategy. As soon as water breakthrough is avoided, the algorithm no longer has a direction in which to optimize. The result is that the optimal control function found may not be optimal for a longer production period. For the NPV objective function, the scope for improvement and the associated optimal control function thus depend on the length of the optimization window. From this point of view, when using a fixed optimization window, it is advisable to optimize for a production period (at least) as long as the one expected for the real case. Alternatively, a variable optimization window length may be used, where the point of zero cash flow is used as the end time criterion.

Results from section 6.3 showed that the scope for improvement may change if uncertainty is included in the optimization. Generally, forecasts for production and well equipment performance will be more reliable for the short than for the long term. Potential improvement in the long term may be associated with a large degree of uncertainty. Yeten *et al.* (2004) showed that the decision on whether or not to deploy smart wells depended on uncertainty in down-hole valve reliability, uncertainty in geology and on the risk attitude of the decision maker. Similarly, in water flood optimization the optimal control function may vary with uncertainty in the short and long term production performance, the downward and upward potential of the control function, and the risk attitude of the decision maker.

7.3 Scope for improvement

The scope for improvement by dynamic flow control depends on various factors. Since its performance is compared to that of a conventional water flood, one important aspect is the performance of the latter. If performing well there may be little scope for improvement by optimizing flow control.

Secondly, the scope for improvement depends on the degree of control on the pressure (potential) distribution and thereby the fluid flow direction in the reservoir. This controllability is influenced by factors like the reservoir properties, the well operating constraints, and the well locations in the reservoir.

7.3.1 Relative well locations

The ability to manipulate the fluid potential gradient and thereby the flow direction in the reservoir depends on the (relative) locations of the wells in the reservoir, as shown schematically in Figure 7.1 for a two-dimensional example. In this schematic flow is principally in the *x*-direction if all injectors and producers are open. If the reservoir is homogeneous and isotropic, L_x and L_y represent the reservoir dimensions $[m]$ in respectively the *x*- and *y*-direction. The angle θ gives an estimate to what degree the average flow direction may be changed by controlling injection and production rates. Locally, however, the flow direction may be significantly different from this average.

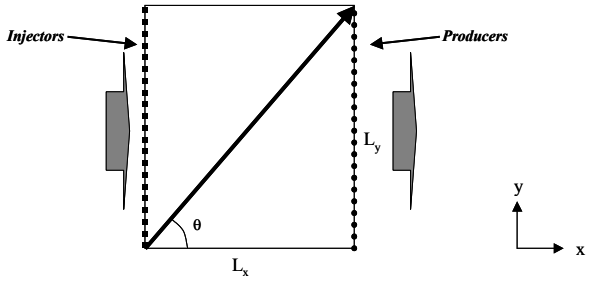

Figure 7.1: Schematic of possible change in flow direction with respect to the main flow directon (x-direction). Top view.

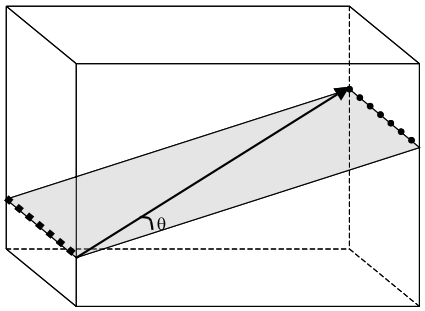

Figure 7.2: Schematic of control on fluid flow direction in a three dimensional setting

The larger the angle θ the more the fluid flow direction can in principle be changed, and the larger the ability to (partly) correct the negative impact of geological features is expected

to be. If the reservoir is not homogeneous and/or isotropic L_x and L_y must be corrected for differences in permeability in the *x*- and *y*-direction.

In the example discussed in section 6.5, the injectors are communicating to multiple producers, lying on opposite sides (Figure 6.33). This enables significant manipulation of the fluid flow direction. Even larger changes in the fluid flow direction are possible in the field-scale pattern flood example (Figure 6.40) of section 6.6. For the three-dimensional examples (Figure 6.47 & 6.51) the control on the fluid flow direction may be less than for the two-dimensional examples, because control will mainly be within the plane in between the wells, as schematically depicted in Figure 7.2. In addition, the controllability will vary with gravity effects.

7.3.2 Reservoir properties

A general observation from the examples investigated in chapter 6 is that the performance of a dynamically controlled water flood is less sensitive to the reservoir properties than a conventional water flood. Therefore, the scope for improvement with respect to a conventional waterflood depends, partly, on the performance of the conventional water flood. The latter varies with the heterogeneity type, as will be explained below. For each separate aspect discussed the others are assumed constant.

Orientation of heterogeneity with respect to the principal flow direction

Figure 7.3 shows a schematic representation of a reservoir with a simple high permeability zone indicated in gray. Injector and producer are located along the left and right edges respectively, as indicated by the black bars. In this figure the angle θ represents the angle between the principal axes of the high permeability zone and the wells.

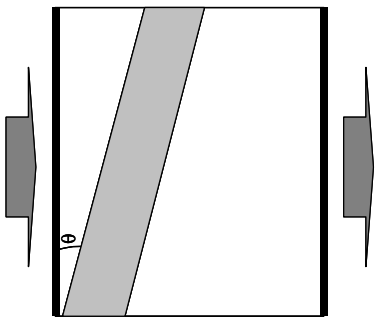

Figure 7.3: Angle (θ) between principal axis of heterogeneity and wells. Top view

If the high permeability streak's principal orientation is parallel or close to parallel to both wells and is extending over the full reservoir width, water does generally not break through early in a conventional waterflooding scenario. This is because the travel time for the injected water to the producer (time of flight) is similar along the well, as shown in Figure 7.4a by the equal lengths of the streamlines in combination with the uniform streamline density[7]. As a result the front moves uniformly from injector to producer. Since there is no significant water breakthrough problem there is also little to no scope for optimization.

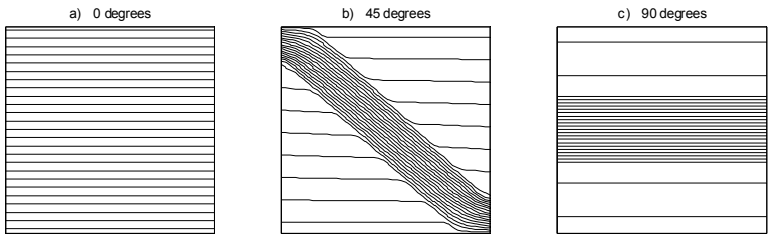

Figure 7.4: Streamline visualization for various angles θ between principal axes of high permeability zone and and wells (Top view). Contrast between high and low permeability zones is a factor 10. Total number of streamlines equals 25.

With increasing angle θ, the variation in effective permeability along flow paths from injector to producer increases along the well. Consequently, flow increasingly tends to follow the high permeability zone. In Figure 7.4 this can be deduced from the higher streamline density in the high permeability zones. This generally results in an increasingly non-uniform movement of the oil-water front towards the producer, and an earlier time of water breakthrough. The latter is most severe if the principal orientation of the streak is at right angles to the wells, i.e. $\theta = 90°$ (Figure 7.4c). In that case the oil-water displacement is generally far from optimal in a conventional water flood, and significant improvement may be possible by optimizing flow control.

Relative position of heterogeneity in the reservoir

The scope for improvement by optimized flow control also depends on the position of the high permeability zone in the reservoir with respect to the wells and the no-flow boundaries. The reason for this is that part of the increased oil sweep is achieved by enhanced injection and production in low permeability zones, and decreased injection and production in the high

[7] In this chapter many streamline illustrations are used, because they clearly show the direction and intensity of flow through the reservoir. All streamline illustrations were constructed with an in-house streamline simulator, developed by Cas Berentsen.

permeability zones. At the injector and producer side this causes the pressure to be locally respectively relatively low and high in the streak. As a result transverse-flow towards the streak occurs at the injection side and transverse-flow out of the streak at the production side. The further away from the high permeability zone injection and production occurs the less severe this transverse-flow generally is, because there is less variation in time of flight along all flow paths from an injector to a producer. This will be illustrated for the simple permeability field, shown in Figure 7.5.

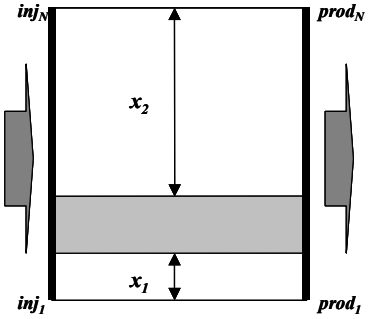

Figure 7.5: Relative position of the high permeability zone with respect to wells and no-flow boundaries. Top view.

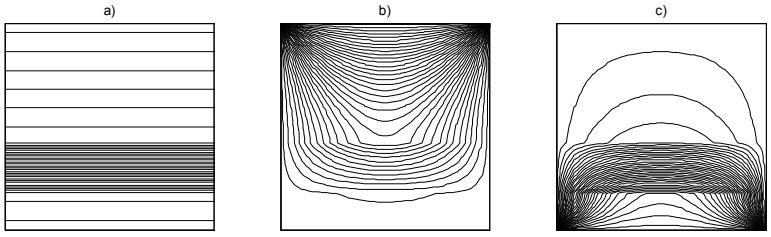

Figure 7.6: a) streamlines resulting from injection and production at constant well flowing pressure in all wells (inj_1-inj_N, and $prod_1$-$prod_N$). b) Injection in inj_N and production from $prod_N$. c) Injection in inj_1 and production from $prod_1$. Contrast between high and low permeability zones is a factor 10. Total number of streamlines in each picture: 35

Figure 7.6b shows that if injection and production only occur in inj_N and $prod_N$ respectively, only a limited number of streamlines go through the high permeability zone, and most flow occurs within low permeability zone x_2. Figure 7.6c shows that for injection and production through only inj_1 and $prod_1$ respectively most flow still goes through the high permeability zone. The injected water generally readily ends up in the high permeability zone due to strong transverse-flow. Similarly, production from $prod_1$ will mainly withdraw fluids from the high permeability zone. The control on fluid flow in zone x_1 may thus be limited, and by that the scope to improve the sweep in it. This explains for heterogeneity type 1 and 2 (section 6.2) why even in the optimized case some parts of the reservoir are left unswept (compare Figure 6.9, 6.10 & 6.11 in this respect).

Permeability contrast between high and low permeability zones

For permeability fields like in Figure 7.5 the capacity of the high permeability zone to transports fluids increase relative to the low permeability areas with increasing contrast between high and low permeability zones, resulting in an increasingly non-uniform movement of the oil-water front towards the producer. In Figure 7.7 this is reflected by the increasing streamline density in the high permeability zone compared to the low permeability zone.

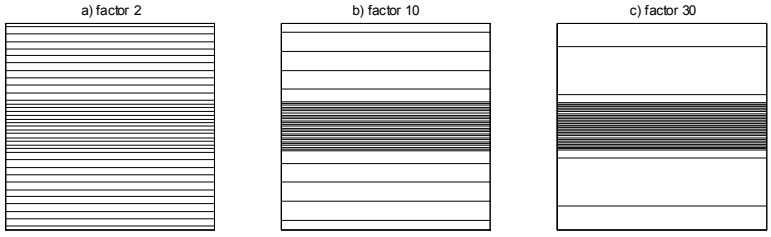

Figure 7.7: Streamlines resulting from injection and production at constant well flowing pressure for various contrasts between high and low permeability zones. a) factor 2, b) factor 10, c) factor 30. Total number of streamlines: 35. Top view.

If contrasts are small the conventional waterflood performance may already be fairly good, and only moderate changes in flow profiles with respect to the reference case are required for compensation. The scope for optimization may then also be limited. Figure 7.8 shows that for large permeability contrasts full compensation may not be possible, due to strong transverse flow towards and from the high permeability zones. Despite this, the scope for improvement may be significant, because a conventional water flood may perform poorly for large permeability contrasts.

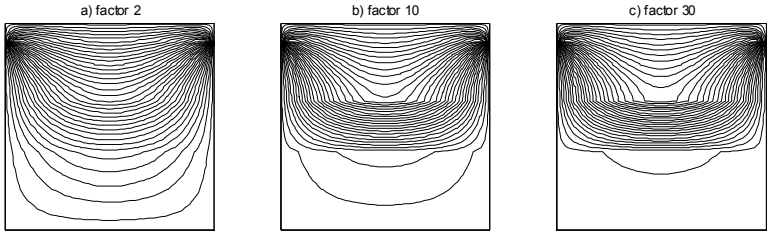

Figure 7.8: Streamlines for various permeability contrasts. Injection is through injector 4, production through producer 4. Top view.

Relative size of the high permeability zone

In previous sections, the effect of the relative position of a heterogeneity in the reservoir, and the effect of the permeability contrast were discussed. The effect of the heterogeneity dimensions, relative to those of the entire reservoir, can be considered a combined effect of these two. Generally the relative flow capacity of a high permeability zone is likely to increase with increasing relative size, as can be deduced from Figure 7.9.

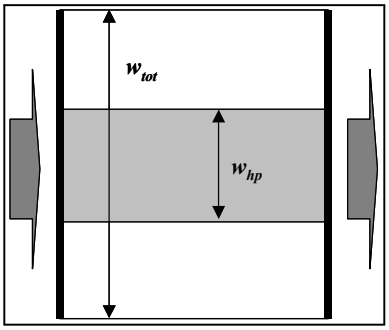

Figure 7.9: Relative width of high permeability zone (w_{hp}) with respect to reservoir width (w_{tot}). Top view.

Secondly, the larger the high permeability zone, the closer to it the wells generally are, and the more severe transverse-flow effects will be if the wells within the high permeability zone are (partly) closed. However, with increasing relative size the percentage of total oil stored

in the high permeability zone generally increases too, so a larger streak does not necessarily cause a larger problem. In the extreme cases where $\frac{w_{hp}}{w_{tot}} \longrightarrow 0$, or $\frac{w_{hp}}{w_{tot}} \longrightarrow 1$ the reservoir becomes homogeneous, and for this two-dimensional, horizontal reservoir with parallel wells the scope for improvement reduces to zero.

Multiple high and low permeability areas

Figure 7.10a shows a schematic of a reservoir having four high permeability streaks. As all wells located in the low permeability are close to at least one high permeability zone, reduced injection and production in the latter expectedly induces strong transverse flow, similar to that in Figure 7.6c.

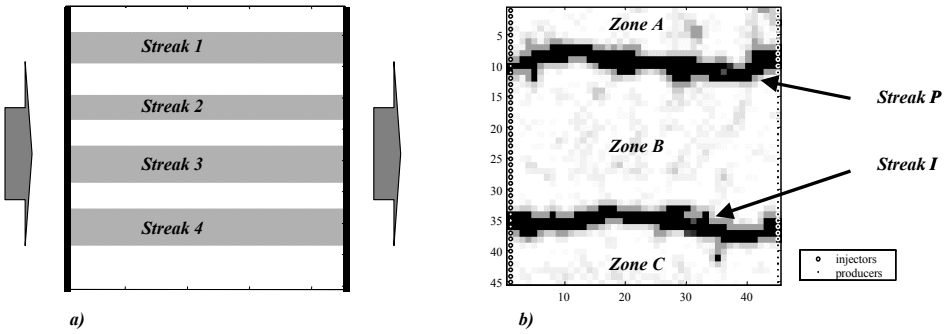

Figure 7.10: a) Schematic of reservoir containing four high permeability zones. b) Permeability field heterogeneity for type 2. Top view.

Results for heterogeneity type 2 (Figure 7.10b), however, indicate that this does not necessarily reduce the scope for optimization. Tables 6.1 & 6.2 and Figure 6.5 & 6.6 show that even for pressure-constrained optimization significant improvements in both cumulative oil recovery and water production are realized. Figure 7.11 shows a streamline representation of the conventional water flood for heterogeneity type 2. It shows that in the conventional water flood most flow is occurring in the two high permeability zones.

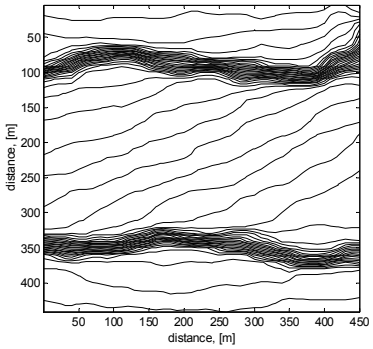

Figure 7.11: Streamlines for heterogeneity type 2, corresponding to a conventional water flood.

Figure 7.12 shows snapshots of the saturation and the flow paths at various times for the non-discounted, pressure-constrained optimized case. It shows that *Streak I* (see Figure 7.10b for definition) is flooded first. Subsequently, production from *Streak I* is stopped and *Zone B* is swept, mainly by water flowing from *Streak I* to *Streak P*, as indicated by the streamline pictures. In this example *Streak I* may be considered to act as an extension of the injection well, whereas *Streak P* may be considered an extension of the producer well. This is in agreement with (unpublished) findings from Dolle and Glandt (N. Dolle and C. Glandt, personal communication), who suggested to consider high permeability zones or fractures as an extension of the well, and actively use those zones to improve sweep of the reservoir. The reason for the poor sweep of *Zone A* and *Zone C* is due to the relative position of the high permeability zones, as discussed on pages 139-141. The streamline pictures in Figure 7.12 show that little flow occurs in these zones.

Figure 7.13a shows the streamlines for a conventional water flood for the heterogeneity containing four high permeability streaks (Figure 7.10a). As in the previous cases, flow occurs predominantly in the high permeability zones. Figure 7.10b shows the flow paths if injection is into *Streak 4* and production from *Streak 1*. Similarly, Figure 7.10c shows the flow direction if injection is into *Streak 1*, and production from *Streak 4*. For both scenarios a significant change in flow direction with respect to the conventional water flood is realized, with more flow going through the low permeability zones. This suggests that an improved sweep of especially the low permeability zones may be possible with either of these strategies.

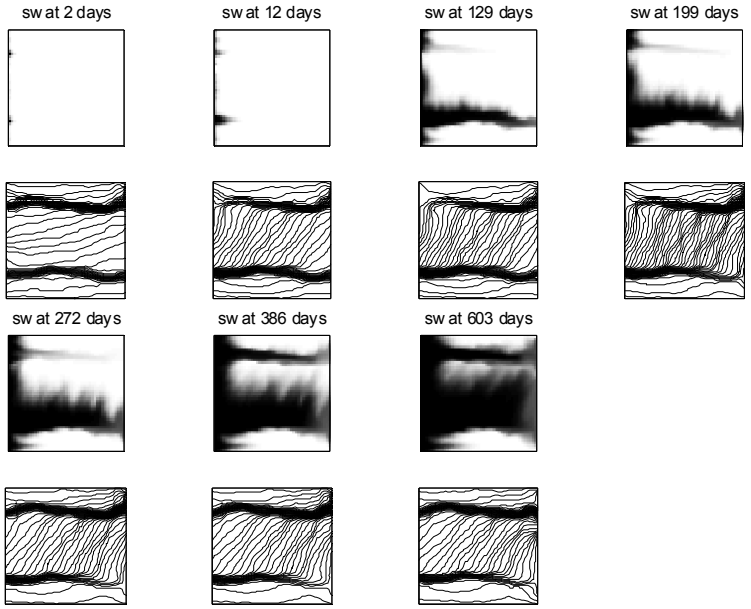

Figure 7.12: Snapshots of water saturation and flow paths at 2, 12, 129, 199, 272, 386, and 603 days (Top view). Water saturated areas are coloured dark.

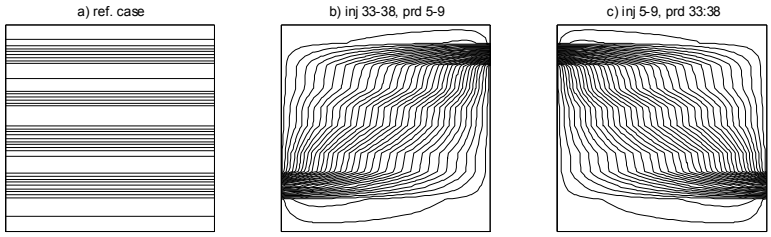

Figure 7.13: a) Injection and production at constant well flowing pressure. b) Injection in wells 33-38, production in wells 5-9. c) Injection in wells 5-9, production in wells 33-38.

7.3.3 Operating constraints

If it is possible to increase the macro-scale sweep in the reservoir by flow control, but only at the cost of flow rate, the scope for optimization may become limited because of economic factors. Results suggest that the scope of improvement is maximal in situations where fluid flow can be controlled without negatively affecting the total injection and production rates, as is the case for rate-controlled optimization. For these operating conditions the scope for improvement is generally in reduced water production, increased cumulative oil production, and accelerated oil production. For pressure-constrained operating conditions the scope for improvement varied from case to case. With tight pressure constraints optimized flow control may result in lower than maximal well rates, and the relative importance of increased sweep, high oil production and low water production rates must therefore be considered. These may be different for different reservoirs. Moreover, the ability to optimize each of the individual aspects may also vary with the reservoir, as will be discussed below.

Well interference

Under pressure-constrained operating conditions, closing one of the wells generally causes a drop in total injection and production rates. However, it also induces a change in the (local) pressure field and hence a change in the (local) fluid flow direction. As a result, injection and production rates in communicating wells may change. Because of this coupling it is not obvious to predict how much the total injection and production rates will be affected.

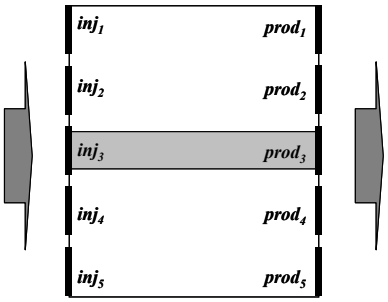

Figure 7.14: Top view of reservoir. Contrast between high and low permeability zone is a factor 6.7.

Figure 7.14 shows a reservoir with five injectors and five producers, producing on constant well flowing pressure. An estimate of the steady state interference between injectors and producers can be obtained by considering the changes in flow rates in the individual wells upon closing one of the wells. Figure 7.15 shows the steady state response between the wells for the permeability field shown in Figure 7.14. Each row in Figure 7.15 represents one well

test. The diagonal contains the rate changes in the wells that are tested (closed), the off-diagonals the responses (rate changes) in the other wells. All rate changes were normalized with respect to the maximum.

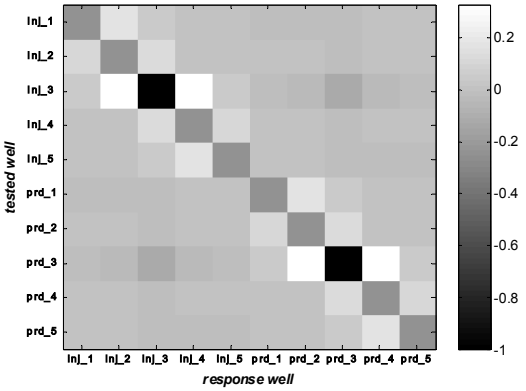

Figure 7.15: Steady state flow rate response. Tested wells are shown on the y-axis, steady state reponses on the x-axis.

The figure shows that each well is at least affecting neighboring wells, and one segment on the opposite side of the reservoir. Responses are small but not zero in wells distant to the tested well. The wells within the high permeability zone (see Figure 7.14, and rows *inj_3* and *prd_3* in Figure 7.15) are affecting all other wells in the reservoir, the degree however varying significantly. The negative correlation between for example tested and neighboring producers indicates that if the rate in one well decreases the rates in the other wells increase, resulting in a drop in the total production rates that is less than would be expected from the tested segment alone. This is attributed to changes in the fluid flow direction, as depicted in Figure 7.16.

Improvement in oil and water production

The scope for reducing water production and increasing cumulative oil production will vary with well interference and the extent to which the fluid flow direction is affected.

If all trajectories from an injector to a producer will water out before the end of the production process, the injector and/or producer should be closed at some point in time. If the resulting change in flow direction is small, and the drop in total production rates is large, the main effect will be a reduction in water production.

If the flow direction is changed significantly, as for example in Figure 7.12 & 7.16c, the newly formed trajectories (streamlines) may on the average contain more oil. Consequently, apart from a reduction in water production an increase in oil production may be feasible, especially if the drop in total production rates is not so severe .

If only part of the trajectories will water out before the end of the production process, it may be necessary to keep the injector and/or producer open in order to maintain oil production in the remaining, oil-bearing trajectories. In these situations a large reduction in water production may not be possible.

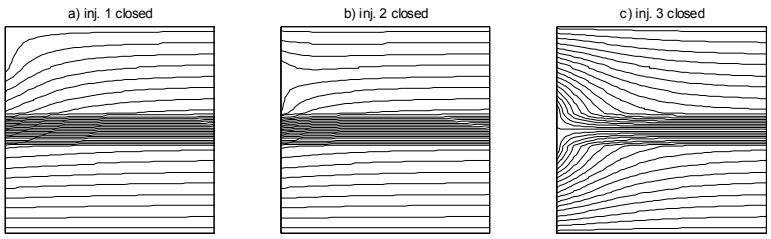

Figure 7.16: Streamlines for: a) injector 1 closed. b) injector 2 closed. c) injector 3 closed. All active wells are operated on constant well flowing pressure. Total number of streamlines equals 25. Top view.

7.3.4 Reduced uncertainty in the outcome

Apart from considering the scope for improvement for each individual example, additional benefits of dynamic water flood optimization are observed when considering the results for all cases. Figure 7.17 shows the ranges in NPV outcome for heterogeneity type 1, 2, and 3 for all reference and optimized runs of section 6.2 (pressure-constrained, rate-constrained, discounted, not discounted, optimization for 1 PV, 2 PV, unit mobility and unfavorable displacement). The figure shows that for all examples considered the range in NPV outcomes lies higher and is narrower for the optimized cases. For pressure-constrained optimization over one PV of injection the range is only slightly narrower, and the ranges for optimized and reference cases partly overlap. For all other examples the ranges do not overlap, and are much narrower for the optimized cases. The narrower distributions suggest that by dynamic flow control negative effects of geological features and fluid properties can (partly) be compensated for, thereby reducing the uncertainty in the outcome. This is in agreement with results from Yeten *et al.* (2004).

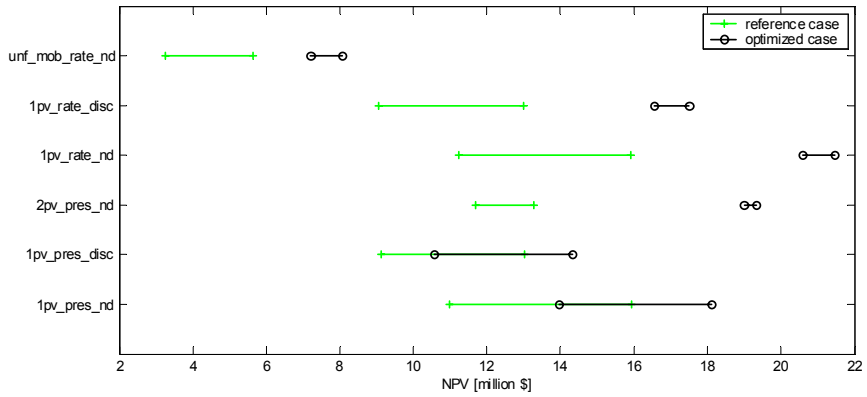

Figure 7.17: Range in NPV outcome for reference and optimized cases in section 6.2.

7.4 General trends for the controls

In section 7.3 the focus was on the scope of improvement. In this section the existence of general trends in the optimal injection and production strategies (optimal control functions) is investigated.

7.4.1 Type of control

In Sudaryanto and Yortsos' approach, the wells were operated according to a "bang bang" type of control, which means that wells only operate on their extremes (on/off) [Sudaryanto (1998), Sudaryanto and Yortsos (2000)]. In their approach maximization of the water saturation at water breakthrough was achieved by optimizing the switch times for the injection wells. In Asheim's approach the well injection or production profiles changed gradually in time. Results from chapter 6 suggest that the type of control depends on a number of factors.

Pressure-constrained operating conditions

For the examples with one smart injector and one smart producer, discussed in section 6.2, the type of control was generally close to an on/off type of control under pressure-constrained well operating conditions. For the examples discussed in sections 6.5, 6.6 & 6.7 the optimal

control functions also comprised intermediate valve-settings. This suggests that the type of control under pressure-constrained operating conditions may vary with the (relative) well locations, the type of reservoir, and the length of the optimization period.

Rate-controlled operating conditions

The optimal control function for the rate-controlled optimized cases were never of the bang bang type. The optimum control functions for the producers often exhibited smooth, gradually changing behavior as found by Asheim (1988), although frequent switching between producer wells was observed at the early stage for the example in section 6.5 (Figure 6.39). More often, frequent switching between injectors was observed at the early stage, generally disappearing at a later stage. Since the frequent switching at the injectors did not occur for all cases it is difficult to interpret the differences in dynamics between injectors and producers. They may be related to distinct differences in properties between injectors and producers. However, the frequent switching at the injectors may also be a numerical artefact, resulting from the fact that the objective function is based only on the production rates. For the producer the gradients $\frac{\partial \mathcal{L}^n}{\partial \mathbf{u}^n}$ are

$$\frac{\partial \mathcal{L}^n}{\partial \mathbf{u}^n} = (\boldsymbol{\lambda}^n)^T \frac{\partial \mathbf{g}^n}{\partial \mathbf{u}^n} + \frac{\partial \mathcal{J}^n}{\partial \mathbf{u}^n}. \tag{7.1}$$

For the injector, however, there is no direct cost to water injection, hence the gradients $\frac{\partial \mathcal{L}^n}{\partial \mathbf{u}^n}$ for the injectors are

$$\frac{\partial \mathcal{L}^n}{\partial \mathbf{u}^n} = (\boldsymbol{\lambda}^n)^T \frac{\partial \mathbf{g}^n}{\partial \mathbf{u}^n}. \tag{7.2}$$

Numerical errors in the adjoint equation, i.e. in the Lagrange multipliers $\boldsymbol{\lambda}$, may have therefore affect the injector gradients (eq. 7.2) to a larger degree than the producer gradients (eq. 7.1). The injector gradients' susceptibility to numerical errors may then be reduced by including separate costs for water injection. Thirdly, the high frequent switching in the injectors may be due to the fact that the number of controllable parameters (equal to the product of the number of wells and the number of time steps) is very large. Just as in history matching, regularization should then be used to smooth the control functions.

7.4.2 Number of well segments required

In this study, a large number of smart well segments were used to enable detailed optimization. Figure 6.7 & 6.8 show that a restricted number of segments may be sufficient if wells are operated on pressure constraints. Adjacent segments with a similar control function for the valve-settings could be grouped together into a single segment. The figures also show that the number of segments required varies with the heterogeneity type. For the rate-controlled optimized cases the number of segments cannot be directly extracted from the optimal control functions, as they show the rates per segment and not the valve-settings. In this case adjacent segments with a similar control function can only be grouped together if the rates have

a similar associated well flowing pressure. However, also for rate-controlled well operating conditions a much smaller number of segments may be sufficient for significant optimization. Similar improvements in oil recovery and water reduction were achieved with the defensive control method (section 2.2.2) and the optimal control method for heterogeneity type 1. In the defensive control method, only 3 segments per well were used and optimization was done for 5 time intervals, whereas in the optimal control method 45 segments per well were used, and flow rates were optimized at each time step [Yeten (2003)].

7.4.3 Timing of optimizing injection and production

For the two-dimensional examples a number of trends in optimizing injectors and producers can be observed for both the pressure and rate-controlled optimized cases. In some pressure-constrained optimized cases control was both at the producers and the injectors. Figure 6.7 & 6.8 show that the optimal injector valve-settings differ only from the reference valve settings (all valves open) at the early stage of the water flooding process, whereas closing of producer segments typically started at a later stage. In other cases only a number of producer segments were closed, typically occurring at a later stage. Under rate-controlled well operating conditions optimization of the flow rates was generally done both in the injectors and the producers. Figure 6.15 & 6.16 show distinct differences between reference and optimal injection and production strategies, but the magnitude of the difference is not directly obvious from these figures. One way of making this better visible is by plotting the normalized sum of the absolute differences γ between reference and optimal wells rates as function of time. For the injectors γ then is

$$\gamma_{inj}^{n} = \frac{\sum_{i=1}^{N_{inj}} \left| q_{ref,inj_i}^{n} - q_{opt,inj_i}^{n} \right|}{\sum_{i=1}^{N_{inj}} \left| q_{ref,inj_i}^{n} \right|}, \tag{7.3}$$

where N_{inj} is the number of injection wells/segments, and n is the discrete time step. Similarly, for the producers γ equals

$$\gamma_{prod}^{n} = \frac{\sum_{j=1}^{N_{prod}} \left| q_{ref,prod_j}^{n} - q_{opt,prod_j}^{n} \right|}{\sum_{j=1}^{N_{prod}} \left| q_{ref,prod_j}^{n} \right|}, \tag{7.4}$$

where N_{prod} is the total number of producer wells/segments. The magnitude of γ is then a measure of the change in control with respect to the reference case. Figure 7.18 & 7.19 show γ_{inj} and γ_{prod} as function of time for heterogeneity type 1 and 2 respectively.

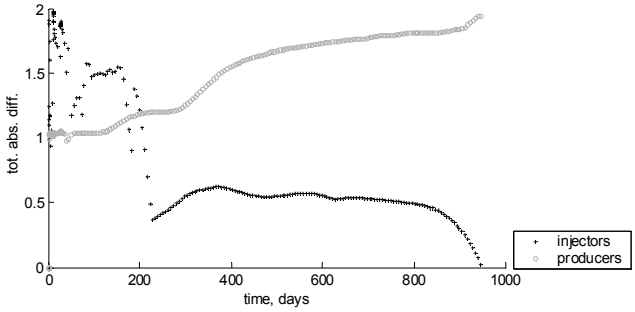

Figure 7.18: γ for injectors and producers for undiscounted, rate-controlled optimization. Heterogeneity type 1.

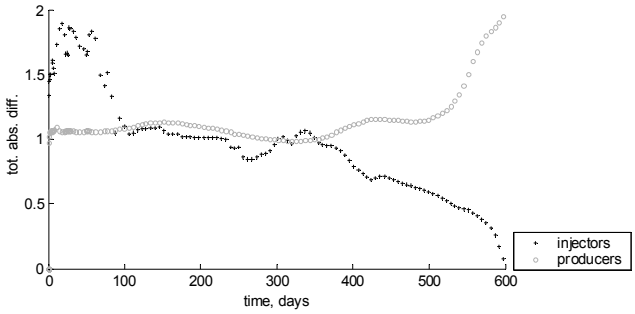

Figure 7.19: γ for injectors and producers for undiscounted, rate-controlled optimization. Heterogeneity type 2.

For the injectors γ decreases with time, reflecting that the optimal injection strategy differs most from the reference case at an early stage. For the producers the overall trend for γ is that it increases with time, indicating that optimization of the producers becomes increasingly important as time progresses. Apart from the fact that trends for injector and producer are opposite, an additional difference is that for the injectors γ reduces to approximately zero at the end time, whereas for the producers γ starts with a nonzero value.

The opposite trends for injectors and producers are in agreement with the opposite trends in sensitivities, discussed in section 5.4 (Figure 5.9). The differences in trends are attributed to the fact that optimization of the water flood is related to maximizing oil production and minimizing water production, in combination with the fact that the water front moves from

the injector towards the producer. As long as the front is close to the injectors largest control on it is in the injectors. Since the front is at this stage generally still far away from the producers, the degree of control on it from the producers may be limited. Furthermore, generally only oil is produced at this stage. As water flooding continues, the front will move away from the injectors. For a certain period the front will be distant to both injectors and producers. Resultingly, the degree of control on it through either injectors or producers may be limited. As the front comes close to the producers it can be controlled mainly through the producers.

Optimization of injection at the early stage may serve to reduce water buildup at the producer at a later stage. This may be important because as soon as the water is close to the production well its production can mainly be controlled by closing valves in the water saturated zones. This may cause divergence of the water to neighboring well segments, as schematically depicted in Figure 7.20 & 7.21.

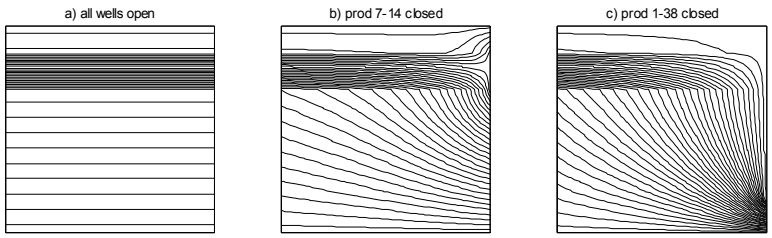

Figure 7.20: Top view of streamlines for: a) all valves open. b) water producing segments in high permeability zone closed. c) most producer segments closed.

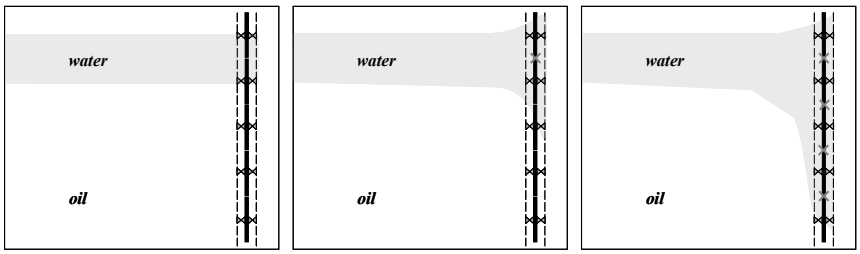

Figure 7.21: Schematic representation of water spreading along smart, segmented producer. Closed valves are cross-marked.

This spread of water may eventually cause the producer to become completely surrounded by water. This effect may be less in the pattern flood example, described in section 6.6, because of the larger distance between producer wells. That may for the pattern flood example also explain why under pressure-constrained well operating conditions optimization of the valve-settings only occurs at the producer wells.

7.4.4 Dynamism of optimal control strategy

The degree of dynamism in the optimal control functions varied considerably from case to case, partly because the optimal fluid trajectory through the reservoir, and thereby the optimal control function, depends on the geological properties. The degree of dynamism in the optimal control function may therefore vary with reservoir properties, as can be deduced from Figure 6.16.

Furthermore, the degree of dynamism expectedly depends on the number of injectors and producers in the reservoir, because with increasing number of wells more detailed optimization may be possible.

Figure 6.7 & 6.16 show that the degree of dynamism in the optimal control function also varies with the well operating constraints, the dynamism being larger for rate-constrained than for pressure-constrained well operating conditions. The reason for this is the difference in pressure available to inject/produce fluids in each scenario. Fluid flow at a certain velocity along the optimal trajectories may often require a larger pressure gradient than along the reference case trajectories, because optimization generally comprises a decreased flow through the high permeability zones and an increased flow through the low permeability zones. The average resistance to flow may therefore generally be higher along the optimal trajectories. As long as field rates can be maintained these optimal trajectories will lead to an improvement in the water flood. This is the case if production is entirely rate-controlled. However, under tight pressure constraints these trajectories are not necessarily optimal, because the higher average resistance to flow will cause a drop in the field rate. This negatively affects the instantaneous oil production rate and possibly also the cumulative oil recovery. The trajectory will only be optimal if the negative impact of the lower oil production rate is more than compensated for in a later stage. The number of feasible optimal trajectories thus depends on the well operating constraints, more specifically on the pressure (energy) available to inject and produce fluids. The expected trend is that the number of feasible optimal trajectories increases with slacker constraints on the pressure.

The degree of dynamism expectedly also depends on the length of the optimization period, more specifically on the fraction of mobile oil produced at the end of the production process. For some rate-controlled optimized cases a steep drop in the oil production rates was observed near the end of the production process (see Figure 6.13, 6.14 & 6.34 in this respect), because at that stage most of the mobile oil had already been produced. A detailed dynamic control strategy may be required to produce the last (relatively small) volumes of oil in the reservoir.

7.4.5 Uniqueness of optimal control functions

In history matching, many different combinations of the spatially distributed parameters are generally possible that give the same production response at the wells. This is because the number of parameters to be estimated is generally larger than the number of measurements. In water flood optimization there may also be different strategies that give the same optimum value for the objective function. The difference in the non-uniqueness between history matching and water flood optimization is that in history matching it is known that the real field has a unique permeability and porosity distribution. In water flood optimization, on the other hand, there may be various injection-production strategies giving the same optimum end result. The existence of a unique optimal control function depends on the objective function, the type of operating constraints, the number of controls, and the physics of the process.

Objective function

Mehos and Ramirez (1989) found different optimal control policies giving approximately the same end result. Similar findings were done by Fathi and Ramirez (1987). They attributed this to a lack of specifications in the objective function that an optimum solution should fulfill. They argued that including additional specifications, like discounting, would narrow the feasible region for the injection policies and increase the possibility of having only one local extremum.

The NPV objective function in this study is based on production rates for the entire production time interval. Therefore, its value can only be evaluated at the end of this production period. As various combinations of injection and production rates may give the same end result in terms of NPV, the optimal control function may not be unique. Results for some of the two-dimensional examples considered suggest that the optimal control functions are not unique, or at least that there are multiple local optima having approximately the same NPV value. Tables 6.5 & 6.6 and Figure 6.13 & 6.14 show for heterogeneity type 1 that, although a change in the discount rate causes a change in the NPV and in the optimal control function, the ultimate oil and water recovery did not change to a significant extent. Applying both the discounted and the non-discounted optimal control functions to the case with zero discounting would therefore give an approximately similar NPV, and cumulative oil and water production. Since the values would not be exactly identical, this can in the strictest sense not be attributed to non-uniqueness. However, the fact remains that different control functions may give similar end results. This also appeared from the comparison study between the defensive and the optimal control method [Yeten (2003)].

Operating constraints

The uniqueness of the solution may also depend on the well operating conditions. The closer the operating conditions are to rate-controlled conditions, the larger the number of possible trajectories from injector to producer may be (see section 7.4.4 in this respect),

and the larger the chance may be on having different combinations of trajectories giving approximately the same end result.

Number of controls

The number of possible control functions increases with increasing number of controls and the frequency at which the controls can be changed. As a result there is an increased possibility that there are multiple optimal control functions that are approximately equivalent in terms of the end result obtained. This may particularly be the case if wells are close to each other and affect similar areas in the reservoir.

7.5 Underlying principles

Section 7.3 discussed the scope for improvement as function of reservoir properties, well operating conditions, and well positions. Section 7.4 discussed some characteristics of the optimal control functions. This section discusses an optimal water flood in terms of possible underlying principles. Since water flood optimization is still a developing area of research, this should be considered a first step.

Results showed that for rate-controlled well operating conditions the improvement in water flooding consisted of increased cumulative oil recovery, reduced cumulative water production, accelerated oil production and delayed water production, realized by increasing the macro-scale sweep efficiency. Under pressure-constrained well operating conditions the improvement depended on the relative importance of reducing water production, increasing the sweep efficiency and maintaining oil production rates as high as possible. In general an optimal water flood may thus be associated with maximizing the macro-scale sweep, while minimizing water production and maximizing oil production rates.

7.5.1 Rate-controlled operating conditions

Time of flight

Results from earlier studies indicated that, for a certain constant total injection and production rate, an improved water flood appeared to be associated with an increased time of flight of the injected water to the producer [Sudaryanto (1998), Sudaryanto and Yortsos (2000), Sudaryanto and Yortsos (2001), Brouwer *et al.* (2001)]. It must be emphasized that this increase in time of flight for a certain constant total injection and production rate is distinct from an increase in the time of flight by simply decreasing the flow rates. Furthermore, since the injected water flows towards the producer along a range of trajectories

(streamlines), the time of flight from injector to producer refers to the shortest time of flight from this set of trajectories.

Figure 7.22 shows the top view of a two-dimensional, homogeneous reservoir with two parallel wells. If both wells are operated at constant well flowing pressure, the oil-water front moves uniformly to the producer and in case of a piston-like displacement only break through after all oil has been produced. Properties of this ideal water flood are that, for a certain constant total injection and production rate, it has a maximum time of flight, and a minimum variation in time of flight for all trajectories from injector to producer. If the displacement is not piston-like, the characteristic of this ideal water flood is that at all times the (fractional) flow of water is minimized. For heterogeneous reservoirs simultaneous breakthrough along the entire well may generally not be feasible, due to the limited control on fluid flow within the reservoir.

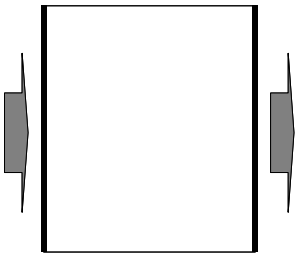

Figure 7.22: Schematic of homogeneous reservoir, with injectors along the left edge and producers along the right edge. Top view.

Sudaryanto (1998), Sudaryanto and Yortsos (2000) and Sudaryanto and Yortsos (2001) maximized the water saturation at the time of water breakthrough. Since optimization was for incompressible flow at constant total production rate, it consisted of maximizing the time of water breakthrough, i.e. maximizing the time of flight from injectors to the producer. The optimal injection policy comprised the start of injection in the most distant injector, often after some time followed by a switch to injection in the closest injector, as shown in Figure 7.23 & 7.24. Rather than a geometric distance, this should be considered the distance from a time of flight point of view. Furthermore, rather than considering the time of flight from injector to producer it may be better to consider the time of flight from the oil-water front to the producer. At the start of the production process these are equivalent since the oil-water front originates at the injector. Figure 7.23 shows that in the optimum water flood the injected fluids from both injectors simultaneously arrive at the producer, pointing at a minimum variation in the time of flight from injectors to producers. The switching from injection in well A to injection in well B occurred at the time that the time of flight from the existing oil-water front to the producer was equal to the time of flight from injector B to the producer. This may indicate that, for a certain constant total injection and production rate,

the time of flight should be maximized at all times and/or that the variation in time of flight should be minimized at all times.

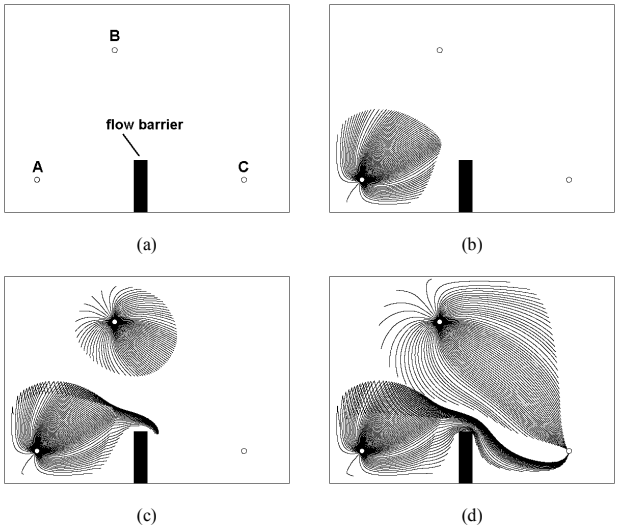

Figure 7.23: Consecutive snapshots of front movement under bang-bang policy. (a) At initial time, (b) at time just before injection switches from well-A to well-B, (c) at time injection is only through well-B, and (d) at breakthrough. [from Sudaryanto (1998), reprinted with permission].

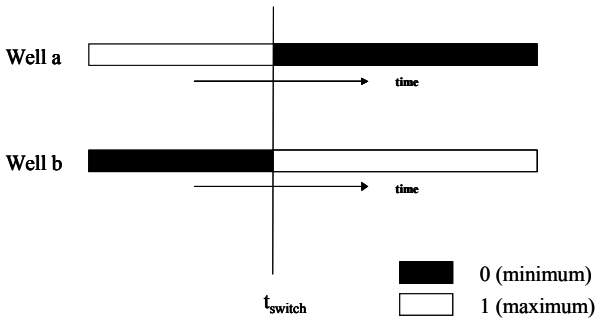

Figure 7.24: Schematic representation of injection rates.

Zakirov *et al.* (1996) investigated optimization of production from a reservoir containing a gas cap, an oil layer and an aquifer. They found an optimal control policy in which production was simultaneous from both wells, such that the GOR in both wells was similar at all times. They interpreted this to correspond to an equal gas-front movement through the reservoir. In the optimum policy the water-oil-ratio was not similar at all times. This may indicate that gas was the component mostly affecting the performance of the production process. The similar evolution of the GOR in both wells may suggest that a minimum variation in time of flight of the gas to the producers was the underlying principle.

In the present study, because all examples considered had many injectors and producers, and because of the more complex permeability fields, it is not directly obvious which injectors-producers combinations are most distant from a time of flight point of view. Generally, however, the plateau production period in the rate-controlled optimized cases is extended due to a delay in water breakthrough, indicating that the time of flight from injectors to producers has increased relative to a conventional water flood.

Results from this and other studies thus suggest that, for a certain constant total injection and production rate, maximizing the time of flight (at all times) and/or minimizing the variation in time of flight (at all times) may be important principles behind an optimal water flood. More research is, however, required to validate this principle.

7.5.2 Pressure-constrained operating conditions

Since the total injection and production rates generally vary in the pressure-constrained optimized cases, the results are more difficult to interpret in terms of possible underlying principles. Interpretation of the results is therefore restricted to describing a number of observations in some detail.

Time of flight

Since total injection and production rates are generally not constant in the pressure constrained optimized case, an increase in the time of flight might result from a drop in the field injection and production rates rather than from an improved macro-scale sweep.

Under pressure-constrained operating conditions, water flood optimization may primarily comprise optimization of the trajectories that have a shorter time of flight than the total production time, i.e. those trajectories along which water breakthrough would occur before the end of the production period if no control would be conducted. In some optimized cases control on water production only occurs at the producers. Producers in or adjacent to the high permeability zone are closed progressively as the oil-water front approaches. Figure 7.20 shows that this increases the length of the flow path from the oil-water front to the active producers. In other cases, control on water production is done both at injectors and producers. Control at the injectors then generally consists of initially closing the injector segments in or adjacent to the high permeability zone, whereas those further away from it

remain open. Figure 7.16c shows that as a result the length of the shortest flow path from injectors to producers increases.

Under pressure constrained operating conditions, the reduction in water production thus appears to be associated with increasing the time of flight along flow paths, that would otherwise cause water breakthrough before the end of the production period. Since the shutting in of wells generally also affects the total injection and production rates, the increase in time of flight is not necessarily directly proportional to the increase in flow path length.

7.5.3 Stages in the production process

Distinct stages in the optimized water flood were reported by Virnovsky (1992) and Virnovsky (1991). The optimal production rates shown in Figures 6.3-6.6, and the associated optimal control functions, shown in Figures 6.7 & 6.8, may also point at the existence of distinct stages. The initial lower-than-maximal production rates are realized by choking at the injector, and serve to avoid water build up at, and production in the production wells at a later stage. The higher oil production rates in the subsequent stage may serve to maximize cumulative oil production. During this stage most well segments are open. In the third stage the total well rates are again much lower due to the closing of producer segments. The main objectives in this stage may be to reduce water production and to increase the macro-scale sweep.

The relative lengths and even the existence of the individual stages may vary with the reservoir, the rock and fluid properties, the well operating constraints, the well locations, the length of the production process, and with discounting. Furthermore, for more complex production scenarios like the pattern flood described in section 6.6 some of these stages may alternatingly become more and less important. It must be emphasized that these stages are based on observations for a restricted number of examples and may as a result be rather speculative and/or incomplete. More simulations on a larger variety of reservoir models and well configurations are needed for verification.

Chapter 8
Conclusions and Recommendations

One objective of this study was to find the optimum injection and production strategy for various types of reservoir models and operating constraints. The use of a gradient based optimization algorithm in combination with optimal control theory appeared very powerful in this respect. A second objective was to investigate the scope for improvement as function of reservoir properties and operating constraints.

8.1 Water Flooding Optimization

8.1.1 Conclusions

For many of the synthetic examples considered significant improvement in NPV of the water flooding process was realized by optimizing the injection and production strategy. Because the optimum strategies were generally dynamic, water flooding optimization expectedly benefits from smart well technology. However, results show that significant improvement may also be possible in a five spot pattern flood with vertical wells, where control may be at the surface. Because the optimization is local, the improvements obtained represent lower limits to improvements possible. Below, the main conclusions on the scope for improvement, the optimal control functions, and the possible principles behind water flooding optimization are given.

Scope for improvement

- The scope for improvement depends on the type of heterogeneity in the permeability field. Because the NPV performance of the optimal water flood depends less on geological features than that of a conventional water flood, the scope for improvement partly depends on the performance of the conventional water flood.

- Under rate-controlled operating conditions there generally is scope for accelerated oil production, increased cumulative oil recovery and decreased water production. Under pressure constrained operating conditions, for the examples and the oil prices and water costs considered, the scope is mainly in reduced water production, although extra cumulative oil production is sometimes also feasible.

- Because under pressure-constrained operating conditions optimized flow control may result in lower-than-maximal well rates, the relative importance of improved sweep, high oil production rates and reduced water production must be considered.

- The scope for improvement also depends on the possibility to affect the pressure distribution, and thereby the fluid flow direction in the reservoir. This may vary with heterogeneity type, the well operating constraints, and the relative well locations in the reservoir.

- The scope for improvement depends on the relative magnitudes of the oil price and the water cost, and on the length of the optimization window.

- Although the displacement efficiency is in an absolute sense much worse if displacement conditions are unfavorable, the scope for improvement by dynamic water flood optimization is relatively higher for unfavorable than for favorable displacement conditions. For the unfavorable displacement case considered part of the improvement resulted from an extension of the production period with positive cash flow.

Preliminary results on water flood optimization in mature oil fields, and water flood optimization with a closed loop assimilation/optimization approach yielded significant NPV improvement. However, since results are based on only one example, general conclusions can not be drawn.

Optimal control functions

- Just like the scope for improvement, the optimal injection and production strategies vary with the relative position of the heterogeneity in the reservoir with respect to the wells and no-flow boundaries, the number of alternating high and low permeability zones, the well operating constraints, and the well locations.

- The optimal control type varies with well operating constraints and to a lesser extent also with the type of reservoir considered. For pressure-constrained well operating conditions an on/off type of optimal control function was often observed, which was never the case under rate-constrained well operating conditions.

- A much smaller number of well segments than used in this study may be sufficient for significant optimization. The exact number of well segments required varies with the type of heterogeneity and with the well operating constraints.

- The importance of control in injectors and producers may change over time. Differences in trends between injector and producer optimal control functions are attributed to the fact that as the water flood progresses the oil-water front moves from the injectors towards the producers.

Principles

- Comparison of the reference and optimal water flood shows that in the latter case there is generally relatively more flow through the low and less through the high permeability zones.
- The characteristics of an optimum water flood seem to vary with well operating conditions. Under rate-controlled well operating conditions the optimization seems associated with an increased time of flight of the oil-water front to the producer in combination with a decreased variation in time of flight. This increased time of flight is distinct from an increase in time of flight realized by simply reducing injection and production rates. Under pressure-constrained well operating conditions, water flood optimization may primarily comprise optimization of the trajectories along which water breakthrough would occur before the end of the production period if no control would be conducted.
- In some examples, the high permeability zones are actively used as extension of the injection or production well

8.1.2 Recommendations

Scope for improvement

The effects of capillary pressure were not investigated in this study. Furthermore, although present in the three-dimensional examples, gravity effects were not studied separately. Results obtained in this study may therefore only be representative for situations were gravity and capillary effects are relatively small. Gravity may positively or negatively affect the sweep efficiency. In fractured reservoirs, capillary effects may significantly contribute to the macro-scale sweep, by causing imbibition of water, present in fractures, into (water-wet) tight matrix blocks. The scope for improvement and the shape of the optimal control functions may thus change if capillary or gravity forces are significant. Therefore, their exact effects should be investigated.

Preliminary results suggest that significant optimization may still be possible in reservoirs that already have a significant non-optimal water flooding history. For the example investigated the scope reduces with optimization starting at a later time. This is, however, partly due to the fact that the end simulation time was fixed. For the scenarios where optimization started close before the end time, the oil production rates were still high at this end time. In practice production would therefore not be stopped at that time. Taking a possible extension of the production period into account, will therefore affect the scope for optimization, something that should be investigated further.

This study primarily focused on investigating the scope for optimization for reservoir models with a priori known properties. For one example the feasibility of a closed loop optimization approach was investigated, yielding significant improvements. Although an encouraging result, it should be considered only a first step. Future work should focus on improving the robustness of this closed loop approach. Apart from addressing divergence issues of the Kalman filter, larger uncertainties in pressure and flow rate measurements must be considered, and estimation of other properties like for example the porosity distribution and the relative permeability curves should be included.

Shape of optimal control functions

Further investigation of the trends observed in the optimal control functions is desirable in order to come up with a better initial guess for the optimization procedure. Knowledge on the shape of the optimal control function may also be useful in field applications, especially if information on reservoir properties is scarce.

8.2 Optimal Control Theory

8.2.1 Conclusions

- Optimal control theory is a suitable optimization procedure for water flood optimization in reservoirs with multiple sources and multiple sinks. The main benefit is in the efficient calculation of the gradients of the objective function with respect to the controllable parameters.
- Stability aspects of the forward dynamic system and the adjoint appeared qualitatively similar.
- Results suggest that for water flood optimization purposes, although formally not exactly the ‘adjoint’, a fully-implicit adjoint scheme can be used in combination with a forward dynamic system formulation that is implicit in the states, and explicit in the state-dependent coefficients.
- The fully-implicit formulation of the adjoint does in principle not require extra computation time compared to the semi-implicit formulation, because the states and the state-dependent coefficients are already known from the forward simulation, and because they are linear in the Lagrange multipliers.

· In a number of cases the gradients obtained with optimal control theory significantly differed from those obtained by numerical perturbation.

8.2.2 Recommendations

The adjoint method is not yet a widely used method for optimization problems in petroleum engineering. Most studies thus far have focused on the applications, rather than the theory itself. Furthermore, the applications in history matching and dynamic process optimization problems seem to have evolved largely independently, each also reporting different difficulties. Since it is a powerful theory with applications in both history matching and dynamic process optimization, it is desirable to study the adjoint method in reservoir simulation applications from a more fundamental point of view. Literature from meteorology, oceanography and hydrology, where adjoint methods have been in use for a longer time, may be very useful in this respect.

Apart from applications in history matching and dynamic process optimization, there may be additional applications of optimal control theory in the petroleum industry. Instead of using the adjoint only to find optimal well rates, it may also be used to select suitable well locations. A first attempt in this directions was done by Virnovsky (1991) and Virnovsky (1992). Secondly, in some applications the adjoint method is used to generate sensitivity coefficients for well bore pressure data and the producing water-oil ratio with respect to reservoir rock properties [Wu *et al.* (1999)]. These sensitivity maps may possibly also be used for optimization purposes, because they may provide information on suitable locations for near-well stimulation and/or shutoff methods.

Instead of only using the gradients obtained by the adjoint method it may also be possible to directly use the values of the Lagrange multipliers. Chapter 4 and 5 showed that they may have a physical meaning that one may make use of. Depending on their exact physical meaning they may possibly be helpful in finding suitable infill well locations or new branches in existing wells.

Nomenclature

This section contains a declaration of the most important symbols, abbreviations and subscripts in chapters 1 - 7.

Greek

α	down-hole valve
α_{eff}	effective valve multiplication factor $[-]$
α_{icv}	multiplication factor representing down-hole interval control valve $[-]$
α_{wh}	multiplication factor representing well head choke $[-]$
$\boldsymbol{\alpha}$	vector containing effective valve multiplication factors
γ	normalized sum of absolute differences between reference and optimal well rates $[-]$
Φ	fluid potential $[Pa]$
$\frac{\partial \mathcal{L}^*}{\partial u}$	modified gradient
ε	weighting factor in steepest descent algorithm
ϕ	porosity $[-]$
λ_l	component mobility $\left[\frac{m^2}{Pa\ s}\right]$
$\boldsymbol{\lambda}$	vector of Lagrange multipliers
μ	fluid viscosity $[Pa\ s]$
ρ_l	density of component l $\left[\frac{kg}{m^3}\right]$
τ	cumulative time $[yr]$
θ	angle between principal axes of the high permeability zone and the wells

Roman

$\mathbf{A}$	system matrix
b	discount rate $\left[\frac{\%}{yr}\right]$
$\mathbf{B}$	storage matrix
B_l	component formation volume factor $\left[\frac{m^3}{m^3}\right]$
C_{CFL}	Courant-Friedrich-Levy condition $[-]$
EOR	enhanced oil recovery
f_{cgo}	gas-oil capillary pressure function $[Pa]$
f_{cow}	oil-water capillary pressure function $[Pa]$
$f_w\left(S_w\right)$	fractional flow of water $[-]$
g	gravitational acceleration factor $\left[\frac{m}{s^2}\right]$
$\mathbf{g}$	dynamic system vector
$\mathbf{G}_{\mathrm{adj}}$	adjoint system matrix
GOR	gas-oil-ratio $\left[\frac{m^3}{m^3}\right]$
h	depth $[m]$
$\mathcal{H}$	Hamiltonian

$\mathbf{I}$	identity matrix
$\bar{\mathcal{J}}$	modified objective function
$\mathcal{J}$	objective function
$\mathcal{J}_j$	cost-to-go objective function
J	objective function
J^n	cash flow for time step n [\$]
J_w^*	value of grid block filled with water [\$]
k	absolute permeability $\left[m^2\right]$
k_{rl}	relative permeability for component l $[-]$
$\mathcal{L}$	Lagrangian
J_o^*	value of grid block filled with oil [\$]
L_x	Reservoir dimension in x-direction $[m]$
$\dot{\mathbf{m}}$	mass rate vector $\left[\frac{kgm}{s}\frac{1}{m^3}\right]$
m	mass $[kg]$
n	discrete time step indicator
N	final time step
N_{inj}	number of injectors
N_{prod}	number of producers
NPV	net present value [\$]
O	order
OCT	optimal control theory
$\hat{\mathbf{p}}$	vector containing primary variables
$\hat{\mathbf{p}}_{wf}^n$	vector containing well flowing pressures
p_{cgo}	gas-oil capillary pressure $[Pa]$
p_{cow}	oil-water capillary pressure $[Pa]$
p_{gb}	grid block pressure $[Pa]$
p_l	component pressure $[Pa]$
p_{wf}	well flowing pressure $[Pa]$
PV	pore volume, total porous volume in reservoir occupied by fluids $\left[m^3\right]$
$\grave{q}$	source term $\left[\frac{kg}{s}\frac{1}{m^3}\right]$
$\mathbf{q}_{\text{adj}}$	source vector for adjoint equation
$\hat{\mathbf{q}}$	vector containing source terms
$\tilde{q}_l$	source term $\left[\frac{1}{s}\right]$
q_l^*	volumetric rate at surface conditions $\left[\frac{m^3}{s}\right]$
r_l	price (+)/cost (-) for production of component l $\left[\frac{\$}{m^3}\right]$

R_s	solution gas-oil ratio $\left[\frac{m^3}{m^3}\right]$
$streak$	zone of high permeability in area of lower permeability
S_l	fractional saturation of component l
S_{or}	residual oil saturation $[-]$
S_{wc}	connate water saturation $[-]$
S_w^*	constraint on maximum water saturation $[-]$
t	time $[s]$
t_{df}	time interval in which flow rates are optimized $[s]$
t_{tot}	total production time $[s]$
$\hat{\mathbf{T}}$	transmissibility matrix
$\mathbf{T_4}$	transmissibility matrix for gravity driven flow
$\mathbf{u}_l$	component velocity vector $\left[\frac{m}{s}\right]$
u_t	total fluid velocity $\left[\frac{m}{s}\right]$
$\mathbf{u}$	input/control variables
V_f	fluid volume in one grid block $\left[m^3\right]$
$\hat{\mathbf{w}}_{pc}^n$	injection/production due to capillary forces
w	well geometric and rock/fluid properties
w_{hp}	width of high permeability zone $[m]$
w_{tot}	width of reservoir $[m]$
$\hat{\mathbf{W}}^n$	matrix containing well geometric factors and fluid mobilities
WOR	water-oil-ratio $\left[\frac{m^3}{m^3}\right]$
x	distance in x-direction $[m]$
$\mathbf{x}$	state vector

Subscripts/superscipts

$_{opt}$	optimal
$_{dg}$	dissolved gas component
$_{fg}$	free gas component
$_{g}$	gas component
$_{h}$	horizontal
$_{inj}$	injection
$_{ref}$	reference (non-optimized) case
$_{r}$	iteration number in optimization loop
$_{t}$	total
$_{v}$	vertical
$_{w}$	water component
$_{l}$	component indicator
$_{o}$	oil component
$^{\max}$	maximum allowed value
$^{\min}$	minimum allowed value

Bibliography

Asheim, H. Optimal Control of Water Drive, paper SPE 15978, provided to the SPE for distribution and possible publication in an SPE journal (1986).

Asheim, H. Maximization of Water Sweep Efficiency by Controlling Production and Injection Rates, paper SPE 18365, presented at the SPE European Petroleum Conference, London, UK, 16-18 October (1988).

Aziz, K. and Settari, A. (1986). *Petroleum Reservoir Simulation*. Elsevier Applied Science Publishers.

Bi, Z., Oliver, D. S., and Reynolds, A. C. (2000). Conditioning 3D Stochastic Channels to Pressure Data. *SPE Jounal*, dec, **5**(4).

Birnovskii, G. A. (1988). On Optimal Control of Multiphase Porous Flow in an Oil Bed. *U.S.S.R. Comput. Maths. Math. Phys.*, **28**(3), 156–163. Article contains error in name of author: Real name is Virnovsky, G.A.

Brouwer, D. R. and Jansen, J. D. Dynamic Optimization of Water Flooding with Smart Wells Using Optimal Control Theory, paper SPE 78278 presented at the 13th SPE European Petroleum Conference (EUROPEC), Aberdeen, Scotland, 29-31 October (2002).

Brouwer, D. R., Jansen, J. D., van der Starre, S., and van Kruijsdijk, C. P. J. W. Recovery Increase through Water Flooding using Smart Well Technology, paper SPE 68979 presented at the SPE European Formation Damage Conference, The Hague, The Netherlands, 21-22 May (2001).

Chavent, C., Dupuy, M., and Lemonnier, P. History Matching by Use of Optimal Control Theory, paper SPE 4627, presented at the SPE-AIME 48th Annual Fall Meeting, Las Vegas, Nevada, 30 September - 3 October (1973).

Chavent, G. (1979). *Identification of Distributed Parameter Systems: About the Output Least Squares Method, its Implementation and Identification and System Parameter Estimation*. Pergamon Press, Darmstadt.

Chavent, G. and Cohen, G. Determination of Relative Permeabilities and Capillary Pressures by an Automatic Adjustment Method, paper SPE 9237, presented at the 55th Annual Fall Technical Conference and Exhibition, Dallas, Texas, 21-24 September (1980).

Chavent, G., Cohen, G., and Espy, M. Determination of relative permeabilities and capillary pressures by an automatic adjustment method, SPE paper 9237, presented at the 55th Annual Fall Technical Conference and Exhibition, Dallas, 21-24 September (1980).

Derber, J. C. (1989). A Variational Continuous Assimilation Technique. *Mon. Wea. Rev.*, **117**, 2437–2446.

Dolle, N., Brouwer, D. R., and Jansen, J. D. Dynamic Optimization of Water Flooding with Multiple Injectors and Producers using Optimal Control Theory, XIVth International Conference on Computational Methods in Water Resources, Delft (2002).

Dougherty, E. L. and Khairkhah, D. a. History Matching of Gas Simulation Models Using Optimal Control Theory, paper SPE 5371, presented at the 45th SPE-AIME Annual California Regional Fall Meeting, Venture, California, 2-4 April (1975).

Erlandsen, S. M. Production Experience from Smart Wells in the Oseberg Field, paper SPE, presented at the Annual Technical Conference and Exhibition, Dallas, Texas, 1-4 October (2000).

Ertekin, T., Abou-Kassem, J. H., and King, G. R. (2001). *Basic Applied Reservoir Simulation*. SPE Textbook Series 7.

Fasanino, G., Molinard, J. E., de Marsily, G., and Pelcé, V. Inverse Modeling in Gas Reservoirs, paper SPE 15592, presented at the 61st SPE Annual Technical Conference and Exhibition, New Orleans, Texas, 5-8 October (1986).

Fathi, Z. (1986). *Optimization of an Enhanced Oil Recovery Process with Boundary Controls - A Large-Scale Nonlinear Maximization*. Ph.D. thesis, University of Colorado.

Fathi, Z. and Ramirez, W. F. (1984). Optimal Injection Policies for Enhanced Recovery: Part 2-Surfactant Flooding. *SPE Journal*, **24**(3), 333–341.

Fathi, Z. and Ramirez, W. F. (1987). Optimization of an Enhanced Oil Recovery Process with Boundary Controls - A Large-scale Non-linear Maximization. *Automatica*, **Vol. 23**(3), 301–310.

Fletcher, R. (1987). *Practical Methods of Optimization*. John Wiley & Sons, New York, 2nd edition edition.

Gai, H. Downhole Flow Control Optimization in the Worlds 1^{st} Extended Reach Multilateral Well at Wytch Farm, paper SPE/IADC, presented at the SPE/IADC Drilling Conference, Amsterdam, The Netherlands, 27 February - 1 March (2001).

Hoffman, J. D. (1992). *Numerical Methods for Engineers and Scientists*. McGraw-Hill, Inc.

Holmes, J. A. (2001). Modeling Advanced Wells in Reservoir Simulation. *Journal of Petroleum Technology*, nov, pp 54–66.

Jacobs, A. (1993). *Timespan Minimisation for Storm Surge Barrier Control*. Ph.D. thesis, Delft University of Technology.

Jansen, J. D., Wagenvoort, A. M., Droppert, V. S., Daling, R., and Glandt, C. A. Smart Well Solutions for Thin Oil Rims: Inflow Switching and the Smart Stinger Completion, paper SPE 77942, presented at the SPE Asia Pacific Oil and Gas Exhibition, Melbourne, Australia, 8-10 October (2002).

Kraaijevanger, J. F. B. M. (2004). Personal Communication.

Li, R., Reynolds, A. C., and Oliver, D. S. History Matching of Three-Phase Flow Production Data, paper SPE 66351, presented at the Reservoir Simulation Symposium, Houston, Texas, 11-14 February (2001).

Li, S. and Petzold, L. (2003). Adjoint Sensitivity Analysis for Time-Dependent Partial Differential Equations with Adaptive Mesh Refinement. *Journal of Computational Physis, to appear*.

Li, Y. and Droegemeier, K. K. (1993). The Influence of Diffusion and Associated Errors on the Adjoint Data Assimilation Technique. *Tellus*, **45A**, 435–448.

Liu, W. and Ramirez, W. F. (1994a). Optimal Control of Three-Dimensional Steam Flooding Processes. *Journ. Of Pet. Sc. and Eng.*, **11**, 137–154.

Liu, W. and Ramirez, W. F. (1994b). Optimal Control of Three-Dimensional Steamflooding Processes. *Journ. of Pet. Sc. and Eng*, **11**, 137–154.

Liu, W., Ramirez, W. F., and Qi, Y. F. Optimal Control of Steamflooding, paper SPE 21619, provided to the SPE for distribution and possible publication in an SPE journal (1990).

Luenberger, D. G. (1979). *Introduction to Dynamic Systems. Theory, Models & Applications*. John Wiley and Sons Inc.

Mehos, G. J. (1986). *Optimal Control Policies for Carbon Dioxide Recovery Miscible Flooding Enhanced Oil Recovery*. Ph.D. thesis, University of Colorado at Boulder.

Mehos, G. J. and Ramirez, W. F. (1989). Use of Optimal Control Theory to Optimize Carbon Dioxide Miscible-Flooding Enhanced Oil Recovery. *Journ. of. Pet. Sc. and Eng*, **2**, 247–260.

Naevdal, G., Mannseth, T., and Vefring, E. H. Instrumented Wells and Near-Well Reservoir Monitoring through Ensemble Kalman Filter, in Proceedings of 8th European Conference on the Mathematics of Oil Recovery, Freiberg, Germany, 3-6 September (2002a).

Naevdal, G., Mannseth, T., and Vefring, E. H. Near-Well Reservoir Monitoring through Ensemble Kalman Filter, paper SPE 75235, presented at the SPE/DOE improved oil recovery symposium, Tulsa, Oklahoma, April (2002b).

Naevdal, G., Johnsen, L. M., Aanonsen, S. I., and Vefring, E. H. Reservoir Monitoring and Continuous Model Updating using Ensemble Kalman Filter, paper SPE 84372, presented at the SPE Annual Technical Conference and Exhibition, Denver, Colorado, 5-8 October (2003).

Palatnik, B. M. and Aanonsen, S. I. (1994). New Technique to Improve the Efficiency of History Matching. *original journal unknown*.

Peaceman, D. W. (1977). *Fundamentals of Numerical Reservoir Simulation*. Elsevier Scientific Publishing Company.

Porzucek, C. Optimal Injection Strategies for Surfactant Flooding Enhanced Oil Recovery using a Streamtube Reservoir Simulator - Part 2, The Optimal Control Problem, paper SPE 17096 provided to the SPE for distribution and possible publication in an SPE journal (1988).

Ramirez, W. F. (1987). *Application of Optimal Control Theory to Enhanced Oil Recovery*, volume 21 of *Developments in Petroleum Science*. Elsevier Science Publishers B.V.

Ramirez, W. F., Fathi, Z., and Cagnol, J. L. (1984). Optimal Injection Policies for Enhanced Recovery: Part 1-Computational Strategies. *SPE Journal*, **24**(3), 328–332.

Ray, W. H. (1981). *Advanced Process Control*. McGraw-Hill.

Saputelli, L. A., Mochizuki, S., Hutchins, L., and Cramer, R. Promoting Real-Time Optimization of Hydrocarbon Producing Systems, paper SPE 83978, presented at Offshore Europe, Aberdeen, United Kingdom, 2-5 September (2003a).

Saputelli, L. A., Nikolaou, M., and Economides, M. J. Self-Learning Reservoir Management, paper SPE 84064, presented at the Annual Technical Conference and Exhibition, Denver, Colorado, 5-8 October (2003b).

Silin, D. B. and Patzek, T. W. Control of Water Injection into a Layered Formation, paper SPE 59300, presented at the 2000 SPE/DOE Improved Oil Recovery Symposium, Tulsa, Oklahoma, 3-5 April (2000).

Silin, D. B. and Patzek, T. W. (2001). Control Model of Water Injection into a Layered Formation. *SPE Jounal*, September, pp 253–261.

Sinha, S., Kumar, R., Vega, L., and Jalali, Y. Flow Equilibration Towards Horizontal Wells Using Downhole Valves, paper SPE 68635, presented at the SPE Asia Pacific Oil and Gas Conference and Exhibition, Jakarta, Indonesia, 17-19 April (2001).

Stengel, R. F. (1994). *Optimal Control and Estimation*. Dover Publications Inc., New York.

Strang, G. (1986). *Introduction to Applied Mathematics*. Wellesley-Cambridge Press.

Sudaryanto, B. (1998). *Optimization of Displacement Efficiency of Oil Recovery in Porous Media using Optimal Control Theory*. Ph.D. thesis, University of Southern California.

Sudaryanto, B. and Yortsos, Y. C. (2000). Optimization of Fluid Front Dynamics in Porous Media using Rate Control. I Equal Mobility Fluids. *Phys. of Fluids*, jul, **12**(7), 1656–1670.

Sudaryanto, B. and Yortsos, Y. C. Optimization of Displacements in Porous Media Using Rate Control, paper SPE 71509, presented at the 2001 Annual Technical Conference and Exhibition, New Orleans, Louisiana, 30 September - 3 October (2001).

Ulbrich, S. (2001). *Optimal Control of Nonlinear Hyperbolic Conservation Laws with Source Terms*. Ph.D. thesis, Technische Universität München, Fakultät für Mathematik.

Valvatne, P. H., Durlofsky, L. J., and Aziz, K. Semi-Analytical Modeling of the Performance of Intelligent Well Completions, paper SPE 66368, presented at the SPE Reservoir Simulation Symposium, Houston, Texas, 11-14 February (2001).

van Delden, R. M., Uv, E. H., and Jalali, Y. A Model-Based Approach to Assist Operation of a Gas-Constrained Multizone Intelligent Completion in the Ness Formation, paper SPE 71824 presented at the Offshore Europe Conference, Aberdeen, Scotland, 4-7 September (2001).

Virnovsky, G. A. Water flooding Strategy Design Using Optimal Control Theory, paper presented at the 6th. European IOR-Symposium, Stavanger, Norway, 21-23 May (1991).

Virnovsky, G. A. Optimization Techniques Application in Oil Recovery Problems, paper SPE 24281, presented at the SPE European Petroleum Computer Conference, Stavanger, Norway, 25-27 May (1992).

Wasserman, M. L., Emanuel, A. S., and Seinfeld, J. H. Practical Applications of Optimal Control Theory to History-Matching Multiphase Simulator Models, paper SPE 5020, presented at the SPE-AIME 49th Annual Fall Meeting, Houston, Texas, 6-9 October (1974).

Watson, A. T., Seinfeld, J. H., Gavalas, G. R., and Woo, P. T. History Matching in Two-Phase Petroleum Reservoirs, paper SPE 8250, presented at the SPE-AIME 54th Annual Fall Technical Conference and Exhibition, Las Vegas, Nevada (1979).

Wu, Z. (1999). *Conditioning Geostatistical Models to Two-Phase Production Data*. Ph.D. thesis, University of Tulsa.

Wu, Z. A Newton-Raphson Iterative Scheme for Integrating Multiphase Production Data into Reservoir Models, paper SPE 62846, presented at the 2000 SPE/AAPG Western Regional Meeting, Long Beach, California, 19-23 June (2000).

Wu, Z. and Datta-Gupta, A. Rapid History Matching Using a Generalized Travel Time Inversion Method, paper SPE 66352 presented at the SPE Reservoir Simulation Symposium, Houston, Texas, 11-14 February (2001).

Wu, Z., Reynolds, A. C., and Oliver, D. S. (1999). Conditioning Geostatistical Models to Two-Phase Production Data. *SPE Jounal*, June, **4**.

Xu, Q. (1996). Generalized Adjoint for Physical Processes with Parameterized Discontinuities. Part I: Basic Issues and Heuristic Examples. *Journal of the Atmospheric Sciences*, **53**(8), 1123–1142.

Yang, D., Zhang, Q., Gu, Y., and Li, L. Integrated Global Optimization of Displacement Efficiency in Hydrocarbon Reservoirs, paper SPE 81035, presented at the SPE Latin American and Caribbean Petroleum Engineering Conference, Port-of-Spain, Trinidad, West-Indies, 27-30 April (2003).

Yang, P. H. and Watson, A. T. Automatic History Matching with Variable-Metric Methods, paper SPE 16977, presented at the SPE 62nd Annual Technical Conference and Exhibition, Dallas, Texas, 27-30 September (1987).

Yeten, B. (2003). *Optimum Deployment of Nonconventional Wells*. Ph.D. thesis, Stanford University.

Yeten, B. and Jalali, Y. Effectiveness of Intelligent Completions in a Multiwell Development Context, paper SPE 68077, presented at the 2001 SPE Middle East Oil Show, Bahrain, 17-20 March (2001).

Yeten, B., Durlofsky, L. J., and Aziz, K. Optimization of Smart Control, paper SPE 79031 presented at the 2002 SPE International Thermal Operations and Heavy Oil Symposium and International Horizontal Well Technology Conference, Calgary, Alberta, Canada, 4-7 November (2002).

Yeten, B., Brouwer, D. R., Durlofsky, L. J., and Aziz, K. (2004). Decision Analysis under Uncertainty for Smart Well Deployment. *Journal of Petroleum Science and Engineering, special issue on risk analysis (accepted)*.

Yu, S., Davies, D. R., and Sherrard, D. W. The Modelling of Advanced "Intelligent" Well – An Application, paper SPE 62950 presented at the 2000 SPE Annual Technical Conference and Exhibition, Dallas, Texas, 1-4 October (2000).

Zakirov, I., Astl, A., Zakirov, E., and Schweng, K. History Matching for Lauchstaedt Underground Gas Storage, paper SPE 39994, presented at the 1998 SPE Gas Technology Symposium, Galgary, Alberta, 15-18 March (1998).

Zakirov, I. S. and Zakirov, E. S. Aquifer Configuration Estimation Through Inverse Problem Solution, paper SPE 51926, presented at the 1999 SPE Reservoir Simulation Symposium, Houston, Texas, 14-17 February (1999).

Zakirov, I. S., Aanonsen, S. I., Zakirov, E. S., and Palatnik, B. M. Optimization of Reservoir Performance by Automatic Allocation of Well Rates, 5th European Conference on the Mathematics of Oil Recovery, Leoben (1996).

Appendix A
The reservoir model

In this study optimization of the water flooding process was investigated both for two-phase (oil and water) flow in the horizontal plane, and three-phase, three-dimensional flow. Two separate reservoir model were used. Since the three-phase, three-dimensional formulation is the most general, it is the one that will be discussed. The black oil formulation described in the following sections is based on the formulation from Aziz and Settari (1986). The three phases that are distinguished are gas, oil, and water. The three components that are distinguished are the light and the heavy hydrocarbon pseudo-components and the water component.

A.1 Three phase flow

A.1.1 Mass Balance equations

In multi-phase flow the mass balance for each individual component per unit rock volume is

$$-\nabla \cdot \dot{\mathbf{m}} + \grave{q} = \frac{\partial(m)}{\partial t}, \tag{A.1}$$

which states that the difference in mass flowing into and out of a unit volume per unit time, plus the mass added or extracted through an external source per unit time and volume $\grave{q}$ $\left[\frac{kg}{s}\frac{1}{m^3}\right]$ must equal the change in mass per unit time and volume $\frac{\partial(m)}{\partial t}$ $\left[\frac{kg}{s}\frac{1}{m^3}\right]$. $\dot{\mathbf{m}}$ is a vector comprising the mass flow in *x*,*y*,*z*-direction and has unit $\left[\frac{kgm}{s}\frac{1}{m^3}\right]$. For a component c it is equal to the product of its density and the velocity of the phase l in which it is present, i.e. $\dot{\mathbf{m}}_c{=}\rho_c\mathbf{u}_l$. The total mass m of component c per unit rock volume can be expressed as the product of the component density ρ_c, the rock porosity ϕ, and the phase saturation S_l (The volume fraction of the porous rock that is occupied by the phase l in which component c is present.), i.e. $m_c = \rho_c\phi S_l$. Substitution into eq. A.1 then gives

$$-\nabla \cdot \rho_c\mathbf{u}_l = \frac{\partial}{\partial t}\left(\rho_c\phi S_l\right) - \rho_c\tilde{q}_l, \tag{A.2}$$

where the source term $\tilde{q}_l$ has unit $\left[\frac{1}{s}\right]$, $\mathbf{u}_l$ $\left[\frac{m}{s}\right]$ is a vector with the phase velocities in *x*,*y*,*z*-direction. The porosity and density are a function of pressure. The component density is generally assumed to be a function of the phase pressure p_l, hence $\rho_c = \rho_c\left(p_l\right)$.

For the heavy hydrocarbon component the mass balance then becomes

$$-\nabla \cdot \bar{\rho}_o \mathbf{u}_o = \frac{\partial}{\partial t}\left(\bar{\rho}_o \phi S_o\right) - \bar{\rho}_o \tilde{q}_o \tag{A.3}$$

where $\bar{\rho}_o$ is the density of the heavy hydrocarbon component in the oil phase. For the water component the material balance is

$$-\nabla \cdot \rho_w \mathbf{u}_w = \frac{\partial}{\partial t}\left(\rho_w \phi S_w\right) - \rho_w \tilde{q}_w \tag{A.4}$$

For the light hydrocarbon component the situation is slightly different since it is present both in the gas phase and in solution in the oil phase.

$$\dot{\mathbf{m}}_g = \bar{\rho}_{dg} \mathbf{u}_o + \rho_g \mathbf{u}_g \tag{A.5}$$

$$m_g = \bar{\rho}_{dg} \phi S_o + \rho_g \phi S_g \tag{A.6}$$

where $\bar{\rho}_{dg}$ is the density of the heavy hydrocarbon component dissolved in the oil phase. The mass balance then is

$$-\nabla \cdot \left(\bar{\rho}_{dg} \mathbf{u}_o + \rho_g \mathbf{u}_g\right) = \frac{\partial}{\partial t}\left(\bar{\rho}_{dg} \phi S_o + \rho_g \phi S_g\right) - \bar{\rho}_{dg} \tilde{q}_o - \rho_g \tilde{q}_{fg} \tag{A.7}$$

The source terms $\bar{\rho}_{dg} \tilde{q}_o$ and $\rho_g \tilde{q}_{fg}$ represent respectively dissolved and free gas production.

A.1.2 Formation Volume Factors and the Solution gas-oil-ratio

Under the assumption of constant reservoir temperature, the relation between the phase volumes at surface conditions and reservoir conditions can be described by the formation volumes factors

$$B_o = \frac{V_{o,RC}}{V_{o,SC}} = f_1 \qquad [-], \tag{A.8}$$

$$B_w = \frac{V_{w,RC}}{V_{w,SC}} = f_2\left(p_w\right) \qquad [-], \tag{A.9}$$

$$B_g = \frac{V_{g,RC}}{V_{fg,SC}} = f_3\left(p_g\right) \qquad [-], \tag{A.10}$$

where V_l stands for the volume occupied by a fixed mass of phase l at reservoir conditions and the subscript SC refers to the volume at standard conditions (atmospheric pressure and temperature) and RC for the volume at reservoir conditions. The oil formation volume factor B_o is a function of both the oil pressure and the bulk hydrocarbon composition in the reservoir. The equilibrium distribution of the light hydrocarbon pseudo component between the oil and gas phases is described by the solution-gas-oil ratio

$$R_s = \left[\frac{V_{dg}}{V_o}\right]_{STC} = f_4 \qquad [-], \tag{A.11}$$

which is the ratio of the SC-volume of dissolved gas over the SC-oil volume. In the black oil approach this equilibrium distribution is assumed to be reached instantaneously throughout the reservoir. For saturated oil, R_s increases with pressure up to the bubble point pressure. The

bubble point pressure (p_{bp}) is the pressure at which all light hydrocarbons are just dissolved in the oil phase. Above p_{bp} the oil is undersaturated, and R_s is therefore constant. Apart from the pressure, p_{bp} and R_s also depend on the bulk hydrocarbon composition in the reservoir. In this study, however, R_s is assumed to be only a function of pressure.

The phase densities at reservoir conditions are related to the component densities at standard conditions in the following way. For the oil phase

$$\begin{aligned} \rho_o &= \tfrac{1}{B_o}\left(\rho_{o_{SC}} + R_s\rho_{g_{SC}}\right) \\ &= \bar{\rho}_o + \bar{\rho}_{dg} \end{aligned}$$

where $\bar{\rho}_o = \frac{1}{B_o}\rho_{o_{STC}}$ is the density of the oil component in the oil phase at reservoir conditions and $\bar{\rho}_{dg} = \frac{R_s}{B_o}\rho_{g_{STC}}$ the density of the dissolved gas component. Similarly for the gas and water phase

$$\rho_w = \tfrac{1}{B_w}\left(\rho_{w_{STC}}\right) \tag{A.12}$$

$$\rho_g = \tfrac{1}{B_g}\left(\rho_{g_{STC}}\right) \tag{A.13}$$

After dividing eq. A.3 by $\rho_{o_{STC}}$ the mass balance for the heavy hydrocarbon component becomes

$$-\nabla\cdot\tfrac{1}{B_o}\mathbf{u}_o = \tfrac{\partial}{\partial t}\left(\tfrac{1}{B_o}\phi S_o\right) - \tfrac{1}{B_o}\tilde{q}_o \tag{A.14}$$

After dividing eq. A.4 by $\rho_{w_{STC}}$ the mass balance for the water component becomes

$$-\nabla\cdot\tfrac{1}{B_w}\mathbf{u}_w = \tfrac{\partial}{\partial t}\left(\tfrac{1}{B_w}\phi S_w\right) - \tfrac{1}{B_w}\tilde{q}_w \tag{A.15}$$

For the gas component dividing eq. A.7 by $\rho_{g_{STC}}$ results in

$$-\nabla\cdot\left(\tfrac{R_s}{B_o}\mathbf{u}_o + \tfrac{1}{B_g}\mathbf{u}_g\right) = \tfrac{\partial}{\partial t}\left(\tfrac{R_s}{B_o}\phi S_o + \tfrac{1}{B_g}\phi S_g\right) - R_s\tfrac{1}{B_o}\tilde{q}_o - \tfrac{1}{B_g}\tilde{q}_{fg} \tag{A.16}$$

All production terms $\tilde{q}_o, \tilde{q}_w, \tilde{q}_{fg}$ have dimension. $\left[\frac{1}{\mathrm{s}}\right]$.

A.1.3 Constitutive equation - Darcy's Law

The fluid flow velocity in permeable media is often described through Darcy's law which for single phase, one dimensional flow reads as

$$u_x = -\tfrac{k}{\mu}\tfrac{\partial\Phi}{\partial x}. \tag{A.17}$$

It states that the fluid velocity u_x $\left[\frac{m}{s}\right]$ is proportional to the fluid potential gradient $\frac{\partial\Phi}{\partial x}$, the rock permeability k $\left[m^2\right]$ and inversely proportional to the fluid viscosity μ $[Pa\ s]$. The same law may be used for multi-phase and multi-dimensional flow. The only extra factor needed is the relative permeability k_{rl} $[-]$, where l is the phase considered. The relative permeability represents a reduction in the permeability for a phase due to interference with another phase.

Furthermore, the fluid potential gradient can be expressed as

$$\nabla\Phi_l = \nabla p_l - \rho_l g \nabla h, \tag{A.18}$$

where p_l is the phase pressure, g is the gravitational acceleration $\left(g = 9.81\ \frac{m}{s^2}\right)$, and h is the depth. Darcy's law for phase l then becomes

$$\mathbf{u}_l = -\frac{k k_{rl}}{\mu_l}\left(\nabla p_l - \rho_l g \nabla h\right). \tag{A.19}$$

The density and viscosity are a function of both pressure and temperature. Constant temperature is assumed in the black oil model, and in this study the densities and viscosities are assumed to be only a function of pressure, i.e. $\rho_l = \rho_l\left(p_l\right)$, and $\mu_l = \mu_l\left(p_l\right)$. The relative permeability is assumed to be only a function of saturation. In three-phase flow with a water-wet rock the relative permeability for the oil phase is typically taken to be a function of both the water (S_w) and the gas saturations (S_g), i.e. $k_{ro} = k_{ro}\left(S_w, S_g\right)$. The relative permeability for the water and gas phases is then generally taken to be a function of only their own phase saturation, i.e. $k_{rw} = k_{rw}\left(S_w\right)$ and $k_{rg} = k_{rg}\left(S_g\right)$. This is done because in a water-wet rock water and gas generally reside in a different part of the pore space and are separated by the oil, as schematically depicted in Figure A.1. Because gas and water do not interface in this situation, changes in saturation of either of them is then assumed to have no (significant) effect on the relative permeability of the other. Since the oil interfaces with both gas and water its relative permeability depends on both saturations. Typically, values for the relative permeability are derived from two-phase flow experiments.

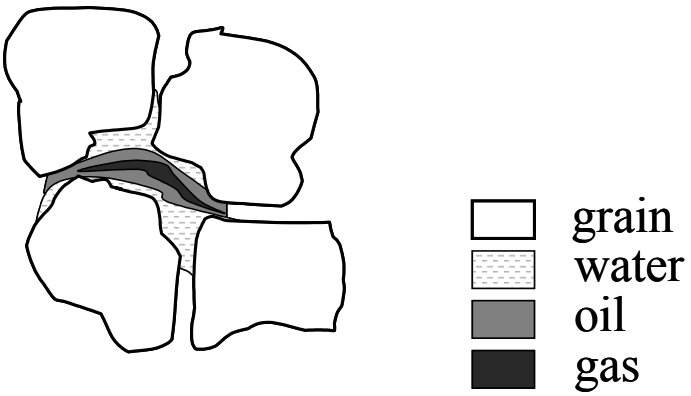

Figure A.1: Schematic of pore space occupied by water phase, oil phase and gas phase in a water wet medium

A.1.4 Mass balance combined wit Darcy's Law

Substituting Darcy's law for each phase into eqs. A.14, A.15, and A.16, and substituting the relation $\lambda_l = \frac{k_{rl}}{B_l \mu_l} k$ for each phase, where λ_l is the mobility of phase l, results in

$$\nabla \cdot (\lambda_o (\nabla p_o - \rho_o g \nabla h)) = \frac{\partial}{\partial t} \left(\frac{1}{B_o} \phi S_o \right) - \frac{1}{B_o} \tilde{q}_o, \tag{A.20}$$

$$\nabla \cdot (\lambda_w (\nabla p_w - \rho_w g \nabla h)) = \frac{\partial}{\partial t} \left(\frac{1}{B_w} \phi S_w \right) - \frac{1}{B_w} \tilde{q}_w, \tag{A.21}$$

$$\begin{aligned} & \nabla \cdot \left(R_s \lambda_o (\nabla p_o - \rho_o g \nabla h) + \lambda_g \left(\nabla p_g - \rho_g g \nabla h \right) \right) \\ = \quad & \frac{\partial}{\partial t} \left(\frac{R_s}{B_o} \phi S_o + \frac{1}{B_g} \phi S_g \right) - \frac{1}{B_o} R_s \tilde{q}_o - \frac{1}{B_g} \tilde{q}_{fg}. \end{aligned} \tag{A.22}$$

A.1.5 Choice of primary variables - Formulation in terms of p_o, S_w, and S_g

With 6 unknowns (p_o, p_w, p_g, S_o, S_w, and S_g) 6 equations are required to complete the system description. Apart from eqs. A.20, A.21 & A.22 these comprise 3 additional equations. The first is a closure equation requiring that the sum of all fractional saturations must always be equal to one, i.e.

$$S_o + S_w + S_g = 1. \tag{A.23}$$

Furthermore, the relation between the individual phase pressures is given by the capillary pressure equations

$$p_{cow} = p_o - p_w = f_{cow} (S_w, S_g), \tag{A.24}$$

$$p_{cgo} = p_g - p_o = f_{cgo} (S_w, S_g), \tag{A.25}$$

where water is assumed to be the wetting phase, oil the intermediate wetting phase, and gas the nonwetting phase. Functions f_{cow} and f_{cgo} are generally empirical relations, derived from core experiments.

In eqs. A.20, A.21, A.22 the primary variables are respectively p_o, p_w, and p_g. Generally a formulation with primary variables being the oil pressure p_o, the fractional water saturation S_w and the fractional gas saturation S_g is used in reservoir simulation. This can be obtained by substituting eqs. A.23, A.24, A.25 into eqs. A.20, A.21, A.22, giving

$$\nabla \cdot (\lambda_o (\nabla p_o - \rho_o g \nabla h)) = \frac{\partial}{\partial t} \left(\frac{1}{B_o} \phi (1 - S_w - S_g) \right) - \frac{1}{B_o} \tilde{q}_o, \tag{A.26}$$

$$\nabla \cdot (\lambda_w (\nabla (p_o - p_{cow}) - \rho_w g \nabla h)) = \frac{\partial}{\partial t} \left(\frac{1}{B_w} \phi S_w \right) - \frac{1}{B_w} \tilde{q}_w, \tag{A.27}$$

$$\begin{aligned} & \nabla \cdot \left(R_s \lambda_o (\nabla p_o - \rho_o g \nabla h) + \lambda_g \left(\nabla (p_o + p_{cgo}) - \rho_g g \nabla h \right) \right) \\ = \quad & \frac{\partial}{\partial t} \left(\frac{R_s}{B_o} \phi (1 - S_w - S_g) + \frac{1}{B_g} \phi S_g \right) - \frac{1}{B_o} R_s \tilde{q}_o - \frac{1}{B_g} \tilde{q}_{fg}. \end{aligned} \tag{A.28}$$

The capillary pressure gradients can be expressed in terms of a saturation gradient using

$$\nabla p_{cow} = \frac{\partial p_{cow}}{\partial S_w}\nabla S_w + \frac{\partial p_{cow}}{\partial S_g}\nabla S_g, \tag{A.29}$$

and

$$\nabla p_{cgo} = \frac{\partial p_{cgo}}{\partial S_w}\nabla S_w + \frac{\partial p_{cgo}}{\partial S_g}\nabla S_g. \tag{A.30}$$

Substitution of eqs. A.29 & A.30 into the left sides of eqs.A.26,A.27 & A.28 then gives

$$\nabla \cdot (\lambda_o \nabla p_o - \lambda_o \rho_o g \nabla h) = \frac{\partial}{\partial t}\left(\frac{1}{B_o}\phi\left(1 - S_w - S_g\right)\right) - \frac{1}{B_o}\tilde{q}_o, \tag{A.31}$$

$$\nabla \cdot \left(\lambda_w \nabla p_o - \lambda_w \frac{\partial p_{cow}}{\partial S_w}\nabla S_w - \lambda_w \frac{\partial p_{cow}}{\partial S_g}\nabla S_g - \lambda_w \rho_w g \nabla h\right) = \frac{\partial}{\partial t}\left(\frac{1}{B_w}\phi S_w\right) - \frac{1}{B_w}\tilde{q}_w, \tag{A.32}$$

and

$$\begin{aligned} & \nabla \cdot \left(\left(R_s\lambda_o + \lambda_g\right)\nabla p_o + \lambda_g \frac{\partial p_{cgo}}{\partial S_w}\nabla S_w + \lambda_g \frac{\partial p_{cgo}}{\partial S_g}\nabla S_g - \left(R_s\lambda_o\rho_o + \lambda_g\rho_g\right) g \nabla h\right) \\ = \; & \frac{\partial}{\partial t}\left(\frac{R_s}{B_o}\phi\left(1 - S_w - S_g\right) + \frac{1}{B_g}\phi S_g\right) - \frac{1}{B_o}R_s\tilde{q}_o - \frac{1}{B_g}\tilde{q}_{fg}. \end{aligned} \tag{A.33}$$

A.2 Discretization

Since the equations can generally not be solved analytically, they must be evaluated numerically. To this purpose the equations are discretized in space and in time. At first discretization of the $\frac{\partial}{\partial t}$ terms in eqs. A.31, A.32, and A.33 is discussed.

A.2.1 Time differencing of the right hand side

The time difference is defined as [Ertekin *et al.* (2001)]

$$\Delta_t\left(x\right) \equiv x^{n+1} - x^n.$$

The $\frac{\partial}{\partial t}$ terms are discretized using a mass-conservative time difference rule

$$\frac{\partial}{\partial t}\left(x\right) \simeq \frac{1}{\Delta t}\Delta_t\left(x\right),$$

where

$$\Delta_t\left(UVX\right) = V^n X^n \Delta_t U + U^{n+1} X^n \Delta_t V + U^{n+1} V^{n+1} \Delta_t X. \tag{A.34}$$

Application of eq. A.34 to the $\frac{\partial}{\partial t}$ term of eq. A.31 gives

$$\begin{aligned}\Delta_t\left(\tfrac{1}{B_o}\phi S_o\right) &= \left(\left(\tfrac{S_o}{B_o}\right)^n \phi^{'} + \phi^{n+1} S_o^n \left(\tfrac{1}{B_o}\right)^{'}\right)\Delta_t p_o \\ &\quad -\phi^{n+1}\left(\tfrac{1}{B_o}\right)^{n+1}\Delta_t S_w - \phi^{n+1}\left(\tfrac{1}{B_o}\right)^{n+1}\Delta_t S_g, \\ &= \beta_{op}\Delta_t p_o - \beta_{os}\Delta_t S_w - \beta_{os}\Delta_t S_g, \end{aligned} \tag{A.35}$$

and thus

$$\frac{\partial}{\partial t}\left(\tfrac{1}{B_o}\phi S_o\right) \simeq \beta_{op}\frac{\Delta_t p_o}{\Delta t} - \beta_{os}\frac{\Delta_t S_w}{\Delta t} - \beta_{os}\frac{\Delta_t S_g}{\Delta t}. \tag{A.36}$$

Similarly for eq. A.32

$$\begin{aligned}\Delta_t\left(\tfrac{1}{B_w}\phi S_w\right) &= \left(\left(\tfrac{1}{B_w}\right)^n {S_w}^n \phi^{'} + \phi^{n+1}{S_w}^n\left(\tfrac{1}{B_w}\right)^{'}\right)\Delta_t p_o, \\ &\quad + \left(\phi^{n+1}\left(\tfrac{1}{B_w}\right)^{n+1} - \phi^{n+1}{S_w}^n\left(\tfrac{1}{B_w}\right)^{'} p'_{cow}\right)\Delta_t S_w, \\ &= \beta_{wp}\Delta_t p_o + \beta_{ws}\Delta_t S_w, \end{aligned} \tag{A.37}$$

and thus

$$\frac{\partial}{\partial t}\left(\tfrac{1}{B_w}\phi S_w\right) \simeq \beta_{wp}\frac{\Delta_t p_o}{\Delta t} + \beta_{ws}\frac{\Delta_t S_w}{\Delta t}. \tag{A.38}$$

For equation A.33

$$\Delta_t\left(\tfrac{R_s}{B_o}\phi S_o + \tfrac{1}{B_g}\phi S_g\right) = \Delta_t\left(\tfrac{1}{B_g}\phi S_g\right) + \left(\tfrac{1}{B_o}\phi S_o\right)^n R'_s\Delta_t p_o + R_s^{n+1}\Delta_t\left(\tfrac{1}{B_o}\phi S_o\right), \tag{A.39}$$

where the first term is

$$\begin{aligned}\Delta_t\left(\tfrac{1}{B_g}\phi S_g\right) &= \left(\tfrac{1}{B_g}\right)^n S_g^n\phi^{'}\Delta_t p_o + \phi^{n+1}S_g^n\left(\tfrac{1}{B_g}\right)^{'}\left(\Delta_t p_o + p'_{cgo}\Delta_t S_g\right) \\ &\quad +\phi^{n+1}\left(\tfrac{1}{B_g}\right)^{n+1}\Delta_t S_g. \end{aligned} \tag{A.40}$$

Substitution of eqs. A.35 & A.40 into eq. A.39 then gives for the gas phase

$$\begin{aligned}\Delta_t\left(\tfrac{R_s}{B_o}\phi S_o + \tfrac{1}{B_g}\phi S_g\right) &= \begin{bmatrix} +\left(\tfrac{1}{B_o}\phi S_o\right)^n R'_s \\ +\left(\left(\tfrac{1}{B_g}\right)^n S_g^n + R_s^{n+1}\left(\tfrac{S_o}{B_o}\right)^n\right)\phi^{'} \\ +\phi^{n+1}\left(R_s^{n+1}S_o^n\left(\tfrac{1}{B_o}\right)^{'} + S_g^n\left(\tfrac{1}{B_g}\right)^{'}\right)\end{bmatrix}\Delta_t p_o, \\ &\quad -R_s^{n+1}\phi^{n+1}\left(\tfrac{1}{B_o}\right)^{n+1}\Delta_t S_w, \\ &\quad + \begin{bmatrix} \phi^{n+1}\left(\tfrac{1}{B_g}\right)^{n+1} + \phi^{n+1}S_g^n\left(\tfrac{1}{B_g}\right)^{'} p'_{cgo} \\ -R_s^{n+1}\phi^{n+1}\left(\tfrac{1}{B_o}\right)^{n+1}\end{bmatrix}\Delta_t S_g, \\ &= \beta_{gp}\Delta_t p_o - \beta_{gsw}\Delta_t S_w + \beta_{gsg}\Delta_t S_g, \end{aligned} \tag{A.41}$$

and thus

$$\frac{\partial}{\partial t}\left(\frac{R_s}{B_o}\phi S_o + \frac{1}{B_g}\phi S_g\right) \simeq \beta_{gp}\frac{\Delta_t p_o}{\Delta t} - \beta_{gsw}\frac{\Delta_t S_w}{\Delta t} + \beta_{gsg}\frac{\Delta_t S_g}{\Delta t}. \tag{A.42}$$

Substituting eqs. A.36, A.38, A.42 into eqs. A.31, A.32, A.33 and multiplying the equation by the grid block volume V_{gb} gives for the oil equation

$$\nabla \cdot V_{gb}\lambda_o \nabla p_o - \nabla \cdot V_{gb}\lambda_o \rho_o g \nabla h = V_{gb}\beta_{op}\frac{\Delta_t p_o}{\Delta t} - V_{gb}\beta_{os}\frac{\Delta_t S_w}{\Delta t} - V_{gb}\beta_{os}\frac{\Delta_t S_g}{\Delta t} - \frac{V_{gb}}{B_o}\tilde{q}_o,$$

which is more compactly written as

$$\nabla \cdot T_{o_1}\nabla p_o - \nabla \cdot T_{o_4}\nabla h = \beta^*_{op}\frac{\Delta_t p_o}{\Delta t} - \beta^*_{os}\frac{\Delta_t S_w}{\Delta t} - \beta^*_{os}\frac{\Delta_t S_g}{\Delta t} - q^*_o. \tag{A.43}$$

The subscripts $1, 4$ in the transmissibility terms are used for convenience. Similarly, the water and gas equations become respectively

$$\begin{aligned} & \nabla \cdot T_{w_1}\nabla p_o - \nabla \cdot T_{w_2}\nabla S_w - \nabla \cdot T_{w_3}\nabla S_g - \nabla \cdot T_{w_4}\nabla h \\ = \;& \beta^*_{wp}\frac{\Delta_t p_o}{\Delta t} + \beta^*_{ws}\frac{\Delta_t S_w}{\Delta t} - q^*_w. \end{aligned} \tag{A.44}$$

and

$$\begin{aligned} & \nabla \cdot T_{g_1}\nabla p_o + \nabla \cdot T_{g_2}\nabla S_w + \nabla \cdot T_{g_3}\nabla S_g - \nabla \cdot T_{g_4}\nabla h \\ = \;& \beta^*_{gp}\frac{\Delta_t p_o}{\Delta t} - \beta^*_{gsw}\frac{\Delta_t S_w}{\Delta t} + \beta^*_{gsg}\frac{\Delta_t S_g}{\Delta t} - q^*_g. \end{aligned} \tag{A.45}$$

Simplifying assumptions for parameters $\beta_{op}, \beta_{os}, \beta_{wp}, \beta_{ws}, \beta_{gp}, \beta_{gsw}, \beta_{gsg}$

The fact that some factors are to be calculated implicitly would require iteration on these parameters. The systems that are considered are, however, of low compressibility, and most pressure dependent parameters therefore hardly change during the simulation. To avoid time consuming iterating on implicitly calculated factors the following simplifying assumptions were made in the forward simulation:

$$\beta_{op} \approx \left(\left(\frac{S_o}{B_o}\right)^n \phi' + \phi^n S_o^n \left(\frac{1}{B_o}\right)'\right), \tag{A.46}$$

$$\beta_{os} \approx \phi^n \left(\frac{1}{B_o}\right)^n, \tag{A.47}$$

$$\beta_{wp} \approx \left(\left(\frac{1}{B_w}\right)^n {S_w}^n \phi' + \phi^n {S_w}^n \left(\frac{1}{B_w}\right)'\right), \tag{A.48}$$

$$\beta_{ws} \approx \left(\phi^n \left(\frac{1}{B_w}\right)^n - \phi^n {S_w}^n \left(\frac{1}{B_w}\right)' p'_{cow}\right), \tag{A.49}$$

$$\beta_{gp} \approx \left[\begin{array}{c} +\left(\frac{1}{B_o}\phi S_o\right)^n R'_s + \left(\left(\frac{1}{B_g}\right)^n S_g^n + R_s^n \left(\frac{S_o}{B_o}\right)^n\right)\phi' \\ +\phi^n \left(R_s^n S_o^n \left(\frac{1}{B_o}\right)' + S_g^n \left(\frac{1}{B_g}\right)'\right) \end{array}\right], \tag{A.50}$$

$$\beta_{gsw} \approx R_s^n \phi^n \left(\frac{1}{B_o}\right)^n, \tag{A.51}$$

$$\beta_{gsg} \approx \left[\phi^n \left(\frac{1}{B_g}\right)^n + \phi^n S_g^n \left(\frac{1}{B_g}\right)' p'_{cgo} - R_s^n \phi^n \left(\frac{1}{B_o}\right)^n\right]. \tag{A.52}$$

A.2.2 Spatial discretization

It is important to note here that the axes of reference are oriented as shown in the figure below.

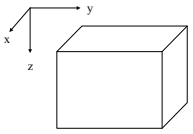

Figure A.2:

Since the spatial discretization leads to rather lengthy equations, they will not all be discussed. Instead, only the oil equation will be treated in some detail. A similar procedure holds for the water and gas equations. Spatial discretization of $\nabla \cdot T_{o_1} \nabla p_o$ in eq. A.43 gives

$$\begin{aligned}
\nabla \cdot T_{o_1} \nabla p_o &= \tfrac{\partial}{\partial x}\left(T_{o_1} \tfrac{\partial p_o}{\partial x}\right) + \tfrac{\partial}{\partial y}\left(T_{o_1} \tfrac{\partial p_o}{\partial y}\right) + \tfrac{\partial}{\partial z}\left(T_{o_1} \tfrac{\partial p_o}{\partial z}\right), \\
&= T_{o_{1_{i+\frac{1}{2},j,k}}} \left(p_{o_{i+1,j,k}} - p_{o_{i,j,k}}\right) - T_{o_{1_{i-\frac{1}{2},j,k}}} \left(p_{o_{i,j,k}} - p_{o_{i-1,j,k}}\right) \\
&\quad + T_{o_{1_{i,j+\frac{1}{2},k}}} \left(p_{o_{i,j+1,k}} - p_{o_{i,j,k}}\right) - T_{o_{1_{i,j-\frac{1}{2},k}}} \left(p_{o_{i,j,k}} - p_{o_{i,j-1,k}}\right) \\
&\quad + T_{o_{1_{i,j,k+\frac{1}{2}}}} \left(p_{o_{i,j,k+1}} - p_{o_{i,j,k}}\right) - T_{o_{1_{i,j,k-\frac{1}{2}}}} \left(p_{o_{i,j,k}} - p_{o_{i,j,k-1}}\right).
\end{aligned} \tag{A.53}$$

Similarly, for the term $\nabla \cdot T_{o_4} \nabla h$

$$\begin{aligned}
\nabla \cdot T_{o_4} \nabla h &= \tfrac{\partial}{\partial x}\left(T_{o_4} \tfrac{\partial h}{\partial x}\right) + \tfrac{\partial}{\partial y}\left(T_{o_4} \tfrac{\partial h}{\partial y}\right) + \tfrac{\partial}{\partial z}\left(T_{o_4} \tfrac{\partial h}{\partial z}\right), \\
&= T_{o_{4_{i+\frac{1}{2},j,k}}} \left(h_{i+1,j,k} - h_{i,j,k}\right) - T_{o_{4_{i-\frac{1}{2},j,k}}} \left(h_{i,j,k} - h_{i-1,j,k}\right) \\
&\quad + T_{o_{4_{i,j+\frac{1}{2},k}}} \left(h_{i,j+1,k} - h_{i,j,k}\right) - T_{o_{4_{i,j-\frac{1}{2},k}}} \left(h_{i,j,k} - h_{i,j-1,k}\right) \\
&\quad + T_{o_{4_{i,j,k+\frac{1}{2}}}} \left(h_{i,j,k+1} - h_{i,j,k}\right) - T_{o_{4_{i,j,k-\frac{1}{2}}}} \left(h_{i,j,k} - h_{i,j,k-1}\right),
\end{aligned} \tag{A.54}$$

where

$$T_{o4_{i+\frac{1}{2},j,k}} = \frac{\Delta y_{i,j,k}\Delta z_{i,j,k}}{\Delta x_{i+\frac{1}{2},j,k}} \lambda_{o_{i+\frac{1}{2},j,k}} \rho_{o_{i+\frac{1}{2},j,k}} g_{i+\frac{1}{2},j,k}.$$

A.2.3 Discretized equations in matrix form

In the discretized system there are three equations per grid block. The total number of equations is thus 3 times the number of grid blocks. These equations could be sorted in different ways. One possibility is to order the equations per phase. However, this leads to a matrix with a large bandwidth, something undesirable from a computational point of view. Ordering the equations per grid block leads to a matrix with a smaller bandwidth, and will therefore be used in this study. The discrete formulation for a 7 point stencil is then

$$\begin{bmatrix} \hat{\mathbf{T}}_o \\ \hat{\mathbf{T}}_w \\ \hat{\mathbf{T}}_g \end{bmatrix} \begin{bmatrix} \hat{\mathbf{p}}_{i,j,k-1} \\ \hat{\mathbf{p}}_{i,j-1,k} \\ \hat{\mathbf{p}}_{i-1,j,k} \\ \hat{\mathbf{p}}_{i,j,k} \\ \hat{\mathbf{p}}_{i+1,j,k} \\ \hat{\mathbf{p}}_{i,j+1,k} \\ \hat{\mathbf{p}}_{i,j,k+1} \end{bmatrix} - \begin{bmatrix} \mathbf{T}_{o_4} \\ \mathbf{T}_{w_4} \\ \mathbf{T}_{g_4} \end{bmatrix} \begin{bmatrix} h_{i,j,k-1} \\ h_{i,j-1,k} \\ h_{i-1,j,k} \\ h_{i,j,k} \\ h_{i+1,j,k} \\ h_{i,j+1,k} \\ h_{i,j,k+1} \end{bmatrix} = \begin{bmatrix} \boldsymbol{\beta}^*_{ot} \\ \boldsymbol{\beta}^*_{wt} \\ \boldsymbol{\beta}^*_{gt} \end{bmatrix} \dot{\hat{\mathbf{p}}} - \hat{\mathbf{q}}, \tag{A.55}$$

where

$$\hat{\mathbf{T}}_o = \begin{bmatrix} \hat{\mathbf{T}}\mathbf{ot}_{i,j,k-\frac{1}{2}} & \hat{\mathbf{T}}\mathbf{ot}_{i,j-\frac{1}{2},k} & \hat{\mathbf{T}}\mathbf{ot}_{i-\frac{1}{2},j,k} & \hat{\mathbf{T}}\mathbf{ot}_{i,j,k} & \hat{\mathbf{T}}\mathbf{ot}_{i+\frac{1}{2},j,k} & \hat{\mathbf{T}}\mathbf{ot}_{i,j+\frac{1}{2},k} & \hat{\mathbf{T}}\mathbf{ot}_{i,j,k+\frac{1}{2}} \end{bmatrix},$$

$$\hat{\mathbf{T}}_w = \begin{bmatrix} \hat{\mathbf{T}}\mathbf{wt}_{i,j,k-\frac{1}{2}} & \hat{\mathbf{T}}\mathbf{wt}_{i,j-\frac{1}{2},k} & \hat{\mathbf{T}}\mathbf{wt}_{i-\frac{1}{2},j,k} & \hat{\mathbf{T}}\mathbf{wt}_{i,j,k} & \hat{\mathbf{T}}\mathbf{wt}_{i+\frac{1}{2},j,k} & \hat{\mathbf{T}}\mathbf{wt}_{i,j+\frac{1}{2},k} & \hat{\mathbf{T}}\mathbf{wt}_{i,j,k+\frac{1}{2}} \end{bmatrix},$$

$$\hat{\mathbf{T}}_g = \begin{bmatrix} \hat{\mathbf{T}}\mathbf{gt}_{i,j,k-\frac{1}{2}} & \hat{\mathbf{T}}\mathbf{gt}_{i,j-\frac{1}{2},k} & \hat{\mathbf{T}}\mathbf{gt}_{i-\frac{1}{2},j,k} & \hat{\mathbf{T}}\mathbf{gt}_{i,j,k} & \hat{\mathbf{T}}\mathbf{gt}_{i+\frac{1}{2},j,k} & \hat{\mathbf{T}}\mathbf{gt}_{i,j+\frac{1}{2},k} & \hat{\mathbf{T}}\mathbf{gt}_{i,j,k+\frac{1}{2}} \end{bmatrix},$$

and

$$\begin{aligned} \hat{\mathbf{T}}\mathbf{ot}_{i,j,k+\frac{1}{2}} &= \begin{bmatrix} T_{o1} & 0 & 0 \end{bmatrix}_{i,j,k+\frac{1}{2}}, \\ \hat{\mathbf{T}}\mathbf{wt}_{i,j,k+\frac{1}{2}} &= \begin{bmatrix} T_{w1} & -T_{w2} & -T_{w3} \end{bmatrix}_{i,j,k+\frac{1}{2}}, \\ \hat{\mathbf{T}}\mathbf{gt}_{i,j,k+\frac{1}{2}} &= \begin{bmatrix} T_{g1} & T_{g2} & T_{g3} \end{bmatrix}_{i,j,k+\frac{1}{2}}, \end{aligned}$$

and

$$\mathbf{T}_{o_4} = \begin{bmatrix} T_{o4_{i,j,k-\frac{1}{2}}} & T_{o4_{i,j-\frac{1}{2},k}} & T_{o4_{i-\frac{1}{2},j,k}} & T_{o4_{i,j,k}} & T_{o4_{i+\frac{1}{2},j,k}} & T_{o4_{i,j+\frac{1}{2},k}} & T_{o4_{i,j,k+\frac{1}{2}}} \end{bmatrix},$$

$$\mathbf{T}_{w_4} = \begin{bmatrix} T_{w4_{i,j,k-\frac{1}{2}}} & T_{w4_{i,j-\frac{1}{2},k}} & T_{w4_{i-\frac{1}{2},j,k}} & T_{w4_{i,j,k}} & T_{w4_{i+\frac{1}{2},j,k}} & T_{w4_{i,j+\frac{1}{2},k}} & T_{w4_{i,j,k+\frac{1}{2}}} \end{bmatrix},$$

$$\mathbf{T}_{g_4} = \begin{bmatrix} T_{g4_{i,j,k-\frac{1}{2}}} & T_{g4_{i,j-\frac{1}{2},k}} & T_{g4_{i-\frac{1}{2},j,k}} & T_{g4_{i,j,k}} & T_{g4_{i+\frac{1}{2},j,k}} & T_{g4_{i,j+\frac{1}{2},k}} & T_{g4_{i,j,k+\frac{1}{2}}} \end{bmatrix},$$

and

$$\hat{\mathbf{p}}_{i,j,k+1} = \begin{bmatrix} p_o \\ S_w \\ S_g \end{bmatrix}_{i,j,k+1},$$

$$\begin{aligned} \boldsymbol{\beta}^*_{ot} &= \begin{bmatrix} \beta^*_{op} & -\beta^*_{os} & -\beta^*_{os} \end{bmatrix}, \\ \boldsymbol{\beta}^*_{wt} &= \begin{bmatrix} \beta^*_{wp} & \beta^*_{ws} & 0 \end{bmatrix}, \\ \boldsymbol{\beta}^*_{gt} &= \begin{bmatrix} \beta^*_{gp} & -\beta^*_{gsw} & \beta^*_{gsg} \end{bmatrix}, \end{aligned}$$

and

$$\dot{\hat{\mathbf{p}}} = \begin{bmatrix} \frac{\Delta_t p_o}{\Delta t} \\ \frac{\Delta_t S_w}{\Delta t} \\ \frac{\Delta_t S_g}{\Delta t} \end{bmatrix},$$

and

$$\hat{\mathbf{q}} = \begin{bmatrix} q^*_o \\ q^*_w \\ q^*_g \end{bmatrix}.$$

Finally the discrete system of equations can be written as

$$\hat{\mathbf{T}}\hat{\mathbf{p}} - \mathbf{T_4}\mathbf{h} = \mathbf{B}\dot{\hat{\mathbf{p}}} - \hat{\mathbf{q}}. \tag{A.56}$$

where the product $\mathbf{T_4}\mathbf{h}$ contains terms due to gravity forces. Eq. A.56 can be rewritten into

$$\mathbf{B}\dot{\hat{\mathbf{p}}} = \hat{\mathbf{T}}\hat{\mathbf{p}} - \mathbf{T_4}\mathbf{h} + \hat{\mathbf{q}}. \tag{A.57}$$

For numerical implementation, the analytical inverse of matrix $\mathbf{B}$ was used. For this block diagonal matrix, the inverse can be calculated analytically by calculating the inverse of the individual blocks. This analytical inverse has been compared with the $inv(\mathbf{B})$ command in MATLAB and maximum differences between the inverted matrices were in the order $1{\cdot}10^{-19}$.

Matrix formulation: Implicit in $\hat{\mathbf{p}}$, explicit in $\hat{\mathbf{T}}, \mathbf{T_4}, \hat{\mathbf{q}}$

In Eq. A.57 $\mathbf{B}$ and $\dot{\hat{\mathbf{p}}}$ have already been determined by mass-conservative time differencing. Therefore, only the choice for the time step at which $\hat{\mathbf{T}}$, $\hat{\mathbf{p}}$, $\mathbf{T_4}$, $\hat{\mathbf{q}}$ are to be calculated must be determined. The choice is to calculate all states $\hat{\mathbf{p}}$ implicitly, and all state dependent coefficients explicitly. Matrix $\mathbf{B}$ is assigned $\mathbf{B}^n$. Eq. A.57 then becomes

$$\mathbf{B}^n \left(\frac{\hat{\mathbf{p}}^{n+1}}{\Delta t^n} - \frac{\hat{\mathbf{p}}^n}{\Delta t^n} \right) = \hat{\mathbf{T}}^n \hat{\mathbf{p}}^{n+1} - \mathbf{T}^n_4 \mathbf{h} + \hat{\mathbf{q}}^n. \tag{A.58}$$

If injection and production rates are assigned directly without using a well model, the fluid mobilities are calculated explicitly. This is still the case if a well model is used, but in this case the grid block pressure used in the well model is calculated implicitly. The well model used in this study equals (see eq. B.21 and appendix B for more details on the well model)

$$\hat{\mathbf{q}}^n = -\hat{\mathbf{W}}^n \hat{\mathbf{p}}^{n+1} + \hat{\mathbf{W}}^n \hat{\mathbf{p}}^n_{wf} + \hat{\mathbf{w}}^n_{pc}. \tag{A.59}$$

Substitution gives, after some rearranging

$$\begin{aligned}\mathbf{g}^n &= \mathbf{0}, \\ &= \left[-\mathbf{I}\tfrac{1}{\Delta t^n} + (\mathbf{B}^n)^{-1}\,\hat{\mathbf{T}}^n - (\mathbf{B}^n)^{-1}\,\hat{\mathbf{W}}^n\right]\hat{\mathbf{p}}^{n+1} \\ &\quad + (\mathbf{B}^n)^{-1}\left(-\mathbf{T}_{\mathbf{4}}^n\mathbf{h} + \hat{\mathbf{W}}^n\hat{\mathbf{p}}_{wf}^n + \hat{\mathbf{w}}_{pc}^n\right) + \mathbf{I}\tfrac{\hat{\mathbf{p}}^n}{\Delta t^n}. \qquad \text{(A.60)}\end{aligned}$$

Appendix B
Well model

The well model used in this study is (after Ertekin *et al.* (2001))

$$p_{wf} - p_{gb_l} = \frac{q_l \mu_l B_l}{2\pi h k_{rl} \sqrt[3]{k_x k_y k_z}} \left(\ln\left(\frac{r_o}{r_w}\right) + S \right), \tag{B.1}$$

where p_{gb_l} is the pressure in the grid block for phase l. The well flowing pressure p_{wf} is assumed to be the same for all phases. μ_l is the fluid viscosity, B_l the formation volume factor, h the grid block thickness in the z-direction $[m]$, k_{rl} the relative permeability. k_x, k_y, k_z are absolute permeabilities in x, y, and z- direction respectively, q_l the injection or production rate $\left[\frac{m^3}{s}\right]$, r_w the well radius $[m]$, and r_o the effective well radius $[m]$, and S the well skin $[-]$. The effective well radius equals

$$r_o = 0.28 \frac{\sqrt{\left\{\left(\sqrt{k_x/k_y}(\Delta x)^2\right) + \left(\sqrt{k_y/k_x}\right)(\Delta y)^2\right\}}}{\sqrt[4]{(k_x/k_y)} + \sqrt[4]{(k_y/k_x)}}. \tag{B.2}$$

Rearranging gives

$$q_l = \frac{1}{B_l} \frac{k_{rl}}{\mu_l} \frac{\left(2\pi h \sqrt[3]{k_x k_y k_z}\right)}{\left(\ln\left(\frac{r_o}{r_w}\right) + S\right)} \left(p_{wf_l} - p_{gb_l}\right) \qquad \left[\frac{m^3}{s}\right]. \tag{B.3}$$

Dividing by the grid block volume gives

$$\begin{aligned} \hat{q}_l &= \frac{1}{B_l} \frac{k_{rl}}{\mu_l} \frac{\left(2\pi h \sqrt[3]{k_x k_y k_z}\right)}{V_{gb}\left(\ln\left(\frac{r_o}{r_w}\right) + S\right)} \left(p_{wf_l} - p_{gb_l}\right) \qquad \left[\frac{m^3}{m^3 s} = \frac{1}{s}\right], \\ &= \frac{1}{B_l} \tilde{q}_l \qquad \left[\frac{1}{s}\right]. \end{aligned} \tag{B.4}$$

In eq. B.4 $\tilde{q}_l$ corresponds to the $\tilde{q}_o$, $\tilde{q}_w$, and $\tilde{q}_g$ used in three phase flow formulation in chapter 3, and appendix A. This can be written as

$$\tilde{q}_l = \frac{k_{rl}}{\mu_l} w \left(p_{wf_l} - p_{gb_l}\right) \qquad \left[\frac{1}{s}\right], \tag{B.5}$$

where $w = \frac{\left(2\pi h \sqrt[3]{k_x k_y k_z}\right)}{V_{gb}\left(\ln\left(\frac{r_o}{r_w}\right) + S\right)}$ contain all parameters that are constant throughout the simulation. The source terms for the individual components are then

$$\tilde{q}_o = \frac{k_{ro}}{\mu_o} w \left(p_{wf_o} - p_{gb_o}\right) \qquad \left[\frac{1}{s}\right], \tag{B.6}$$

$$\tilde{q}_w = \frac{k_{rw}}{\mu_w} w \left(p_{wf_w} - p_{gb_w}\right) \qquad \left[\frac{1}{s}\right], \tag{B.7}$$

$$\begin{aligned}\tilde{q}_g &= \tilde{q}_{dg} + \tilde{q}_{fg}, \\ &= R_s\tilde{q}_o + \tilde{q}_{fg}, \\ &= R_s\frac{k_{ro}}{\mu_o}w\left(p_{wf_o} - p_{gb_o}\right) + \frac{k_{rg}}{\mu_g}w\left(p_{wf_g} - p_{gb_g}\right) \qquad \left[\frac{1}{s}\right].\end{aligned} \tag{B.8}$$

Since only the oil pressure p_o is calculated the relations $p_w = p_o - p_{cow}$, and $p_g = p_o + p_{cgo}$ must be substituted into eqs. B.7 and B.8 respectively. Eq. B.7 then becomes

$$\tilde{q}_w = \frac{k_{rw}}{\mu_w}w\left(p_{wf} - p_{gb_o}\right) + \frac{k_{rw}}{\mu_w}wp_{cow} \qquad \left[\frac{1}{s}\right], \tag{B.9}$$

and eq. B.8

$$\tilde{q}_g = \left(R_s\frac{k_{ro}}{\mu_o} + \frac{k_{rg}}{\mu_g}\right)w\left(p_{wf} - p_{gb_o}\right) - \frac{k_{rg}}{\mu_g}wp_{cgo} \qquad \left[\frac{1}{s}\right]. \tag{B.10}$$

Adding the effective choke position α_{eff}, with $\alpha_{eff} = \alpha_{wh}\alpha_{icv}$ to eqs. B.6, B.9, & B.10 then gives

$$\tilde{q}_o = \alpha_{eff}\frac{k_{ro}}{\mu_o}w\left(p_{wf} - p_{gb_o}\right) \qquad \left[\frac{1}{s}\right], \tag{B.11}$$

$$\tilde{q}_w = \alpha_{eff}\left(\frac{k_{rw}}{\mu_w}w\left(p_{wf} - p_{gb_o}\right) \; + \frac{k_{rw}}{\mu_w}wp_{cow}\right) \qquad \left[\frac{1}{s}\right], \tag{B.12}$$

$$\tilde{q}_g = \alpha_{eff}\left(\left(R_s\frac{k_{ro}}{\mu_o} + \frac{k_{rg}}{\mu_g}\right)w\left(p_{wf} - p_{gb_o}\right) - \frac{k_{rg}}{\mu_g}wp_{cgo}\right) \qquad \left[\frac{1}{s}\right]. \tag{B.13}$$

The total production rate is then

$$\begin{aligned}\tilde{q}_{t_p} &= \tilde{q}_o + \tilde{q}_w + \tilde{q}_g, \\ &= \alpha_{eff}\left\{\begin{array}{c}\left[\frac{k_{ro}}{\mu_o} + \frac{k_{rw}}{\mu_w} + \left(R_s\frac{k_{ro}}{\mu_o} + \frac{k_{rg}}{\mu_g}\right)\right]w\left(p_{wf} - p_{gb_o}\right) \\ + \frac{k_{rw}}{\mu_w}wp_{cow} - \frac{k_{rg}}{\mu_g}wp_{cgo}\end{array}\right\}.\end{aligned} \tag{B.14}$$

For an injector the injection rate is dependent on the total fluid mobility around the well, i.e. the sum of the oil mobility $\frac{k_{ro}}{\mu_o}$, the water mobility $\frac{k_{rw}}{\mu_w}$, and the free gas mobility $\frac{k_{rg}}{\mu_g}$, i.e.

$$\tilde{q}_{t_{inj}} = \alpha_{eff}\left\{\left[\frac{k_{ro}}{\mu_o} + \frac{k_{rw}}{\mu_w} + \frac{k_{rg}}{\mu_g}\right]w\left(p_{wf} - p_{gb_o}\right) + \frac{k_{rw}}{\mu_w}wp_{cow} - \frac{k_{rg}}{\mu_g}wp_{cgo}\right\}. \tag{B.15}$$

The production rates q_o^*, q_w^*, & q_g^* (see chapter 3 and appendix A) are then

$$\begin{aligned}q_o^* &= \frac{V_{gb}}{B_o}\tilde{q}_o, \\ &= \alpha_{eff}V_{gb}w\frac{k_{ro}}{B_o\mu_o}\left(p_{wf} - p_{gb_o}\right),\end{aligned} \tag{B.16}$$

$$\begin{aligned} q_w^* &= \tfrac{V_{gb}}{B_w}\tilde{q}_w, \\ &= \alpha_{eff} V_{gb} w \frac{k_{rw}}{B_w \mu_w} \left(p_{wf} - p_{gb_o}\right), \\ &\quad + \alpha_{eff} V_{gb} w \frac{k_{rw}}{B_w \mu_w} p_{cow}, \end{aligned} \tag{B.17}$$

$$\begin{aligned} q_g^* &= \frac{V_{gb}}{B_o} R_s \tilde{q}_o + \frac{V_{gb}}{B_g} \tilde{q}_{fg}, \\ &= \alpha_{eff} V_{gb} w \left(R_s \frac{k_{ro}}{B_o \mu_o} + \frac{k_{rg}}{B_g \mu_g} \right) \left(p_{wf} - p_{gb_o}\right) - \alpha_{eff} V_{gb} w \frac{k_{rg}}{B_g \mu_g} p_{cgo}. \end{aligned} \tag{B.18}$$

This can be written in matrix form as

$$\begin{aligned} \begin{bmatrix} q_o^* \\ q_w^* \\ q_g^* \end{bmatrix} &= - \begin{bmatrix} \alpha_{eff} V_{gb} w \frac{k_{ro}}{B_o \mu_o} & 0 & 0 \\ \alpha_{eff} V_{gb} w \frac{k_{rw}}{B_w \mu_w} & 0 & 0 \\ \alpha_{eff} V_{gb} w \left(R_s \frac{k_{ro}}{B_o \mu_o} + \frac{k_{rg}}{B_g \mu_g} \right) & 0 & 0 \end{bmatrix} \begin{bmatrix} p_o \\ S_w \\ S_g \end{bmatrix} \\ &\quad + \begin{bmatrix} \alpha_{eff} V_{gb} w \frac{k_{ro}}{B_o \mu_o} & 0 & 0 \\ \alpha_{eff} V_{gb} w \frac{k_{rw}}{B_w \mu_w} & 0 & 0 \\ \alpha_{eff} V_{gb} w \left(R_s \frac{k_{ro}}{B_o \mu_o} + \frac{k_{rg}}{B_g \mu_g} \right) & 0 & 0 \end{bmatrix} \begin{bmatrix} p_{wf} \\ 0 \\ 0 \end{bmatrix} \\ &\quad + \begin{bmatrix} 0 \\ \alpha_{eff} V_{gb} w \frac{k_{rw}}{B_w \mu_w} p_{cow} \\ -\alpha_{eff} V_{gb} w \frac{k_{rg}}{B_g \mu_g} p_{cgo} \end{bmatrix}, \end{aligned} \tag{B.19}$$

or

$$\hat{\mathbf{q}}_p = -\hat{\mathbf{W}}_p \hat{\mathbf{p}} + \hat{\mathbf{W}}_p \hat{\mathbf{p}}_{wf} + \hat{\mathbf{w}}_{p_{pc}}. \tag{B.20}$$

If only the states are calculated implicitly, and all other parameters explicitly this becomes

$$\hat{\mathbf{q}}^n = -\hat{\mathbf{W}}^n \hat{\mathbf{p}}^{n+1} + \hat{\mathbf{W}}^n \hat{\mathbf{p}}^n_{wf} + \hat{\mathbf{w}}^n_{pc}. \tag{B.21}$$

For a water injector the injection rate is dependent on the total fluid mobility around the well, i.e. the sum of the oil mobility $\frac{k_{ro}}{\mu_o}$, the water mobility $\frac{k_{rw}}{\mu_w}$, and the free gas mobility $\frac{k_{rg}}{\mu_g}$, i.e.

$$\begin{aligned} q_{w_{inj}}^* &= \tfrac{V_{gb}}{B_w}\tilde{q}_t, \\ &= \tfrac{V_{gb}}{B_w}\left(\tilde{q}_o + \tilde{q}_w + \tilde{q}_{fg}\right), \\ &= \alpha_{eff} \tfrac{V_{gb}}{B_w} w \left(\left[\frac{k_{ro}}{\mu_o} + \frac{k_{rw}}{\mu_w} + \frac{k_{rg}}{\mu_g} \right] \left(p_{wf} - p_{gb_o}\right) + \frac{k_{rw}}{\mu_w} p_{cow} - \frac{k_{rg}}{\mu_g} p_{cgo} \right), \end{aligned}$$

which can be written as

$$\begin{aligned}
\begin{bmatrix} q_o^* \\ q_w^* \\ q_g^* \end{bmatrix} &= -\begin{bmatrix} 0 & 0 & 0 \\ \alpha_{eff} V_{gb} w \frac{1}{B_w} \left[\frac{k_{ro}}{\mu_o} + \frac{k_{rw}}{\mu_w} + \frac{k_{rg}}{\mu_g} \right] & 0 & 0 \\ 0 & 0 & 0 \end{bmatrix} \begin{bmatrix} p_o \\ S_w \\ S_g \end{bmatrix} \\
&+ \begin{bmatrix} 0 & 0 & 0 \\ \alpha_{eff} V_{gb} w \frac{1}{B_w} \left[\frac{k_{ro}}{\mu_o} + \frac{k_{rw}}{\mu_w} + \frac{k_{rg}}{\mu_g} \right] & 0 & 0 \\ 0 & 0 & 0 \end{bmatrix} \begin{bmatrix} p_{wf} \\ 0 \\ 0 \end{bmatrix} \\
&+ \begin{bmatrix} 0 \\ \alpha_{eff} w \frac{V_{gb}}{B_w} \left(\frac{k_{rw}}{\mu_w} p_{cow} - \frac{k_{rg}}{\mu_g} p_{cgo} \right) \\ 0 \end{bmatrix}, \qquad \text{(B.22)}
\end{aligned}$$

or

$$\hat{\mathbf{q}}_{in} = -\hat{\mathbf{W}}_{in}\hat{\mathbf{p}} + \hat{\mathbf{W}}_{in}\hat{\mathbf{p}}_{wf} + \hat{\mathbf{w}}_{in_{pc}}. \qquad \text{(B.23)}$$

Appendix C
Optimal Control Theory - Derivatives

The derivatives for the optimal control problem are based on a fully implicit description of the dynamic system. Derivatives that have to be calculated are $\frac{\partial \mathbf{g}^{n-1}}{\partial \mathbf{x}^n}$, $\frac{\partial \mathbf{g}^n}{\partial \mathbf{x}^n}$, $\frac{\partial \mathbf{g}^n}{\partial \boldsymbol{\alpha}_{eff}^n}$, $\frac{\partial \mathcal{J}^n}{\partial \mathbf{x}^n}$, and $\frac{\partial \mathcal{J}^n}{\partial \boldsymbol{\alpha}_{eff}^n}$.

C.1 Derivatives $\frac{\partial \mathbf{g}^{n-1}}{\partial \mathbf{x}^n}$

C.1.1 The oil equation

Fully written out the discrete oil equation for grid block i, j, k is

$$\begin{aligned} g_{o_{i,j,k}}^{n-1} &= -\begin{bmatrix} T_{o1}\left(p_{o_{i+1,j,k}} - p_{o_{i,j,k}}\right) + T_{o1}\left(p_{o_{i-1,j,k}} - p_{o_{i,j,k}}\right) \\ +T_{o1}\left(p_{o_{i,j+1,k}} - p_{o_{i,j,k}}\right) + T_{o1}\left(p_{o_{i,j-1,k}} - p_{o_{i,j,k}}\right) \\ +T_{o1}\left(p_{o_{i,j,k+1}} - p_{o_{i,j,k}}\right) + T_{o1}\left(p_{o_{i,j,k-1}} - p_{o_{i,j,k}}\right) \end{bmatrix}^n \\ &+ \begin{bmatrix} T_{o4}\left(h_{i+1,j,k} - h_{i,j,k}\right) + T_{o4}\left(h_{i-1,j,k} - h_{i,j,k}\right) \\ +T_{o4}\left(h_{i,j+1,k} - h_{i,j,k}\right) + T_{o4}\left(h_{i,j-1,k} - h_{i,j,k}\right) \\ +T_{o4}\left(h_{i,j,k+1} - h_{i,j,k}\right) + T_{o4}\left(h_{i,j,k-1} - h_{i,j,k}\right) \end{bmatrix}^n \\ &+ \left(\beta_{op}^*\right)^n \frac{p_o^n - p_o^{n-1}}{\Delta t^n} - \left(\beta_{os}^*\right)^n \frac{S_w^n - S_w^{n-1}}{\Delta t^n} - \left(\beta_{os}^*\right)^n \frac{S_g^n - S_g^{n-1}}{\Delta t^n} \\ &- \left(q_o^*\right)^n, \end{aligned} \tag{C.1}$$

where

$$\begin{aligned} T_{o1}\left(p_{o_{i+1,j,k}} - p_{o_{i,j,k}}\right) &= T_{o1}{}_{i+\frac{1}{2},j,k}\left(p_{o_{i+1,j,k}} - p_{o_{i,j,k}}\right), \\ &\vdots \\ T_{o4}\left(h_{i,j,k-1} - h_{i,j,k}\right) &= T_{o4}{}_{i,j,k-\frac{1}{2}}\left(h_{i,j,k-1} - h_{i,j,k}\right) \end{aligned} \tag{C.2}$$

is used to shorten notation. Similarly for grid block $i-1, j, k$ we obtain

$$
\begin{aligned}
g^{n-1}_{o_{i-1,j,k}} \;=\; & -\left[\begin{array}{c} T_{o1}\left(p_{o_{i,j,k}}-p_{o_{i-1,j,k}}\right)+T_{o1}\left(p_{o_{i-2,j,k}}-p_{o_{i-1,j,k}}\right) \\ +T_{o1}\left(p_{o_{i-1,j+1,k}}-p_{o_{i-1,j,k}}\right)+T_{o1}\left(p_{o_{i-1,j-1,k}}-p_{o_{i-1,j,k}}\right) \\ +T_{o1}\left(p_{o_{i-1,j,k+1}}-p_{o_{i-1,j,k}}\right)+T_{o1}\left(p_{o_{i-1,j,k-1}}-p_{o_{i-1,j,k}}\right)\end{array}\right]^n \\
& +\left[\begin{array}{c} T_{o4}\left(h_{i,j,k}-h_{i-1,j,k}\right)+T_{o4}\left(h_{i-2,j,k}-h_{i-1,j,k}\right) \\ +T_{o4}\left(h_{i-1,j+1,k}-h_{i-1,j,k}\right)+T_{o4}\left(h_{i-1,j-1,k}-h_{i-1,j,k}\right) \\ +T_{o4}\left(h_{i-1,j,k+1}-h_{i-1,j,k}\right)+T_{o4}\left(h_{i-1,j,k-1}-h_{i-1,j,k}\right)\end{array}\right]^n \\
& +\left(\beta^*_{op}\right)^n_{i-1,j,k}\left(\frac{p^n_o-p^{n-1}_o}{\Delta t^n}\right)_{i-1,j,k}-\left(\beta^*_{os}\right)^n_{i-1,j,k}\left(\frac{S^n_w-S^{n-1}_w}{\Delta t^n}\right)_{i-1,j,k} \\
& -\left(\beta^*_{os}\right)^n_{i-1,j,k}\left(\frac{S^n_g-S^{n-1}_g}{\Delta t^n}\right)_{i-1,j,k}-\left(q^*_o\right)^n_{i-1,j,k}\,. \qquad \text{(C.3)}
\end{aligned}
$$

Derivatives with respect to the oil pressure $\frac{\partial g^{n-1}_{o_{i-1,j,k}}}{\partial p^n_{o_{i,j,k}}}$

Eq. C.3 can be considered the starting equation for derivatives $\frac{\partial g^{n-1}_{o_{i\pm1,j\pm1,k\pm1}}}{\partial p^n_{o_{i,j,k}}}$, which are

$$
\begin{aligned}
\frac{\partial g^{n-1}_{o_{i,j,k-1}}}{\partial p^n_{o_{i,j,k}}} &= -{T_{o1}}_{i,j,k-\frac{1}{2}}-\frac{\partial {T_{o1}}_{i,j,k-\frac{1}{2}}}{\partial p^n_{o_{i,j,k}}}\left(p_{o_{i,j,k}}-p_{o_{i,j,k-1}}\right)+\frac{\partial {T_{o4}}_{i,j,k-\frac{1}{2}}}{\partial p^n_{o_{i,j,k}}}\left(h_{i,j,k}-h_{i,j,k-1}\right), \\
\frac{\partial g^{n-1}_{o_{i,j-1,k}}}{\partial p^n_{o_{i,j,k}}} &= -{T_{o1}}_{i,j-\frac{1}{2},k}-\frac{\partial {T_{o1}}_{i,j-\frac{1}{2},k}}{\partial p^n_{o_{i,j,k}}}\left(p_{o_{i,j,k}}-p_{o_{i,j-1,k}}\right)+\frac{\partial {T_{o4}}_{i,j-\frac{1}{2},k}}{\partial p^n_{o_{i,j,k}}}\left(h_{i,j,k}-h_{i,j-1,k}\right), \\
\frac{\partial g^{n-1}_{o_{i-1,j,k}}}{\partial p^n_{o_{i,j,k}}} &= -{T_{o1}}_{i-\frac{1}{2},j,k}-\frac{\partial {T_{o1}}_{i-\frac{1}{2},j,k}}{\partial p^n_{o_{i,j,k}}}\left(p_{o_{i,j,k}}-p_{o_{i-1,j,k}}\right)+\frac{\partial {T_{o4}}_{i-\frac{1}{2},j,k}}{\partial p^n_{o_{i,j,k}}}\left(h_{i,j,k}-h_{i-1,j,k}\right), \\
\frac{\partial g^{n-1}_{o_{i+1,j,k}}}{\partial p^n_{o_{i,j,k}}} &= -{T_{o1}}_{i+\frac{1}{2},j,k}-\frac{\partial {T_{o1}}_{i+\frac{1}{2},j,k}}{\partial p^n_{o_{i,j,k}}}\left(p_{o_{i,j,k}}-p_{o_{i+1,j,k}}\right)+\frac{\partial {T_{o4}}_{i+\frac{1}{2},j,k}}{\partial p^n_{o_{i,j,k}}}\left(h_{i,j,k}-h_{i+1,j,k}\right), \\
\frac{\partial g^{n-1}_{o_{i,j+1,k}}}{\partial p^n_{o_{i,j,k}}} &= -{T_{o1}}_{i,j+\frac{1}{2},k}-\frac{\partial {T_{o1}}_{i,j+\frac{1}{2},k}}{\partial p^n_{o_{i,j,k}}}\left(p_{o_{i,j,k}}-p_{o_{i,j+1,k}}\right)+\frac{\partial {T_{o4}}_{i,j+\frac{1}{2},k}}{\partial p^n_{o_{i,j,k}}}\left(h_{i,j,k}-h_{i,j+1,k}\right), \\
\frac{\partial g^{n-1}_{o_{i,j,k+1}}}{\partial p^n_{o_{i,j,k}}} &= -{T_{o1}}_{i,j,k+\frac{1}{2}}-\frac{\partial {T_{o1}}_{i,j,k+\frac{1}{2}}}{\partial p^n_{o_{i,j,k}}}\left(p_{o_{i,j,k}}-p_{o_{i,j,k+1}}\right)+\frac{\partial {T_{o4}}_{i,j,k+\frac{1}{2}}}{\partial p^n_{o_{i,j,k}}}\left(h_{i,j,k}-h_{i,j,k+1}\right),
\end{aligned}
$$

(C.4)

Eq. C.1 forms the basis for derivative $\frac{\partial g^{n-1}_{o_{i,j,k}}}{\partial p^n_{o_{i,j,k}}}$, that equals

$$
\begin{aligned}
\frac{\partial g^{n-1}_{o_{i,j,k}}}{\partial p^n_{o_{i,j,k}}} = & \begin{bmatrix}
-\frac{\partial {To1}_{i+\frac{1}{2},j,k}}{\partial p^n_{o_{i,j,k}}}\left(p_{o_{i+1,j,k}} - p_{o_{i,j,k}}\right) + \frac{\partial {To4}_{i+\frac{1}{2},j,k}}{\partial p^n_{o_{i,j,k}}}\left(h_{i+1,j,k} - h_{i,j,k}\right) \\
-\frac{\partial {To1}_{i-\frac{1}{2},j,k}}{\partial p^n_{o_{i,j,k}}}\left(p_{o_{i-1,j,k}} - p_{o_{i,j,k}}\right) + \frac{\partial {To4}_{i-\frac{1}{2},j,k}}{\partial p^n_{o_{i,j,k}}}\left(h_{i-1,j,k} - h_{i,j,k}\right) \\
-\frac{\partial {To1}_{i,j+\frac{1}{2},k}}{\partial p^n_{o_{i,j,k}}}\left(p_{o_{i,j+1,k}} - p_{o_{i,j,k}}\right) + \frac{\partial {To4}_{i,j+\frac{1}{2},k}}{\partial p^n_{o_{i,j,k}}}\left(h_{i,j+1,k} - h_{i,j,k}\right) \\
-\frac{\partial {To1}_{i,j-\frac{1}{2},k}}{\partial p^n_{o_{i,j,k}}}\left(p_{o_{i,j-1,k}} - p_{o_{i,j,k}}\right) + \frac{\partial {To4}_{i,j-\frac{1}{2},k}}{\partial p^n_{o_{i,j,k}}}\left(h_{i,j-1,k} - h_{i,j,k}\right) \\
-\frac{\partial {To1}_{i,j,k+\frac{1}{2}}}{\partial p^n_{o_{i,j,k}}}\left(p_{o_{i,j,k+1}} - p_{o_{i,j,k}}\right) + \frac{\partial {To4}_{i,j,k+\frac{1}{2}}}{\partial p^n_{o_{i,j,k}}}\left(h_{i,j,k+1} - h_{i,j,k}\right) \\
-\frac{\partial {To1}_{i,j,k-\frac{1}{2}}}{\partial p^n_{o_{i,j,k}}}\left(p_{o_{i,j,k-1}} - p_{o_{i,j,k}}\right) + \frac{\partial {To4}_{i,j,k-\frac{1}{2}}}{\partial p^n_{o_{i,j,k}}}\left(h_{i,j,k-1} - h_{i,j,k}\right)
\end{bmatrix} \\
& + {To1}_{i+\frac{1}{2},j,k} + {To1}_{i-\frac{1}{2},j,k} + {To1}_{i,j+\frac{1}{2},k} + {To1}_{i,j-\frac{1}{2},k} + {To1}_{i,j,k+\frac{1}{2}} + {To1}_{i,j,k-\frac{1}{2}} \\
& + \frac{\partial\left(\beta^*_{op}\right)^n}{\partial p^n_{o_{i,j,k}}}\left(\frac{p^n_o - p^{n-1}_o}{\Delta t^n}\right) + \left(\beta^*_{op}\right)^n \frac{1}{\Delta t^n} - \frac{\partial(\beta^*_{os})^n}{\partial p^n_{o_{i,j,k}}}\left(\frac{S^n_w - S^{n-1}_w}{\Delta t^n}\right) \\
& - \frac{\partial(\beta^*_{os})^n}{\partial p^n_{o_{i,j,k}}}\left(\frac{S^n_g - S^{n-1}_g}{\Delta t^n}\right) - \frac{\partial(q^*_o)^n}{\partial p^n_{o_{i,j,k}}}.
\end{aligned} \tag{C.5}
$$

This can be rearranged as

$$
\begin{aligned}
\frac{\partial g^{n-1}_{o_{i,j,k}}}{\partial p^n_{o_{i,j,k}}} = & \begin{bmatrix}
+\frac{\partial {To1}_{i+\frac{1}{2},j,k}}{\partial p^n_{o_{i,j,k}}}\left(+p_{o_{i,j,k}} - p_{o_{i+1,j,k}}\right) - \frac{\partial {To4}_{i+\frac{1}{2},j,k}}{\partial p^n_{o_{i,j,k}}}\left(+h_{i,j,k} - h_{i+1,j,k}\right) \\
+\frac{\partial {To1}_{i-\frac{1}{2},j,k}}{\partial p^n_{o_{i,j,k}}}\left(+p_{o_{i,j,k}} - p_{o_{i-1,j,k}}\right) - \frac{\partial {To4}_{i-\frac{1}{2},j,k}}{\partial p^n_{o_{i,j,k}}}\left(+h_{i,j,k} - h_{i-1,j,k}\right) \\
+\frac{\partial {To1}_{i,j+\frac{1}{2},k}}{\partial p^n_{o_{i,j,k}}}\left(+p_{o_{i,j,k}} - p_{o_{i,j+1,k}}\right) - \frac{\partial {To4}_{i,j+\frac{1}{2},k}}{\partial p^n_{o_{i,j,k}}}\left(+h_{i,j,k} - h_{i,j+1,k}\right) \\
+\frac{\partial {To1}_{i,j-\frac{1}{2},k}}{\partial p^n_{o_{i,j,k}}}\left(+p_{o_{i,j,k}} - p_{o_{i,j-1,k}}\right) - \frac{\partial {To4}_{i,j-\frac{1}{2},k}}{\partial p^n_{o_{i,j,k}}}\left(+h_{i,j,k} - h_{i,j-1,k}\right) \\
+\frac{\partial {To1}_{i,j,k+\frac{1}{2}}}{\partial p^n_{o_{i,j,k}}}\left(+p_{o_{i,j,k}} - p_{o_{i,j,k+1}}\right) - \frac{\partial {To4}_{i,j,k+\frac{1}{2}}}{\partial p^n_{o_{i,j,k}}}\left(+h_{i,j,k} - h_{i,j,k+1}\right) \\
+\frac{\partial {To1}_{i,j,k-\frac{1}{2}}}{\partial p^n_{o_{i,j,k}}}\left(+p_{o_{i,j,k}} - p_{o_{i,j,k-1}}\right) - \frac{\partial {To4}_{i,j,k-\frac{1}{2}}}{\partial p^n_{o_{i,j,k}}}\left(+h_{i,j,k} - h_{i,j,k-1}\right)
\end{bmatrix} \\
& + {To1}_{i+\frac{1}{2},j,k} + {To1}_{i-\frac{1}{2},j,k} + {To1}_{i,j+\frac{1}{2},k} + {To1}_{i,j-\frac{1}{2},k} + {To1}_{i,j,k+\frac{1}{2}} + {To1}_{i,j,k-\frac{1}{2}} \\
& + \frac{\partial\left(\beta^*_{op}\right)^n}{\partial p^n_{o_{i,j,k}}}\left(\frac{p^n_o - p^{n-1}_o}{\Delta t^n}\right) + \left(\beta^*_{op}\right)^n \frac{1}{\Delta t^n} - \frac{\partial(\beta^*_{os})^n}{\partial p^n_{o_{i,j,k}}}\left(\frac{S^n_w - S^{n-1}_w}{\Delta t^n}\right) \\
& - \frac{\partial(\beta^*_{os})^n}{\partial p^n_{o_{i,j,k}}}\left(\frac{S^n_g - S^{n-1}_g}{\Delta t^n}\right) - \frac{\partial(q^*_o)^n}{\partial p^n_{o_{i,j,k}}}.
\end{aligned} \tag{C.6}
$$

Substitution of eqs. C.4 into eq. C.6 then gives finally

$$\begin{aligned}\frac{\partial g^{n-1}_{o_{i,j,k}}}{\partial p^n_{o_{i,j,k}}} &= -\left(\frac{\partial g^{n-1}_{o_{i,j,k-1}}}{\partial p^n_{o_{i,j,k}}}+\frac{\partial g^{n-1}_{o_{i,j-1,k}}}{\partial p^n_{o_{i,j,k}}}+\frac{\partial g^{n-1}_{o_{i-1,j,k}}}{\partial p^n_{o_{i,j,k}}}+\frac{\partial g^{n-1}_{o_{i+1,j,k}}}{\partial p^n_{o_{i,j,k}}}+\frac{\partial g^{n-1}_{o_{i,j+1,k}}}{\partial p^n_{o_{i,j,k}}}+\frac{\partial g^{n-1}_{o_{i,j,k+1}}}{\partial p^n_{o_{i,j,k}}}\right)\\ &+\frac{\partial\left(\beta^*_{op}\right)^n}{\partial p^n_{o_{i,j,k}}}\left(\frac{p^n_o-p^{n-1}_o}{\Delta t^n}\right)+\frac{\left(\beta^*_{op}\right)^n}{\Delta t^n}\\ &-\frac{\partial(\beta^*_{os})^n}{\partial p^n_{o_{i,j,k}}}\left(\frac{S^n_w-S^{n-1}_w}{\Delta t^n}\right)-\frac{\partial(\beta^*_{os})^n}{\partial p^n_{o_{i,j,k}}}\left(\frac{S^n_g-S^{n-1}_g}{\Delta t^n}\right)\\ &-\frac{\partial(q^*_o)^n}{\partial p^n_{o_{i,j,k}}}.\end{aligned} \tag{C.7}$$

In eq. C.7 the derivative $\frac{\partial\left(\beta^*_{op}\right)^n}{\partial p^n_{o_{i,j,k}}}$ is

$$\frac{\partial\left(\beta^*_{op}\right)^n}{\partial p^n_{o_{i,j,k}}} = V_{gb}S^{n-1}_o\left(\left(\frac{1}{B_o}\right)^{n-1}\frac{\partial\phi'}{\partial p^n_{o_{i,j,k}}}+\phi^n\frac{\partial\left(\frac{1}{B_o}\right)'}{\partial p^n_{o_{i,j,k}}}+\left(\frac{1}{B_o}\right)'\frac{\partial\phi^n}{\partial p^n_{o_{i,j,k}}}\right), \tag{C.8}$$

where

$$\frac{\partial\left(\frac{1}{B_o}\right)^{n-1}}{\partial p^n_{o_{i,j,k}}} = 0. \tag{C.9}$$

In eq. C.7 the derivative $\frac{\partial(\beta^*_{os})^n}{\partial p^n_{o_{i,j,k}}}$ is equal to

$$\frac{\partial(\beta^*_{os})^n}{\partial p^n_{o_{i,j,k}}} = V_{gb}\left(\phi^n a_o+\left(\frac{1}{B_o}\right)^n\frac{\partial\phi^n}{\partial p^n_{o_{i,j,k}}}\right), \tag{C.10}$$

where

$$a_o = \frac{\partial\left(\frac{1}{B_o}\right)^n}{\partial p^n_{o_{i,j,k}}}. \tag{C.11}$$

Derivatives with respect to the water saturation $\frac{\partial g^{n-1}_{o_{i,j,k-1}}}{\partial S^n_{w_{i,j,k}}}$

Eq. C.3 is the starting equation for derivatives $\frac{\partial g^{n-1}_{o_{i\pm1,j\pm1,k\pm1}}}{\partial S^n_{w_{i,j,k}}}$. Derivative $\frac{\partial g^{n-1}_{o_{i,j,k-1}}}{\partial S^n_{w_{i,j,k}}}$ equals

$$\frac{\partial g^{n-1}_{o_{i,j,k-1}}}{\partial S^n_{w_{i,j,k}}} = -\frac{\partial {T_{o1}}_{i,j,k-\frac{1}{2}}}{\partial S^n_{w_{i,j,k}}}\left(p_{o_{i,j,k}}-p_{o_{i,j,k-1}}\right)+\frac{\partial {T_{o4}}_{i,j,k-\frac{1}{2}}}{\partial S^n_{w_{i,j,k}}}\left(h_{i,j,k}-h_{i,j,k-1}\right). \tag{C.12}$$

Derivatives $\frac{\partial g^{n-1}_{o_{i,j-1,k}}}{\partial S^n_{w_{i,j,k}}}$, $\frac{\partial g^{n-1}_{o_{i-1,j,k}}}{\partial S^n_{w_{i,j,k}}}$, $\frac{\partial g^{n-1}_{o_{i+1,j,k}}}{\partial S^n_{w_{i,j,k}}}$, $\frac{\partial g^{n-1}_{o_{i,j+1,k}}}{\partial S^n_{w_{i,j,k}}}$, and $\frac{\partial g^{n-1}_{o_{i,j,k+1}}}{\partial S^n_{w_{i,j,k}}}$ are obtained similarly. Eq. C.1 forms the basis for derivative $\frac{\partial g^{n-1}_{o_{i,j,k}}}{\partial S^n_{w_{i,j,k}}}$, which becomes after substituting eqs. C.12,

and some rearranging

$$\begin{aligned}\frac{\partial g^{n-1}_{o_{i,j,k}}}{\partial S^n_{w_{i,j,k}}} &= -\left(\frac{\partial g^{n-1}_{o_{i,j,k-1}}}{\partial S^n_{w_{i,j,k}}}+\frac{\partial g^{n-1}_{o_{i,j-1,k}}}{\partial S^n_{w_{i,j,k}}}+\frac{\partial g^{n-1}_{o_{i-1,j,k}}}{\partial S^n_{w_{i,j,k}}}+\frac{\partial g^{n-1}_{o_{i+1,j,k}}}{\partial S^n_{w_{i,j,k}}}+\frac{\partial g^{n-1}_{o_{i,j+1,k}}}{\partial S^n_{w_{i,j,k}}}+\frac{\partial g^{n-1}_{o_{i,j,k+1}}}{\partial S^n_{w_{i,j,k}}}\right)\\ &+\frac{\partial\left(\beta^*_{op}\right)^n}{\partial S^n_{w_{i,j,k}}}\left(\frac{p^n_o-p^{n-1}_o}{\Delta t^n}\right)-\frac{\partial(\beta^*_{os})^n}{\partial S^n_{w_{i,j,k}}}\left(\frac{S^n_w-S^{n-1}_w}{\Delta t^n}\right)-\frac{(\beta^*_{os})^n}{\Delta t^n}\\ &-\frac{\partial(\beta^*_{os})^n}{\partial S^n_{w_{i,j,k}}}\left(\frac{S^n_g-S^{n-1}_g}{\Delta t^n}\right)-\frac{\partial(q^*_o)^n}{\partial S^n_{w_{i,j,k}}}. \end{aligned} \tag{C.13}$$

In eq. C.13 the derivatives $\frac{\partial\left(\beta^*_{op}\right)^n}{\partial S^n_{w_{i,j,k}}}$ and $\frac{\partial(\beta^*_{os})^n}{\partial S^n_{w_{i,j,k}}}$ are zero, i.e.

$$\begin{aligned}\frac{\partial\left(\beta^*_{op}\right)^n}{\partial S^n_{w_{i,j,k}}} &= V_{gb}\frac{\partial}{\partial S^n_{w_{i,j,k}}}\left(\left(\frac{S_o}{B_o}\right)^{n-1}\phi^{'}+\phi^n S_o^{n-1}\left(\frac{1}{B_o}\right)^{'}\right)\\ &= 0, \end{aligned} \tag{C.14}$$

and

$$\begin{aligned}\frac{\partial(\beta^*_{os})^n}{\partial S^n_{w_{i,j,k}}} &= V_{gb}\frac{\partial}{\partial S^n_{w_{i,j,k}}}\left(\phi^n\left(\frac{1}{B_o}\right)^n\right)\\ &= 0. \end{aligned} \tag{C.15}$$

Derivatives with respect to the gas saturation $\frac{\partial g^{n-1}_{o_{i,j,k-1}}}{\partial S^n_{g_{i,j,k}}}$

Eq. C.3 is the starting equation for derivatives $\frac{\partial g^{n-1}_{o_{i\pm1,j\pm1,k\pm1}}}{\partial S^n_{g_{i,j,k}}}$. Derivative $\frac{\partial g^{n-1}_{o_{i,j,k-1}}}{\partial S^n_{g_{i,j,k}}}$ equals

$$\frac{\partial g^{n-1}_{o_{i,j,k-1}}}{\partial S^n_{g_{i,j,k}}} = -\frac{\partial {To1}_{i,j,k-\frac{1}{2}}}{\partial S^n_{g_{i,j,k}}}\left(p_{o_{i,j,k}}-p_{o_{i,j,k-1}}\right)+\frac{\partial {To4}_{i,j,k-\frac{1}{2}}}{\partial S^n_{g_{i,j,k}}}\left(h_{i,j,k}-h_{i,j,k-1}\right). \tag{C.16}$$

Eq. C.1 forms the basis for derivative $\frac{\partial g^{n-1}_{o_{i,j,k}}}{\partial S^n_{g_{i,j,k}}}$, which becomes after substituting eqs. C.16, and some rearranging

$$\begin{aligned}\frac{\partial g^{n-1}_{o_{i,j,k}}}{\partial S^n_{g_{i,j,k}}} &= -\left(\frac{\partial g^{n-1}_{o_{i,j,k-1}}}{\partial S^n_{g_{i,j,k}}}+\frac{\partial g^{n-1}_{o_{i,j-1,k}}}{\partial S^n_{g_{i,j,k}}}+\frac{\partial g^{n-1}_{o_{i-1,j,k}}}{\partial S^n_{g_{i,j,k}}}+\frac{\partial g^{n-1}_{o_{i+1,j,k}}}{\partial S^n_{g_{i,j,k}}}+\frac{\partial g^{n-1}_{o_{i,j+1,k}}}{\partial S^n_{g_{i,j,k}}}+\frac{\partial g^{n-1}_{o_{i,j,k+1}}}{\partial S^n_{g_{i,j,k}}}\right)\\ &+\frac{\partial\left(\beta^*_{op}\right)^n}{\partial S^n_{g_{i,j,k}}}\left(\frac{p^n_o-p^{n-1}_o}{\Delta t^n}\right)-\frac{\partial(\beta^*_{os})^n}{\partial S^n_{g_{i,j,k}}}\left(\frac{S^n_w-S^{n-1}_w}{\Delta t^n}\right)\\ &-\frac{\partial(\beta^*_{os})^n}{\partial S^n_{g_{i,j,k}}}\left(\frac{S^n_g-S^{n-1}_g}{\Delta t^n}\right)-\frac{(\beta^*_{os})^n}{\Delta t^n}-\frac{\partial(q^*_o)^n}{\partial S^n_{g_{i,j,k}}}. \end{aligned} \tag{C.17}$$

In eq. C.17 the derivatives $\frac{\partial\left(\beta^*_{op}\right)^n}{\partial S^n_{g_{i,j,k}}}$ and $\frac{\partial(\beta^*_{os})^n}{\partial S^n_{g_{i,j,k}}}$ are zero, i.e.

$$\begin{aligned}\frac{\partial\left(\beta^*_{op}\right)^n}{\partial S^n_{g_{i,j,k}}} &= V_{gb}\frac{\partial}{\partial S^n_{g_{i,j,k}}}\left(\left(\frac{S_o}{B_o}\right)^{n-1}\phi^{'}+\phi^n S_o^{n-1}\left(\frac{1}{B_o}\right)^{'}\right)\\ &= 0, \end{aligned} \tag{C.18}$$

and

$$\begin{aligned}\frac{\partial(\beta^*_{os})^n}{\partial S^n_{g_{i,j,k}}} &= V_{gb}\frac{\partial}{\partial S^n_{g_{i,j,k}}}\left(\phi^n\left(\frac{1}{B_o}\right)^n\right)\\ &= 0. \end{aligned} \tag{C.19}$$

C.1.2 The water equation

Fully written out the discrete water equation for grid block i,j,k is

$$\begin{aligned} g^{n-1}_{w_{i,j,k}} &= -\left[\begin{array}{l} T_{w1_{i+\frac{1}{2},j,k}}\left(p_{o_{i+1,j,k}}-p_{o_{i,j,k}}\right)+T_{w1_{i-\frac{1}{2},j,k}}\left(p_{o_{i-1,j,k}}-p_{o_{i,j,k}}\right)\\ +T_{w1_{i,j+\frac{1}{2},k}}\left(p_{o_{i,j+1,k}}-p_{o_{i,j,k}}\right)+T_{w1_{i,j-\frac{1}{2},k}}\left(p_{o_{i,j-1,k}}-p_{o_{i,j,k}}\right)\\ +T_{w1_{i,j,k+\frac{1}{2}}}\left(p_{o_{i,j,k+1}}-p_{o_{i,j,k}}\right)+T_{w1_{i,j,k-\frac{1}{2}}}\left(p_{o_{i,j,k-1}}-p_{o_{i,j,k}}\right)\end{array}\right]^n\\ &+\left[\begin{array}{l} T_{w2_{i+\frac{1}{2},j,k}}\left(S_{w_{i+1,j,k}}-S_{w_{i,j,k}}\right)+T_{w2_{i-\frac{1}{2},j,k}}\left(S_{w_{i-1,j,k}}-S_{w_{i,j,k}}\right)\\ +T_{w2_{i,j+\frac{1}{2},k}}\left(S_{w_{i,j+1,k}}-S_{w_{i,j,k}}\right)+T_{w2_{i,j-\frac{1}{2},k}}\left(S_{w_{i,j-1,k}}-S_{w_{i,j,k}}\right)\\ +T_{w2_{i,j,k+\frac{1}{2}}}\left(S_{w_{i,j,k+1}}-S_{w_{i,j,k}}\right)+T_{w2_{i,j,k-\frac{1}{2}}}\left(S_{w_{i,j,k-1}}-S_{w_{i,j,k}}\right)\end{array}\right]^n\\ &+\left[\begin{array}{l} T_{w3_{i+\frac{1}{2},j,k}}\left(S_{g_{i+1,j,k}}-S_{g_{i,j,k}}\right)+T_{w3_{i-\frac{1}{2},j,k}}\left(S_{g_{i-1,j,k}}-S_{g_{i,j,k}}\right)\\ +T_{w3_{i,j+\frac{1}{2},k}}\left(S_{g_{i,j+1,k}}-S_{g_{i,j,k}}\right)+T_{w3_{i,j-\frac{1}{2},k}}\left(S_{g_{i,j-1,k}}-S_{g_{i,j,k}}\right)\\ +T_{w3_{i,j,k+\frac{1}{2}}}\left(S_{g_{i,j,k+1}}-S_{g_{i,j,k}}\right)+T_{w3_{i,j,k-\frac{1}{2}}}\left(S_{g_{i,j,k-1}}-S_{g_{i,j,k}}\right)\end{array}\right]^n\\ &+\left[\begin{array}{l} T_{w4_{i+\frac{1}{2},j,k}}\left(h_{i+1,j,k}-h_{i,j,k}\right)+T_{w4_{i-\frac{1}{2},j,k}}\left(h_{i-1,j,k}-h_{i,j,k}\right)\\ +T_{w4_{i,j+\frac{1}{2},k}}\left(h_{i,j+1,k}-h_{i,j,k}\right)+T_{w4_{i,j-\frac{1}{2},k}}\left(h_{i,j-1,k}-h_{i,j,k}\right)\\ +T_{w4_{i,j,k+\frac{1}{2}}}\left(h_{i,j,k+1}-h_{i,j,k}\right)+T_{w4_{i,j,k-\frac{1}{2}}}\left(h_{i,j,k-1}-h_{i,j,k}\right)\end{array}\right]^n\\ &+\left(\beta^*_{wp}\right)^n_{i,j,k}\left(\frac{p^n_o-p^{n-1}_o}{\Delta t^n}\right)_{i,j,k}+\left(\beta^*_{ws}\right)^n_{i,j,k}\left(\frac{S^n_w-S^{n-1}_w}{\Delta t^n}\right)_{i,j,k}-\left(q^*_w\right)^n_{i,j,k}. \end{aligned} \tag{C.20}$$

Derivatives with respect to the oil pressure $\frac{\partial g^{n-1}_{w_{i,j,k-1}}}{\partial p^n_{o_{i,j,k}}}$

Derivative $\frac{\partial g^{n-1}_{w_{i,j,k-1}}}{\partial p^n_{o_{i,j,k}}}$ equals

$$\begin{aligned}\frac{\partial g^{n-1}_{w_{i,j,k-1}}}{\partial p^n_{o_{i,j,k}}} &= -T_{w1}{}_{i,j,k-\frac{1}{2}} \\ &\quad -\frac{\partial T_{w1}{}_{i,j,k-\frac{1}{2}}}{\partial p^n_{o_{i,j,k}}}\left(p_{o_{i,j,k}}-p_{o_{i,j,k-1}}\right)+\frac{\partial T_{w2}{}_{i,j,k-\frac{1}{2}}}{\partial p^n_{o_{i,j,k}}}\left(S_{w_{i,j,k}}-S_{w_{i,j,k-1}}\right) \\ &\quad +\frac{\partial T_{w3}{}_{i,j,k-\frac{1}{2}}}{\partial p^n_{o_{i,j,k}}}\left(S_{g_{i,j,k}}-S_{g_{i,j,k-1}}\right)+\frac{\partial T_{w4}{}_{i,j,k-\frac{1}{2}}}{\partial p^n_{o_{i,j,k}}}\left(h_{i,j,k}-h_{i,j,k-1}\right).\end{aligned} \tag{C.21a}$$

It is representative for derivatives $\frac{\partial g^{n-1}_{w_{i\pm1,j\pm1,k\pm1}}}{\partial p^n_{o_{i,j,k}}}$.

Eq. C.20 forms the starting point for derivative $\frac{\partial g^{n-1}_{w_{i,j,k}}}{\partial p^n_{o_{i,j,k}}}$ which becomes, after substituting eqs. C.21 and some rearranging

$$\begin{aligned}\frac{\partial g^{n-1}_{w_{i,j,k}}}{\partial p^n_{o_{i,j,k}}} &= -\left(\begin{array}{c}\frac{\partial g^{n-1}_{w_{i,j,k-1}}}{\partial p^n_{o_{i,j,k}}}+\frac{\partial g^{n-1}_{w_{i,j-1,k}}}{\partial p^n_{o_{i,j,k}}}+\frac{\partial g^{n-1}_{w_{i-1,j,k}}}{\partial p^n_{o_{i,j,k}}} \\ +\frac{\partial g^{n-1}_{w_{i+1,j,k}}}{\partial p^n_{o_{i,j,k}}}+\frac{\partial g^{n-1}_{w_{i,j+1,k}}}{\partial p^n_{o_{i,j,k}}}+\frac{\partial g^{n-1}_{w_{i,j,k+1}}}{\partial p^n_{o_{i,j,k}}}\end{array}\right) \\ &\quad +\frac{\partial\left(\beta^*_{wp}\right)^n}{\partial p^n_{o_{i,j,k}}}\left(\frac{p^n_o-p^{n-1}_o}{\Delta t^n}\right)+\frac{\left(\beta^*_{wp}\right)^n}{\Delta t^n}+\frac{\partial(\beta^*_{ws})^n}{\partial p^n_{o_{i,j,k}}}\left(\frac{S^n_w-S^{n-1}_w}{\Delta t^n}\right)-\frac{\partial(q^*_w)^n}{\partial p^n_{o_{i,j,k}}}.\end{aligned} \tag{C.22}$$

In eq. C.22 the derivative $\frac{\partial\left(\beta^*_{wp}\right)^n}{\partial p^n_{o_{i,j,k}}}$ is

$$\frac{\partial\left(\beta^*_{wp}\right)^n}{\partial p^n_{o_{i,j,k}}}=V_{gb}S^{n-1}_w\left(\left(\frac{1}{B_w}\right)^{n-1}\frac{\partial\phi'}{\partial p^n_{o_{i,j,k}}}+\phi^n\frac{\partial\left(\frac{1}{B_w}\right)'}{\partial p^n_{o_{i,j,k}}}+\left(\frac{1}{B_w}\right)'\frac{\partial\phi^n}{\partial p^n_{o_{i,j,k}}}\right), \tag{C.23}$$

noting that

$$\frac{\partial p^n_w}{\partial p^n_{o_{i,j,k}}}=\frac{\partial(p^n_o-p^n_{cow})}{\partial p^n_{o_{i,j,k}}}=1, \tag{C.24}$$

and thus

$$\frac{\partial\left(\frac{1}{B_w}\right)^n}{\partial p^n_{o_{i,j,k}}}=\frac{\partial\left(\frac{1}{B_w}\right)^n}{\partial p^n_{w_{i,j,k}}}\frac{\partial p^n_{w_{i,j,k}}}{\partial p^n_{o_{i,j,k}}}=\frac{\partial\left(\frac{1}{B_w}\right)^n}{\partial p^n_{w_{i,j,k}}}=a_w. \tag{C.25}$$

In eq. C.22 the derivative $\frac{\partial(\beta^*_{ws})^n}{\partial p^n_{o_{i,j,k}}}$ is

$$\frac{\partial(\beta^*_{ws})^n}{\partial p^n_{o_{i,j,k}}}=V_{gb}\left[\begin{array}{c}\left(\left(\frac{1}{B_w}\right)^n-S^{n-1}_w\left(\frac{1}{B_w}\right)'p'_{cow}\right)\frac{\partial\phi^n}{\partial p^n_{o_{i,j,k}}} \\ +\phi^n\left(\frac{\partial\left(\frac{1}{B_w}\right)^n}{\partial p^n_{o_{i,j,k}}}-S^{n-1}_w p'_{cow}\frac{\partial\left(\frac{1}{B_w}\right)'}{\partial p^n_{o_{i,j,k}}}\right)\end{array}\right]. \tag{C.26}$$

Derivatives with respect to the water saturation $\frac{\partial g^{n-1}_{w_{i,j,k-1}}}{\partial S^n_{w_{i,j,k}}}$

For derivatives like $\frac{\partial g^{n-1}_{w_{i\pm1,j\pm1,k\pm1}}}{\partial S^n_{w_{i,j,k}}}$, $\frac{\partial g^{n-1}_{w_{i,j,k-1}}}{\partial S^n_{w_{i,j,k}}}$ is used as an example, i.e.

$$\begin{aligned}\frac{\partial g^{n-1}_{w_{i,j,k-1}}}{\partial S^n_{w_{i,j,k}}} &= -\frac{\partial {T_{w1}}_{i,j,k-\frac{1}{2}}}{\partial S^n_{w_{i,j,k}}}\left(p_{o_{i,j,k}} - p_{o_{i,j,k-1}}\right) \\ &+{T_{w2}}_{i,j,k-\frac{1}{2}} + \frac{\partial {T_{w2}}_{i,j,k-\frac{1}{2}}}{\partial S^n_{w_{i,j,k}}}\left(S_{w_{i,j,k}} - S_{w_{i,j,k-1}}\right) \\ &+\frac{\partial {T_{w3}}_{i,j,k-\frac{1}{2}}}{\partial S^n_{w_{i,j,k}}}\left(S_{g_{i,j,k}} - S_{g_{i,j,k-1}}\right) + \frac{\partial {T_{w4}}_{i,j,k-\frac{1}{2}}}{\partial S^n_{w_{i,j,k}}}\left(h_{i,j,k} - h_{i,j,k-1}\right).\end{aligned} \tag{C.27}$$

Eq. C.20 forms again the starting point for derivative $\frac{\partial g^{n-1}_{w_{i,j,k}}}{\partial S^n_{w_{i,j,k}}}$ which becomes, after some rearranging

$$\begin{aligned}\frac{\partial g^{n-1}_{w_{i,j,k}}}{\partial S^n_{w_{i,j,k}}} &= -\left(\begin{array}{c}\frac{\partial g^{n-1}_{w_{i,j,k-1}}}{\partial S^n_{w_{i,j,k}}} + \frac{\partial g^{n-1}_{w_{i,j-1,k}}}{\partial S^n_{w_{i,j,k}}} + \frac{\partial g^{n-1}_{w_{i-1,j,k}}}{\partial S^n_{w_{i,j,k}}} \\ +\frac{\partial g^{n-1}_{w_{i+1,j,k}}}{\partial S^n_{w_{i,j,k}}} + \frac{\partial g^{n-1}_{w_{i,j+1,k}}}{\partial S^n_{w_{i,j,k}}} + \frac{\partial g^{n-1}_{w_{i,j,k+1}}}{\partial S^n_{w_{i,j,k}}}\end{array}\right) \\ &+\frac{\partial\left(\beta^*_{wp}\right)^n}{\partial S^n_{w_{i,j,k}}}\left(\frac{p^n_o - p^{n-1}_o}{\Delta t^n}\right) + \frac{\partial(\beta^*_{ws})^n}{\partial S^n_{w_{i,j,k}}}\left(\frac{S^n_w - S^{n-1}_w}{\Delta t^n}\right) + \frac{(\beta^*_{ws})^n}{\Delta t^n} - \frac{\partial(q^*_w)^n}{\partial S^n_{w_{i,j,k}}}.\end{aligned} \tag{C.28}$$

In eq. C.28 the derivative $\frac{\partial\left(\beta^*_{wp}\right)^n}{\partial S^n_{w_{i,j,k}}}$ is zero, i.e.

$$\begin{aligned}\frac{\partial\left(\beta^*_{wp}\right)^n}{\partial S^n_{w_{i,j,k}}} &= V_{gb}\frac{\partial}{\partial S^n_{w_{i,j,k}}}\left(\left(\frac{1}{B_w}\right)^{n-1} S_w^{n-1}\phi' + \phi^n S_w^{n-1}\left(\frac{1}{B_w}\right)'\right) \\ &= 0.\end{aligned} \tag{C.29}$$

The derivative $\frac{\partial(\beta^*_{ws})^n}{\partial S^n_{w_{i,j,k}}}$ equals

$$\begin{aligned}\frac{\partial(\beta^*_{ws})^n}{\partial S^n_{w_{i,j,k}}} &= V_{gb}\frac{\partial\left(\phi^n\left(\frac{1}{B_w}\right)^n - \phi^n S_w^{n-1}\left(\frac{1}{B_w}\right)' p'_{cow}\right)}{\partial S^n_{w_{i,j,k}}}, \\ &= V_{gb}\left(-\phi^n S_w^{n-1}\left(\frac{1}{B_w}\right)'\frac{\partial p'_{cow}}{\partial S^n_{w_{i,j,k}}}\right).\end{aligned} \tag{C.30}$$

Derivatives with respect to the gas saturation $\frac{\partial g^{n-1}_{w_{i,j,k-1}}}{\partial S^n_{g_{i,j,k}}}$

The derivatives $\frac{\partial g^{n-1}_{w_{i\pm1,j\pm1,k\pm1}}}{\partial S^n_{g_{i,j,k}}}$ are like

$$\begin{aligned}\frac{\partial g^{n-1}_{w_{i,j,k-1}}}{\partial S^n_{g_{i,j,k}}} &= -\frac{\partial {T_{w1}}_{i,j,k-\frac{1}{2}}}{\partial S^n_{g_{i,j,k}}}\left(p_{o_{i,j,k}}-p_{o_{i,j,k-1}}\right)+\frac{\partial {T_{w2}}_{i,j,k-\frac{1}{2}}}{\partial S^n_{g_{i,j,k}}}\left(S_{w_{i,j,k}}-S_{w_{i,j,k-1}}\right)\\ &\quad+\frac{\partial {T_{w3}}_{i,j,k-\frac{1}{2}}}{\partial S^n_{g_{i,j,k}}}\left(S_{g_{i,j,k}}-S_{g_{i,j,k-1}}\right)\\ &\quad+{T_{w3}}_{i,j,k-\frac{1}{2}}+\frac{\partial {T_{w4}}_{i,j,k-\frac{1}{2}}}{\partial S^n_{g_{i,j,k}}}\left(h_{i,j,k}-h_{i,j,k-1}\right). \qquad \text{(C.31)}\end{aligned}$$

Eq. C.20 forms again the starting point for derivative $\frac{\partial g^{n-1}_{w_{i,j,k}}}{\partial S^n_{g_{i,j,k}}}$ which becomes, after substituting eqs. C.31 and some rearranging

$$\begin{aligned}\frac{\partial g^{n-1}_{w_{i,j,k}}}{\partial S^n_{g_{i,j,k}}} &= -\left(\begin{array}{l}\frac{\partial g^{n-1}_{w_{i,j,k-1}}}{\partial S^n_{g_{i,j,k}}}+\frac{\partial g^{n-1}_{w_{i,j-1,k}}}{\partial S^n_{g_{i,j,k}}}+\frac{\partial g^{n-1}_{w_{i-1,j,k}}}{\partial S^n_{g_{i,j,k}}}\\ +\frac{\partial g^{n-1}_{w_{i+1,j,k}}}{\partial S^n_{g_{i,j,k}}}+\frac{\partial g^{n-1}_{w_{i,j+1,k}}}{\partial S^n_{g_{i,j,k}}}+\frac{\partial g^{n-1}_{w_{i,j,k+1}}}{\partial S^n_{g_{i,j,k}}}\end{array}\right)\\ &\quad+\frac{\partial\left(\beta^*_{wp}\right)^n}{\partial S^n_{g_{i,j,k}}}\left(\frac{p^n_o-p^{n-1}_o}{\Delta t^n}\right)+\frac{\partial(\beta^*_{ws})^n}{\partial S^n_{g_{i,j,k}}}\left(\frac{S^n_w-S^{n-1}_w}{\Delta t^n}\right)-\frac{\partial(q^*_w)^n}{\partial S^n_{g_{i,j,k}}}. \qquad \text{(C.32)}\end{aligned}$$

In eq. C.32 the derivatives $\frac{\partial\left(\beta^*_{wp}\right)^n}{\partial S^n_{g_{i,j,k}}}$ and $\frac{\partial(\beta^*_{ws})^n}{\partial S^n_{g_{i,j,k}}}$ are zero, i.e.

$$\begin{aligned}\frac{\partial\left(\beta^*_{wp}\right)^n}{\partial S^n_{g_{i,j,k}}} &= V_{gb}\frac{\partial}{\partial S^n_{g_{i,j,k}}}\left(\left(\frac{1}{B_w}\right)^{n-1}S_w^{n-1}\phi^{'}+\phi^n S_w^{n-1}\left(\frac{1}{B_w}\right)^{'}\right)\\ &= 0, \qquad \text{(C.33)}\end{aligned}$$

and

$$\begin{aligned}\frac{\partial(\beta^*_{ws})^n}{\partial S^n_{g_{i,j,k}}} &= V_{gb}\frac{\partial\left(\phi^n\left(\frac{1}{B_w}\right)^n-\phi^n S_w^{n-1}\left(\frac{1}{B_w}\right)^{'}p'_{cow}\right)}{\partial S^n_{g_{i,j,k}}}\\ &= 0. \qquad \text{(C.34)}\end{aligned}$$

C.1.3 The gas equation

The discrete gas equation for grid block i, j, k is

$$
\begin{aligned}
g^{n-1}_{g_{i,j,k}} \;=\; & -\left[\begin{array}{l} T_{g1}{}_{i+\frac{1}{2},j,k}\left(p_{o_{i+1,j,k}}-p_{o_{i,j,k}}\right)+T_{g1}{}_{i-\frac{1}{2},j,k}\left(p_{o_{i-1,j,k}}-p_{o_{i,j,k}}\right) \\ +T_{g1}{}_{i,j+\frac{1}{2},k}\left(p_{o_{i,j+1,k}}-p_{o_{i,j,k}}\right)+T_{g1}{}_{i,j-\frac{1}{2},k}\left(p_{o_{i,j-1,k}}-p_{o_{i,j,k}}\right) \\ +T_{g1}{}_{i,j,k+\frac{1}{2}}\left(p_{o_{i,j,k+1}}-p_{o_{i,j,k}}\right)+T_{g1}{}_{i,j,k-\frac{1}{2}}\left(p_{o_{i,j,k-1}}-p_{o_{i,j,k}}\right) \end{array}\right]^n \\
& -\left[\begin{array}{l} T_{g2}{}_{i+\frac{1}{2},j,k}\left(S_{w_{i+1,j,k}}-S_{w_{i,j,k}}\right)+T_{g2}{}_{i-\frac{1}{2},j,k}\left(S_{w_{i-1,j,k}}-S_{w_{i,j,k}}\right) \\ +T_{g2}{}_{i,j+\frac{1}{2},k}\left(S_{w_{i,j+1,k}}-S_{w_{i,j,k}}\right)+T_{g2}{}_{i,j-\frac{1}{2},k}\left(S_{w_{i,j-1,k}}-S_{w_{i,j,k}}\right) \\ +T_{g2}{}_{i,j,k+\frac{1}{2}}\left(S_{w_{i,j,k+1}}-S_{w_{i,j,k}}\right)+T_{g2}{}_{i,j,k-\frac{1}{2}}\left(S_{w_{i,j,k-1}}-S_{w_{i,j,k}}\right) \end{array}\right]^n \\
& -\left[\begin{array}{l} T_{g3}{}_{i+\frac{1}{2},j,k}\left(S_{g_{i+1,j,k}}-S_{g_{i,j,k}}\right)+T_{g3}{}_{i-\frac{1}{2},j,k}\left(S_{g_{i-1,j,k}}-S_{g_{i,j,k}}\right) \\ +T_{g3}{}_{i,j+\frac{1}{2},k}\left(S_{g_{i,j+1,k}}-S_{g_{i,j,k}}\right)+T_{g3}{}_{i,j-\frac{1}{2},k}\left(S_{g_{i,j-1,k}}-S_{g_{i,j,k}}\right) \\ +T_{g3}{}_{i,j,k+\frac{1}{2}}\left(S_{g_{i,j,k+1}}-S_{g_{i,j,k}}\right)+T_{g3}{}_{i,j,k-\frac{1}{2}}\left(S_{g_{i,j,k-1}}-S_{g_{i,j,k}}\right) \end{array}\right]^n \\
& +\left[\begin{array}{l} T_{g4}{}_{i+\frac{1}{2},j,k}\left(h_{i+1,j,k}-h_{i,j,k}\right)+T_{g4}{}_{i-\frac{1}{2},j,k}\left(h_{i-1,j,k}-h_{i,j,k}\right) \\ +T_{g4}{}_{i,j+\frac{1}{2},k}\left(h_{i,j+1,k}-h_{i,j,k}\right)+T_{g4}{}_{i,j-\frac{1}{2},k}\left(h_{i,j-1,k}-h_{i,j,k}\right) \\ +T_{g4}{}_{i,j,k+\frac{1}{2}}\left(h_{i,j,k+1}-h_{i,j,k}\right)+T_{g4}{}_{i,j,k-\frac{1}{2}}\left(h_{i,j,k-1}-h_{i,j,k}\right) \end{array}\right]^n \\
& +\left(\beta^*_{gp}\right)^n_{i,j,k}\left(\tfrac{p^n_o-p^{n-1}_o}{\Delta t^n}\right)_{i,j,k}-\left(\beta^*_{gsw}\right)^n_{i,j,k}\left(\tfrac{S^n_w-S^{n-1}_w}{\Delta t^n}\right)_{i,j,k} \\
& +\left(\beta^*_{gsg}\right)^n_{i,j,k}\left(\tfrac{S^n_g-S^{n-1}_g}{\Delta t^n}\right)_{i,j,k}-\left(q^*_g\right)^n_{i,j,k}. \qquad \text{(C.35)}
\end{aligned}
$$

Derivatives with respect to the oil pressure $\frac{\partial g^{n-1}_{g_{i-1,j,k}}}{\partial p^n_{o_{i,j,k}}}$

The derivatives $\frac{\partial g^{n-1}_{g_{i\pm1,j\pm1,k\pm1}}}{\partial p^n_{o_{i,j,k}}}$ are like

$$
\begin{aligned}
\frac{\partial g^{n-1}_{g_{i,j,k-1}}}{\partial p^n_{o_{i,j,k}}} \;=\; & -T_{g1}{}_{i,j,k-\frac{1}{2}}-\frac{\partial T_{g1}{}_{i,j,k-\frac{1}{2}}}{\partial p^n_{o_{i,j,k}}}\left(p_{o_{i,j,k}}-p_{o_{i,j,k-1}}\right) \\
& -\frac{\partial T_{g2}{}_{i,j,k-\frac{1}{2}}}{\partial p^n_{o_{i,j,k}}}\left(S_{w_{i,j,k}}-S_{w_{i,j,k-1}}\right)-\frac{\partial T_{g3}{}_{i,j,k-\frac{1}{2}}}{\partial p^n_{o_{i,j,k}}}\left(S_{g_{i,j,k}}-S_{g_{i,j,k-1}}\right) \\
& +\frac{\partial T_{g4}{}_{i,j,k-\frac{1}{2}}}{\partial p^n_{o_{i,j,k}}}\left(h_{i,j,k}-h_{i,j,k-1}\right). \qquad \text{(C.36)}
\end{aligned}
$$

Eq. C.35 forms the starting point for derivative $\frac{\partial g_{g_{i,j,k}}^{n-1}}{\partial p_{o_{i,j,k}}^{n}}$ which becomes, after some rearranging

$$\begin{aligned}\frac{\partial g_{g_{i,j,k}}^{n-1}}{\partial p_{o_{i,j,k}}^{n}} &= -\left(\begin{array}{c}\frac{\partial g_{g_{i,j,k-1}}^{n-1}}{\partial p_{o_{i,j,k}}^{n}}+\frac{\partial g_{g_{i,j-1,k}}^{n-1}}{\partial p_{o_{i,j,k}}^{n}}+\frac{\partial g_{g_{i-1,j,k}}^{n-1}}{\partial p_{o_{i,j,k}}^{n}}\\ +\frac{\partial g_{g_{i+1,j,k}}^{n-1}}{\partial p_{o_{i,j,k}}^{n}}+\frac{\partial g_{g_{i,j+1,k}}^{n-1}}{\partial p_{o_{i,j,k}}^{n}}+\frac{\partial g_{g_{i,j,k+1}}^{n-1}}{\partial p_{o_{i,j,k}}^{n}}\end{array}\right)\\ &+\frac{\partial\left(\beta_{gp}^{*}\right)_{i,j,k}^{n}}{\partial p_{o_{i,j,k}}^{n}}\left(\frac{p_o^n-p_o^{n-1}}{\Delta t^n}\right)_{i,j,k}+\frac{\left(\beta_{gp}^{*}\right)_{i,j,k}^{n}}{\Delta t^n}-\frac{\partial\left(\beta_{gsw}^{*}\right)_{i,j,k}^{n}}{\partial p_{o_{i,j,k}}^{n}}\left(\frac{S_w^n-S_w^{n-1}}{\Delta t^n}\right)_{i,j,k}\\ &+\frac{\partial\left(\beta_{gsg}^{*}\right)_{i,j,k}^{n}}{\partial p_{o_{i,j,k}}^{n}}\left(\frac{S_g^n-S_g^{n-1}}{\Delta t^n}\right)_{i,j,k}-\frac{\partial\left(q_g^{*}\right)_{i,j,k}^{n}}{\partial p_{o_{i,j,k}}^{n}}. \qquad \text{(C.37)}\end{aligned}$$

In eq. C.37 the derivative $\frac{\partial\left(\beta_{gp}^{*}\right)^{n}}{\partial p_{o_{i,j,k}}^{n}}$ is

$$\frac{\partial\left(\beta_{gp}^{*}\right)^{n}}{\partial p_{o_{i,j,k}}^{n}}=V_{gb}\left[\begin{array}{c}\left(\frac{1}{B_o}\phi S_o\right)^{n-1}\frac{\partial R_s'}{\partial p_{o_{i,j,k}}^{n}}+\left(\left(\frac{1}{B_g}\right)^{n-1}S_g^{n-1}+R_s^n\left(\frac{S_o}{B_o}\right)^{n-1}\right)\frac{\partial\phi'}{\partial p_{o_{i,j,k}}^{n}}\\ +\phi'\left(\frac{S_o}{B_o}\right)^{n-1}\frac{\partial R_s^n}{\partial p_{o_{i,j,k}}^{n}}+\left(R_s^nS_o^{n-1}\left(\frac{1}{B_o}\right)'+S_g^{n-1}\left(\frac{1}{B_g}\right)'\right)\frac{\partial\phi^n}{\partial p_{o_{i,j,k}}^{n}}\\ +\phi^n\left(S_o^{n-1}\left(\frac{1}{B_o}\right)'\frac{\partial R_s^n}{\partial p_{o_{i,j,k}}^{n}}+R_s^nS_o^{n-1}\frac{\partial\left(\frac{1}{B_o}\right)'}{\partial p_{o_{i,j,k}}^{n}}+S_g^{n-1}\frac{\partial\left(\frac{1}{B_g}\right)'}{\partial p_{o_{i,j,k}}^{n}}\right)\end{array}\right]. \qquad \text{(C.38)}$$

Since

$$\frac{\partial p_g^n}{\partial p_{o_{i,j,k}}^{n}}=\frac{\partial\left(p_o^n+p_{cgo}^n\right)}{\partial p_{o_{i,j,k}}^{n}}=\frac{\partial(p_o^n)}{\partial p_{o_{i,j,k}}^{n}}=1, \qquad \text{(C.39)}$$

the derivative $\frac{\partial\left(\frac{1}{B_g}\right)^{n}}{\partial p_{o_{i,j,k}}^{n}}$ becomes

$$\frac{\partial\left(\frac{1}{B_g}\right)^{n}}{\partial p_{o_{i,j,k}}^{n}}=\frac{\partial\left(\frac{1}{B_g}\right)^{n}}{\partial p_{g_{i,j,k}}^{n}}\frac{\partial p_{g_{i,j,k}}^{n}}{\partial p_{o_{i,j,k}}^{n}}=\frac{\partial\left(\frac{1}{B_g}\right)^{n}}{\partial p_{g_{i,j,k}}^{n}}=a_g^n. \qquad \text{(C.40)}$$

In eq. C.37 the derivative $\frac{\partial\left(\beta_{gsw}^{*}\right)^{n}}{\partial p_{o_{i,j,k}}^{n}}$ is

$$\frac{\partial\left(\beta_{gsw}^{*}\right)^{n}}{\partial p_{o_{i,j,k}}^{n}}=V_{gb}\left[R_s^n\phi^na_o+R_s^n\left(\frac{1}{B_o}\right)^{n}\frac{\partial\phi^n}{\partial p_{o_{i,j,k}}^{n}}+\phi^n\left(\frac{1}{B_o}\right)^{n}\frac{\partial R_s^n}{\partial p_{o_{i,j,k}}^{n}}\right] \qquad \text{(C.41)}$$

and the derivative $\frac{\partial\left(\beta_{gsg}^{*}\right)^{n}}{\partial p_{o_{i,j,k}}^{n}}$ is equal to

$$\frac{\partial\left(\beta_{gsg}^{*}\right)^{n}}{\partial p_{o_{i,j,k}}^{n}}=V_{gb}\left[\begin{array}{c}\left(\frac{1}{B_g}\right)^{n}\frac{\partial\phi^n}{\partial p_{o_{i,j,k}}^{n}}+\phi^na_g^n+S_g^{n-1}p_{cgo}'\left(\left(\frac{1}{B_g}\right)'\frac{\partial\phi^n}{\partial p_{o_{i,j,k}}^{n}}+\phi^n\frac{\partial\left(\frac{1}{B_g}\right)'}{\partial p_{o_{i,j,k}}^{n}}\right)\\ -R_s^n\phi^na_o^n-R_s^n\left(\frac{1}{B_o}\right)^{n}\frac{\partial\phi^n}{\partial p_{o_{i,j,k}}^{n}}-\phi^n\left(\frac{1}{B_o}\right)^{n}\frac{\partial R_s^n}{\partial p_{o_{i,j,k}}^{n}}\end{array}\right]$$

Derivatives with respect to the water saturation $\frac{\partial g^{n-1}_{g_{i-1,j,k}}}{\partial S^n_{w_{i,j,k}}}$

The derivatives $\frac{\partial g^{n-1}_{g_{i\pm1,j\pm1,k\pm1}}}{\partial S^n_{w_{i,j,k}}}$ are like

$$\begin{aligned}\frac{\partial g^{n-1}_{g_{i,j,k-1}}}{\partial S^n_{w_{i,j,k}}} &= -\frac{\partial {T_{g1}}_{i,j,k-\frac{1}{2}}}{\partial S^n_{w_{i,j,k}}}\left(p_{o_{i,j,k}}-p_{o_{i,j,k-1}}\right)-{T_{g2}}_{i,j,k-\frac{1}{2}}\\ &\quad-\frac{\partial {T_{g2}}_{i,j,k-\frac{1}{2}}}{\partial S^n_{w_{i,j,k}}}\left(S_{w_{i,j,k}}-S_{w_{i,j,k-1}}\right)-\frac{\partial {T_{g3}}_{i,j,k-\frac{1}{2}}}{\partial S^n_{w_{i,j,k}}}\left(S_{g_{i,j,k}}-S_{g_{i,j,k-1}}\right)\\ &\quad+\frac{\partial {T_{g4}}_{i,j,k-\frac{1}{2}}}{\partial S^n_{w_{i,j,k}}}\left(h_{i,j,k}-h_{i,j,k-1}\right). \end{aligned}\tag{C.42}$$

Eq. C.35 forms the starting point for derivative $\frac{\partial g^{n-1}_{g_{i,j,k}}}{\partial S^n_{w_{i,j,k}}}$ which becomes, after some rearranging

$$\begin{aligned}\frac{\partial g^{n-1}_{g_{i,j,k}}}{\partial S^n_{w_{i,j,k}}} &= -\left(\begin{array}{c}\frac{\partial g^{n-1}_{g_{i,j,k-1}}}{\partial S^n_{w_{i,j,k}}}+\frac{\partial g^{n-1}_{g_{i,j-1,k}}}{\partial S^n_{w_{i,j,k}}}+\frac{\partial g^{n-1}_{g_{i-1,j,k}}}{\partial S^n_{w_{i,j,k}}}\\ +\frac{\partial g^{n-1}_{g_{i+1,j,k}}}{\partial S^n_{w_{i,j,k}}}+\frac{\partial g^{n-1}_{g_{i,j+1,k}}}{\partial S^n_{w_{i,j,k}}}+\frac{\partial g^{n-1}_{g_{i,j,k+1}}}{\partial S^n_{w_{i,j,k}}}\end{array}\right)\\ &\quad+\frac{\partial\left(\beta^*_{gp}\right)^n_{i,j,k}}{\partial S^n_{w_{i,j,k}}}\left(\frac{p^n_o-p^{n-1}_o}{\Delta t^n}\right)_{i,j,k}-\frac{\partial\left(\beta^*_{gsw}\right)^n_{i,j,k}}{\partial S^n_{w_{i,j,k}}}\left(\frac{S^n_w-S^{n-1}_w}{\Delta t^n}\right)_{i,j,k}-\frac{\left(\beta^*_{gsw}\right)^n_{i,j,k}}{\Delta t^n}\\ &\quad+\frac{\partial\left(\beta^*_{gsg}\right)^n_{i,j,k}}{\partial S^n_{w_{i,j,k}}}\left(\frac{S^n_g-S^{n-1}_g}{\Delta t^n}\right)_{i,j,k}-\frac{\partial\left(q^*_g\right)^n_{i,j,k}}{\partial S^n_{w_{i,j,k}}}. \end{aligned}\tag{C.43}$$

In eq. C.43 the derivatives $\frac{\partial\left(\beta^*_{gp}\right)^n_{i,j,k}}{\partial S^n_{w_{i,j,k}}}$, $\frac{\partial\left(\beta^*_{gsw}\right)^n_{i,j,k}}{\partial S^n_{w_{i,j,k}}}$, and $\frac{\partial\left(\beta^*_{gsg}\right)^n_{i,j,k}}{\partial S^n_{w_{i,j,k}}}$ are zero, i.e.

$$\begin{aligned}\frac{\partial\left(\beta^*_{gp}\right)^n}{\partial S^n_{w_{i,j,k}}} &= V_{gb}\frac{\partial}{\partial S^n_{w_{i,j,k}}}\left[\begin{array}{c}+\left(\frac{1}{B_o}\phi S_o\right)^{n-1}R'_s+\left(\left(\frac{1}{B_g}\right)^{n-1}S^{n-1}_g+R^n_s\left(\frac{S_o}{B_o}\right)^{n-1}\right)\phi'\\ +\phi^n\left(R^n_sS^{n-1}_o\left(\frac{1}{B_o}\right)'+S^{n-1}_g\left(\frac{1}{B_g}\right)'\right)\end{array}\right]\\ &= 0. \end{aligned}\tag{C.44}$$

$$\begin{aligned}\frac{\partial\left(\beta^*_{gsw}\right)^n}{\partial S^n_{w_{i,j,k}}} &= V_{gb}\frac{\partial\left(R^n_s\phi^n\left(\frac{1}{B_o}\right)^n\right)}{\partial S^n_{w_{i,j,k}}}\\ &= 0 \end{aligned}\tag{C.45}$$

$$\begin{aligned}\frac{\partial\left(\beta^*_{gsg}\right)^n}{\partial S^n_{w_{i,j,k}}} &= V_{gb}\frac{\partial\left(\phi^n\left(\frac{1}{B_g}\right)^n+\phi^nS^{n-1}_g\left(\frac{1}{B_g}\right)'p'_{cgo}-R^n_s\phi^n\left(\frac{1}{B_o}\right)^n\right)}{\partial S^n_{w_{i,j,k}}}\\ &= 0 \end{aligned}\tag{C.46}$$

Derivatives with respect to the gas saturation $\frac{\partial g^{n-1}_{g_{i-1,j,k}}}{\partial S^n_{g_{i,j,k}}}$

The derivatives $\frac{\partial g^{n-1}_{g_{i\pm1,j\pm1,k\pm1}}}{\partial S^n_{g_{i,j,k}}}$ are like

$$\begin{aligned}\frac{\partial g^{n-1}_{g_{i,j,k-1}}}{\partial S^n_{g_{i,j,k}}} &= -\frac{\partial {T_{g1}}_{i,j,k-\frac{1}{2}}}{\partial S^n_{g_{i,j,k}}}\left(p_{o_{i,j,k}}-p_{o_{i,j,k-1}}\right)-\frac{\partial {T_{g2}}_{i,j,k-\frac{1}{2}}}{\partial S^n_{g_{i,j,k}}}\left(S_{w_{i,j,k}}-S_{w_{i,j,k-1}}\right)\\ &\quad -{T_{g3}}_{i,j,k-\frac{1}{2}}-\frac{\partial {T_{g3}}_{i,j,k-\frac{1}{2}}}{\partial S^n_{g_{i,j,k}}}\left(S_{g_{i,j,k}}-S_{g_{i,j,k-1}}\right)\\ &\quad +\frac{\partial {T_{g4}}_{i,j,k-\frac{1}{2}}}{\partial S^n_{g_{i,j,k}}}\left(h_{i,j,k}-h_{i,j,k-1}\right). \end{aligned} \tag{C.47}$$

Eq. C.35 forms the starting point for derivative $\frac{\partial g^{n-1}_{g_{i,j,k}}}{\partial S^n_{g_{i,j,k}}}$ which becomes, after substituting eqs. C.47 and some rearranging

$$\begin{aligned}\frac{\partial g^{n-1}_{g_{i,j,k}}}{\partial S^n_{g_{i,j,k}}} &= -\left(\frac{\partial g^{n-1}_{g_{i,j,k-1}}}{\partial S^n_{g_{i,j,k}}}+\frac{\partial g^{n-1}_{g_{i,j-1,k}}}{\partial S^n_{g_{i,j,k}}}+\frac{\partial g^{n-1}_{g_{i-1,j,k}}}{\partial S^n_{g_{i,j,k}}}+\frac{\partial g^{n-1}_{g_{i+1,j,k}}}{\partial S^n_{g_{i,j,k}}}+\frac{\partial g^{n-1}_{g_{i,j+1,k}}}{\partial S^n_{g_{i,j,k}}}+\frac{\partial g^{n-1}_{g_{i,j,k+1}}}{\partial S^n_{g_{i,j,k}}}\right)\\ &\quad +\frac{\partial\left(\beta^*_{gp}\right)^n_{i,j,k}}{\partial S^n_{g_{i,j,k}}}\left(\frac{p^n_o-p^{n-1}_o}{\Delta t^n}\right)_{i,j,k}-\frac{\partial\left(\beta^*_{gsw}\right)^n_{i,j,k}}{\partial S^n_{g_{i,j,k}}}\left(\frac{S^n_w-S^{n-1}_w}{\Delta t^n}\right)_{i,j,k}\\ &\quad +\frac{\partial\left(\beta^*_{gsg}\right)^n_{i,j,k}}{\partial S^n_{g_{i,j,k}}}\left(\frac{S^n_g-S^{n-1}_g}{\Delta t^n}\right)_{i,j,k}+\frac{\left(\beta^*_{gsg}\right)^n_{i,j,k}}{\Delta t^n}-\frac{\partial\left(q^*_g\right)^n_{i,j,k}}{\partial S^n_{g_{i,j,k}}}. \end{aligned} \tag{C.48}$$

In eq. C.48 the derivatives $\frac{\partial\left(\beta^*_{gp}\right)^n_{i,j,k}}{\partial S^n_{g_{i,j,k}}}$ and $\frac{\partial\left(\beta^*_{gsw}\right)^n_{i,j,k}}{\partial S^n_{g_{i,j,k}}}$ are zero, i.e.

$$\begin{aligned}\frac{\partial\left(\beta^*_{gp}\right)^n}{\partial S^n_{g_{i,j,k}}} &= V_{gb}\frac{\partial}{\partial S^n_{g_{i,j,k}}}\left[\begin{array}{c}+\left(\frac{1}{B_o}\phi S_o\right)^{n-1}R'_s+\left(\left(\frac{1}{B_g}\right)^{n-1}S^{n-1}_g+R^n_s\left(\frac{S_o}{B_o}\right)^{n-1}\right)\phi'\\ +\phi^n\left(R^n_sS^{n-1}_o\left(\frac{1}{B_o}\right)'+S^{n-1}_g\left(\frac{1}{B_g}\right)'\right)\end{array}\right]\\ &= 0, \end{aligned} \tag{C.49}$$

and

$$\frac{\partial\left(\beta^*_{gsw}\right)^n}{\partial S^n_{g_{i,j,k}}}=V_{gb}\frac{\partial\left(R^n_s\phi^n\left(\frac{1}{B_o}\right)^n\right)}{\partial S^n_{g_{i,j,k}}}=0 \tag{C.50}$$

In eq. C.48 the derivative $\frac{\partial\left(\beta^*_{gsg}\right)^n}{\partial S^n_{g_{i,j,k}}}$ is

$$\frac{\partial\left(\beta^*_{gsg}\right)^n}{\partial S^n_{g_{i,j,k}}}=V_{gb}\phi^nS^{n-1}_g\left(\frac{1}{B_g}\right)'\frac{\partial\left(p'_{cgo}\right)}{\partial S^n_{g_{i,j,k}}} \tag{C.51}$$

C.2 Derivatives $\frac{\partial \mathbf{g}^n}{\partial \mathbf{x}^n}$

C.2.1 The oil equation

For grid block $i-1,j,k$ the discrete oil equation is, using notation similar to that in eqs. C.1 & C.2,

$$\begin{aligned} g^n_{o_{i-1,j,k}} &= -\left[\begin{array}{c} +T_{o1}\left(p_{o_{i,j,k}}-p_{o_{i-1,j,k}}\right)+T_{o1}\left(p_{o_{i-2,j,k}}-p_{o_{i-1,j,k}}\right) \\ +T_{o1}\left(p_{o_{i-1,j+1,k}}-p_{o_{i-1,j,k}}\right)+T_{o1}\left(p_{o_{i-1,j-1,k}}-p_{o_{i-1,j,k}}\right) \\ +T_{o1}\left(p_{o_{i-1,j,k+1}}-p_{o_{i-1,j,k}}\right)+T_{o1}\left(p_{o_{i-1,j,k-1}}-p_{o_{i-1,j,k}}\right) \end{array}\right]^{n+1} \\ &+\left[\begin{array}{c} +T_{o4}\left(h_{i,j,k}-h_{i-1,j,k}\right)+T_{o4}\left(h_{i-2,j,k}-h_{i-1,j,k}\right) \\ +T_{o4}\left(h_{i-1,j+1,k}-h_{i-1,j,k}\right)+T_{o4}\left(h_{i-1,j-1,k}-h_{i-1,j,k}\right) \\ +T_{o4}\left(h_{i-1,j,k+1}-h_{i-1,j,k}\right)+T_{o4}\left(h_{i-1,j,k-1}-h_{i-1,j,k}\right) \end{array}\right]^{n+1} \\ &+\left(\beta^*_{op}\right)^{n+1}_{i-1,j,k}\left(\tfrac{p^{n+1}_o-p^n_o}{\Delta t^{n+1}}\right)_{i-1,j,k}-\left(\beta^*_{os}\right)^{n+1}_{i-1,j,k}\left(\tfrac{S^{n+1}_w-S^n_w}{\Delta t^{n+1}}\right)_{i-1,j,k} \\ &-\left(\beta^*_{os}\right)^{n+1}_{i-1,j,k}\left(\tfrac{S^{n+1}_g-S^n_g}{\Delta t^{n+1}}\right)_{i-1,j,k}-\left(q^*_o\right)^{n+1}_{i-1,j,k}. \end{aligned} \tag{C.52}$$

Derivatives with respect to the oil pressure $\frac{\partial g^n_{o_{i-1,j,k}}}{\partial p^n_{o_{i,j,k}}}$

All parameters on line 1 and 2 of eq. C.52 are at time level $n+1$, and thus the derivatives for these terms are $\frac{\partial()^{n+1}}{\partial()^n}=0$. All parameters on line 3 and 4 of eq. C.52 are only a function of the states in grid block $i-1,j,k$, and thus the derivatives $\frac{\partial()_{i-1,j,k}}{\partial()_{i,j,k}}$ are zero. Consequently all derivatives $\frac{\partial g^n_{o_{i\pm1,j\pm1,k\pm1}}}{\partial p^n_{o_{i,j,k}}}$ are zero, i.e.

$$\begin{aligned} \frac{\partial g^n_{o_{i,j,k-1}}}{\partial p^n_{o_{i,j,k}}} &= 0,\ \frac{\partial g^n_{o_{i,j-1,k}}}{\partial p^n_{o_{i,j,k}}}=0,\ \frac{\partial g^n_{o_{i-1,j,k}}}{\partial p^n_{o_{i,j,k}}}=0, \\ \frac{\partial g^n_{o_{i+1,j,k}}}{\partial p^n_{o_{i,j,k}}} &= 0,\ \frac{\partial g^n_{o_{i,j+1,k}}}{\partial p^n_{o_{i,j,k}}}=0,\ \frac{\partial g^n_{o_{i,j,k+1}}}{\partial p^n_{o_{i,j,k}}}=0. \end{aligned} \tag{C.53}$$

Derivative $\frac{\partial g^n_{o_{i,j,k}}}{\partial p^n_{o_{i,j,k}}}$ equals

$$\begin{aligned} \frac{\partial g^n_{o_{i,j,k}}}{\partial p^n_{o_{i,j,k}}} &= -\frac{\beta^{*n+1}_{op}}{\Delta t^{n+1}}+\left(\tfrac{p^{n+1}_o-p^n_o}{\Delta t^{n+1}}\right)\frac{\partial \beta^{*n+1}_{op}}{\partial p^n_{o_{i,j,k}}} \\ &-\left(\tfrac{S^{n+1}_w-S^n_w}{\Delta t^{n+1}}\right)\frac{\partial(\beta^*_{os})^{n+1}}{\partial p^n_{o_{i,j,k}}}-\left(\tfrac{S^{n+1}_g-S^n_g}{\Delta t^{n+1}}\right)\frac{\partial(\beta^*_{os})^{n+1}}{\partial p^n_{o_{i,j,k}}}. \end{aligned} \tag{C.54}$$

In eq. C.54 the derivative $\frac{\partial\left(\beta^*_{op}\right)^{n+1}}{\partial p^n_{o_{i,j,k}}}$ equals

$$\frac{\partial\left(\beta^*_{op}\right)^{n+1}}{\partial p^n_{o_{i,j,k}}}=V_{gb}\left[\left(\tfrac{S_o}{B_o}\right)^n\frac{\partial\left(\phi'\right)}{\partial p^n_{o_{i,j,k}}}+S^n_o\phi' a^n_o+\phi^{n+1}S^n_o\frac{\partial\left(\frac{1}{B_o}\right)'}{\partial p^n_{o_{i,j,k}}}\right]. \tag{C.55}$$

In eq. C.54 the derivative $\frac{\partial(\beta_{os}^*)^{n+1}}{\partial p_{o_{i,j,k}}^n}$ is zero, i.e.

$$\begin{aligned}\frac{\partial(\beta_{os}^*)^{n+1}}{\partial p_{o_{i,j,k}}^n} &= V_{gb}\frac{\partial\left(\phi^{n+1}\left(\frac{1}{B_o}\right)^{n+1}\right)}{\partial p_{o_{i,j,k}}^n} \\ &= 0. \end{aligned} \tag{C.56}$$

Derivatives with respect to the water saturation $\frac{\partial g_{o_{i-1,j,k}}^n}{\partial S_{w_{i,j,k}}^n}$

For the same reasons as described in section 1 all derivatives $\frac{\partial g_{o_{i\pm1,j\pm1,k\pm1}}^n}{\partial S_{w_{i,j,k}}^n}$ are zero, i.e.

$$\begin{aligned}\frac{\partial g_{o_{i,j,k-1}}^n}{\partial S_{w_{i,j,k}}^n} &= 0,\ \frac{\partial g_{o_{i,j-1,k}}^n}{\partial S_{w_{i,j,k}}^n} = 0,\ \frac{\partial g_{o_{i-1,j,k}}^n}{\partial S_{w_{i,j,k}}^n} = 0, \\ \frac{\partial g_{o_{i+1,j,k}}^n}{\partial S_{w_{i,j,k}}^n} &= 0,\ \frac{\partial g_{o_{i,j+1,k}}^n}{\partial S_{w_{i,j,k}}^n} = 0,\ \frac{\partial g_{o_{i,j,k+1}}^n}{\partial S_{w_{i,j,k}}^n} = 0 \end{aligned} \tag{C.57}$$

Derivative $\frac{\partial g_{o_{i,j,k}}^n}{\partial S_{w_{i,j,k}}^n}$ equals

$$\frac{\partial g_{o_{i,j,k}}^n}{\partial S_{w_{i,j,k}}^n} = \left(\frac{p_o^{n+1}-p_o^n}{\Delta t^{n+1}}\right)\frac{\partial\left(\beta_{op}^*\right)^{n+1}}{\partial S_{w_{i,j,k}}^n} + \frac{\left(\beta_{os}^*\right)^{n+1}}{\Delta t^{n+1}} + \left(-\left(\frac{S_w^{n+1}-S_w^n}{\Delta t^{n+1}}\right) - \left(\frac{S_g^{n+1}-S_g^n}{\Delta t^{n+1}}\right)\right)\frac{\partial(\beta_{os}^*)^{n+1}}{\partial S_{w_{i,j,k}}^n},$$

in which derivative $\frac{\partial\left(\beta_{op}^*\right)^{n+1}}{\partial S_{w_{i,j,k}}^n}$ equals

$$\frac{\partial\left(\beta_{op}^*\right)^{n+1}}{\partial S_{w_{i,j,k}}^n} = -V_{gb}\left(\left(\frac{1}{B_o}\right)^n\phi^{'} + \phi^{n+1}\left(\frac{1}{B_o}\right)^{'}\right), \tag{C.58}$$

and derivative $\frac{\partial(\beta_{os}^*)^{n+1}}{\partial S_{w_{i,j,k}}^n}$ is zero, i.e.

$$\begin{aligned}\frac{\partial(\beta_{os}^*)^{n+1}}{\partial S_{w_{i,j,k}}^n} &= V_{gb}\frac{\partial\left(\phi^{n+1}\left(\frac{1}{B_o}\right)^{n+1}\right)}{\partial S_{w_{i,j,k}}^n} \\ &= 0. \end{aligned} \tag{C.59}$$

Derivatives with respect to the gas saturation $\frac{\partial g_{o_{i-1,j,k}}^n}{\partial S_{g_{i,j,k}}^n}$

Again all derivatives $\frac{\partial g_{o_{i\pm1,j\pm1,k\pm1}}^n}{\partial S_{g_{i,j,k}}^n}$ are zero, i.e.

$$\begin{aligned}\frac{\partial g_{o_{i,j,k-1}}^n}{\partial S_{g_{i,j,k}}^n} &= 0,\ \frac{\partial g_{o_{i,j-1,k}}^n}{\partial S_{g_{i,j,k}}^n} = 0,\ \frac{\partial g_{o_{i-1,j,k}}^n}{\partial S_{g_{i,j,k}}^n} = 0, \\ \frac{\partial g_{o_{i+1,j,k}}^n}{\partial S_{g_{i,j,k}}^n} &= 0,\ \frac{\partial g_{o_{i,j+1,k}}^n}{\partial S_{g_{i,j,k}}^n} = 0,\ \frac{\partial g_{o_{i,j,k+1}}^n}{\partial S_{g_{i,j,k}}^n} = 0. \end{aligned} \tag{C.60}$$

Derivative $\frac{\partial g^n_{o_{i,j,k}}}{\partial S^n_{g_{i,j,k}}}$ equals

$$\begin{aligned}\frac{\partial g^n_{o_{i,j,k}}}{\partial S^n_{g_{i,j,k}}} &= \left(\frac{p_o^{n+1}-p_o^n}{\Delta t^{n+1}}\right)\frac{\partial\left(\beta^*_{op}\right)^{n+1}}{\partial S^n_{g_{i,j,k}}} + \frac{\left(\beta^*_{os}\right)^{n+1}}{\Delta t^{n+1}} \\ &\quad + \left(-\left(\frac{S_w^{n+1}-S_w^n}{\Delta t^{n+1}}\right) - \left(\frac{S_g^{n+1}-S_g^n}{\Delta t^{n+1}}\right)\right)\frac{\partial(\beta^*_{os})^{n+1}}{\partial S^n_{g_{i,j,k}}} \end{aligned} \tag{C.61}$$

In eq. C.61 the derivative $\frac{\partial\left(\beta^*_{op}\right)^{n+1}}{\partial S^n_{g_{i,j,k}}}$ is

$$\frac{\partial\left(\beta^*_{op}\right)^{n+1}}{\partial S^n_{g_{i,j,k}}} = -V_{gb}\left(\left(\frac{1}{B_o}\right)^n \phi^{'} + \phi^{n+1}\left(\frac{1}{B_o}\right)^{'}\right). \tag{C.62}$$

The derivative $\frac{\partial(\beta^*_{os})^{n+1}}{\partial S^n_{g_{i,j,k}}}$ is zero

$$\begin{aligned}\frac{\partial(\beta^*_{os})^{n+1}}{\partial S^n_{g_{i,j,k}}} &= V_{gb}\frac{\partial\left(\phi^{n+1}\left(\frac{1}{B_o}\right)^{n+1}\right)}{\partial S^n_{g_{i,j,k}}} \\ &= 0. \end{aligned} \tag{C.63}$$

C.2.2 The water equation

For grid block $i-1, j, k$ the discrete water equation is, using notation similar to that in eqs. C.1 & C.2,

$$\begin{aligned} g^n_{w_{i-1,j,k}} &= -\left[\begin{array}{c} T_{w1}\left(p_{o_{i,j,k}} - p_{o_{i-1,j,k}}\right) + T_{w1}\left(p_{o_{i-2,j,k}} - p_{o_{i-1,j,k}}\right) \\ +T_{w1}\left(p_{o_{i-1,j+1,k}} - p_{o_{i-1,j,k}}\right) + T_{w1}\left(p_{o_{i-1,j-1,k}} - p_{o_{i-1,j,k}}\right) \\ +T_{w1}\left(p_{o_{i-1,j,k+1}} - p_{o_{i-1,j,k}}\right) + T_{w1}\left(p_{o_{i-1,j,k-1}} - p_{o_{i-1,j,k}}\right) \end{array}\right]^{n+1} \\ &\quad + \left[\begin{array}{c} T_{w2}\left(S_{w_{i,j,k}} - S_{w_{i-1,j,k}}\right) + T_{w2}\left(S_{w_{i-2,j,k}} - S_{w_{i-1,j,k}}\right) \\ +T_{w2}\left(S_{w_{i-1,j+1,k}} - S_{w_{i-1,j,k}}\right) + T_{w2}\left(S_{w_{i-1,j-1,k}} - S_{w_{i-1,j,k}}\right) \\ +T_{w2}\left(S_{w_{i-1,j,k+1}} - S_{w_{i-1,j,k}}\right) + T_{w2}\left(S_{w_{i-1,j,k-1}} - S_{w_{i-1,j,k}}\right) \end{array}\right]^{n+1} \\ &\quad + \left[\begin{array}{c} T_{w3}\left(S_{g_{i,j,k}} - S_{g_{i-1,j,k}}\right) + T_{w3}\left(S_{g_{i-2,j,k}} - S_{g_{i-1,j,k}}\right) \\ +T_{w3}\left(S_{g_{i-1,j+1,k}} - S_{g_{i-1,j,k}}\right) + T_{w3}\left(S_{g_{i-1,j-1,k}} - S_{g_{i-1,j,k}}\right) \\ +T_{w3}\left(S_{g_{i-1,j,k+1}} - S_{g_{i-1,j,k}}\right) + T_{w3}\left(S_{g_{i-1,j,k-1}} - S_{g_{i-1,j,k}}\right) \end{array}\right]^{n+1} \\ &\quad + \left[\begin{array}{c} T_{w4}\left(h_{i,j,k} - h_{i-1,j,k}\right) + T_{w4}\left(h_{i-2,j,k} - h_{i-1,j,k}\right) \\ +T_{w4}\left(h_{i-1,j+1,k} - h_{i-1,j,k}\right) + T_{w4}\left(h_{i-1,j-1,k} - h_{i-1,j,k}\right) \\ +T_{w4}\left(h_{i-1,j,k+1} - h_{i-1,j,k}\right) + T_{w4}\left(h_{i-1,j,k-1} - h_{i-1,j,k}\right) \end{array}\right]^{n+1} \\ &\quad + \left(\beta^*_{wp}\right)^{n+1}_{i-1,j,k}\left(\frac{p_o^{n+1}-p_o^n}{\Delta t^{n+1}}\right)_{i-1,j,k} + \left(\beta^*_{ws}\right)^{n+1}_{i-1,j,k}\left(\frac{S_w^{n+1}-S_w^n}{\Delta t^{n+1}}\right)_{i-1,j,k} \\ &\quad - \left(q^*_w\right)^{n+1}_{i-1,j,k}. \end{aligned} \tag{C.64}$$

Derivatives with respect to the oil pressure $\frac{\partial g^n_{w_{i-1,j,k}}}{\partial p^n_{o_{i,j,k}}}$

Again all derivatives $\frac{\partial g^n_{w_{i\pm1,j\pm1,k\pm1}}}{\partial p^n_{o_{i,j,k}}}$ are zero

$$\begin{aligned}\frac{\partial g^n_{w_{i,j,k-1}}}{\partial p^n_{o_{i,j,k}}} &= 0,\ \frac{\partial g^n_{w_{i,j-1,k}}}{\partial p^n_{o_{i,j,k}}} = 0,\ \frac{\partial g^n_{w_{i-1,j,k}}}{\partial p^n_{o_{i,j,k}}} = 0,\\ \frac{\partial g^n_{w_{i+1,j,k}}}{\partial p^n_{o_{i,j,k}}} &= 0,\ \frac{\partial g^n_{w_{i,j+1,k}}}{\partial p^n_{o_{i,j,k}}} = 0,\ \frac{\partial g^n_{w_{i,j,k+1}}}{\partial p^n_{o_{i,j,k}}} = 0.\end{aligned} \tag{C.65}$$

Derivative $\frac{\partial g^n_{w_{i,j,k}}}{\partial p^n_{o_{i,j,k}}}$ equals

$$\begin{aligned}\frac{\partial g^n_{w_{i,j,k}}}{\partial p^n_{o_{i,j,k}}} &= \frac{\partial\left(+\left(\beta^*_{wp}\right)^{n+1}_{i,j,k}\left(\frac{p^{n+1}_o-p^n_o}{\Delta t^{n+1}}\right)_{i,j,k}+(\beta^*_{ws})^{n+1}_{i,j,k}\left(\frac{S^{n+1}_w-S^n_w}{\Delta t^{n+1}}\right)_{i,j,k}-(q^*_w)^{n+1}_{i,j,k}\right)}{\partial p^n_{o_{i,j,k}}}\\ &= -\frac{\left(\beta^*_{wp}\right)^{n+1}_{i,j,k}}{\Delta t^{n+1}}+\left(\frac{p^{n+1}_o-p^n_o}{\Delta t^{n+1}}\right)_{i,j,k}\frac{\partial\left(\beta^*_{wp}\right)^{n+1}_{i,j,k}}{\partial p^n_{o_{i,j,k}}}+\left(\frac{S^{n+1}_w-S^n_w}{\Delta t^{n+1}}\right)_{i,j,k}\frac{\partial(\beta^*_{ws})^{n+1}_{i,j,k}}{\partial p^n_{o_{i,j,k}}}.\end{aligned} \tag{C.66}$$

In eq. C.66 the derivative $\frac{\partial\left(\beta^*_{wp}\right)^{n+1}}{\partial p^n_{o_{i,j,k}}}$ is

$$\frac{\partial\left(\beta^*_{wp}\right)^{n+1}}{\partial p^n_{o_{i,j,k}}} = V_{gb}\left[S^n_w\left(\left(\frac{1}{B_w}\right)^n\frac{\partial\phi'}{\partial p^n_{o_{i,j,k}}}+\phi'\frac{\partial\left(\frac{1}{B_w}\right)^n}{\partial p^n_{o_{i,j,k}}}\right)+\phi^{n+1}S^n_w\frac{\partial\left(\frac{1}{B_w}\right)'}{\partial p^n_{o_{i,j,k}}}\right]. \tag{C.67}$$

In eq. C.66 the derivative $\frac{\partial(\beta^*_{ws})^{n+1}}{\partial p^n_{o_{i,j,k}}}$ equals

$$\frac{\partial(\beta^*_{ws})^{n+1}}{\partial p^n_{o_{i,j,k}}} = -V_{gb}\phi^{n+1}S^n_w p'_{cow}\frac{\partial\left(\frac{1}{B_w}\right)'}{\partial p^n_{o_{i,j,k}}}. \tag{C.68}$$

Derivatives with respect to the water saturation $\frac{\partial g^n_{w_{i-1,j,k}}}{\partial S^n_{w_{i,j,k}}}$

All derivatives $\frac{\partial g^n_{w_{i\pm1,j\pm1,k\pm1}}}{\partial S^n_{w_{i,j,k}}}$ are zero

$$\begin{aligned}\frac{\partial g^n_{w_{i,j,k-1}}}{\partial S^n_{w_{i,j,k}}} &= 0,\ \frac{\partial g^n_{w_{i,j-1,k}}}{\partial S^n_{w_{i,j,k}}} = 0,\ \frac{\partial g^n_{w_{i-1,j,k}}}{\partial S^n_{w_{i,j,k}}} = 0,\\ \frac{\partial g^n_{w_{i+1,j,k}}}{\partial S^n_{w_{i,j,k}}} &= 0,\ \frac{\partial g^n_{w_{i,j+1,k}}}{\partial S^n_{w_{i,j,k}}} = 0,\ \frac{\partial g^n_{w_{i,j,k+1}}}{\partial S^n_{w_{i,j,k}}} = 0.\end{aligned} \tag{C.69}$$

Derivative $\frac{\partial g^n_{w_{i,j,k}}}{\partial S^n_{w_{i,j,k}}}$ equals

$$\frac{\partial g^n_{w_{i,j,k}}}{\partial S^n_{w_{i,j,k}}} = \left(\frac{p_o^{n+1}-p_o^n}{\Delta t^{n+1}}\right)_{i,j,k} \frac{\partial\left(\beta^*_{wp}\right)^{n+1}_{i,j,k}}{\partial S^n_{w_{i,j,k}}} - \frac{(\beta^*_{ws})^{n+1}_{i,j,k}}{\Delta t^{n+1}} + \left(\frac{S_w^{n+1}-S_w^n}{\Delta t^{n+1}}\right)_{i,j,k} \frac{\partial(\beta^*_{ws})^{n+1}_{i,j,k}}{\partial S^n_{w_{i,j,k}}}. \quad \text{(C.70)}$$

In eq. C.70 the derivative $\frac{\partial\left(\beta^*_{wp}\right)^{n+1}}{\partial S^n_{w_{i,j,k}}}$ is

$$\frac{\partial\left(\beta^*_{wp}\right)^{n+1}}{\partial S^n_{w_{i,j,k}}} = V_{gb}\left[\left(\frac{1}{B_w}\right)^n \phi^{'} + \phi^{n+1}\left(\frac{1}{B_w}\right)^{'}\right], \quad \text{(C.71)}$$

and the derivative $\frac{\partial(\beta^*_{ws})^{n+1}}{\partial S^n_{w_{i,j,k}}}$ is equal to

$$\frac{\partial(\beta^*_{ws})^{n+1}}{\partial S^n_{w_{i,j,k}}} = -V_{gb}\phi^{n+1}\left(\frac{1}{B_w}\right)^{'}\left(p'_{cow} + S^n_w \frac{\partial p'_{cow}}{\partial S^n_{w_{i,j,k}}}\right). \quad \text{(C.72)}$$

Derivatives with respect to the gas saturation $\frac{\partial g^n_{w_{i-1,j,k}}}{\partial S^n_{g_{i,j,k}}}$

The derivatives $\frac{\partial g^n_{w_{i\pm1,j\pm1,k\pm1}}}{\partial S^n_{g_{i,j,k}}}$ are zero, i.e.

$$\begin{aligned}
\frac{\partial g^n_{w_{i,j,k-1}}}{\partial S^n_{g_{i,j,k}}} &= 0,\ \frac{\partial g^n_{w_{i,j-1,k}}}{\partial S^n_{g_{i,j,k}}} = 0,\ \frac{\partial g^n_{w_{i-1,j,k}}}{\partial S^n_{g_{i,j,k}}} = 0, \\
\frac{\partial g^n_{w_{i+1,j,k}}}{\partial S^n_{g_{i,j,k}}} &= 0,\ \frac{\partial g^n_{w_{i,j+1,k}}}{\partial S^n_{g_{i,j,k}}} = 0,\ \frac{\partial g^n_{w_{i,j,k+1}}}{\partial S^n_{g_{i,j,k}}} = 0.
\end{aligned} \quad \text{(C.73)}$$

Derivative $\frac{\partial g^n_{w_{i,j,k}}}{\partial S^n_{g_{i,j,k}}}$ equals

$$\frac{\partial g^n_{w_{i,j,k}}}{\partial S^n_{g_{i,j,k}}} = \left(\frac{p_o^{n+1}-p_o^n}{\Delta t^{n+1}}\right)_{i,j,k} \frac{\partial\left(\beta^*_{wp}\right)^{n+1}_{i,j,k}}{\partial S^n_{g_{i,j,k}}} + \left(\frac{S_w^{n+1}-S_w^n}{\Delta t^{n+1}}\right)_{i,j,k} \frac{\partial(\beta^*_{ws})^{n+1}_{i,j,k}}{\partial S^n_{g_{i,j,k}}} \quad \text{(C.74)}$$

In eq. C.74 the derivatives $\frac{\partial\left(\beta^*_{wp}\right)^{n+1}}{\partial S^n_{g_{i,j,k}}}$ and $\frac{\partial(\beta^*_{ws})^{n+1}}{\partial S^n_{g_{i,j,k}}}$ are zero

$$\begin{aligned}
\frac{\partial\left(\beta^*_{wp}\right)^{n+1}}{\partial S^n_{g_{i,j,k}}} &= V_{gb}\frac{\partial\left(\left(\frac{1}{B_w}\right)^n S_w^n \phi^{'} + \phi^{n+1} S_w^n \left(\frac{1}{B_w}\right)^{'}\right)}{\partial S^n_{g_{i,j,k}}} \\
&= 0,
\end{aligned} \quad \text{(C.75)}$$

and

$$\begin{aligned}
\frac{\partial(\beta^*_{ws})^{n+1}}{\partial S^n_{g_{i,j,k}}} &= V_{gb}\frac{\partial\left(\phi^{n+1}\left(\frac{1}{B_w}\right)^{n+1} - \phi^{n+1} S_w^n \left(\frac{1}{B_w}\right)^{'} p'_{cow}\right)}{\partial S^n_{g_{i,j,k}}} \\
&= 0.
\end{aligned} \quad \text{(C.76)}$$

C.2.3 The gas equation

For grid block $i-1,j,k$ the discrete gas equation is, using notation similar to that in eqs. C.1 & C.2,

$$\begin{aligned}
g^n_{g_{i-1,j,k}} \;=\; & -\left[\begin{array}{c} T_{g1}\left(p_{o_{i,j,k}}-p_{o_{i-1,j,k}}\right)+T_{g1}\left(p_{o_{i-2,j,k}}-p_{o_{i-1,j,k}}\right) \\ +T_{g1}\left(p_{o_{i-1,j+1,k}}-p_{o_{i-1,j,k}}\right)+T_{g1}\left(p_{o_{i-1,j-1,k}}-p_{o_{i-1,j,k}}\right) \\ +T_{g1}\left(p_{o_{i-1,j,k+1}}-p_{o_{i-1,j,k}}\right)+T_{g1}\left(p_{o_{i-1,j,k-1}}-p_{o_{i-1,j,k}}\right)\end{array}\right]^{n+1} \\
& -\left[\begin{array}{c} T_{g2}\left(S_{w_{i,j,k}}-S_{w_{i-1,j,k}}\right)+T_{g2}\left(S_{w_{i-2,j,k}}-S_{w_{i-1,j,k}}\right) \\ +T_{g2}\left(S_{w_{i-1,j+1,k}}-S_{w_{i-1,j,k}}\right)+T_{g2}\left(S_{w_{i-1,j-1,k}}-S_{w_{i-1,j,k}}\right) \\ +T_{g2}\left(S_{w_{i-1,j,k+1}}-S_{w_{i-1,j,k}}\right)+T_{g2}\left(S_{w_{i-1,j,k-1}}-S_{w_{i-1,j,k}}\right)\end{array}\right]^{n+1} \\
& -\left[\begin{array}{c} T_{g3}\left(S_{g_{i,j,k}}-S_{g_{i-1,j,k}}\right)+T_{g3}\left(S_{g_{i-2,j,k}}-S_{g_{i-1,j,k}}\right) \\ +T_{g3}\left(S_{g_{i-1,j+1,k}}-S_{g_{i-1,j,k}}\right)+T_{g3}\left(S_{g_{i-1,j-1,k}}-S_{g_{i-1,j,k}}\right) \\ +T_{g3}\left(S_{g_{i-1,j,k+1}}-S_{g_{i-1,j,k}}\right)+T_{g3}\left(S_{g_{i-1,j,k-1}}-S_{g_{i-1,j,k}}\right)\end{array}\right]^{n+1} \\
& +\left[\begin{array}{c} T_{g4}\left(h_{i,j,k}-h_{i-1,j,k}\right)+T_{g4}\left(h_{i-2,j,k}-h_{i-1,j,k}\right) \\ +T_{g4}\left(h_{i-1,j+1,k}-h_{i-1,j,k}\right)+T_{g4}\left(h_{i-1,j-1,k}-h_{i-1,j,k}\right) \\ +T_{g4}\left(h_{i-1,j,k+1}-h_{i-1,j,k}\right)+T_{g4}\left(h_{i-1,j,k-1}-h_{i-1,j,k}\right)\end{array}\right]^{n+1} \\
& +\left(\beta^*_{gp}\right)^{n+1}_{i-1,j,k}\left(\tfrac{p_o^{n+1}-p_o^n}{\Delta t^{n+1}}\right)_{i-1,j,k}-\left(\beta^*_{gsw}\right)^{n+1}_{i-1,j,k}\left(\tfrac{S_w^{n+1}-S_w^n}{\Delta t^{n+1}}\right)_{i-1,j,k} \\
& +\left(\beta^*_{gsg}\right)^{n+1}_{i-1,j,k}\left(\tfrac{S_g^{n+1}-S_g^n}{\Delta t^{n+1}}\right)_{i-1,j,k}-\left(q^*_g\right)^{n+1}_{i-1,j,k}. \qquad \text{(C.77)}
\end{aligned}$$

Derivatives with respect to the oil pressure $\frac{\partial g^n_{g_{i-1,j,k}}}{\partial p^n_{o_{i,j,k}}}$

Just as for the oil and water equations the derivatives $\frac{\partial g^n_{g_{i\pm1,j\pm1,k\pm1}}}{\partial p^n_{o_{i,j,k}}}$ are zero

$$\begin{aligned}
\tfrac{\partial g^n_{g_{i,j,k-1}}}{\partial p^n_{o_{i,j,k}}} &= 0,\ \tfrac{\partial g^n_{g_{i,j-1,k}}}{\partial p^n_{o_{i,j,k}}}=0,\ \tfrac{\partial g^n_{g_{i-1,j,k}}}{\partial p^n_{o_{i,j,k}}}=0, \\
\tfrac{\partial g^n_{g_{i+1,j,k}}}{\partial p^n_{o_{i,j,k}}} &= 0,\ \tfrac{\partial g^n_{g_{i,j+1,k}}}{\partial p^n_{o_{i,j,k}}}=0,\ \tfrac{\partial g^n_{g_{i,j,k+1}}}{\partial p^n_{o_{i,j,k}}}=0. \qquad \text{(C.78)}
\end{aligned}$$

Derivative $\frac{\partial g^n_{g_{i,j,k}}}{\partial p^n_{o_{i,j,k}}}$ equals

$$\begin{aligned}
\tfrac{\partial g^n_{g_{i,j,k}}}{\partial p^n_{o_{i,j,k}}} \;=\; & -\frac{\left(\beta^*_{gp}\right)^{n+1}}{\Delta t^{n+1}}+\left(\tfrac{p_o^{n+1}-p_o^n}{\Delta t^{n+1}}\right)\tfrac{\partial\left(\beta^*_{gp}\right)^{n+1}}{\partial p^n_{o_{i,j,k}}} \\
& -\left(\tfrac{S_w^{n+1}-S_w^n}{\Delta t^{n+1}}\right)\tfrac{\partial\left(\beta^*_{gsw}\right)^{n+1}}{\partial p^n_{o_{i,j,k}}}+\left(\tfrac{S_g^{n+1}-S_g^n}{\Delta t^{n+1}}\right)\tfrac{\partial\left(\beta^*_{gsg}\right)^{n+1}}{\partial p^n_{o_{i,j,k}}} \qquad \text{(C.79)}
\end{aligned}$$

In eq. C.79 the derivative $\frac{\partial\left(\beta^*_{gp}\right)^{n+1}}{\partial p^n_{o_{i,j,k}}}$ equals

$$\frac{\partial\left(\beta^*_{gp}\right)^{n+1}}{\partial p^n_{o_{i,j,k}}} = V_{gb}\left[\begin{array}{c}\left(\frac{1}{B_o}\phi S_o\right)^n \frac{\partial\left(R'_s\right)}{\partial p^n_{o_{i,j,k}}} + R'_s S^n_o\left(\left(\frac{1}{B_o}\right)^n \frac{\partial\phi^n}{\partial p^n_{o_{i,j,k}}} + \phi^n \frac{\partial\left(\frac{1}{B_o}\right)^n}{\partial p^n_{o_{i,j,k}}}\right) \\ +\phi^{'}\left(S^n_g \frac{\partial\left(\frac{1}{B_g}\right)^n}{\partial p^n_{o_{i,j,k}}} + R^{n+1}_s S^n_o \frac{\partial\left(\left(\frac{1}{B_o}\right)^n\right)}{\partial p^n_{o_{i,j,k}}}\right) \\ +\left(\left(\frac{1}{B_g}\right)^n S^n_g + R^{n+1}_s\left(\frac{S_o}{B_o}\right)^n\right)\frac{\partial\phi^{'}}{\partial p^n_{o_{i,j,k}}} \\ +\phi^{n+1}\left(R^{n+1}_s S^n_o \frac{\partial\left(\frac{1}{B_o}\right)^{'}}{\partial p^n_{o_{i,j,k}}} + S^n_g \frac{\partial\left(\frac{1}{B_g}\right)^{'}}{\partial p^n_{o_{i,j,k}}}\right)\end{array}\right]. \tag{C.80}$$

Because

$$\frac{\partial p^n_g}{\partial p^n_{o_{i,j,k}}} = \frac{\partial\left(p^n_o + p^n_{cog}\right)}{\partial p^n_{o_{i,j,k}}} = \frac{\partial\left(p^n_o\right)}{\partial p^n_{o_{i,j,k}}} = 1,$$

derivative $\frac{\partial\left(\frac{1}{B_g}\right)^n}{\partial p^n_{o_{i,j,k}}}$ becomes

$$\frac{\partial\left(\frac{1}{B_g}\right)^n}{\partial p^n_{o_{i,j,k}}} = \frac{\partial\left(\frac{1}{B_g}\right)^n}{\partial p^n_{g_{i,j,k}}}\frac{\partial p^n_g}{\partial p^n_{o_{i,j,k}}} = a^n_g.$$

In eq. C.79 the derivative $\frac{\partial\left(\beta^*_{gsw}\right)^{n+1}}{\partial p^n_{o_{i,j,k}}}$ is zero

$$\begin{aligned}\frac{\partial\left(\beta^*_{gsw}\right)^{n+1}}{\partial p^n_{o_{i,j,k}}} &= V_{gb}\frac{\partial\left(R^{n+1}_s \phi^{n+1}\left(\frac{1}{B_o}\right)^{n+1}\right)}{\partial p^n_{o_{i,j,k}}} \\ &= 0,\end{aligned} \tag{C.81}$$

and derivative $\frac{\partial\left(\beta^*_{gsg}\right)^{n+1}}{\partial p^n_{o_{i,j,k}}}$ is equal to

$$\frac{\partial\left(\beta^*_{gsg}\right)^{n+1}}{\partial p^n_{o_{i,j,k}}} = V_{gb}\phi^{n+1} S^n_g p'_{cgo}\frac{\partial\left(\frac{1}{B_g}\right)^{'}}{\partial p^n_{o_{i,j,k}}}. \tag{C.82}$$

Derivatives with respect to the water saturation $\frac{\partial g^n_{g_{i-1,j,k}}}{\partial S^n_{w_{i,j,k}}}$

The derivatives $\frac{\partial g^n_{g_{i\pm1,j\pm1,k\pm1}}}{\partial S^n_{w_{i,j,k}}}$ are again zero

$$\begin{aligned}\frac{\partial g^n_{g_{i,j,k-1}}}{\partial S^n_{w_{i,j,k}}} &= 0,\ \frac{\partial g^n_{g_{i,j-1,k}}}{\partial S^n_{w_{i,j,k}}} = 0,\ \frac{\partial g^n_{g_{i-1,j,k}}}{\partial S^n_{w_{i,j,k}}} = 0,\\ \frac{\partial g^n_{g_{i+1,j,k}}}{\partial S^n_{w_{i,j,k}}} &= 0,\ \frac{\partial g^n_{g_{i,j+1,k}}}{\partial S^n_{w_{i,j,k}}} = 0,\ \frac{\partial g^n_{g_{i,j,k+1}}}{\partial S^n_{w_{i,j,k}}} = 0.\end{aligned} \tag{C.83}$$

Derivative $\frac{\partial g^n_{g_{i,j,k}}}{\partial S^n_{w_{i,j,k}}}$ equals

$$\begin{aligned}\frac{\partial g^n_{g_{i,j,k}}}{\partial S^n_{w_{i,j,k}}} &= \left(\frac{p_o^{n+1}-p_o^n}{\Delta t^{n+1}}\right)\frac{\partial\left(\beta^*_{gp}\right)^{n+1}}{\partial S^n_{w_{i,j,k}}} + \frac{\left(\beta^*_{gsw}\right)^{n+1}}{\Delta t^{n+1}}\\ &\quad - \left(\frac{S_w^{n+1}-S_w^n}{\Delta t^{n+1}}\right)\frac{\partial\left(\beta^*_{gsw}\right)^{n+1}}{\partial S^n_{w_{i,j,k}}} + \left(\frac{S_g^{n+1}-S_g^n}{\Delta t^{n+1}}\right)\frac{\partial\left(\beta^*_{gsg}\right)^{n+1}}{\partial S^n_{w_{i,j,k}}}.\end{aligned} \tag{C.84}$$

In eq. C.84 the derivative $\frac{\partial\left(\beta^*_{gp}\right)^{n+1}}{\partial S^n_{w_{i,j,k}}}$ is equal to

$$\frac{\partial\left(\beta^*_{gp}\right)^{n+1}}{\partial S^n_{w_{i,j,k}}} = V_{gb}\left[-\left(\frac{1}{B_o}\phi\right)^n R_s' - R_s^{n+1}\left(\frac{1}{B_o}\right)^n\phi' - \phi^{n+1}R_s^{n+1}\left(\frac{1}{B_o}\right)'\right] \tag{C.85}$$

The derivatives $\frac{\partial\left(\beta^*_{gsw}\right)^{n+1}}{\partial S^n_{w_{i,j,k}}}$ and $\frac{\partial\left(\beta^*_{gsg}\right)^{n+1}}{\partial S^n_{w_{i,j,k}}}$ are zero, i.e.

$$\begin{aligned}\frac{\partial\left(\beta^*_{gsw}\right)^{n+1}}{\partial S^n_{w_{i,j,k}}} &= V_{gb}\frac{\partial\left(R_s^{n+1}\phi^{n+1}\left(\frac{1}{B_o}\right)^{n+1}\right)}{\partial S^n_{w_{i,j,k}}}\\ &= 0,\end{aligned} \tag{C.86}$$

and

$$\begin{aligned}\frac{\partial\left(\beta^*_{gsg}\right)^{n+1}}{\partial S^n_{w_{i,j,k}}} &= V_{gb}\frac{\partial\left(\phi^{n+1}\left(\frac{1}{B_g}\right)^{n+1}+\phi^{n+1}S_g^n\left(\frac{1}{B_g}\right)'p'_{cgo}-R_s^{n+1}\phi^{n+1}\left(\frac{1}{B_o}\right)^{n+1}\right)}{\partial S^n_{w_{i,j,k}}}\\ &= 0.\end{aligned} \tag{C.87}$$

Derivatives with respect to the gas saturation $\frac{\partial g^n_{g_{i-1,j,k}}}{\partial S^n_{g_{i,j,k}}}$

The derivatives $\frac{\partial g^n_{g_{i\pm1,j\pm1,k\pm1}}}{\partial S^n_{g_{i,j,k}}}$ are again zero

$$\begin{aligned}\frac{\partial g^n_{g_{i,j,k-1}}}{\partial S^n_{g_{i,j,k}}} &= 0,\ \frac{\partial g^n_{g_{i,j-1,k}}}{\partial S^n_{g_{i,j,k}}} = 0,\ \frac{\partial g^n_{g_{i-1,j,k}}}{\partial S^n_{g_{i,j,k}}} = 0,\\ \frac{\partial g^n_{g_{i+1,j,k}}}{\partial S^n_{g_{i,j,k}}} &= 0,\ \frac{\partial g^n_{g_{i,j+1,k}}}{\partial S^n_{g_{i,j,k}}} = 0,\ \frac{\partial g^n_{g_{i,j,k+1}}}{\partial S^n_{g_{i,j,k}}} = 0.\end{aligned} \tag{C.88}$$

Derivative $\frac{\partial g^n_{g_{i,j,k}}}{\partial S^n_{g_{i,j,k}}}$ equals

$$\begin{aligned}\frac{\partial g^n_{g_{i,j,k}}}{\partial S^n_{g_{i,j,k}}} &= +\left(\frac{p_o^{n+1}-p_o^n}{\Delta t^{n+1}}\right)\frac{\partial\left(\beta^*_{gp}\right)^{n+1}}{\partial S^n_{g_{i,j,k}}} - \left(\frac{S_w^{n+1}-S_w^n}{\Delta t^{n+1}}\right)\frac{\partial\left(\beta^*_{gsw}\right)^{n+1}}{\partial S^n_{g_{i,j,k}}} \\ &\quad -\frac{\left(\beta^*_{gsg}\right)^{n+1}}{\Delta t^{n+1}} + \left(\frac{S_g^{n+1}-S_g^n}{\Delta t^{n+1}}\right)\frac{\partial\left(\beta^*_{gsg}\right)^{n+1}}{\partial S^n_{g_{i,j,k}}}. \end{aligned} \tag{C.89}$$

In eq. C.89 the derivative $\frac{\partial\left(\beta^*_{gp}\right)^{n+1}}{\partial S^n_{g_{i,j,k}}}$ is equal to

$$\frac{\partial\left(\beta^*_{gp}\right)^{n+1}}{\partial S^n_{g_{i,j,k}}} = V_{gb}\left[\begin{array}{c} -\left(\frac{1}{B_o}\phi\right)^n R_s' + \phi^{'}\left(\left(\frac{1}{B_g}\right)^n - R_s^{n+1}\left(\frac{1}{B_o}\right)^n\right) \\ +\phi^{n+1}\left(-R_s^{n+1}\left(\frac{1}{B_o}\right)' + \left(\frac{1}{B_g}\right)'\right) \end{array}\right]. \tag{C.90}$$

The derivative $\frac{\partial\left(\beta^*_{gsw}\right)^{n+1}}{\partial S^n_{g_{i,j,k}}}$ is zero

$$\begin{aligned}\frac{\partial\left(\beta^*_{gsw}\right)^{n+1}}{\partial S^n_{g_{i,j,k}}} &= V_{gb}\frac{\partial\left(R_s^{n+1}\phi^{n+1}\left(\frac{1}{B_o}\right)^{n+1}\right)}{\partial S^n_{g_{i,j,k}}} \\ &= 0, \end{aligned} \tag{C.91}$$

and the derivative $\frac{\partial\left(\beta^*_{gsg}\right)^{n+1}}{\partial S^n_{g_{i,j,k}}}$ is equal to

$$\frac{\partial\left(\beta^*_{gsg}\right)^{n+1}}{\partial S^n_{g_{i,j,k}}} = V_{gb}\phi^{n+1}\left(\frac{1}{B_g}\right)'\left(S_g^n\frac{\partial p'_{cgo}}{\partial S^n_{g_{i,j,k}}} + p'_{cgo}\right). \tag{C.92}$$

C.3 Transmissibility and well model derivatives

C.3.1 The oil equation

Derivatives with respect to the oil pressure

Derivatives like $\frac{\partial {T_{o1}}_{i+\frac{1}{2},j,k}}{\partial p^n_{o_{i,j,k}}}$ are

$$\frac{\partial {T_{o1}}_{i+\frac{1}{2},j,k}}{\partial p^n_{o_{i,j,k}}} = \frac{\Delta y_{i,j,k}\Delta z_{i,j,k}}{\Delta x_{i+\frac{1}{2},j,k}}\frac{\partial {\lambda_o}_{i+\frac{1}{2},j,k}}{\partial p^n_{o_{i,j,k}}}, \tag{C.93}$$

where

$$\frac{\partial \lambda_{o_{i+\frac{1}{2},j,k}}}{\partial p^n_{o_{i,j,k}}} = k_{i+\frac{1}{2},j,k} k_{ro_{i+\frac{1}{2},j,k}} \left(\frac{1}{\mu_{o_{i+\frac{1}{2},j,k}}} \frac{\partial \left(\frac{1}{B_o}\right)_{i+\frac{1}{2},j,k}}{\partial p^n_{o_{i,j,k}}} + \frac{1}{B_{o_{i+\frac{1}{2},j,k}}} \frac{\partial \left(\frac{1}{\mu_o}\right)_{i+\frac{1}{2},j,k}}{\partial p^n_{o_{i,j,k}}} \right).$$

Derivatives $\frac{\partial T_{o1}{}_{i\pm\frac{1}{2},j\pm\frac{1}{2},k\pm\frac{1}{2}}}{\partial p^n_{o_{i,j,k}}}$ are obtained in a similar way.

For terms $T_{o4}{}_{i+\frac{1}{2},j,k}$ the derivative is

$$\frac{\partial T_{o4}{}_{i+\frac{1}{2},j,k}}{\partial p^n_{o_{i,j,k}}} = g \left(\rho_{o_{i+\frac{1}{2},j,k}} \frac{\partial T_{o1}{}_{i+\frac{1}{2},j,k}}{\partial p^n_{o_{i,j,k}}} + \frac{\partial \rho_{o_{i+\frac{1}{2},j,k}}}{\partial p^n_{o_{i,j,k}}} T_{o1}{}_{i+\frac{1}{2},j,k} \right). \tag{C.94}$$

The general equation for the well model derivative is

$$\frac{\partial (q^*_o)^n}{\partial p^n_{o_{i,j,k}}} = \frac{\partial}{\partial p^n_{o_{i,j,k}}} \left(\frac{V_{gb}}{B_o} \left(\alpha_{eff} \frac{k_{ro}}{\mu_o} w \left(p_{wf} - p_{gb_o} \right) \right) \right). \tag{C.95}$$

For an injector this derivative is zero since no oil is injected, hence

$$\left(\frac{\partial (q^*_o)^n}{\partial p^n_{o_{i,j,k}}} \right)_{inj} = 0.$$

For a producer the derivative $\frac{\partial q^*_o}{\partial p^n_{o_{i,j,k}}}$ is equal to

$$\left(\frac{\partial q^*_o}{\partial p^n_{o_{i,j,k}}} \right)_{prod} = \alpha_{eff} V_{gb} w k_{ro} \begin{pmatrix} \frac{1}{\mu_o} \left(p_{wf} - p_{gb_o} \right) \frac{\partial}{\partial p^n_{o_{i,j,k}}} \left(\frac{1}{B_o} \right) \\ + \frac{1}{B_o} \left(p_{wf} - p_{gb_o} \right) \frac{\partial}{\partial p^n_{o_{i,j,k}}} \left(\frac{1}{\mu_o} \right) \\ - \frac{1}{B_o} \frac{1}{\mu_o} \end{pmatrix}. \tag{C.96}$$

Derivatives with respect to the water saturation

Derivative $\frac{\partial T_{o1}{}_{i+\frac{1}{2},j,k}}{\partial S^n_{w_{i,j,k}}}$ equals

$$\frac{\partial T_{o1}{}_{i+\frac{1}{2},j,k}}{\partial S^n_{w_{i,j,k}}} = \frac{\Delta y_{i,j,k} \Delta z_{i,j,k}}{\Delta x_{i+\frac{1}{2},j,k}} \frac{\partial \lambda_{o_{i+\frac{1}{2},j,k}}}{\partial S^n_{w_{i,j,k}}}, \tag{C.97}$$

where

$$\frac{\partial \lambda_{o_{i+\frac{1}{2},j,k}}}{\partial S^n_{w_{i,j,k}}} = \frac{\partial \left(k \frac{k_{ro}}{B_o \mu_o} \right)_{i+\frac{1}{2},j,k}}{\partial S^n_{w_{i,j,k}}} = \left(\frac{k}{B_o \mu_o} \right)_{i+\frac{1}{2},j,k} \frac{\partial (k_{ro})_{i+\frac{1}{2},j,k}}{\partial S^n_{w_{i,j,k}}}. \tag{C.98}$$

For the gravity term the derivative is

$$\frac{\partial T_{o4}{}_{i+\frac{1}{2},j,k}}{\partial S^n_{w_{i,j,k}}} = \rho_{o_{i+\frac{1}{2},j,k}} g \frac{\partial T_{o1}{}_{i+\frac{1}{2},j,k}}{\partial S^n_{w_{i,j,k}}}. \tag{C.99}$$

The general well model derivative is

$$\frac{\partial (q_o^*)^n}{\partial S^n_{w_{i,j,k}}} = \frac{\partial}{\partial S^n_{w_{i,j,k}}} \left(\frac{V_{gb}}{B_o} \left[\alpha_{eff} \frac{k_{ro}}{\mu_o} w \left(p_{wf} - p_{gb_o} \right) \right] \right) \tag{C.100}$$

For an injector this derivative is zero since no oil is injected, i.e.

$$\left(\frac{\partial q_o^*}{\partial S^n_{w_{i,j,k}}} \right)_{inj} = 0. \tag{C.101}$$

For a producer the derivative $\frac{\partial (q_o^*)^n}{\partial S^n_{w_{i,j,k}}}$ is equal to

$$\left(\frac{\partial (q_o^*)^n}{\partial S^n_{w_{i,j,k}}} \right)_{prod} = \alpha_{eff} \frac{V_{gb}}{B_o \mu_o} w \left(p_{wf} - p_{gb_o} \right) \frac{\partial k_{ro}}{\partial S^n_{w_{i,j,k}}}. \tag{C.102}$$

Derivatives with respect to the gas saturation

Derivative $\frac{\partial {T_{o1}}_{i+\frac{1}{2},j,k}}{\partial S^n_{g_{i,j,k}}}$ equals

$$\frac{\partial {T_{o1}}_{i+\frac{1}{2},j,k}}{\partial S^n_{g_{i,j,k}}} = \frac{\Delta y_{i,j,k} \Delta z_{i,j,k}}{\Delta x_{i+\frac{1}{2},j,k}} \frac{\partial {\lambda_o}_{i+\frac{1}{2},j,k}}{\partial S^n_{g_{i,j,k}}}, \tag{C.103}$$

where

$$\frac{\partial {\lambda_o}_{i+\frac{1}{2},j,k}}{\partial S^n_{g_{i,j,k}}} = \left(\frac{k}{B_o \mu_o} \right)_{i+\frac{1}{2},j,k} \frac{\partial {(k_{ro})}_{i+\frac{1}{2},j,k}}{\partial S^n_{g_{i,j,k}}}. \tag{C.104}$$

The derivative $\frac{\partial {T_{o4}}_{i+\frac{1}{2},j,k}}{\partial S^n_{g_{i,j,k}}}$ is

$$\frac{\partial {T_{o4}}_{i+\frac{1}{2},j,k}}{\partial S^n_{g_{i,j,k}}} = {\rho_o}_{i+\frac{1}{2},j,k} g \frac{\partial {T_{o1}}_{i+\frac{1}{2},j,k}}{\partial S^n_{g_{i,j,k}}}. \tag{C.105}$$

The general derivative for the well model is

$$\frac{\partial (q_o^*)^n}{\partial S^n_{g_{i,j,k}}} = \frac{\partial \left(\frac{V_{gb}}{B_o} \left[\alpha_{eff} \frac{k_{ro}}{\mu_o} w (p_{wf} - p_{gb_o}) \right] \right)^n}{\partial S^n_{g_{i,j,k}}} \tag{C.106}$$

For a producer this derivative is zero since no oil is injected, i.e.

$$\left(\frac{\partial q_o^*}{\partial S^n_{g_{i,j,k}}} \right)_{inj} = 0. \tag{C.107}$$

For a producer the derivative is

$$\left(\frac{\partial (q_o^*)^n}{\partial S^n_{g_{i,j,k}}} \right)_{prod} = \alpha_{eff} \frac{V_{gb}}{B_o \mu_o} w \left(p_{wf} - p_{gb_o} \right) \frac{\partial k^n_{ro}}{\partial S^n_{g_{i,j,k}}}. \tag{C.108}$$

C.3.2 The water equation

Derivatives with respect to the oil pressure

For term $T_{w1_{i+\frac{1}{2},j,k}}$ the derivative with respect to $p^n_{o_{i,j,k}}$ equals

$$\frac{\partial T_{w1}{}_{i+\frac{1}{2},j,k}}{\partial p^n_{o_{i,j,k}}} = \frac{\Delta y_{i,j,k}\Delta z_{i,j,k}}{\Delta x_{i+\frac{1}{2},j,k}} \frac{\partial \lambda_{w}{}_{i+\frac{1}{2},j,k}}{\partial p^n_{o_{i,j,k}}}, \tag{C.109}$$

where

$$\frac{\partial \lambda_{w}{}_{i+\frac{1}{2},j,k}}{\partial p^n_{o_{i,j,k}}} = kk_{rw}\left(\frac{1}{B_w} \frac{\partial\left(\frac{1}{\mu_w}\right)}{\partial p^n_{o_{i,j,k}}}{}_{i+\frac{1}{2},j,k} + \frac{1}{\mu_w} \frac{\partial\left(\frac{1}{B_w}\right)}{\partial p^n_{o_{i,j,k}}}{}_{i+\frac{1}{2},j,k} \right). \tag{C.110}$$

For term $T_{w2_{i+\frac{1}{2},j,k}}$ the derivative equals

$$\frac{\partial T_{w2}{}_{i+\frac{1}{2},j,k}}{\partial p^n_{o_{i,j,k}}} = \left(\frac{\partial p_{cow}}{\partial S_w}\right)_{i+\frac{1}{2},j,k} \frac{\partial T_{w1}{}_{i+\frac{1}{2},j,k}}{\partial p^n_{o_{i,j,k}}}. \tag{C.111}$$

Similarly, for term $T_{w3_{i+\frac{1}{2},j,k}}$

$$\frac{\partial T_{w3}{}_{i+\frac{1}{2},j,k}}{\partial p^n_{o_{i,j,k}}} = \left(\frac{\partial p_{cow}}{\partial S_g}\right)_{i+\frac{1}{2},j,k} \frac{\partial T_{w1}{}_{i+\frac{1}{2},j,k}}{\partial p^n_{o_{i,j,k}}}. \tag{C.112}$$

Finally, for term $T_{w4_{i+\frac{1}{2},j,k}}$

$$\frac{\partial T_{w4}{}_{i+\frac{1}{2},j,k}}{\partial p^n_{o_{i,j,k}}} = g\left(\rho_{w}{}_{i+\frac{1}{2},j,k} \frac{\partial T_{w1}{}_{i+\frac{1}{2},j,k}}{\partial p^n_{o_{i,j,k}}} + T_{w1}{}_{i+\frac{1}{2},j,k} \frac{\partial \rho_{w}{}_{i+\frac{1}{2},j,k}}{\partial p^n_{o_{i,j,k}}} \right). \tag{C.113}$$

If water is the injected fluid, the derivative of the water injection rate with respect to the pressure is

$$\begin{aligned} \left(\frac{\partial q^*_w}{\partial p^n_{o_{i,j,k}}}\right)_{inj} &= \frac{\partial q^*_{t_{inj}}}{\partial p^n_{o_{i,j,k}}}, \qquad \text{(C.114)} \\ &= V_{gb}\alpha_{eff}\left(\begin{array}{c} \left\{\lambda_{rt} w\left(p_{wf} - p_{gb_o}\right) + \frac{k_{rw}}{\mu_w} w p_{cow} - \frac{k_{rg}}{\mu_g} w p_{cgo}\right\} \frac{\partial\left(\frac{1}{B_w}\right)}{\partial p^n_{o_{i,j,k}}} \\ +\frac{1}{B_w}\left\{ \begin{array}{c} \lambda_{rt} w \frac{\partial(p_{wf} - p_{gb_o})}{\partial p^n_{o_{i,j,k}}} + w\left(p_{wf} - p_{gb_o}\right) \frac{\partial \lambda_{rt}}{\partial p^n_{o_{i,j,k}}} \\ +k_{rw} w p_{cow} \frac{\partial\left(\frac{1}{\mu_w}\right)}{\partial p^n_{o_{i,j,k}}} - k_{rg} w p_{cgo} \frac{\partial\left(\frac{1}{\mu_g}\right)}{\partial p^n_{o_{i,j,k}}} \end{array} \right\} \end{array} \right), \end{aligned}$$

where

$$\frac{\partial \lambda_{rt}}{\partial p^n_{o_{i,j,k}}} = k_{ro} \frac{\partial\left(\frac{1}{\mu_o}\right)}{\partial p^n_{o_{i,j,k}}} + k_{rw} \frac{\partial\left(\frac{1}{\mu_w}\right)}{\partial p^n_{o_{i,j,k}}} + k_{rg} \frac{\partial\left(\frac{1}{\mu_g}\right)}{\partial p^n_{o_{i,j,k}}} \tag{C.115}$$

If no water is injected

$$\left(\frac{\partial (q_w^*)^n}{\partial p_{o_{i,j,k}}^n}\right)_{inj} = 0. \tag{C.116}$$

For a producer the derivative is equal to

$$\left(\frac{\partial (q_w^*)^n}{\partial p_{o_{i,j,k}}^n}\right)_{prod} = \alpha_{eff} V_{gb} k_{rw} w \begin{pmatrix} \frac{1}{\mu_w}\left[(p_{wf} - p_{gb_o}) + p_{cow}\right] \frac{\partial}{\partial p_{o_{i,j,k}}^n}\left(\frac{1}{B_w}\right) \\ +\frac{1}{B_w}\left[(p_{wf} - p_{gb_o}) + p_{cow}\right] \frac{\partial}{\partial p_{o_{i,j,k}}^n}\left(\frac{1}{\mu_w}\right) \\ -\frac{1}{B_w}\frac{1}{\mu_w} \end{pmatrix}. \tag{C.117}$$

Derivatives with respect to the water saturation

For term ${Tw1}_{i+\frac{1}{2},j,k}$, the derivative with respect to the water saturation is

$$\frac{\partial {Tw1}_{i+\frac{1}{2},j,k}}{\partial S_{w_{i,j,k}}^n} = \frac{\Delta y_{i,j,k} \Delta z_{i,j,k}}{\Delta x_{i+\frac{1}{2},j,k}} \frac{\partial {\lambda_w}_{i+\frac{1}{2},j,k}}{\partial S_{w_{i,j,k}}^n}, \tag{C.118}$$

where

$$\frac{\partial {\lambda_w}_{i+\frac{1}{2},j,k}}{\partial S_{w_{i,j,k}}^n} = \left(\frac{k}{B_w \mu_w}\right)_{i+\frac{1}{2},j,k} \frac{\partial {(k_{rw})}_{i+\frac{1}{2},j,k}}{\partial S_{w_{i,j,k}}^n}. \tag{C.119}$$

For term ${Tw2}_{i+\frac{1}{2},j,k}$ the derivative is

$$\frac{\partial {Tw2}_{i+\frac{1}{2},j,k}}{\partial S_{w_{i,j,k}}^n} = \left(\frac{\partial p_{cow}}{\partial S_w}\right)_{i+\frac{1}{2},j,k} \frac{\partial {Tw1}_{i+\frac{1}{2},j,k}}{\partial S_{w_{i,j,k}}^n} + \frac{\partial \left(\frac{\partial p_{cow}}{\partial S_w}\right)_{i+\frac{1}{2},j,k}}{\partial S_{w_{i,j,k}}^n} {Tw1}_{i+\frac{1}{2},j,k}. \tag{C.120}$$

For term ${Tw3}_{i+\frac{1}{2},j,k}$

$$\frac{\partial {Tw3}_{i+\frac{1}{2},j,k}}{\partial S_{w_{i,j,k}}^n} = \left(\frac{\partial p_{cow}}{\partial S_g}\right)_{i+\frac{1}{2},j,k} \frac{\partial {Tw1}_{i+\frac{1}{2},j,k}}{\partial S_{w_{i,j,k}}^n}, \tag{C.121}$$

which is zero if $p_{cow} = p_{cow}\,(S_w)$.

Finally, for term ${Tw4}_{i+\frac{1}{2},j,k}$ the derivative is equal to

$$\frac{\partial {Tw4}_{i+\frac{1}{2},j,k}}{\partial S_{w_{i,j,k}}^n} = \rho_{w_{i+\frac{1}{2},j,k}} g \frac{\partial {Tw1}_{i+\frac{1}{2},j,k}}{\partial S_{w_{i,j,k}}^n} \tag{C.122}$$

If water is the injected liquid the derivative $\frac{\partial (q_w^*)^n}{\partial S_{w_{i,j,k}}^n}$ equals

$$\left(\frac{\partial q_w^*}{\partial S_{w_{i,j,k}}^n}\right)_{inj} = \frac{\partial q_{tw}^*}{\partial S_{w_{i,j,k}}^n} \tag{C.123}$$

$$= \frac{V_{gb}}{B_w} \alpha_{eff} w \begin{pmatrix} (p_{wf} - p_{gb_o}) \frac{\partial \lambda_{rt}}{\partial S_{w_{i,j,k}}^n} + \frac{1}{\mu_w} p_{cow} \frac{\partial k_{rw}}{\partial S_{w_{i,j,k}}^n} \\ +\frac{k_{rw}}{\mu_w} \frac{\partial p_{cow}}{\partial S_{w_{i,j,k}}^n} - \frac{1}{\mu_g} p_{cgo} \frac{\partial k_{rg}}{\partial S_{w_{i,j,k}}^n} - \frac{k_{rg}}{\mu_g} \frac{\partial p_{cgo}}{\partial S_{w_{i,j,k}}^n} \end{pmatrix},$$

where

$$\frac{\partial \lambda_{rt}}{\partial S^n_{w_{i,j,k}}} = \frac{1}{\mu_o}\frac{\partial k_{ro}}{\partial S^n_{w_{i,j,k}}} + \frac{1}{\mu_w}\frac{\partial k_{rw}}{\partial S^n_{w_{i,j,k}}} + \frac{1}{\mu_g}\frac{\partial k_{rg}}{\partial S^n_{w_{i,j,k}}}. \tag{C.124}$$

If no water is injected, the $\frac{\partial q^*_w}{\partial S^n_{w_{i,j,k}}}$ derivative equals

$$\left(\frac{\partial q^*_w}{\partial S^n_{w_{i,j,k}}}\right)_{inj} = 0. \tag{C.125}$$

For a producer the derivative is equal to

$$\left(\frac{\partial (q^*_w)^n}{\partial S^n_{w_{i,j,k}}}\right)_{prod} = \alpha_{eff}\frac{V_{gb}}{B_w \mu_w} w\left((p_{wf} - p_{gb_o}) \ + p_{cow}\right)\frac{\partial k_{rw}}{\partial S^n_{w_{i,j,k}}} \tag{C.126}$$

Derivatives with respect to the gas saturation

For term ${T_w1}_{i+\frac{1}{2},j,k}$ the derivative with respect to the gas saturation is

$$\frac{\partial {T_w1}_{i+\frac{1}{2},j,k}}{\partial S^n_{g_{i,j,k}}} = \frac{\Delta y_{i,j,k}\Delta z_{i,j,k}}{\Delta x_{i+\frac{1}{2},j,k}}\frac{\partial {\lambda_w}_{i+\frac{1}{2},j,k}}{\partial S^n_{g_{i,j,k}}}, \tag{C.127}$$

where

$$\frac{\partial {\lambda_w}_{i+\frac{1}{2},j,k}}{\partial S^n_{g_{i,j,k}}} = \left(\frac{k}{B_w \mu_w}\right)_{i+\frac{1}{2},j,k}\frac{\partial {k_{rw}}_{i+\frac{1}{2},j,k}}{\partial S^n_{g_{i,j,k}}} \tag{C.128}$$

For term ${T_w2}_{i+\frac{1}{2},j,k}$ the derivative is

$$\frac{\partial {T_w2}_{i+\frac{1}{2},j,k}}{\partial S^n_{g_{i,j,k}}} = \left(\frac{\partial p_{cow}}{\partial S_w}\right)_{i+\frac{1}{2},j,k}\frac{\partial {T_w1}_{i+\frac{1}{2},j,k}}{\partial S^n_{g_{i,j,k}}}. \tag{C.129}$$

For term ${T_w3}_{i+\frac{1}{2},j,k}$

$$\frac{\partial {T_w3}_{i+\frac{1}{2},j,k}}{\partial S^n_{g_{i,j,k}}} = \left(\frac{\partial p_{cow}}{\partial S_g}\right)_{i+\frac{1}{2},j,k}\frac{\partial {T_w1}_{i+\frac{1}{2},j,k}}{\partial S^n_{g_{i,j,k}}} + \frac{\partial\left(\frac{\partial p_{cow}}{\partial S_g}\right)_{i+\frac{1}{2},j,k}}{\partial S^n_{g_{i,j,k}}}{T_w1}_{i+\frac{1}{2},j,k}, \tag{C.130}$$

which is zero if $p_{cow} = p_{cow}\,(S_w)$.

Finally for term ${T_w4}_{i+\frac{1}{2},j,k}$ the derivative is

$$\frac{\partial {T_w4}_{i+\frac{1}{2},j,k}}{\partial S^n_{g_{i,j,k}}} = {\rho_w}_{i+\frac{1}{2},j,k}\, g\frac{\partial {T_w1}_{i+\frac{1}{2},j,k}}{\partial S^n_{g_{i,j,k}}}. \tag{C.131}$$

If water is the injected liquid the derivative $\frac{\partial q_w^*}{\partial S^n_{w_{i,j,k}}}$ equals

$$\left(\frac{\partial q_w^*}{\partial S^n_{w_{i,j,k}}}\right)_{inj} = \frac{\partial q_{tw}^*}{\partial S^n_{g_{i,j,k}}} \tag{C.132}$$

$$= \frac{V_{gb}}{B_w}\alpha_{eff} w \left(\begin{array}{c} (p_{wf} - p_{gb_o}) \frac{\partial \lambda_{rt}}{\partial S^n_{g_{i,j,k}}} + \frac{1}{\mu_w} p_{cow} \frac{\partial k_{rw}}{\partial S^n_{g_{i,j,k}}} \\ + \frac{k_{rw}}{\mu_w} \frac{\partial p_{cow}}{\partial S^n_{g_{i,j,k}}} - \frac{1}{\mu_g} p_{cgo} \frac{\partial k_{rg}}{\partial S^n_{g_{i,j,k}}} - \frac{k_{rg}}{\mu_g} \frac{\partial p_{cgo}}{\partial S^n_{g_{i,j,k}}} \end{array} \right),$$

where

$$\frac{\partial \lambda_{rt}}{\partial S^n_{g_{i,j,k}}} = \frac{1}{\mu_o}\frac{\partial k_{ro}}{\partial S^n_{g_{i,j,k}}} + \frac{1}{\mu_w}\frac{\partial k_{rw}}{\partial S^n_{g_{i,j,k}}} + \frac{1}{\mu_g}\frac{\partial k_{rg}}{\partial S^n_{g_{i,j,k}}}. \tag{C.133}$$

If no water is injected

$$\left(\frac{\partial q_w^*}{\partial S^n_{g_{i,j,k}}}\right)_{inj} = 0. \tag{C.134}$$

For a producer the derivative is equal to

$$\frac{\partial (q_w^*)^n}{\partial S^n_{g_{i,j,k}}} = \alpha_{eff}\frac{V_{gb}}{B_w \mu_w} w \left((p_{wf} - p_{gb_o}) \ + p_{cow} \right) \frac{\partial k_{rw}}{\partial S^n_{g_{i,j,k}}} \tag{C.135}$$

$$= 0. \tag{C.136}$$

C.3.3 The gas equation

Derivatives with respect to the oil pressure

For term ${T_{g1}}_{i+\frac{1}{2},j,k}$ the derivative with respect to the oil pressure equals

$$\frac{\partial {T_{g1}}_{i+\frac{1}{2},j,k}}{\partial p^n_{o_{i,j,k}}} = \frac{\Delta y_{i,j,k}\Delta z_{i,j,k}}{\Delta x_{i+\frac{1}{2},j,k}} \left({\lambda_o}_{i+\frac{1}{2},j,k} \frac{\partial {R_s}_{i+\frac{1}{2},j,k}}{\partial p^n_{o_{i,j,k}}} + {R_s}_{i+\frac{1}{2},j,k} \frac{\partial {\lambda_o}_{i+\frac{1}{2},j,k}}{\partial p^n_{o_{i,j,k}}} \right)$$

$$+ \frac{\Delta y_{i,j,k}\Delta z_{i,j,k}}{\Delta x_{i+\frac{1}{2},j,k}} \left(\frac{\partial {\lambda_g}_{i+\frac{1}{2},j,k}}{\partial p^n_{o_{i,j,k}}} \right)$$

$$= \frac{\partial {T_{go1}}_{i+\frac{1}{2},j,k}}{\partial p^n_{o_{i,j,k}}} + \frac{\partial {T_{gg1}}_{i+\frac{1}{2},j,k}}{\partial p^n_{o_{i,j,k}}}, \tag{C.137}$$

where

$$\frac{\partial {\lambda_g}_{i+\frac{1}{2},j,k}}{\partial p^n_{o_{i,j,k}}} = k_{i+\frac{1}{2},j,k} {k_{rg}}_{i+\frac{1}{2},j,k} \left(\begin{array}{c} \frac{1}{B_g} \frac{\partial \left(\frac{1}{\mu_g}\right)_{i+\frac{1}{2},j,k}}{\partial p^n_{o_{i,j,k}}} + \frac{1}{\mu_g} \frac{\partial \left(\frac{1}{B_g}\right)_{i+\frac{1}{2},j,k}}{\partial p^n_{o_{i,j,k}}} \\ \end{array} \right). \tag{C.138}$$

For term ${Tg2}_{i+\frac{1}{2},j,k}$ the derivative equals

$$\frac{\partial {Tg2}_{i+\frac{1}{2},j,k}}{\partial p^n_{o_{i,j,k}}} = \left(\frac{\partial p_{cgo}}{\partial S_w}\right)_{i+\frac{1}{2},j,k} \frac{\partial {Tgg1}_{i+\frac{1}{2},j,k}}{\partial p^n_{o_{i,j,k}}}. \tag{C.139}$$

For term ${Tg3}_{i+\frac{1}{2},j,k}$

$$\frac{\partial {Tg3}_{i+\frac{1}{2},j,k}}{\partial p^n_{o_{i,j,k}}} = \left(\frac{\partial p_{cgo}}{\partial S_g}\right)_{i+\frac{1}{2},j,k} \frac{\partial {Tgg1}_{i+\frac{1}{2},j,k}}{\partial p^n_{o_{i,j,k}}}. \tag{C.140}$$

Finally for the term ${Tg4}_{i+\frac{1}{2},j,k}$ the derivative is

$$\frac{\partial {Tg4}_{i+\frac{1}{2},j,k}}{\partial p^n_{o_{i,j,k}}} = g \left(\begin{array}{c} \rho_{o_{i+\frac{1}{2},j,k}} \frac{\partial {Tgo1}_{i+\frac{1}{2},j,k}}{\partial p^n_{o_{i,j,k}}} + \frac{\partial \rho_{o_{i+\frac{1}{2},j,k}}}{\partial p^n_{o_{i,j,k}}} {Tgo1}_{i+\frac{1}{2},j,k} \\ +\rho_{g_{i+\frac{1}{2},j,k}} \frac{\partial {Tgg1}_{i+\frac{1}{2},j,k}}{\partial p^n_{o_{i,j,k}}} + \frac{\partial \rho_{g_{i+\frac{1}{2},j,k}}}{\partial p^n_{o_{i,j,k}}} {Tgg1}_{i+\frac{1}{2},j,k} \end{array} \right) \tag{C.141}$$

If gas is the injected fluid, the derivative $\frac{\partial q^{*n}_g}{\partial p^n_{o_{i,j,k}}}$ is

$$\begin{aligned} \left(\frac{\partial q^{*n}_g}{\partial p^n_{o_{i,j,k}}}\right)_{inj} &= \frac{\partial q^*_{t_{inj}}}{\partial p^n_{o_{i,j,k}}} \qquad (C.142) \\ &= V_{gb}\alpha_{eff} \left(\begin{array}{c} \left\{ \lambda_{rt} w \left(p_{wf} - p_{gb_o}\right) + \frac{k_{rw}}{\mu_w} w p_{cow} - \frac{k_{rg}}{\mu_g} w p_{cgo} \right\} \frac{\partial\left(\frac{1}{B_g}\right)}{\partial p^n_{o_{i,j,k}}} \\ +\frac{1}{B_g} \left\{ \begin{array}{c} \lambda_{rt} w \frac{\partial (p_{wf} - p_{gb_o})}{\partial p^n_{o_{i,j,k}}} + w \left(p_{wf} - p_{gb_o}\right) \frac{\partial \lambda_{rt}}{\partial p^n_{o_{i,j,k}}} \\ +k_{rw} w p_{cow} \frac{\partial\left(\frac{1}{\mu_w}\right)}{\partial p^n_{o_{i,j,k}}} - k_{rg} w p_{cgo} \frac{\partial\left(\frac{1}{\mu_g}\right)}{\partial p^n_{o_{i,j,k}}} \end{array} \right\} \end{array} \right) \end{aligned}$$

where

$$\frac{\partial \lambda_{rt}}{\partial p^n_{o_{i,j,k}}} = k_{ro} \frac{\partial\left(\frac{1}{\mu_o}\right)}{\partial p^n_{o_{i,j,k}}} + k_{rw} \frac{\partial\left(\frac{1}{\mu_w}\right)}{\partial p^n_{o_{i,j,k}}} + k_{rg} \frac{\partial\left(\frac{1}{\mu_g}\right)}{\partial p^n_{o_{i,j,k}}} \tag{C.143}$$

If no gas is injected

$$\left(\frac{\partial q^{*n}_g}{\partial p^n_{o_{i,j,k}}}\right)_{inj} = 0. \tag{C.144}$$

For a producer the derivative is

$$\left(\frac{\partial \left(q^*_g\right)^n}{\partial p^n_{o_{i,j,k}}}\right)_{prod} = V_{gb} \left(\begin{array}{c} R_s \tilde{q}_o \frac{\partial\left(\frac{1}{B_o}\right)}{\partial p^n_{o_{i,j,k}}} + \frac{1}{B_o} \tilde{q}_o \frac{\partial R_s}{\partial p^n_{o_{i,j,k}}} + \frac{1}{B_o} R_s \frac{\partial \tilde{q}_o}{\partial p^n_{o_{i,j,k}}} \\ +\tilde{q}_{fg} \frac{\partial\left(\frac{1}{B_g}\right)}{\partial p^n_{o_{i,j,k}}} + \frac{1}{B_g} \frac{\partial \tilde{q}_{fg}}{\partial p^n_{o_{i,j,k}}} \end{array} \right), \tag{C.145}$$

where

$$\frac{\partial \tilde{q}_o}{\partial p^n_{o_{i,j,k}}} = \alpha_{eff} k_{ro} w \left(\left(p_{wf} - p_{gb_o}\right) \frac{\partial\left(\frac{1}{\mu_o}\right)}{\partial p^n_{o_{i,j,k}}} - \frac{1}{\mu_o} \right), \tag{C.146}$$

and

$$\frac{\partial \tilde{q}_{fg}}{\partial p^n_{o_{i,j,k}}} = \alpha_{eff} k_{rg} w \left(\left(\left(p_{wf} - p_{gb_o}\right) - p_{cgo}\right) \frac{\partial\left(\frac{1}{\mu_g}\right)}{\partial p^n_{o_{i,j,k}}} - \frac{1}{\mu_g} \right) \tag{C.147}$$

Derivatives with respect to the water saturation

For term ${Tg1}_{i+\frac{1}{2},j,k}$ the derivative with respect to the water saturation equals

$$\begin{aligned}\frac{\partial {Tg1}_{i+\frac{1}{2},j,k}}{\partial S^n_{w_{i,j,k}}} &= \frac{\Delta y_{i,j,k}\Delta z_{i,j,k}}{\Delta x_{i+\frac{1}{2},j,k}}\left(R_{s_{i+\frac{1}{2},j,k}}\frac{\partial {\lambda_o}_{i+\frac{1}{2},j,k}}{\partial S^n_{w_{i,j,k}}}+\frac{\partial {\lambda_g}_{i+\frac{1}{2},j,k}}{\partial S^n_{w_{i,j,k}}}\right)\\ &= \frac{\partial {To1}_{i+\frac{1}{2},j,k}}{\partial S^n_{w_{i,j,k}}}+\frac{\partial {Tg1}_{i+\frac{1}{2},j,k}}{\partial S^n_{w_{i,j,k}}},\end{aligned} \tag{C.148}$$

where

$$\frac{\partial {\lambda_g}_{i+\frac{1}{2},j,k}}{\partial S^n_{w_{i,j,k}}}=\left(\frac{k}{B_g\mu_g}\right)_{i+\frac{1}{2},j,k}\frac{\partial {(k_{rg})}_{i+\frac{1}{2},j,k}}{\partial S^n_{w_{i,j,k}}}. \tag{C.149}$$

For term ${Tg2}_{i+\frac{1}{2},j,k}$ the derivative is

$$\frac{\partial {Tg2}_{i+\frac{1}{2},j,k}}{\partial S^n_{w_{i,j,k}}}=\left(\frac{\partial p_{cgo}}{\partial S_w}\right)_{i+\frac{1}{2},j,k}\frac{\partial {Tg1}_{i+\frac{1}{2},j,k}}{\partial S^n_{w_{i,j,k}}}+\frac{\partial\left(\frac{\partial p_{cgo}}{\partial S_w}\right)_{i+\frac{1}{2},j,k}}{\partial S^n_{w_{i,j,k}}}{Tgg1}_{i+\frac{1}{2},j,k}, \tag{C.150}$$

which is zero if $p_{cgo}=p_{cgo}\left(S_g\right)$.

For term ${Tg3}_{i+\frac{1}{2},j,k}$ the derivative is

$$\frac{\partial {Tg3}_{i+\frac{1}{2},j,k}}{\partial S^n_{w_{i,j,k}}}=\left(\frac{\partial p_{cgo}}{\partial S_g}\right)_{i+\frac{1}{2},j,k}\frac{\partial {Tg1}_{i+\frac{1}{2},j,k}}{\partial S^n_{w_{i,j,k}}}+\frac{\partial\left(\frac{\partial p_{cgo}}{\partial S_g}\right)_{i+\frac{1}{2},j,k}}{\partial S^n_{w_{i,j,k}}}{Tgg1}_{i+\frac{1}{2},j,k}. \tag{C.151}$$

Finally, for the term ${Tg4}_{i+\frac{1}{2},j,k}$ the derivative is

$$\frac{\partial {Tg4}_{i+\frac{1}{2},j,k}}{\partial S^n_{w_{i,j,k}}}=g\left(\rho_{o_{i+\frac{1}{2},j,k}}\frac{\partial {To1}_{i+\frac{1}{2},j,k}}{\partial S^n_{w_{i,j,k}}}+\rho_{g_{i+\frac{1}{2},j,k}}\frac{\partial {Tg1}_{i+\frac{1}{2},j,k}}{\partial S^n_{w_{i,j,k}}}\right). \tag{C.152}$$

If gas is the injected fluid, the derivative $\frac{\partial q^{*n}_g}{\partial S^n_{w_{i,j,k}}}$ equals

$$\left(\frac{\partial q^{*n}_g}{\partial S^n_{w_{i,j,k}}}\right)_{inj} = \frac{\partial q^*_{t_{inj}}}{\partial S^n_{w_{i,j,k}}} \tag{C.153}$$

$$= \frac{V_{gb}}{B_g}\alpha_{eff}w\left(\left\{\begin{array}{c}\left[\begin{array}{c}(1+R_s)\frac{1}{\mu_o}\frac{\partial k_{ro}}{\partial S^n_{w_{i,j,k}}}\\ +\frac{1}{\mu_w}\frac{\partial k_{rw}}{\partial S^n_{w_{i,j,k}}}\\ +\frac{1}{\mu_g}\frac{\partial k_{rg}}{\partial S^n_{w_{i,j,k}}}\end{array}\right]\left(p_{wf}-p_{gb_o}\right)\\ +\frac{1}{\mu_w}\frac{\partial k_{rw}}{\partial S^n_{w_{i,j,k}}}p_{cow}+\frac{k_{rw}}{\mu_w}\frac{\partial p_{cow}}{\partial S^n_{w_{i,j,k}}}\\ -\frac{1}{\mu_g}\frac{\partial k_{rg}}{\partial S^n_{w_{i,j,k}}}p_{cgo}-\frac{k_{rg}}{\mu_g}\frac{\partial p_{cgo}}{\partial S^n_{w_{i,j,k}}}\end{array}\right\}\right).$$

If no gas is injected

$$\left(\frac{\partial q^{*n}_g}{\partial S^n_{w_{i,j,k}}}\right)_{inj}=0. \tag{C.154}$$

For a producer well the derivative is

$$\left(\frac{\partial\left(q_g^*\right)^n}{\partial S^n_{w_{i,j,k}}}\right)_{prod} = V_{gb}\left(\frac{1}{B_o}R_s\frac{\partial\tilde{q}_o}{\partial S^n_{w_{i,j,k}}} + \frac{1}{B_g}\frac{\partial\tilde{q}_{fg}}{\partial S^n_{w_{i,j,k}}}\right), \tag{C.155}$$

where

$$\frac{\partial\tilde{q}_o}{\partial S^n_{w_{i,j,k}}} = \alpha_{eff}\frac{1}{\mu_o}w\left(p_{wf} - p_{gb_o}\right)\frac{\partial k_{ro}}{\partial S^n_{w_{i,j,k}}}, \tag{C.156}$$

and

$$\frac{\partial\tilde{q}_{fg}}{\partial S^n_{w_{i,j,k}}} = \alpha_{eff}\frac{1}{\mu_g}w\left(\left(\left(p_{wf} - p_{gb_o}\right) - p_{cgo}\right)\frac{\partial k_{rg}}{\partial S^n_{w_{i,j,k}}} - k_{rg}\frac{\partial p_{cgo}}{\partial S^n_{w_{i,j,k}}}\right). \tag{C.157}$$

Derivatives with respect to the gas saturation

For term ${Tg1}_{i+\frac{1}{2},j,k}$ the derivative with respect to the gas saturation is

$$\begin{aligned}\frac{\partial {Tg1}_{i+\frac{1}{2},j,k}}{\partial S^n_{g_{i,j,k}}} &= \frac{\Delta y_{i,j,k}\Delta z_{i,j,k}}{\Delta x_{i+\frac{1}{2},j,k}}{R_s}_{i+\frac{1}{2},j,k}\frac{\partial {\lambda_o}_{i+\frac{1}{2},j,k}}{\partial S^n_{g_{i,j,k}}} + \frac{\Delta y_{i,j,k}\Delta z_{i,j,k}}{\Delta x_{i+\frac{1}{2},j,k}}\frac{\partial {\lambda_g}_{i+\frac{1}{2},j,k}}{\partial S^n_{g_{i,j,k}}} \\ &= \frac{\partial {To1}_{i+\frac{1}{2},j,k}}{\partial S^n_{g_{i,j,k}}} + \frac{\partial {Tgg1}_{i+\frac{1}{2},j,k}}{\partial S^n_{g_{i,j,k}}},\end{aligned} \tag{C.158}$$

where

$$\frac{\partial {\lambda_g}_{i+\frac{1}{2},j,k}}{\partial S^n_{g_{i,j,k}}} = \left(\frac{k}{B_g\mu_g}\right)_{i+\frac{1}{2},j,k}\frac{\partial {(k_{rg})}_{i+\frac{1}{2},j,k}}{\partial S^n_{g_{i,j,k}}}. \tag{C.159}$$

For term ${Tg2}_{i+\frac{1}{2},j,k}$ the derivative is

$$\begin{aligned}\frac{\partial {Tg2}_{i+\frac{1}{2},j,k}}{\partial S^n_{g_{i,j,k}}} &= \frac{\partial}{\partial S^n_{g_{i,j,k}}}\left(\frac{\Delta y_{i,j,k}\Delta z_{i,j,k}}{\Delta x_{i+\frac{1}{2},j,k}}\lambda_{g_{i+\frac{1}{2},j,k}}\left(\frac{\partial p_{cgo}}{\partial S_w}\right)_{i+\frac{1}{2},j,k}\right) \\ &= \left(\frac{\partial p_{cgo}}{\partial S_w}\right)_{i+\frac{1}{2},j,k}\frac{\partial {Tgg1}_{i+\frac{1}{2},j,k}}{\partial S^n_{g_{i,j,k}}} + \frac{\partial\left(\frac{\partial p_{cgo}}{\partial S_w}\right)_{i+\frac{1}{2},j,k}}{\partial S^n_{g_{i,j,k}}}{Tgg1}_{i+\frac{1}{2},j,k},\end{aligned} \tag{C.160}$$

which is zero if $p_{cgo} = p_{cgo}\left(S_g\right)$.

For term ${Tg3}_{i+\frac{1}{2},j,k}$ the derivative is

$$\frac{\partial {Tg3}_{i+\frac{1}{2},j,k}}{\partial S^n_{g_{i,j,k}}} = \left(\frac{\partial p_{cgo}}{\partial S_g}\right)_{i+\frac{1}{2},j,k}\frac{\partial {Tgg1}_{i+\frac{1}{2},j,k}}{\partial S^n_{g_{i,j,k}}} + \frac{\partial\left(\frac{\partial p_{cgo}}{\partial S_g}\right)_{i+\frac{1}{2},j,k}}{\partial S^n_{g_{i,j,k}}}{Tgg1}_{i+\frac{1}{2},j,k}. \tag{C.161}$$

For the term ${Tg4}_{i+\frac{1}{2},j,k}$ the derivative is

$$\frac{\partial {Tg4}_{i+\frac{1}{2},j,k}}{\partial S^n_{g_{i,j,k}}} = g\left(\rho_{o_{i+\frac{1}{2},j,k}}\frac{\partial {To1}_{i+\frac{1}{2},j,k}}{\partial S^n_{g_{i,j,k}}} + \rho_{g_{i+\frac{1}{2},j,k}}\frac{\partial {Tgg1}_{i+\frac{1}{2},j,k}}{\partial S^n_{g_{i,j,k}}}\right). \tag{C.162}$$

If gas is the injected fluid, the derivative $\frac{\partial q_g^{*n}}{\partial S_{g_{i,j,k}}^n}$ is

$$\left(\frac{\partial q_g^{*n}}{\partial S_{g_{i,j,k}}^n}\right)_{inj} = \frac{\partial q_{t_{inj}}^*}{\partial S_{g_{i,j,k}}^n} \tag{C.163}$$

$$= \frac{V_{gb}}{B_g}\alpha_{eff} w \begin{pmatrix} \begin{bmatrix} (1+R_s)\frac{1}{\mu_o}\frac{\partial k_{ro}}{\partial S_{g_{i,j,k}}^n} \\ +\frac{1}{\mu_w}\frac{\partial k_{rw}}{\partial S_{g_{i,j,k}}^n} \\ +\frac{1}{\mu_g}\frac{\partial k_{rg}}{\partial S_{g_{i,j,k}}^n} \end{bmatrix} (p_{wf} - p_{gb_o}) \\ +\frac{1}{\mu_w}\frac{\partial k_{rw}}{\partial S_{g_{i,j,k}}^n} p_{cow} + \frac{k_{rw}}{\mu_w}\frac{\partial p_{cow}}{\partial S_{g_{i,j,k}}^n} \\ -\frac{1}{\mu_g}\frac{\partial k_{rg}}{\partial S_{g_{i,j,k}}^n} p_{cgo} - \frac{k_{rg}}{\mu_g}\frac{\partial p_{cgo}}{\partial S_{g_{i,j,k}}^n} \end{pmatrix}.$$

If no gas is injected,

$$\left(\frac{\partial q_g^{*n}}{\partial S_{g_{i,j,k}}^n}\right)_{inj} = 0. \tag{C.164}$$

For a producer the derivative is

$$\left(\frac{\partial \left(q_g^*\right)^n}{\partial S_{g_{i,j,k}}^n}\right)_{prod} = V_{gb} \begin{pmatrix} \frac{1}{B_o} R_s \frac{\partial \tilde{q}_o}{\partial S_{g_{i,j,k}}^n} \\ +\frac{1}{B_g}\frac{\partial \tilde{q}_{fg}}{\partial S_{g_{i,j,k}}^n} \end{pmatrix}, \tag{C.165}$$

where

$$\frac{\partial \tilde{q}_o}{\partial S_{g_{i,j,k}}^n} = \alpha_{eff}\frac{1}{\mu_o} w \left(p_{wf} - p_{gb_o}\right)\frac{\partial k_{ro}}{\partial S_{g_{i,j,k}}^n}, \tag{C.166}$$

and

$$\frac{\partial \tilde{q}_{fg}}{\partial S_{g_{i,j,k}}^n} = \alpha_{eff}\frac{1}{\mu_g} w \left(\left(\left(p_{wf} - p_{gb_o}\right) - p_{cgo}\right)\frac{\partial k_{rg}}{\partial S_{g_{i,j,k}}^n} - k_{rg}\frac{\partial p_{cgo}}{\partial S_{g_{i,j,k}}^n}\right). \tag{C.167}$$

C.4 Derivatives $\frac{\partial \mathbf{g}^n}{\partial \boldsymbol{\alpha}_{eff}^n}$

C.4.1 The oil equation

If an injector is located in the grid block this derivative is zero since no oil is injected, hence

$$\left(\frac{\partial g_o^n}{\partial \alpha_{eff}^n}\right)_{inj} = -\frac{\partial \left(q_o^*\right)^{n+1}}{\partial \alpha_{eff}^n} = 0. \tag{C.168}$$

If a producer is located in the grid block the derivative is

$$\frac{\partial g_o^n}{\partial \alpha_{eff}^n} = -\left(\frac{V_{gb}}{B_o}\left(\frac{k_{ro}}{\mu_o} w \left(p_{wf} - p_{gb_o}\right)\right)\right)^{n+1}. \tag{C.169}$$

C.4.2 The water equation

If a water injector is located in the grid block the derivative is

$$\frac{\partial g_w^n}{\partial \alpha_{eff}^n} = -\left(\frac{\partial \left(q_{t_w}^*\right)^{n+1}}{\partial \alpha_{eff}^n}\right)_{inj}, \tag{C.170}$$

where

$$\left(\frac{\partial (q_{tw}^*)^{n+1}}{\partial \alpha_{eff}^n}\right)_{inj} = \left(\frac{V_{gb}}{B_w}\left\{\begin{array}{c}\left[(1+R_s)\frac{k_{ro}}{\mu_o}+\frac{k_{rw}}{\mu_w}+\frac{k_{rg}}{\mu_g}\right]w\left(p_{wf}-p_{gb_o}\right)\\ +\frac{k_{rw}}{\mu_w}wp_{cow}-\frac{k_{rg}}{\mu_g}wp_{cgo}\end{array}\right\}\right)^{n+1}. \tag{C.171}$$

If no water is injected

$$\left(\frac{\partial (q_{tw}^*)^{n+1}}{\partial \alpha_{eff}^n}\right)_{inj} = 0. \tag{C.172}$$

If a producer is located in the grid block the derivative is

$$\begin{aligned}\frac{\partial g_w^n}{\partial \alpha_{eff}^n} &= -\frac{\partial (q_w^*)^{n+1}}{\partial \alpha_{eff}^n}\\ &= -\left(\frac{V_{gb}}{B_w}\left(\left[\frac{k_{rw}}{\mu_w}w\left(p_{wf}-p_{gb_o}\right)+\frac{k_{rw}}{\mu_w}wp_{cow}\right]\right)\right)^{n+1}.\end{aligned} \tag{C.173}$$

C.4.3 The gas equation

If the well in the grid block is a gas injector, the derivative is

$$\frac{\partial g_g^n}{\partial \alpha_{eff}^n} = -\left(\frac{\partial \left(q_g^*\right)^{n+1}}{\partial \alpha_{eff}^n}\right)_{inj} = -\left(\frac{\partial q_{tg}^{*n+1}}{\partial \alpha_{eff}^n}\right)_{inj}, \tag{C.174}$$

where

$$\left(\frac{\partial \left(q_{tg}^*\right)^{n+1}}{\partial \alpha_{eff}^n}\right)_{inj} = \left(\frac{V_{gb}}{B_g}\left\{\begin{array}{c}\left[(1+R_s)\frac{k_{ro}}{\mu_o}+\frac{k_{rw}}{\mu_w}+\frac{k_{rg}}{\mu_g}\right]w\left(p_{wf}-p_{gb_o}\right)\\ +\frac{k_{rw}}{\mu_w}wp_{cow}-\frac{k_{rg}}{\mu_g}wp_{cgo}\end{array}\right\}\right)^{n+1}. \tag{C.175}$$

If no gas is injected

$$\left(\frac{\partial q_{tg}^{*n+1}}{\partial \alpha_{eff}^n}\right)_{inj} = 0. \tag{C.176}$$

If a producer is located in the grid block the derivative is

$$\begin{aligned}\frac{\partial g_g^n}{\partial \alpha_{eff}^n} &= -\left(\frac{\partial \left(q_g^*\right)^{n+1}}{\partial \alpha_{eff}^n}\right)_{prod}\\ &= -V_{gb}\left[\frac{1}{B_o}R_s\frac{\partial \tilde{q}_o}{\partial \alpha_{eff}^n}+\frac{1}{B_g}\frac{\partial \tilde{q}_{fg}}{\partial \alpha_{eff}^n}\right]^{n+1},\end{aligned} \tag{C.177}$$

where

$$\frac{\partial \tilde{q}_o}{\partial \alpha^n_{eff}} = \left(\frac{k_{ro}}{\mu_o} w \left(p_{wf} - p_{gb_o} \right) \right)^{n+1}, \tag{C.178}$$

and

$$\frac{\partial \tilde{q}_{fg}}{\partial \alpha^n_{eff}} = \left(\frac{k_{rg}}{\mu_g} w \left(p_{wf} - p_{gb_o} \right) - \frac{k_{rg}}{\mu_g} w p_{cgo} \right)^{n+1}. \tag{C.179}$$

C.5 Derivatives of the objective function

The Net Present Value objective function for three phase flow can be written as

$$\begin{aligned} \mathcal{J} &= \sum_{n=0}^{N-1} \sum_{k=1}^{N_{prod}} \frac{-r_o \left(q_o^* \right)^n_k - r_w \left(q_w^* \right)^n_k - r_g \left(q_g^* \right)^n_k}{\left(1 + \frac{b}{100} \right)^{\tau^n}} \Delta t^n \\ &= \sum_{n=0}^{N-1} \mathcal{J}^n \end{aligned} \tag{C.180}$$

It is based only on the production wells, and thus only on oil, water and gas production rates. Furthermore, the cost/revenue parameters are thus those related to oil, water and total gas production. The cost of gas and water injection is thus not taken into account.

C.5.1 Derivative $\frac{\partial \mathcal{J}^n}{\partial x^n}$

At producer locations the derivatives of the objective function with respect to the states are

$$\left(\frac{\partial \mathcal{J}^n}{\partial p_o^n} \right)_{i,j,k} = \left(\frac{-r_w \frac{\partial (q_w^*)^n_k}{\partial p_o^n} - r_g \frac{\partial \left(q_g^* \right)^n_k}{\partial p_o^n} - r_o \frac{\partial (q_o^*)^n_k}{\partial p_o^n}}{\left(1 + \frac{b}{100} \right)^{\tau^n}} \right) \Delta t^n, \tag{C.181}$$

$$\left(\frac{\partial \mathcal{J}^n}{\partial S_w^n} \right)_{i,j,k} = \left(\frac{-r_w \frac{\partial (q_w^*)^n_k}{\partial S_w^n} - r_g \frac{\partial \left(q_g^* \right)^n_k}{\partial S_w^n} - r_o \frac{\partial (q_o^*)^n_k}{\partial S_w^n}}{\left(1 + \frac{b}{100} \right)^{\tau^n}} \right) \Delta t^n, \tag{C.182}$$

$$\left(\frac{\partial \mathcal{J}^n}{\partial S_g^n} \right)_{i,j,k} = \left(\frac{-r_w \frac{\partial (q_w^*)^n_k}{\partial S_g^n} - r_g \frac{\partial \left(q_g^* \right)^n_k}{\partial S_g^n} - r_o \frac{\partial (q_o^*)^n_k}{\partial S_g^n}}{\left(1 + \frac{b}{100} \right)^{\tau^n}} \right) \Delta t^n. \tag{C.183}$$

C.5.2 Derivative $\frac{\partial \mathcal{J}^n}{\partial \alpha_{eff}^n}$

At producer locations, the derivative of the objective function $\mathcal{J}$ with respect to the control α_{eff}^n is

$$\frac{\partial \mathcal{J}^n}{\partial \alpha_{eff}^n} = \left(\frac{-r_w \frac{\partial (q_w^*)_k^n}{\partial \alpha_{eff}^n} - r_g \frac{\partial \left(q_g^*\right)_k^n}{\partial \alpha_{eff}^n} - r_o \frac{\partial (q_o^*)_k^n}{\partial \alpha_{eff}^n}}{\left(1 + \frac{b}{100}\right)^{\tau^n}} \right) \Delta t^n. \tag{C.184}$$

Appendix D
One dimensional fractional flow problem

D.1 Dynamic system

The one dimensional fractional flow equation for incompressible fluids without capillary pressure is, after Aziz and Settari (1986),

$$\frac{\partial S_w}{\partial t} = -\frac{u_t}{\phi}\frac{\partial f_w}{\partial x} - \frac{q_w}{\phi} + \frac{f_w q_t}{\phi}, \tag{D.1}$$

where S_w is the water saturation $[-]$, u_t the total fluid velocity $\left[\frac{m}{s}\right]$, ϕ the porosity $[-]$, f_w the fractional flow of water $[-]$, x the distance in the x-direction $[m]$, and q_w and q_t are respectively the water and total injection or production rates.

The term $\frac{\partial f_w}{\partial x}$ is discretized with an upstream weighting scheme, assuming the flow is from i to $i+1$, i.e.

$$\left[\frac{\partial f_w}{\partial x}\right]_i \approx \frac{f_{w_i} - f_{w_{i-1}}}{\Delta x}. \tag{D.2}$$

Substituting eq. D.2 into eq. D.1 and discretizing explicitly in time (and replacing $\approx$ with $=$) gives, after some rearranging

$$\begin{aligned} S_{w_i}^{n+1} &= \frac{\Delta t}{\phi}\left[-u_{t_i}^n\left(\frac{f_{w_i} - f_{w_{i-1}}}{\Delta x}\right) - q_{w_i}^n + f_{w_i}^n q_{t_i}^n\right] + S_{w_i}^n, \\ &= f_i^n. \end{aligned} \tag{D.3}$$

The time step size Δt is taken constant and the porosity ϕ is the same in every grid block. The left boundary ($i = 0$) is a no-flow boundary, hence $u_{t_0}^n = 0$. The initial saturation at this boundary equals the connate water saturation, just like in all other grid blocks. All flow is directly related to injection of water, and for the corresponding grid block the equation thus reduces to

$$\begin{aligned} S_{w_0}^{n+1} &= \frac{\Delta t}{\phi}\left(-1 + f_{w_0}^n\right) q_{t_0}^n + S_{w_0}^n, \\ &= f_0^n, \end{aligned} \tag{D.4}$$

where the injection rate $q_{t_0}^n$ has negative sign. For all grid blocks without a source term the equation is

$$\begin{aligned} S_{w_i}^{n+1} &= -\Delta t\frac{u_{t_i}^n}{\phi}\left(\frac{f_{w_i} - f_{w_{i-1}}}{\Delta x}\right) + S_{w_i}^n, \\ &= f_i^n, \end{aligned} \tag{D.5}$$

where the relation between the total injection rate q_t^n and the total fluid velocity $u_{t_i}^n$ is given by

$$u_{t_i}^n = -q_t^n \Delta x. \tag{D.6}$$

For the right boundary ($i = r$), the production equals the flow through this boundary. The equation then becomes

$$\begin{aligned} S_{w_r}^{n+1} &= \frac{u_{t_r}^n}{\Delta x}\frac{\Delta t}{\phi} f_{w_{r-1}}^n - \frac{\Delta t}{\phi}\frac{u_{t_r}^n}{\Delta x} f_{w_r}^n + S_{w_r}^n, & \text{(D.7)} \\ &= f_r^n, & \text{(D.8)} \end{aligned}$$

where the term $-\frac{u_{t_r}^n}{\Delta x} f_{w_r}^n$ corresponds to the water production rate from this grid block.

D.2 Objective function

The objective function to be optimized is again the NPV objective function

$$\begin{aligned} J &= \sum_{n=0}^{N-1} \left(-V_{gb} \frac{\left[(1 - f_w^n)\, r_o + f_w^n r_w \right] q_t^n \Delta t^n}{(1+b)^{t^n}} \right), \\ &= \sum_{n=0}^{N-1} J^n, \end{aligned} \tag{D.9}$$

where V_{gb} is the grid block volume $\left[m^3\right]$, r_o is the oil revenue $\left[\frac{\$}{m^3}\right]$ which is positive, r_w is the water cost $\left[\frac{\$}{m^3}\right]$ which is negative, b is the discount factor $\left[\frac{\%}{yr}\right]$, t is the cumulative time $[yr]$, and the total production rate equals the total injection rate q_t^n, since flow is incompressible. Parameter n represent the discrete time step, and N the final time step. The objective function is evaluated from the production rates in grid block r.

D.3 Optimal control formulation

The optimal control problem is again a fixed end time, free terminal state optimal control problem. The objective function that has to be maximized is the NPV objective function, described in the previous section

$$J = \sum_{n=0}^{N-1} J^n. \tag{D.10}$$

The dynamic system is added to this objective function with a set of Lagrange multipliers, with one multiplier for each grid block. The result is the modified objective function

$$\bar{J} = \sum_{n=0}^{N-1} \left[J^n - \left(\left(\boldsymbol{\lambda}^{n+1}\right)^T \mathbf{S}_{\mathbf{w}}^{n+1} - \left(\boldsymbol{\lambda}^{n+1}\right)^T \mathbf{f}^n \right) \right]. \tag{D.11}$$

For this system an auxiliary function $\mathcal{H}^n$ is defined as

$$\mathcal{H}^n = J^n + \left(\boldsymbol{\lambda}^{n+1}\right)^T \mathbf{f}^n. \tag{D.12}$$

Eq. D.12 is referred to as the *Hamiltonian*. Substitution into eq. D.11 gives

$$\bar{J} = \sum_{n=0}^{N-1} \left(\mathcal{H}^n - \left(\boldsymbol{\lambda}^{n+1}\right)^T \mathbf{S}_{\mathbf{w}}^{n+1} \right). \tag{D.13}$$

Taking the first variation gives

$$\delta \bar{J} = \sum_{n=0}^{N-1} \left[\begin{array}{c} \left(\frac{\partial \mathcal{H}^n}{\partial \mathbf{S}_{\mathbf{w}}^n}\right) \delta \mathbf{S}_{\mathbf{w}}^n - \left(\boldsymbol{\lambda}^{n+1}\right)^T \delta \mathbf{S}_{\mathbf{w}}^{n+1} \\ + \left(\frac{\partial \mathcal{H}^n}{\partial \boldsymbol{\lambda}^{n+1}} - \mathbf{S}_{\mathbf{w}}^{T\,n+1}\right) \delta \boldsymbol{\lambda}^{n+1} + \left(\frac{\partial \mathcal{H}^n}{\partial \mathbf{q}_{\mathbf{t}}^n}\right) \delta \mathbf{q}_{\mathbf{t}}^n \end{array} \right], \tag{D.14}$$

where $\frac{\partial \mathcal{H}^n}{\partial \mathbf{S}_{\mathbf{w}}^n}$, $\left(\boldsymbol{\lambda}^{n+1}\right)^T$, $\frac{\partial \mathcal{H}^n}{\partial \boldsymbol{\lambda}^{n+1}}$, $\mathbf{S}_{\mathbf{w}}^{T\,n+1}$, and $\frac{\partial \mathcal{H}^n}{\partial \mathbf{q}_{\mathbf{t}}^n}$ are row vectors. Changing the index of summation (discrete summation by parts) for the second term in eq. D.14 gives

$$\begin{aligned} \sum_{n=0}^{N-1} \left(\boldsymbol{\lambda}^{n+1}\right)^T \delta \mathbf{S}_{\mathbf{w}}^{n+1} &= \sum_{n=1}^{N} \left(\boldsymbol{\lambda}^n\right)^T \delta \mathbf{S}_{\mathbf{w}}^n, \\ &= \sum_{n=1}^{N-1} \left(\left(\boldsymbol{\lambda}^n\right)^T \delta \mathbf{S}_{\mathbf{w}}^n \right) + \left(\boldsymbol{\lambda}^N\right)^T \delta \mathbf{S}_{\mathbf{w}}^N. \end{aligned} \tag{D.15}$$

Substitution of eq. D.15 into eq. D.14 gives, after some rearranging

$$\begin{aligned} \delta \bar{J} &= -\left(\boldsymbol{\lambda}^N\right)^T \delta \mathbf{S}_{\mathbf{w}}^N + \sum_{n=1}^{N-1} \left[\left(\frac{\partial \mathcal{H}^n}{\partial \mathbf{S}_{\mathbf{w}}^n} - \left(\boldsymbol{\lambda}^n\right)^T \right) \delta \mathbf{S}_{\mathbf{w}}^n \right] \\ &\quad + \sum_{n=0}^{N-1} \left[\left(\frac{\partial \mathcal{H}^n}{\partial \boldsymbol{\lambda}^{n+1}} - \mathbf{S}_{\mathbf{w}}^{T\,n+1} \right) \delta \boldsymbol{\lambda}^{n+1} + \left(\frac{\partial \mathcal{H}^n}{\partial \mathbf{q}_{\mathbf{t}}^n} \right) \delta \mathbf{q}_{\mathbf{t}}^n \right]. \end{aligned} \tag{D.16}$$

In an optimum the terms $\left(\boldsymbol{\lambda}^N\right)^T$, $\left(\frac{\partial \mathcal{H}^n}{\partial \mathbf{S}_{\mathbf{w}}^n} - \left(\boldsymbol{\lambda}^n\right)^T\right)$, $\left(\frac{\partial \mathcal{H}^n}{\partial \boldsymbol{\lambda}^{n+1}} - \mathbf{S}_{\mathbf{w}}^{T\,n+1}\right)$, $\left(\frac{\partial \mathcal{H}^n}{\partial \mathbf{q}_{\mathbf{t}}^n}\right)$ should be zero. The adjoint equation

$$\left(\boldsymbol{\lambda}^n\right)^T = \frac{\partial \mathcal{H}^n}{\partial \mathbf{S}_{\mathbf{w}}^n} = \frac{\partial \left(J^n + \left(\boldsymbol{\lambda}^{n+1}\right)^T \mathbf{f}^n \right)}{\partial \mathbf{S}_{\mathbf{w}}^n} = \frac{\partial J^n}{\partial \mathbf{S}_{\mathbf{w}}^n} + \left(\boldsymbol{\lambda}^{n+1}\right)^T \frac{\partial \mathbf{f}^n}{\partial \mathbf{S}_{\mathbf{w}}^n} \tag{D.17}$$

can be calculated backward in time using the Final Conditions $\left(\boldsymbol{\lambda}^N\right)^T = \mathbf{0}$ as initial conditions.

D.4 Derivatives for the dynamic system

For the dynamic system equations in most grid blocks there are two nonzero derivatives with respect to the water saturation S_w. For the dynamic system in grid block i these nonzero derivatives are $\frac{\partial f^n_{w_i}}{\partial S^n_{w_i}}$ and $\frac{\partial f^n_{w_i}}{\partial S^n_{w_{i-1}}}$.

D.4.1 Derivatives $\frac{\partial f^n_{w_i}}{\partial S^n_{w_i}}$

For the grid block at the left boundary, containing only water injection, i.e. $q^n_{w_i} = q^n_{t_i}$ the derivative of the dynamic system becomes

$$\frac{\partial f^n_0}{\partial S^n_{w_0}} = \frac{\Delta t}{\phi} q^n_{t_0} \frac{\partial f^n_{w_0}}{\partial S^n_{w_0}} + 1. \tag{D.18}$$

In grid blocks without a source the derivative is

$$\frac{\partial f^n_i}{\partial S^n_{w_i}} = -\Delta t \frac{u^n_{t_i}}{\Delta x \phi} \frac{\partial f_{w_i}}{\partial S^n_{w_i}} + 1. \tag{D.19}$$

For the last grid block, at the right boundary, the derivative is

$$\frac{\partial f^n_r}{\partial S^n_{w_r}} = -\frac{\Delta t}{\phi} \frac{u^n_{t_r}}{\Delta x} \frac{\partial f^n_{w_r}}{\partial S^n_{w_r}} + 1. \tag{D.20}$$

D.4.2 Derivatives $\frac{\partial f^n_{w_i}}{\partial S^n_{w_{i-1}}}$

For the grid block at the left boundary this derivative is

$$\frac{\partial f_0}{\partial S^n_{w_{0-1}}} = 0. \tag{D.21}$$

For grid blocks without source terms

$$\frac{\partial f^n_i}{\partial S^n_{w_{i-1}}} = \Delta t \frac{u^n_{t_i}}{\Delta x \phi} \frac{\partial f_{w_{i-1}}}{\partial S^n_{w_{i-1}}}. \tag{D.22}$$

For the last grid block

$$\frac{\partial f_r^n}{\partial S_{w_{r-1}}^n} = \frac{u_{t_r}^n}{\Delta x}\frac{\Delta t}{\phi}\frac{\partial f_{w_{r-1}}^n}{\partial S_{w_{r-1}}^n}. \tag{D.23}$$

D.4.3 Derivative with respect to q_t^n

The control parameter is the total injection/production rate q_t^n. For the grid block at the left boundary, the derivative with respect to q_t^n is

$$\frac{\partial f_0^n}{\partial q_t^n} = \frac{\Delta t}{\phi}\left(-1 + f_{w_0}^n\right). \tag{D.24}$$

For grid blocks without source terms

$$\frac{\partial f_i^n}{\partial q_t^n} = -\frac{\Delta t}{\phi}\left(\frac{f_{w_i} - f_{w_{i-1}}}{\Delta x}\right)\frac{\partial u_{t_i}^n}{\partial q_t^n}. \tag{D.25}$$

The derivative $\frac{\partial u_{t_i}^n}{\partial q_t^n}$ can be calculated by using eq. D.6

$$\frac{\partial u_{t_i}^n}{\partial q_t^n} = \frac{\partial\left(-q_t^n \Delta x\right)}{\partial q_t^n} = -\Delta x. \tag{D.26}$$

For the last grid block the derivative with respect to q_t^n is

$$\frac{\partial f_r^n}{\partial q_t^n} = \left(\frac{\Delta t}{\Delta x \phi} f_{w_{r-1}}^n - \frac{\Delta t}{\phi \Delta x} f_{w_r}^n\right)\frac{\partial u_{t_r}^n}{\partial q_t^n}. \tag{D.27}$$

D.5 Derivatives of the objective function

Since the objective function is based on the production rates in grid block r it has only nonzero derivatives with respect to the water saturation in this grid block $\left(S_{w_r}^n\right)$

$$\frac{\partial J^n}{\partial S_{w_r}^n} = -V_{gb}\frac{q_t^n \Delta t^n}{(1+b)^{t^n}}\left(-r_o + r_w\right)\frac{\partial f_{w_r}^n}{\partial S_{w_r}^n}. \tag{D.28}$$

The derivative with respect to the control q_t^n is

$$\frac{\partial J^n}{\partial q_t^n} = -V_{gb}\frac{\left[\left(1 - f_w^n\right) r_o + f_w^n r_w\right] \Delta t^n}{(1+b)^{t^n}}. \tag{D.29}$$

Appendix E
Meaning of the Lagrange multipliers

In this appendix the general formulation for the (physical) meaning of the Lagrange multipliers is derived, based on Kraaijevanger (2004). We consider a dynamic system of type $g^n\left(x^{n+1}, x^n, u^n\right) = 0$.

E.1 Perturbation in the state

We consider the objective function $\mathcal{J}$, defined as

$$\mathcal{J} = \sum_{n=0}^{N-1} \mathcal{J}^n\left(x^n, u^n\right). \tag{E.1}$$

Furthermore, we consider a perturbation in the state x at time step j, from x^j to $\left(x^j + \delta x^j\right)$. Because of this perturbation the states at subsequent time steps k (with $k = j+1, j+2, .., N-1$) will generally be affected, as opposed to the states at prior time steps p (with $0 \leq p \leq j-1$) which are not affected. Due to the perturbation in the state the objective function will change by $d\mathcal{J}$. Because the perturbation occurs at j only the part of the objective function for time steps $j, j+1, .., N-1$ will be affected. For this reason we define a cost-to-go objective function $\mathcal{J}_j$ as

$$\mathcal{J}_j = \sum_{n=j}^{N-1} \mathcal{J}^n\left(x^n, u^n\right). \tag{E.2}$$

$\mathcal{J}_j$ is a function of the state x^j and the controls $u^j, u^{j+1}, .., u^{N-1}$, i.e.

$$\mathcal{J}_j = \mathcal{J}_j\left(x^j, u^j, u^{j+1}, .., u^{N-1}\right). \tag{E.3}$$

The states at time steps x^k (with $k = j+1, j+2, .., N-1$) are calculated from x^j and u^j, $u^{j+1}, .., u^{N-1}$ through the dynamic system

$$g^n\left(x^{n+1}, x^n, u^n\right) = 0, \text{ with } n = j, j+1, .., N-2. \tag{E.4}$$

For perturbation of only x^j, keeping $u^j, u^{j+1}, .., u^{N-1}$ fixed, the total differential of eq. E.2 is equal to

$$d\mathcal{J}_j = \sum_{n=j}^{N-1} \frac{\partial \mathcal{J}^n\left(x^n, u^n\right)}{\partial x^n} dx^n. \tag{E.5}$$

Furthermore, the total differential of eq. E.4 is

$$dg^n = \frac{\partial g^n}{\partial x^{n+1}} dx^{n+1} + \frac{\partial g^n}{\partial x^n} dx^n = 0. \tag{E.6}$$

The derivative $\frac{\partial \mathcal{J}^n(x^n,u^n)}{\partial x^n}$ can be obtained from the adjoint equation

$$-\left(\lambda^n\right)^T \frac{\partial g^{n-1}}{\partial x^n} = \left(\lambda^{n+1}\right)^T \frac{\partial g^n}{\partial x^n} - \frac{\partial \mathcal{J}^n}{\partial x^n} \tag{E.7}$$

(like eq. 4.12). Substitution into eq. E.5 gives

$$\begin{aligned} d\mathcal{J}_j &= \sum_{n=j}^{N-1} \left[-\left(\lambda^n\right)^T \frac{\partial g^{n-1}}{\partial x^n} - \left(\lambda^{n+1}\right)^T \frac{\partial g^n}{\partial x^n} \right] dx^n \\ &= -\sum_{n=j}^{N-1} \left(\lambda^n\right)^T \frac{\partial g^{n-1}}{\partial x^n} dx^n - \sum_{n=j}^{N-1} \left(\lambda^{n+1}\right)^T \frac{\partial g^n}{\partial x^n} dx^n. \end{aligned} \tag{E.8}$$

The first summation on the second line of eq. E.8 can be rewritten as

$$\begin{aligned} \sum_{n=j}^{N-1} \left(\lambda^n\right)^T \frac{\partial g^{n-1}}{\partial x^n} dx^n &= \left(\lambda^j\right)^T \frac{\partial g^{j-1}}{\partial x^j} dx^j + \sum_{n=j+1}^{N-1} \left(\lambda^n\right)^T \frac{\partial g^{n-1}}{\partial x^n} dx^n \\ &= \left(\lambda^j\right)^T \frac{\partial g^{j-1}}{\partial x^j} dx^j + \sum_{n=j}^{N-2} \left(\lambda^{n+1}\right)^T \frac{\partial g^n}{\partial x^{n+1}} dx^{n+1}. \end{aligned} \tag{E.9}$$

The second summation on the second line of eq. E.8 can be rewritten as

$$\sum_{n=j}^{N-1} \left(\lambda^{n+1}\right)^T \frac{\partial g^n}{\partial x^n} dx^n = \left(\lambda^N\right)^T \frac{\partial g^{N-1}}{\partial x^{N-1}} dx^{N-1} + \sum_{n=j}^{N-2} \left(\lambda^{n+1}\right)^T \frac{\partial g^n}{\partial x^n} dx^n. \tag{E.10}$$

Substitution of eqs. E.9 & E.10 into eq. E.8, using the *Final Condition* $\lambda^N = 0$ (like eq. 4.10), yields

$$\begin{aligned} d\mathcal{J}_j &= -\left(\lambda^j\right)^T \frac{\partial g^{j-1}}{\partial x^j} dx^j - \sum_{n=j}^{N-2} \left(\lambda^{n+1}\right)^T \frac{\partial g^n}{\partial x^{n+1}} dx^{n+1} - \sum_{n=j}^{N-2} \left(\lambda^{n+1}\right)^T \frac{\partial g^n}{\partial x^n} dx^n \\ &= -\left(\lambda^j\right)^T \frac{\partial g^{j-1}}{\partial x^j} dx^j - \sum_{n=j}^{N-2} \left(\lambda^{n+1}\right)^T \left(\frac{\partial g^n}{\partial x^{n+1}} dx^{n+1} + \frac{\partial g^n}{\partial x^n} dx^n \right). \end{aligned} \tag{E.11}$$

Substitution of eq. E.6 gives

$$d\mathcal{J}_j = -\left(\lambda^j\right)^T \frac{\partial g^{j-1}}{\partial x^j} dx^j. \tag{E.12}$$

Eq. E.12 describes the first order change in the cost-to-go objective function resulting from a perturbation in the state x^j at time step j. For systems of type $g^n = x^{n+1} - f\left(x^n, u^n\right)$, like the fractional flow problem in section 5.5 and appendix D, the derivative $\frac{\partial g^{j-1}}{\partial x^j} = 1$. For these systems eq. E.12 reduces to

$$d\mathcal{J}_j = -\left(\lambda^j\right)^T dx^j. \tag{E.13}$$

In eq. E.13 the Lagrange multiplier, apart from the minus sign, directly reflects the sensitivity of the objective function with respect to slight changes in the state. The minus sign difference

could be removed by defining the adjoint equation (eq. E.7) as

$$(\lambda^n)^T \frac{\partial g^{n-1}}{\partial x^n} = -\left(\lambda^{n+1}\right)^T \frac{\partial g^n}{\partial x^n} - \frac{\partial \mathcal{J}^n}{\partial x^n}. \tag{E.14}$$

E.2 Perturbation in the constraint

In this section a perturbation in the constraint is considered. At time step $j-1$ the constraint is equal to

$$g^{j-1}\left(x^j, x^{j-1}, u^{j-1}\right) = 0. \tag{E.15}$$

Because x^{j-1} and u^{j-1} are fixed at time step $j-1$, the derivative of eq. E.15 can be written as

$$dg^{j-1} = \frac{\partial g^{j-1}}{\partial x^j} dx^j \tag{E.16}$$

Substitution into eq. E.12 then gives

$$d\mathcal{J}_j = -\left(\lambda^j\right)^T dg^{j-1}. \tag{E.17}$$

Eq. E.17 describes the first order change in the cost-to-go objective function resulting from a perturbation in the constraint g at time step j.

Summary

During the oil production process water is generally injected into the reservoir to maintain reservoir pressure and to displace the oil towards the production wells. Ideally, as the production process continues the injected water will slowly move through the reservoir in the direction of the producers, in the meantime sweeping the oil in between. However, because the rock properties vary spatially, the displacement generally does not occur uniformly. There may be preferential, high permeability flow paths through which the injected water channels to the producer. Oil outside these channels may as a result not be displaced by the injected water. Because of this non-uniform displacement water production often starts at an early stage. With conventional wells there is little that can be done to remedy this early water production without significant costs. This early water production can also hardly be prevented, because identification of possible preferential flow paths is difficult due to the reservoir's limited accessibility. As a result of the uncertainty and the lack of control on the production process typically only a relatively small percentage (30-40 percent) of the oil present in the reservoir can be recovered economically. Hence, the world's recoverable reserves may be increased if a larger percentage of oil can be recovered from the reservoir.

In de last few years a variety of technologies to better measure and control the production process through the wells have been developed. These technologies are typically installed within the well and they can be operated remotely. A well equipped with this type of measurement and control technology is generally referred to as a smart, intelligent or instrumented well. With down-hole control valves and isolating packers a well can be split up in segments that can be controlled separately. This enables an increased control on fluid flow into or out of the well. By manipulating the valve-settings it is to some degree possible to change the pressure distribution and thereby the fluid flow direction in the reservoir. The objective of this thesis work is to examine if by doing this it is possible to increase the percentage of oil recovered from the reservoir. An important part of this study comprises the calculation of the valve-settings that will optimize the net present value of the displacement process. To be able to do this for various reservoirs a numerical reservoir model was used, instead of a real reservoir. The calculation of the optimal valve-settings was done with a gradient-based optimization routine, the derivative information was calculated with optimal control theory.

The results show that significant improvement in the water flooding process can be achieved by dynamically controlling the valve-settings in the injection and production wells. In fields equipped with smart wells this is realized by controlling the down-hole valves, in fields equipped with vertical conventional wells by controlling the valves at the surface. The degree of improvement depends on the fluid properties and on the spatial variation in the rock properties. The scope for improvement also depends on constraints on the well operating conditions, it generally increases with increasing pressure available to inject or produce fluids. In addition the scope for improvement depends on the relative well locations, because these partly determine to what extent the fluid flow direction in the reservoir can be affected. The improvement partly results from the fact that through dynamic flow control the negative impact of geological features can be mitigated.

Because the rock properties are poorly known in reality, the displacement optimization must be calculated based on estimated reservoir properties. We investigated if significant improvement in the water flooding process can also be realized if some of the reservoir properties must be estimated from production data. To this end the gradient-based optimization routine was combined with an ensemble Kalman filter data-assimilation method, developed in RF-Rogaland Research. The Kalman filter was used to frequently update the estimated pressure-, saturation, and permeability distribution in the reservoir, based on production data. After each update of the reservoir model, the optimum valve-settings were recalculated for the remaining producing period. First results indicate that significant improvements may be possible with this closed-loop approach.

Samenvatting

Tijdens het olieproductieproces dient vaak water geïnjecteerd te worden teneinde de druk in het reservoir op een voldoende hoog peil te houden. Dit geïnjecteerde water dient er tevens toe de in de porieruimte van het gesteente opgeslagen olie in de richting van de productieputten te verdringen. Doordat de gesteente-eigenschappen veelal ruimtelijk variëren geschiedt deze verdringing over het algemeen niet gelijkmatig. Vanwege ruimtelijke verschillen in permeabiliteit (vloeistofdoorlaatbaarheid) kan kanalisering van de vloeistofstroming optreden, welke er dan toe leidt dat het geïnjecteerde water voornamelijk olie in deze hoog permeabele kanalen verdringt. Dit heeft tevens vaak tot gevolg dat waterproductie al in een vroeg stadium aanvangt, hetgeen de olieproductie negatief kan beïnvloeden. Veelal kan er weinig aan deze waterproductie gedaan worden zonder aanzienlijke extra investeringen. Deze vroegtijdige waterdoorbraak is ook moeilijk te voorkomen, aangezien de ruimtelijke variatie in gesteenteeigenschappen vanwege de beperkte toegankelijkheid tot het reservoir grotendeels onbekend is, en eventuele kanalisering derhalve moeilijk is te voorspellen.

De grote onzekerheden in de gesteente-eigenschappen en de beperkte controle over het productieproces hebben tot gevolg dat over het algemeen slechts een beperkt percentage (circa 30-40 procent) van de in het reservoir aanwezige olie op economische wijze gewonnen kan worden. De winbare wereldwijde olievoorrraden zouden in principe dus vergroot kunnen worden als een hoger percentage van de in het reservoir aanwezige olie gewonnen kan worden.

In de laatste jaren zijn verschillende technieken ontwikkeld waarmee het productieproces beter gemeten en geregeld kan worden. Een put uitgerust met deze meet- en regelapparatuur wordt vaak aangeduid als een slimme of intelligente put. Door kleppen in de put te installeren kan deze in vescheidene zones worden ingedeeld die elk afzonderlijk van het oppervlak bestuurd kunnen worden. Hierdoor kan beter geregeld worden waar de vloeistoffen de put in- of uitstromen.

Door het veranderen van de klepstanden in de putten kan de drukverdeling en daarmee de stromingsrichting in het reservoir tot op zekere hoogte beïnvloed worden. Het doel van dit proefschrift is om te onderzoeken of het hierdoor mogelijk is om een groter percentage van de olie uit het reservoir te produceren. Een belangrijk deel van het onderzoek omvat het uitrekenen van de klepstanden als funktie van de tijd die de economische waarde van het verdringingproces optimaliseren. Om dit voor een groot aantal verschillende soorten reservoirs te kunnen doen is in plaats van een echt reservoir gebruik gemaakt van een numeriek reservoir model.

Voor het uitrekenen van de klepstanden is gebruik gemaakt van de steilste afdalingsmethode waarbij optimale besturingstheorie is gebruikt om de benodigde gradiënten uit te rekenen.

Het blijkt dat wanneer de vloeistof- en gesteente-eigenschappen bekend zijn een significante verbetering van het olie-water verdringsproces vaak mogelijk is door dynamische aansturing van de klepstanden in de injectie- en productieputten. In slimme putten kan dit bereikt worden door het controleren van de ondergrondse kleppen, in conventionele vertikale putten door het controleren van de kleppen aan het oppervlak. Aanzienlijke verbeteringen blijken in principe

ook mogelijk in reservoirs die reeds geruime tijd op niet-optimale wijze geëxploiteerd zijn. De mate van verbetering is onder andere afhankelijk van de vloeistofeigenschappen en van de ruimtelijke variatie in de permeabiliteit. Een negatief effect van de laatste kan door middel van dynamische aansturing vaak deels tenietgedaan worden. De realiseerbare verbetering is daarnaast ook sterk afhankelijk van restricties op de putbesturing. Grotere verbeteringen zijn haalbaar naarmate een grotere overduk voor vloeistofinjectie of een grotere onderdruk voor vloeistofproductie mogelijk is.

Omdat met name de gesteente-eigenschappen in de werkelijkheid slecht bekend zijn, is ook onderzocht of verbeteringen gerealiseerd kunnen worden wanneer de ruimtelijke variatie in het permeabiliteitsveld aanvankelijk onbekend is en geschat dient te worden op basis van meetgegevens van het productieproces. In deze aanpak werd de op optimale besturingstheorie gebaseerde optimalisatiemethode gecombineerd met een, elders ontwikkelde, parameter identificatiemethode (Kalman filter). Het Kalman filter werd gebruikt om op gezette tijden, op basis van de meetgegevens van het productieproces, een nieuwe schatting van de druk-, de waterverzadigings- en de permeabiliteitsverdeling in het reservoir te verkrijgen. Op basis van de nieuw geschatte verdelingen werd de optimale aansturingsfunctie opnieuw uitgerekend voor het resterende deel van het productieproces. De eerste resultaten duiden erop dat aanzienlijke verbeteringen haalbaar zijn met deze gesloten-lus aanpak.

Acknowledgments

The front cover of this dissertation contains only one name. However, it has been shaped by many people. I would like to sincerely thank everybody who, either directly or indirectly, contributed!

Having been an active member of the "Utrechtse Geologen Vereniging" gives moving to "Mijnbouw" in Delft something extra. Quite curious to what these " former competitors" would be like I happily accepted the invitation from Arjen Wagenvoort to join the Barbara drinks in 't Noorden. Being initially a little worried to end up in the canal, I quickly discovered that the mining people are not too different from the average geologist in Utrecht. It was really a pleasure to work, talk and hang out with the students. In particular I would like to thank Arjen and Vincent for learning me a lot about the oil business and about mining behaviors (Glück Auf!). Somewhere in the second year the project became more mathematical of nature. Working together with Norbert during this phase has been great, both for developing the algorithms and for keeping a good atmosphere during the periods of debugging. At the final stage, the work from Ali Vakili has helped greatly in improving the contents of my thesis, for which I want to thank him a lot. I would also like to thank Saskia, Tim and Leendert for being nice room mates.

At the start of my Ph.D. most topics present in this thesis were completely new to me. Therefore, I would not have been able to do this project without a number of key reference books on reservoir engineering, reservoir simulation, numerical methods, and optimal control theory. Throughout the years I intensively used a number of books, among which Aziz and Settari (1986) for the reservoir simulation part of the study, Luenberger (1979) to learn about optimal control theory, and Stengel (1994) to get a better understanding of the physical meaning of the Lagrange multipliers. In addition books/dissertations from Mehos (1986), Ramirez (1987), and Sudaryanto (1998) have been of great help. I would like to express my appreciation and gratitude for the effort they have put into making them.

A number of people have played an important role in enabling, creating and coordinating the project. I would like to thank Pieter Kapteijn from Shell for funding the project. In addition, I would like to thank Cor van Kruijsdijk, first of all for hiring me (despite the fact that my background was probably not the most suitable one), secondly for coming up with the idea to apply "blaasvoetbal" (I don't know how to translate this other than with "blow-soccer") to petroleum reservoirs, and finally for the pleasant cooperation over the last years. I am also truly grateful to Jan-Dirk Jansen, for the many things I have learned from him, for the many personal and professional discussions, and for the nice daily cooperation. Rarely have I seen someone who can work as hard and as enthousiastic as he can, and who simultaneously manages two jobs, about four different research subjects with as many Ph.D.'s, probably twice as many M.Sc.'s, and a busy family life!

Many thanks too to Hans Bruining, it was a pleasure to get into his office, generally at the end of the day, and to have an extended discussion on a variety of subjects.....somehow I always left laughing! I also would like to thank Hans Kraaijevanger for meticulously reviewing my dissertation, and for his help on a number of aspects of the adjoint equation.

Doing a Ph.D. is not always easy, especially when one is completely stuck in a particular problem (Sometimes I am wondering if the latter is the very definition of a Ph.D.). In these situations it is great to talk to Ph.D. fellows who are, have been, or will be in the same situation. I would like to thank all my Ph.D. colleagues, in particular Ainhoa, Antonio, Tanguy, Marco, Quoc, Cas, Willem-Jan, Renato, Joris, Maarten, and Talal, for the serious and not so serious talks and discussions, and for being nice colleagues. A special word of thank to Nicolai who became a close friend during the last few years.

Doing a project that involves computers for most of the time makes you really to get to know and appreciate the IT people. Many thanks to, amongst others, Rob, Vincent, Guus, Mongi, Jaap, and Nick from Stanford, for helping me out with all sorts of IT issues.

During my Ph.D. I had the pleasant opportunity to visit Stanford university for about three months. Many thanks to everybody there for making my stay a very pleasant one. I would like to thank professor Durlofsky and professor Aziz for hosting my stay, and for giving me the opportunity to participate in the annual SUPRI-meetings, and in writing a paper. Many thanks to Amisha and Alex for letting me join them to the Redwoods in North California. Many many thanks to Burak, for jointly writing a paper, for showing me around, for loaning me his car while he was off to Turkey, for the sessions in the Nut House, for the very nice smoking breaks, and for his very funny way of referring to things in general, and articles and dissertations in particular.

Apart from the people who were directly involved in my Ph.D. many people helped me in other ways. I would like to thank all my friends, for the great fun I am always having when hanging out with them, and for them supporting me in many ways. I am especially grateful to my parents Dick and Heleen, and my sister Marleen for their continuous presence and support, not only in the last years but thoughout my entire life.

Last, but definitely not least, I want to thank Barbara.....for too many things to mention here.

About the author

Roald Brouwer was born on 1 June 1974 in Assen, The Netherlands. In 1992 he received his V.W.O. degree from College de Klop in Utrecht. From 1992 to 1997 he studied at Utrecht University, getting his propaedeutics in Geology in 1993 and his Masters degree in Geochemistry in 1997. From 1997 to 1999 he worked in various companies, both inside and outside the oil industry. In September 1999 he started a Ph.D. at the department of Geotechnology (at the time the "faculteit Mijnbouw") of Delft University of Technology. On 1 January 2005 he started at Shell International Exploration and Production in Rijswijk, The Netherlands.